UNIVERSITY OF SOUTHAMPTON

FACULTY OF ENGINEERING AND THE ENVIRONMENT

INSTITUTE OF SOUND AND VIBRATION RESEARCH

BIODYNAMICS OF THE SEATED HUMAN BODY WITH DUAL-AXIS EXCITATION: NONLINEARITY AND CROSS-AXIS COUPLING

by

Guangtai Zheng

Thesis for the degree of Doctor of Philosophy

February 2012

UNIVERSITY OF SOUTHAMPTON

ABSTRACT

FACULTY OF ENGINEERING AND THE ENVIRONMENT

INSTITUTE OF SOUND AND VIBRATION RESEARCH

Doctor of Philosophy

BIODYNAMICS OF THE SEATED HUMAN BODY WITH DUAL-AXIS EXCITATION: NONLINEARITY AND CROSS-AXIS COUPLING

By Guangtai Zheng

The apparent mass of the seated human body and the transmissibility to the upper-body (i.e., the spine and the pelvis) during vertical vibration excitation have been reported to have resonance frequencies around 5 Hz. With fore-and-aft excitation the apparent mass shows a first peak around 1 Hz and second mode around 2 to 3 Hz. Little is known about how the motion of the upper-body during excitation in one direction is affected by the addition of vibration in an orthogonal direction (i.e., the cross-axis coupling). The principal objective of the research reported in this thesis was to identify how the resonances in the apparent mass and transmissibility, and their association, depends on the magnitude of the inline vibration excitation and the addition of an orthogonal vibration excitation. The research was also designed to investigate the characteristics necessary in mathematical models that represent the cross-axis coupling and nonlinearity evident in the biodynamic responses of the human body.

The movement of the body (over the first, fifth and twelfth thoracic vertebrae, the third lumbar vertebra, and the pelvis) in the fore-and-aft and vertical directions (and in pitch at the pelvis) was measured in 12 seated male subjects during random vertical vibration excitation (over the range 0.25 to 20 Hz) at three vibration magnitudes (0.25, 0.5 and 1.0 ms^{-2} r.m.s.) and during fore-and-aft vibration excitation over the same frequency range and at the same three vibration magnitudes. At the highest magnitude of vertical excitation the effect of adding fore-aft excitation (at 0.25, 0.5, and 1.0 ms^{-2} r.m.s.) was investigated. Similarly, at the highest magnitude of fore-and-aft excitation the effect of adding vertical vibration (at 0.25, 0.5, and 1.0 ms^{-2} r.m.s.) was investigated. The forces in the fore-and-aft and vertical directions on the seat surface were also measured so as to calculate apparent masses. The subjects adopted a normal upright posture, an erect posture, and a slouched posture. Resonance frequencies in the apparent mass and transmissibility during vertical excitation decreased with increasing magnitude of vertical excitation and with the addition of fore-and-aft excitation. The modulus of the first peak in the apparent mass and transmissibility during fore-and-aft excitation decreased with increasing magnitude of fore-and-aft excitation and with the addition of vertical excitation. Complex vibration modes in the upper-body appear to be responsible for the resonances in both the vertical and the fore-and-aft apparent masses. Compared to the normal upright posture, the erect posture tended to increase the resonance frequency in the apparent mass and transmissibility associated with vertical excitation but decrease the resonance frequency in the apparent mass and transmissibility associated with fore-and-aft excitation. The association between resonances in the transmissibility to the upper body and the resonance in the apparent mass varied with vertical excitation but not with fore-aft excitation.

A seven degree-of-freedom multi-body model indicated that the resonance frequency in the vertical apparent mass on the seat and the vertical transmissibility to the upper-body with either vertical or dual-axis excitation is sensitive to the vertical stiffness of tissues beneath the pelvis and closely related to the vertical motion of the upper body. It has also been shown that the first mode of the fore-and-aft apparent mass and the fore-and-aft transmissibility can be attributed to

the fore-and-aft movement of the upper-body due to the pelvis pitch, while the second mode can be attributed to the fore-and-aft movement of the upper-body caused by shear deformation of the pelvis tissue. It is suggested that a mathematical model developed with single-axis excitation can represent the biodynamic response with dual-axis excitation by changing these sensitive parameters (e.g., the stiffness of the tissue beneath the pelvis).

A finite element human body model with flexible bodies representing the tissue beneath the pelvis and thighs and rigid bodies representing other body segments provided sensible prediction of the first resonance frequencies and the associated modulus in the vertical inline and fore-and-aft cross-axis apparent mass on the seat and the transmissibility to the lumbar spine, as well as the pressure distribution on the seat surface. With the flexible bodies assigned the material properties of nonlinear low density foam, the model was allowed to reflect the softening effect (i.e., a reduce in the resonance frequency of the vertical apparent mass) when the when the magnitude of the vertical excitation was increased.

CONTENTS

DECLARATION OF AUTHORSHIP

I, GUANGTAI ZHENG,

declare that the thesis entitled

BIODYNAMICS OF THE SEATED HUMAN BODY WITH DUAL-AXIS EXCITATION: NONLINEARITY AND CROSS-AXIS COUPLING

and the work presented in the thesis are both my own, and have been generated by me as the result of my own original research. I confirm that:

- this work was done wholly or mainly while in candidature for a research degree at this University;
- where any part of this thesis has previously been submitted for a degree or any other qualification at this University or any other institution, this has been clearly stated;
- where I have consulted the published work of others, this is always clearly attributed;
- where I have quoted from the work of others, the source is always given. With the exception of such quotations, this thesis is entirely my own work;
- I have acknowledged all main sources of help;
- where the thesis is based on work done by myself jointly with others, I have made clear exactly what was done by others and what I have contributed myself;

Parts of this work have been published as:

Zheng G, Qiu Y, and Griffin MJ (2011a) An analytic model of the in-line and cross-axis apparent mass of the seated human body exposed to vertical vibration with and without a backrest. Journal of Sound and Vibration 330 (26), 6509-6525.

Zheng G, Qiu Y, and Griffin MJ (2011b) Vertical vibration of the seated human body: nonlinearity, cross-axis coupling, and associations between resonances in transmissibility and apparent mass. Submitted to Journal of Sound and Vibration Research.

Signed: ……..

Date: ……..….

ACKNOWLEDGEMENTS

I would like to express my sincerest thanks to my supervisors, Dr. Yi Qiu and Professor Michael J Griffin, for their tailored supervision and promptly encouragement.

Many thanks to Dr. Chris Lewis, Dr. Martin Toward, Mr Peter Russell, Mr Gary Parker, Mrs Louise and Dr. Weidong Gong for their technical support for my experiment and data analysis.

I am grateful to Professor Brian Mace, Dr. Tim Waters and Dr. Miyuki Morioka for their time on my PhD review and valued suggestions on my research work.

Thank you to all the other members of the Human Factors Research Unit. I have been enjoying the collaborative work with you and benefiting from your friendship.

To my parents and younger sister!

CHAPTER 1: INTRODUCTION

Human bodies are frequently exposed to various whole-body vibrations in daily life and work. Study of how the vibration is transmitted to and through the human body will help advance understanding of the mechanisms of how body responds to the external vibration and help human body modelling. Such a study involves biodynamic research.

Previous studies have shown that biodynamic response to whole-body single-axis excitation is affected by factors such as body mass (e.g., Fairley and Griffin, 1989), gender (e.g., Lundström *and* Holmlund, 1998), sitting posture (e.g., Mansfield and Griffin, 2002), backrest contact (e.g., Wang *et al*., 2004), muscle activity (e.g., Mansfield *et al*., 2006), vibration magnitude (e.g., Nawayseh and Griffin, 2003), and the frequency (e.g., Toward, 2003). It is widely accepted that biodynamic response shows nonlinearity: the resonance frequency decreasing with increasing vibration magnitude. The extent of the nonlinearity in biodynamic response appears to depend on factors such as sitting postures, vibration magnitude and the spectrum of the applied vibration.

Biodynamic response with multi-axis excitation is similar to that with single-axis excitation: the resonance frequency of apparent mass (the complex ratio of the force and the acceleration at the same location) reduces with increasing number of vibration axes from single axis to dual or multi-axis (e.g., Hinz *et al*., 2006a; Qiu and Griffin, 2010). Knowledge of the motion of human body, especially the spine during dual-axis excitation will advance understanding of the modes associated with the resonance of the apparent mass.

Various models of biodynamic responses with vertical excitation or fore-and-aft excitation have been developed to interpret experimental findings. Majority of models have been proposed assuming the human body is a linear system so that the models are effective in predicting the human response within specific testing conditions. Nevertheless, models that take into account the nonlinearity in resonance or the coupling effect of multi-axis excitation are much more complex and need a more comprehensive calibration.

The research undertaken in this thesis is designed to investigate the effects of vibration magnitude and addition of an orthogonal excitation on the biodynamic response and how these effects could be reflected with a mathematical model.

The thesis is divided into ten chapters including this introductory chapter.

Chapter 2 reviews and discusses the up to date knowledge of the apparent mass and transmissibility with various excitations. The research scope of this thesis is defined.

Chapter 3 proposes a multi-body human body model to consider the contributions of the principal body segments to the dynamic responses with vertical excitation, especially the primary resonance.

Chapter 4 investigates the effect of the magnitude of vertical excitation and the addition of the fore-and-aft excitation on the resonances in apparent mass and transmissibility of 12 seated subjects.

Chapter 5 investigates the effect of the magnitude of fore-and-aft excitation and the addition of the vertical excitation on the resonances in apparent mass and transmissibility of 12 seated subjects.

Chapter 6 examines the effect of siting posture on the resonances in apparent mass and transmissibility of 12 seated subjects with single-axis and dual-axis excitation.

Chapter 7 investigates how the human body model working for the vertical excitation could be extended to work for the dual-axis excitation so as to improve understanding of the relation between the mechanical properties of human body and the dynamic responses with dual-axis vibration.

Chapter 8 develops a finite element human body model to take into account the nonlinearity in the resonance of vertical apparent mass with increasing vibration magnitudes and reflect the pressure distribution on the seat-occupant surface..

Chapter 9 presents a general discussion of the main findings reported in the thesis.

Chapter 10 presents the main conclusion of the thesis and provide recommendation for the future work.

CHAPTER 2: LITERATURE REVIEW

2.1 Introduction

Biodynamic response contains useful information for the evaluation and optimization of ride comfort of seats and vehicles. A review of the up to date knowledge of various factors affecting biodynamic response and how biodynamic response could be reflected with a mathematical model is presented in this chapter.

Biodynamic response is measured and represented by transfer functions that fall into two categories (Griffin 1990). Those involving the measurement and ratios of motions at different locations on the human body are grouped as transmissibility, for example, seat-to-spine or seat-to-head transmissibility. The other type which measures and calculates the complex ratio of forces and motion at the same point (e.g. acceleration, velocity) is typified as the driving-point response.

Apparent mass or driving point apparent mass is defined as the complex ratio of force, $F(\omega)$, and acceleration, $A(\omega)$, at the same location on the interface between human body and the seat:

$$M(\omega) = \frac{F(\omega)}{A(\omega)} \tag{2.1}$$

where, ω is the angular frequency of the input.

When the force is measured in the same direction as the input acceleration, the ratio between them is called the “inline apparent mass”. If the force is perpendicular to the acceleration, the ratio is called the “cross-axis apparent mass”. For example, when human body is exposed to vertical vibration, the ratios of forces $F_z(\omega)$, $F_x(\omega)$, $F_y(\omega)$ and the acceleration are apparent mass (vertical apparent mass), fore-and-aft cross-axis apparent mass and lateral cross-axis apparent mass, respectively.

The apparent mass of the body is normally used for measurements at an interface between the human body and a seat. However, there are also some studies reporting the measurement of forces and accelerations on the backrest and footrest. The ratio of force and the acceleration defined as Equation (2.1) is adopted as well to represent the dynamic response at these locations.

Mechanical impedance, or the driving point mechanical impedance, is the complex ratio of force $F(\omega)$ to velocity $V(\omega)$ at the same location:

$$Z(\omega) = \frac{F(\omega)}{V(\omega)} = i\omega M(\omega) \tag{2.2}$$

The transmissibility of the body represents how much vibration is transferred from the seat-occupant interface to different locations of the human body, such as the spine or head. Acceleration is widely adopted for the transmissibility studies. Transmissibility is defined as the complex ratio of motion at the output location to the motion at the input reference point. For example, transmissibility from seat to vertebrae level T12 can be defined as:

$$T(\omega) = \frac{a_{T12}(\omega)}{a_s(\omega)} \tag{2.3}$$

where,

a_{T12} (ω) is frequency response of the acceleration at the tenth thoracic spine;

a_s (ω) is frequency response of the acceleration at the seat interface.

Motion of the head when the human body is exposed to vertical vibration has been measured and reported in many studies on the basis that the head is a vital part of the body that is associated with vibration discomfort or that its movements affect vision (Griffin 1990). Measurements of motion at locations along the spine have also been published. Investigations of the spine motion have not only focused on the translational acceleration in the vertical, fore-and-aft, and lateral directions but have also concerned on the roll, pitch and yaw motion in some studies.

Apparent mass or mechanical impedance is often the measurement and representation of the overall dynamic response at the seat-occupant interface which takes into account the local body system and the whole-body movement. Transmissibility is often used to investigate the transmission path and vibration modes contributing to the resonances of the human body. If a human body is simplified to be represented with the single degree-of-freedom model shown as Figure 2.1 (a), then the equation of motion is defined as

$$m\ddot{q}_z + kq_z + c\dot{q}_z = kq_{z0} + c\dot{q}_{z0} \tag{2.4}$$

where m is the mass of the human body supported on the seat, k and c are stiffness and damping respectively. Apparent mass M and transmissibility T_r are defined as follows according to Equations (2.1) and (2.3).

$$M = m\frac{k + cs}{ms^2 + cs + k} \tag{2.5}$$

$$T_r = \frac{k + cs}{ms^2 + cs + k} \tag{2.6}$$

With m=60 kg, k=70000 N m^{-1}, c=2000 Ns m^{-1}, the modulus of the calculated vertical apparent mass and the vertical transmissibility to human body are shown in Figure 2.1 (b-c).

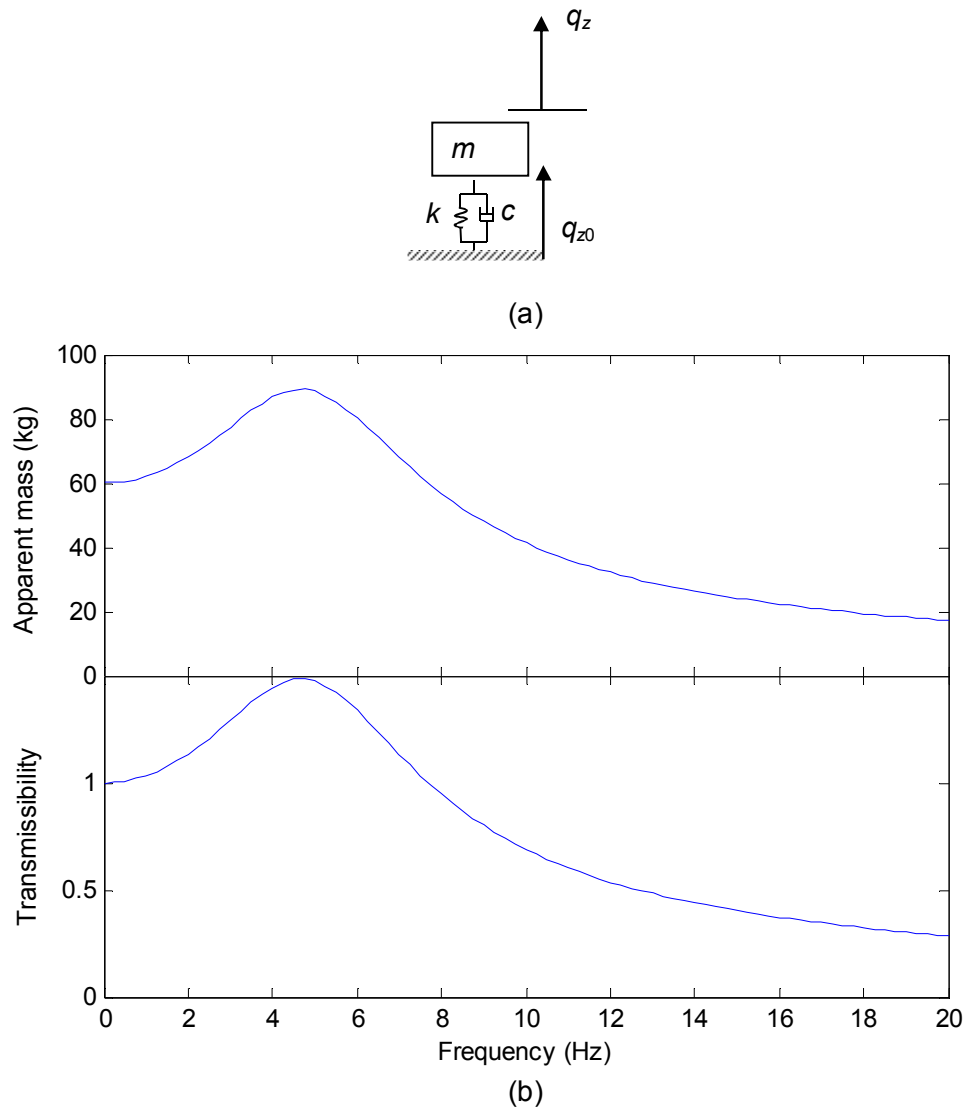

Figure 2.1 A single degree-of-freedom model (a) and calculated apparent mass and transmissibility (b) of a seated human body.

It is shown that at low frequencies, the modulus of apparent mass is close to the mass seated on the seat while the transmissibility is close to unity. The resonance frequency of apparent mass is the same as the resonance frequency of transmissibility.

2.2 Apparent mass of the seated human body with vertical excitation

Many studies investigating apparent mass have reported a first resonance at around 4-6 Hz and a second resonance in the region of 8-12 Hz for the vertical apparent mass (e.g., Fairley and Griffin, 1989; Kitazaki and Griffin, 1998; Mansfield and Griffin, 2000; Mansfield and Griffin, 2002; Matsumoto and Griffin, 2002a; Matsumoto and Griffin, 2002b; Nawayseh and Griffin 2003, Mansfield and Maeda 2006; Qiu and Griffin, 2010). Some studies have reported considerable forces in the fore-and-aft direction on the seat with vertical excitation with the principal resonance frequency in the vicinity of 5 Hz (e.g. Nawayseh and Griffin 2003; Mansfield and Maeda, 2005a; Qiu and Griffin, 2010).

Subject variability in human response to whole-body vibration has been observed and reported extensively (Fairley and Griffin, 1989; Seidel, 1996; Boileau *et al*., 1998; Paddan and Griffin, 1998; Holmlund *et al*., 2000; Mansfield and Griffin, 2000; Wang *et al*. 2004, Qiu and Griffin, 2010). Variability induced by various factors such as differences in body mass, age, gender, height, size among subjects are classified as inter-subject variability, as shown in Figure 2.2. The primary resonance frequencies of the 60 subjects were negatively correlated with the mass of each subject but positively correlated with the static sitting weight of subjects divided by their sitting height; the peak magnitudes of the apparent mass increased with increasing sitting weight while the normalized apparent mass (to be discussed in the following paragraphs) at their resonance frequency was correlated with their total body weight. The normalized apparent mass at 20 Hz was correlated with subject age.

Difference in the body mass has been found to be the largest contributor to the variation in apparent mass of the individual subject. At certain selected frequencies and specific sitting postures, the modulus of the apparent mass was linearly dependent on body mass with the correlation higher at lower frequencies (from 3 to 6 Hz) than at frequencies greater than 12 Hz (Wang *et al*., 2004). It was also found that static body mass supported on the seat was the main contributor to the inter-subject variability while gender and age had less effect. Similarly, the effects of age, gender, stature, and BMI (body mass index, kg m^{-2}) on the apparent masses of the subject groups have been reported to be small relative to the large and systematic effects of subject mass (Toward

and Griffin, 2010).

To minimize the effect of body mass on apparent mass, two methods have been generally adopted. One method is to group the measured data in different mass ranges (e.g., 55 kg, 75 kg and 90 kg) as was used in ISO 5982 (2001), so other factors influencing the dynamic response can be studied in a narrow mass range. Alternatively, apparent mass is normalised with respect to the static mass, as performed by Fairley and Griffin (1989) to limit the variance due to the large influence of body mass on the response data. The apparent mass was normalized by dividing it with the apparent mass at 0.5 Hz. The normalized apparent mass (Figure 2.3) showed far smaller variance than the un-normalised apparent mass. Normalization has been reported to significantly reduce the standard deviation of the rationalized peak magnitude of apparent mass (i.e. the apparent mass of each subject divided by the mean response of the subject group at resonance for both measured and normalized apparent mass) (from 0.255 to 0.105; p<0.001, Levene) (Toward and Griffin, 2010).

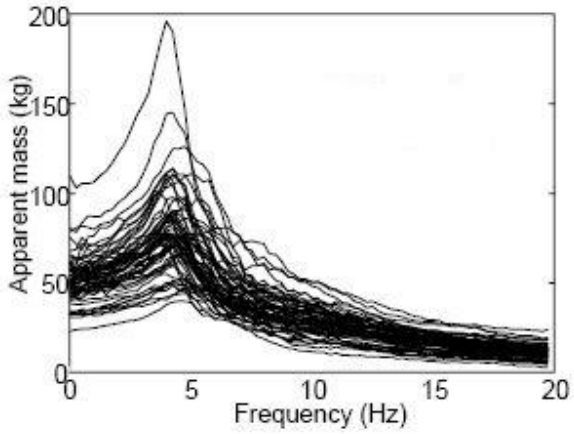

Figure 2.2 Vertical apparent masses of 60 subjects measured during 64-s exposures to 1.0 ms^{-2} r.m.s. random vibration (0.25-20 Hz) without backrest but with vibration at the feet and the seat: inter-subject variability (Fairley and Griffin 1989a).

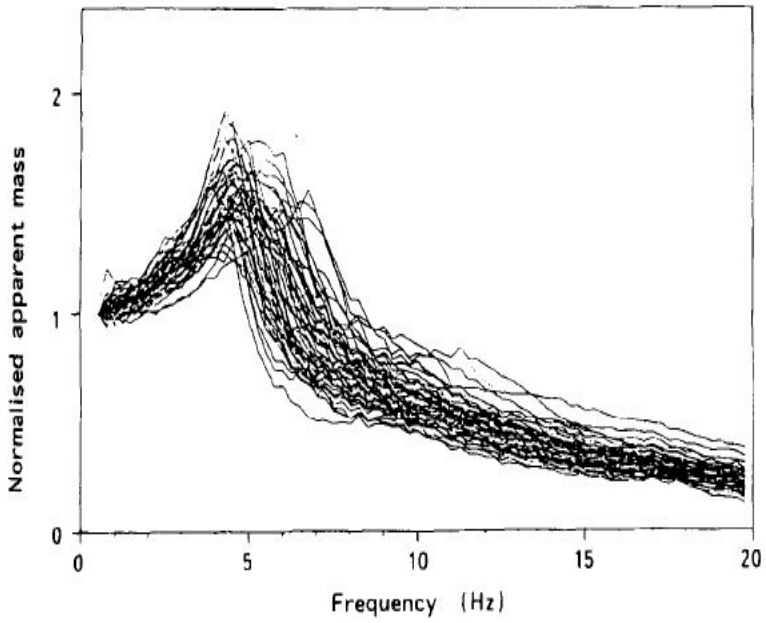

Figure 2.3 Normalized vertical apparent mass of 60 subjects measured during 64 s exposures to 1.0 ms^{-2} r.m.s. random vibration (0.25-20 Hz) without backrest but with vibration on the feet and the seat: inter-subject variability (Fairley and Griffin 1989a).

Apparent mass has been reported to be marginally dependent on gender in some studies. For example, although the mean normalized apparent masses of men, women, and children were similar (Fairley and Griffin, 1989), a slightly lower resonance frequency was observed with female subjects (Lundström and Holmlund, 1998). Females had a less distinct peak in their mechanical impedance than males (Holmlund *et al.*, 2000) whereas females had a greater normalized apparent mass than men at frequencies between 15 and 40 Hz (Wang *et al.*, 2004). The apparent mass was greater for males than females at 0.6 Hz and at 12 Hz with a rigid inclined backrest (Toward and Griffin, 2011). However, it is noted that a larger apparent mass for male might be contributed by body mass besides the gender effect. To reduce the inter-subject variability, only male subjects are used in the experiments conducted for this thesis.

2.2.1 Effect of postures and muscular tension

Many studies have reported significant effects of sitting posture on the biodynamic responses (Fairley and Griffin, 1989; Kitazaki and Griffin, 1998; Lundström and Holmlund, 1998; Holmlund *et al.*, 2000, Wang *et al.*, 2004). A higher resonance frequency was observed for “erect” and “tense” postures than for a “normal” posture (Fairley and Griffin, 1989, Figure 2.4; Lundström and Holmlund, 1998; Matsumoto and Griffin, 2002b; Mansfield *et al.*, 2005; Huang and Griffin, 2006). An increase in the mean

resonance frequency from 4.4 to 5.2 Hz when eight subjects sat in “erect” instead of “slouched” postures (Kitazaki and Griffin, 1998) was observed. The change can be explained by a stiffening effect with erect postures.

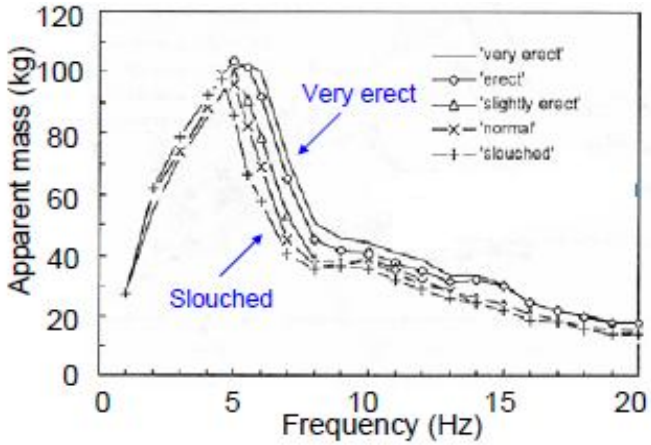

Figure 2.4 The apparent mass of one person exposed to vertical random vibration (0.25-20 Hz) at 1.0 ms^{-2} r.m.s. in five postures: slouched, normal, slightly erect, erect, and very erect (Fairley and Griffin, 1989).

By exposing 12 male subjects to vertical random whole-body vibration in four postures (“back on”, “back off”, “twist”, “move”) at 0.4 ms^{-2} r.m.s. (Mansfield and Maeda, 2005a), apparent mass showed peaks at around 5 Hz and 12 Hz for individuals in “back on”, “back off” and “twist” postures. The peak at 5 Hz was less evident in “move” condition (the condition which comprised a repeated 8 s sequence where subjects twisted to the left and right accompanied by arm movements) than other postures and the second resonance at around 12 Hz was not observed for any subjects. The normalized apparent mass was lower for a “back on” condition than a “back off” condition between 1 and 2 Hz. This might be attributed to less weight being supported by the seat when there was backrest. The normalized apparent masses of all but two subjects were similar. Many of the subjects had a lower normalized apparent mass at resonance frequencies and higher frequencies in “move” condition than the other three conditions (Figure 2.5). Reductions in the peak apparent mass in the “move” condition was suggested to be due to the difference in posture with the hypothesis that stretched arms might act as a dynamic vibration absorber resulting in reduced resultant force acting in the torso.

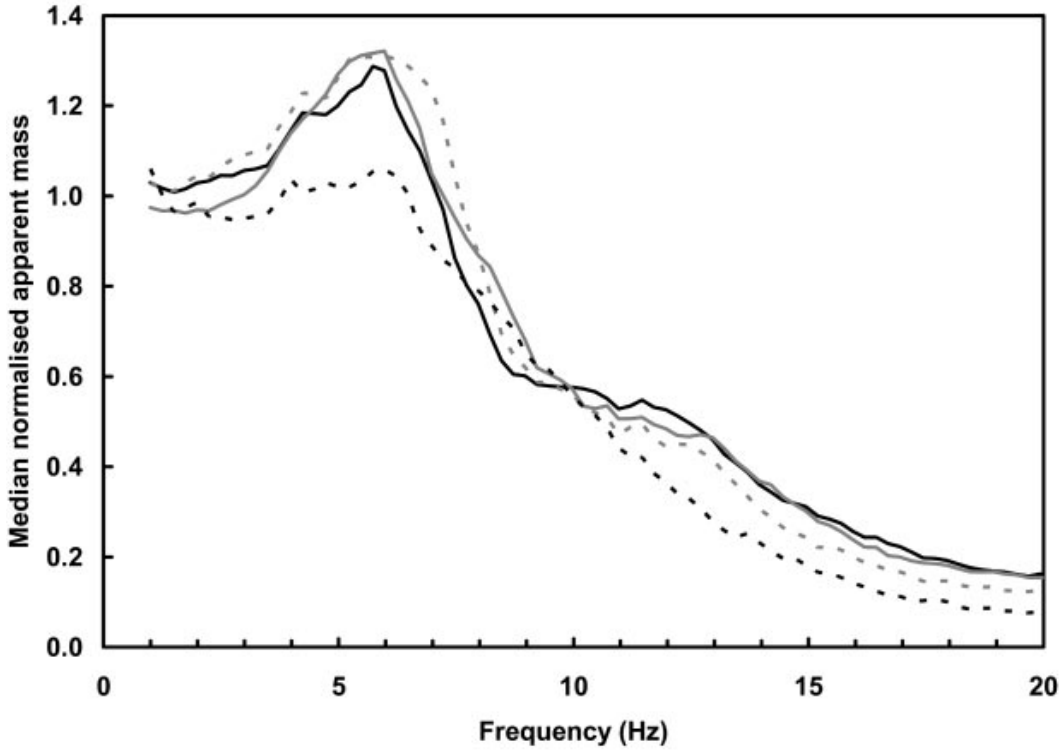

Figure 2.5 Median normalised apparent masses for 12 subjects in four postures exposed to random whole-body vertical vibration in the frequency range of 1 to 20 Hz with a magnitude of 0.4 ms^{-2} r.m.s. ——, back off; **——**, back on; - - -, twist; **- - -**, move (Mansfield and Maeda, 2005a).

The fore-and-aft cross-axis apparent mass had a peak at around 6 Hz for the “back-off”, “back-on” and “twist” conditions but the peak was eliminated for the “move” condition (Mansfield and Maeda, 2005a, Figure 2.6). The peak modulus of the fore-and-aft cross-axis apparent mass were significantly different for different conditions with the lowest modulus for the “move” posture. The apparent mass in the lateral direction was far smaller than that in the fore-and-aft direction and the peaks were not evident.

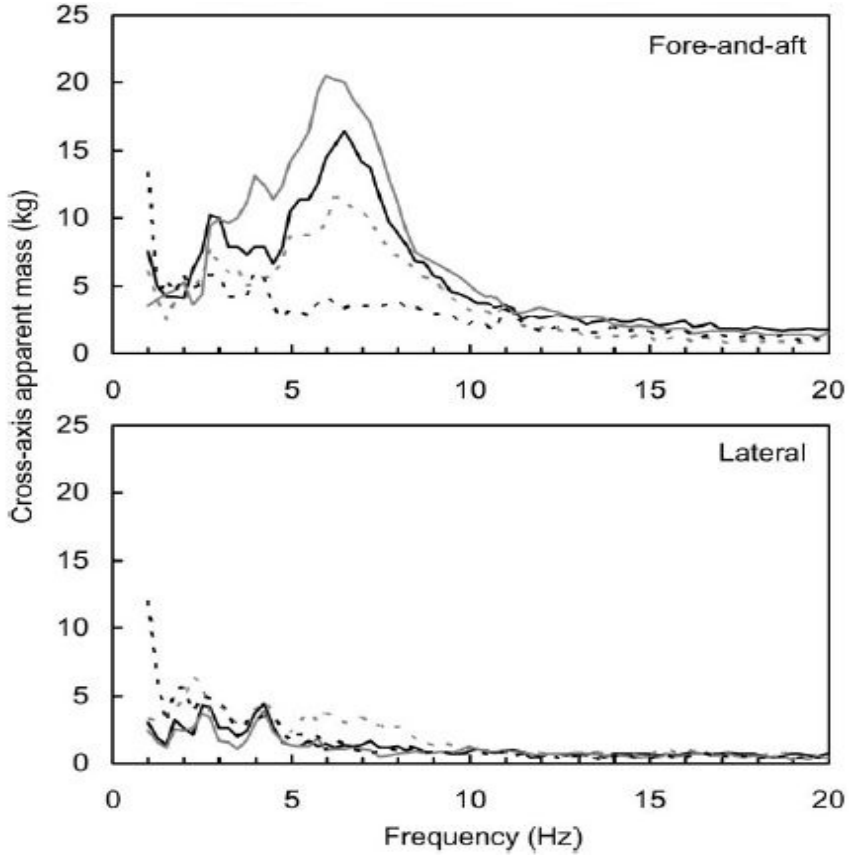

Figure 2.6 Median cross-axis apparent mass of twelve subjects exposed to whole-body vertical vibration at 0.4 ms^{-2} r.m.s. in four postures: ——, back off; **——**, back on; - - -, twist; **- - -**, move (Mansfield and Maeda, 2005a).

Differences in apparent masses of 12 subjects in nine sitting conditions (i.e., "upright", "anterior lean", "posterior lean", "kyphotic", "back-on", "pelvis support", "inverted SIT-BAR", "bead cushion", see Figure 2.7) have been reported (Mansfield and Griffin, 2002). Although there were not significant changes in apparent mass with different postures, peaks in the normalized apparent mass were lower for the "kyphotic" condition. Compared to the upright posture, a significant difference in the apparent mass resonance frequency was found for the "anterior lean" posture at 0.2 ms^{-2} r.m.s. In the "cushion" condition, the resonance frequency of the apparent mass was found to be decreased compared to the upright posture. When an upright posture was changed to "inverted SIT-BAR" condition representing an increase in tissue pressure, there was no evident difference in the resonance frequency of the apparent mass.

Apart from the muscle tension, the force exerted by hands or feet has been reported to influence apparent mass (Figures 2.8 and 2.9; Toward and Griffin, 2010). Either

increasing the applied force on a steering wheel or on a footrest reduced the apparent mass at the primary resonance frequency. The resonance frequency was increased with increasing applied force on the steering wheel from 0 to 150 N but was unaffected by changing the force exerted on the footrest.

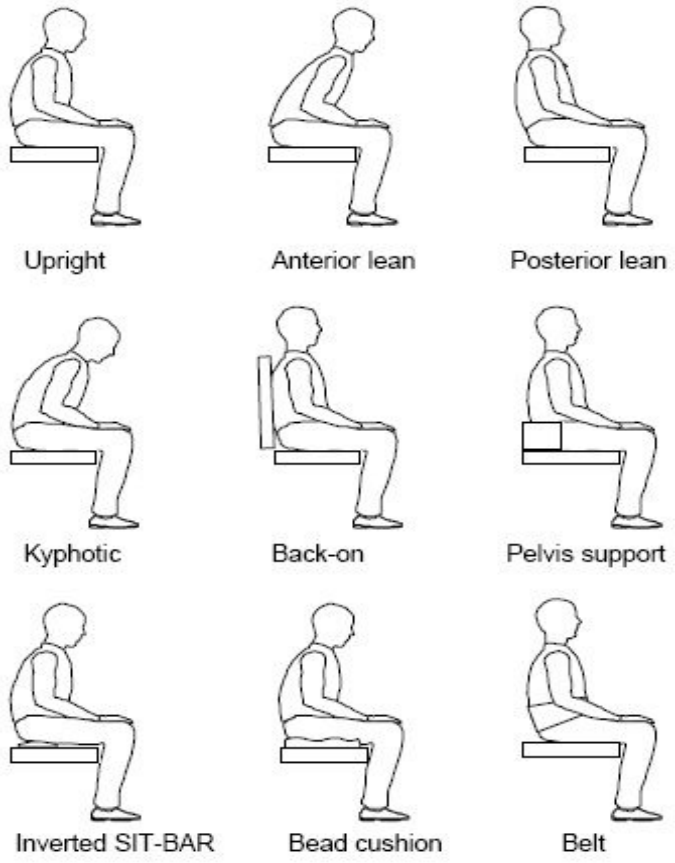

Figure 2.7 Diagrammatic representation of the nine postures used in the experiment (Mansfield and Griffin 2002).

It is shown from the reviewed studies that the changes in sitting posture or muscle tension that introduced variation in the apparent mass were generally associated with a change in stiffness of human tissue or spine geometry. It is desirable to study the effect of sitting posture on the apparent mass in the way in which the resonance in the apparent mass could be changed effectively. Changing the stiffness of pelvis tissue might be the most effective way to do this. This could be achieved by simply adjusting sitting postures, e.g., from a normal upright to an erect posture.

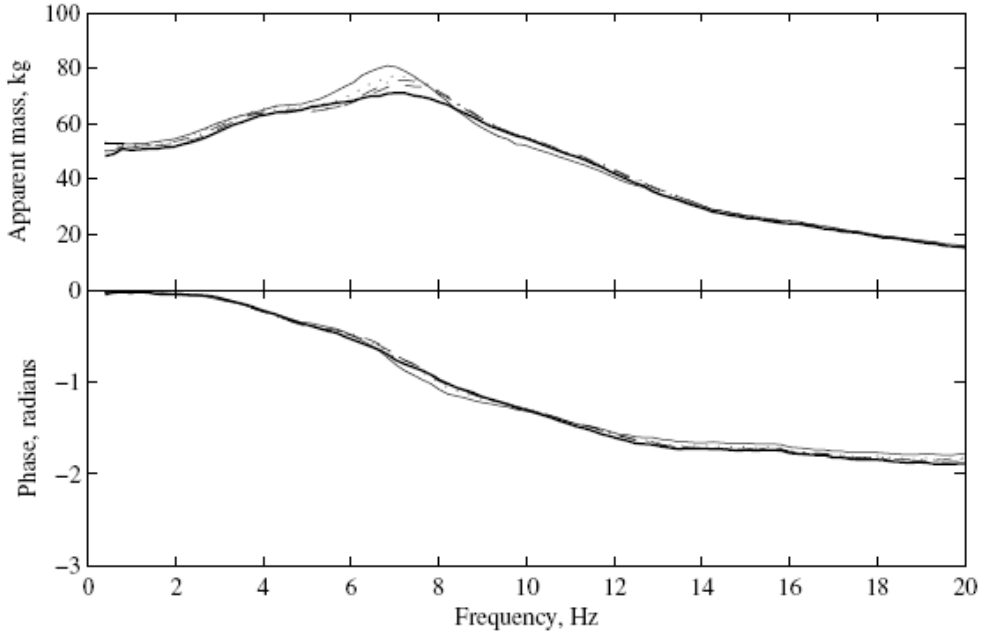

Figure 2.8 Effect of force applied to the steering wheel on apparent mass (medians of 12 subjects with the hands at S_{H3} and the feet at F_{H4}): 0 N (——), 50 N (- - -), 100 N (—.—), 150 N (— —) and 200 N (▬▬) at 1.0 ms^{-2} r.m.s. (Toward and Griffin, 2010).

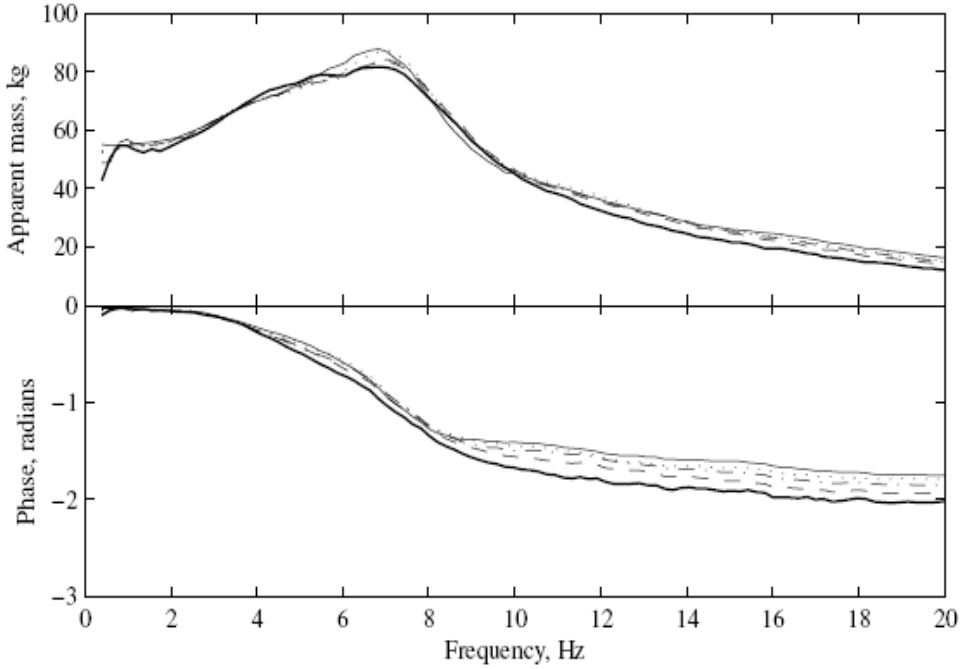

Figure 2.9 Effect of force applied to the footrest on apparent mass (medians of 12 subjects with the hands in lap and footrest at F_{H4}): 0 N (——), 50 N (:), 100 N (—.—), 150 N (— —), and 200 N (———) at 1.0 ms^{-2} r.m.s. (Toward and Griffin, 2010).

2.2.2 Effect of body support

Backrests affect biodynamic responses to whole-body vibration, possibly by changing occupant stiffness and spine geometry (Fairley and Griffin, 1990). The resonance frequency of the apparent mass increased with back supported by a backrest (Fairley and Griffin, 1989; Nawayseh and Griffin 2003, Figure 2.10; Toward, 2003; Mansfield and Maeda, 2006). This might be associated with a decrease in the body mass supported by the seat that was observed when there was a backrest support (e.g., Qiu and Griffin, 2010; Toward and Martin, 2009). The apparent mass at frequencies greater than the resonance frequency was also found to be higher with a back–supported posture (e.g., Toward and Griffin, 2009). The backrest was also found to constrain the vibration mode around 1 Hz, as the first resonance in the fore-and-aft cross-axis apparent mass observed without a backrest was eliminated when there was a backrest (Qiu and Griffin, 2010).

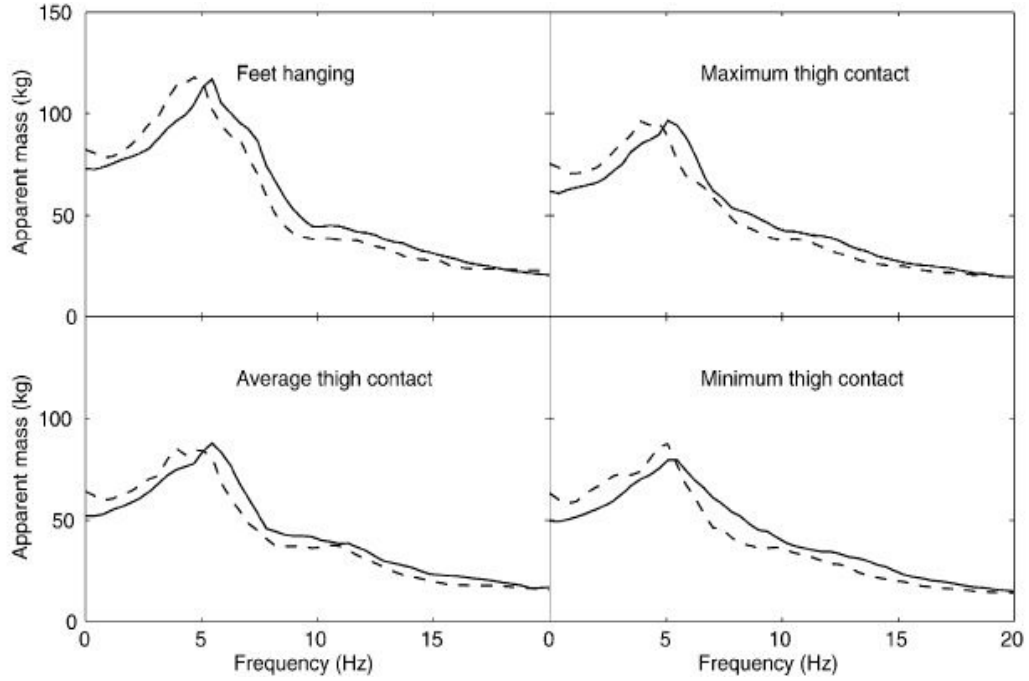

Figure 2.10 Median vertical apparent mass of 11 subjects measured on a seat at 1.25 ms^{-2} r.m.s. in four sitting postures: effect of backrest. ——, with backrest; - - -, without backrest (Nawayseh and Griffin 2003).

Apparent mass of two groups of 13 female and 14 male subjects during exposure to vertical vibration have been obtained to identify the variation in biodynamic response with a total of 36 different sitting postures (Wang *et al*., 2004). The measurements were

conducted on a rigid seat that could be adjusted in terms of height, pan angle, and backrest inclination (Figure 2.11).

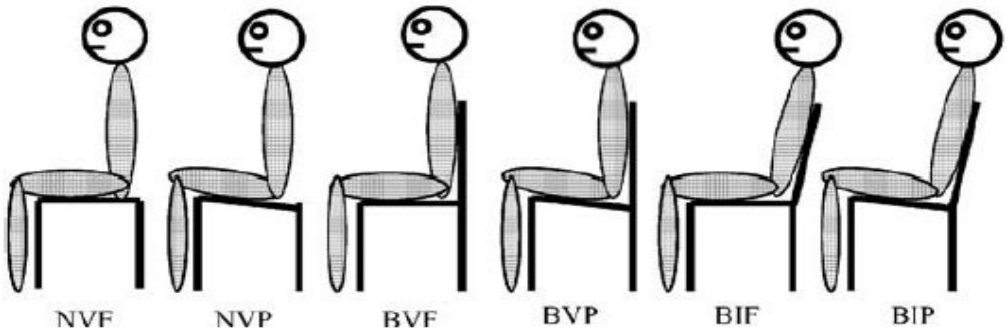

Figure 2.11 Sitting postures configurations to determine the effect of body support on apparent mass. NVF: flat seat without backrest; NVP: inclined seat without backrest; BVF: flat seat with vertical backrest; BVP: inclined seat with vertical backrest; BIF: flat seat with inclined backrest; BIP: inclined seat with inclined backrest (Wang *et al*, 2004).

The resonance region of the apparent mass for the posture without backrest was sharp while vertical and inclined backrests increased the bandwidth of the peak magnitude response (Figure 2.12).

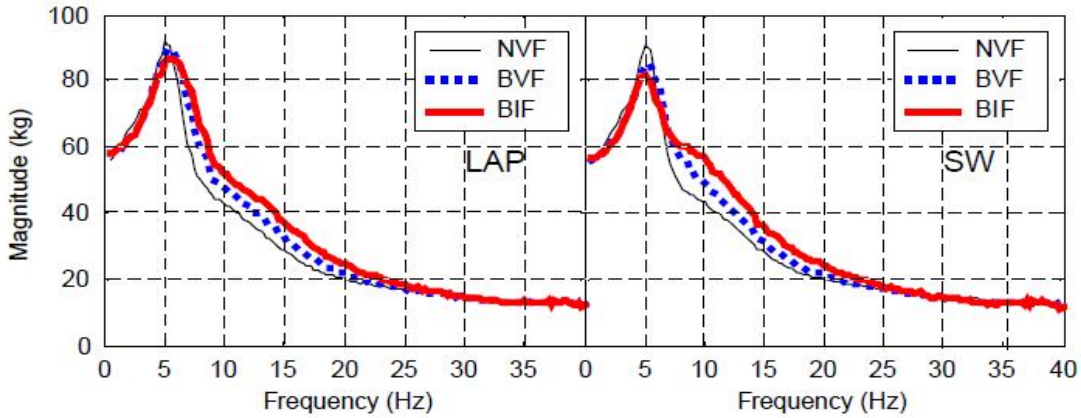

Figure 2.12 Influence of backrest on the mean apparent mass magnitude response of 27 subjects, sitting height: 460 mm, excitation: 1.0 ms^{-2} r.m.s. LAP: hands in the lap; SW: hands on the steering wheel. NVF: without backrest; BVF: vertical backrest; BIF: inclined backrest (Wang *et al*., 2004).

Backrest contact was reported to increase the median resonance frequency of the vertical apparent mass of 12 subjects from 4.8 Hz to 6.7 Hz (Toward and Griffin, 2010). However, the apparent mass at the lowest frequencies (i.e., static mass supported on the seat surface), and at the resonance frequency decreased significantly with a backrest contact.

An inclined backrest tended to introduce a further increase in the resonance frequency in the vertical apparent mass on the seat compared to that with a vertical backrest (Toward and Griffin, 2009). The mean resonance frequency in the vertical apparent mass was found to be at 7.8 Hz (Rakheja *et al.*, 2002; the seat pan was installed at an angle of 13º with respect to horizontal, while the angle between the pan and the backrest was fixed at 101º), higher than the resonance frequency (i.e., around 5 Hz) reported for studies where subjects were unsupported by a backrest or supported by an upright backrest. An increase trend for the resonance frequency in the vertical apparent mass at the seat was observed as a rigid backrest was reclined from 0 to 20° (Wei, 2000). When a backrest was reclined to 90°, the mean resonance frequency in the apparent mass in a semi-supine posture was found to be between 7.8 and 9.6 Hz (Huang and Griffin, 2008). The primary resonance frequencies in the apparent mass increased with increasing rigid backrest inclination while the resonance frequencies decreased with increasing foam backrest inclination (Figure 2.13, Toward and Griffin, 2009).

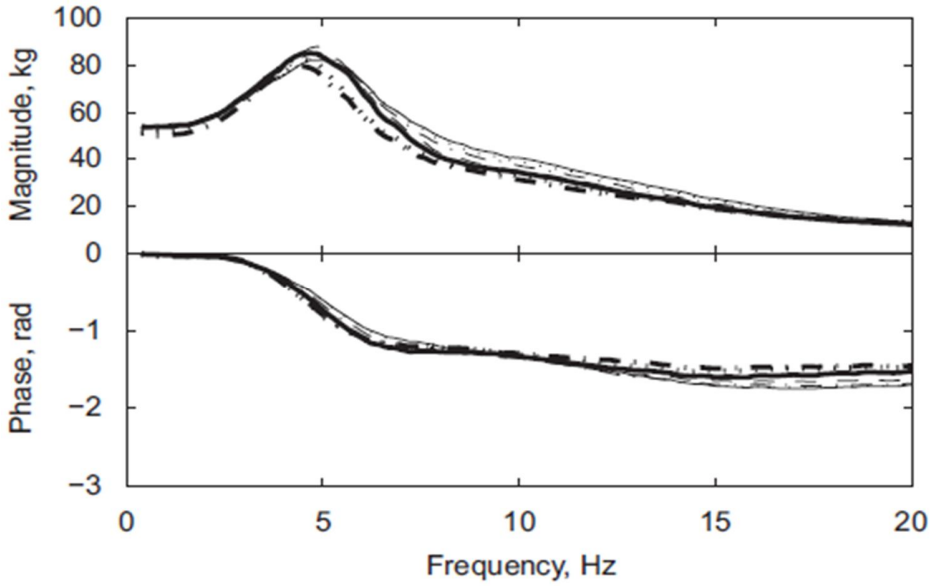

Figure 2.13 Effect of inclination of a 100 mm foam backrest on the median vertical apparent masses of 12 subjects measured on the seat: ——, 0º; . . . . , 5º; —.—, 10º; - - -, 15º; ——, 20º; . . . , 25º; —.—, 30º (Toward and Griffin, 2009).

It might be expected that the body mass supported by a seat with the hands on a steering wheel is lower than that with hands in lap posture. Lower peaks were observed for the hands on steering wheel posture than the hands in lap posture with the same backrest support (Wang *et al.*, 2004; Figure 2.14). The same decrease was observed by Toward and Griffin (2010) when hands were holding a steering wheel in which case a

second resonance occurred. The authors (Toward and Griffin, 2010) suggested the second mode was associated with the motion of the arm and shoulder. When the steering wheel was moved forward away from the subjects, the apparent mass at the primary resonance frequency was further decreased (Figure 2.15).Changing the vertical position of the steering wheel did not influence the apparent mass at any frequency (Figure 2.16).

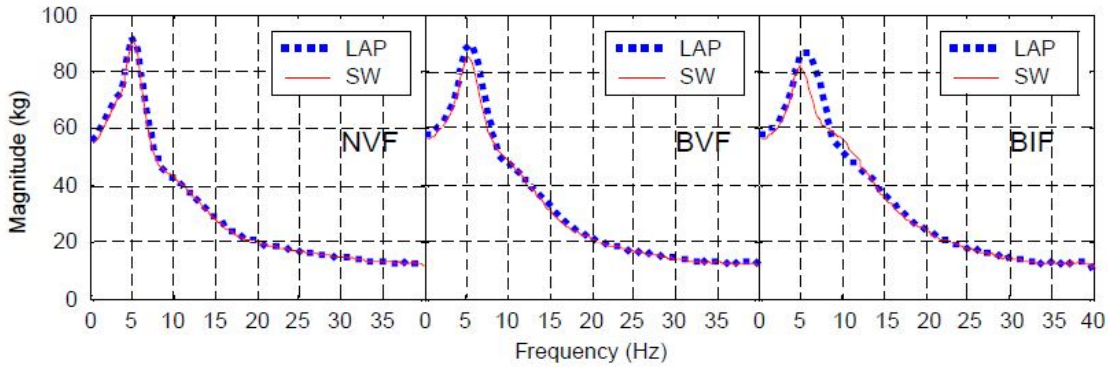

Figure 2.14 Influence of hand position on the mean apparent mass magnitude response of 27 subjects exposed to vertical excitation at 1.0 ms^{-2} r.m.s. with a sitting height of 460 mm, LAP: hands in the lap; SW: hands on the steering wheel. NVF: without backrest; BVF: vertical backrest; BIF: inclined backrest (Wang *et al.,* 2004).

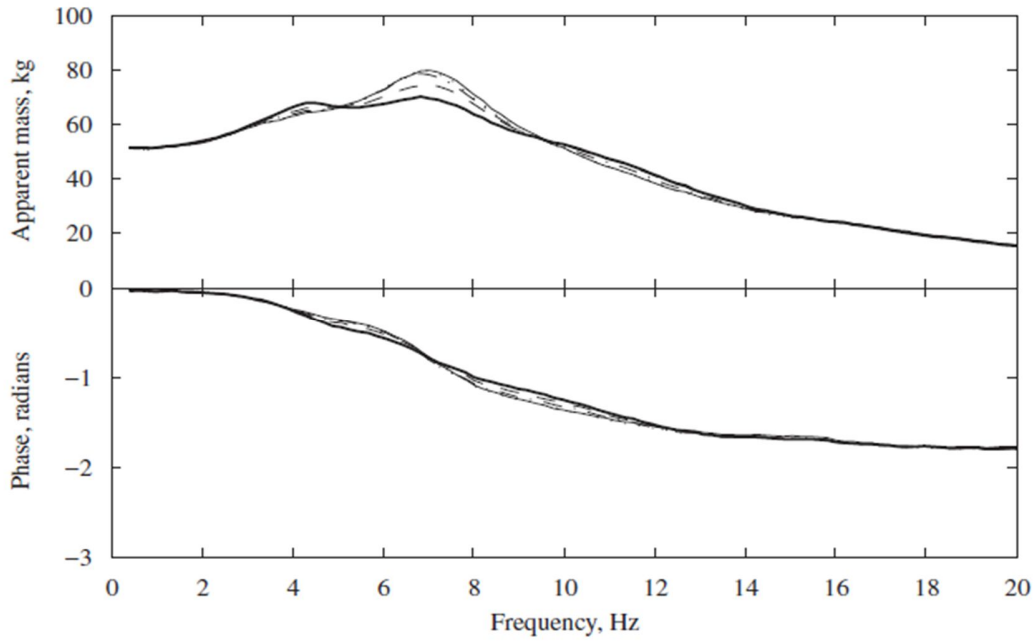

Figure 2.15 Effect of horizontal position of the steering wheel on apparent mass (medians of 12 subjects with steering wheel at vertical position S_{V3} and footrest at F_{H4}): S_{H1} (——), S_{H2} (. . .), S_{H3} (—.—), S_{H4} (- - -) and S_{H5} (——) (Toward and Griffin, 2010).

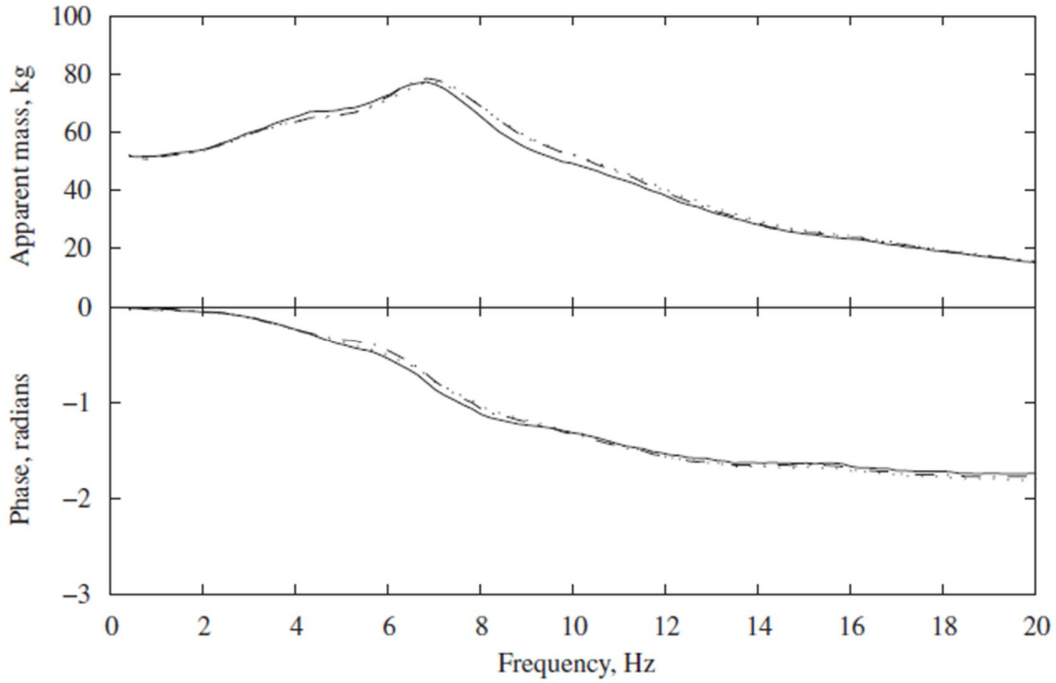

Figure 2.16 Effect of vertical position of the steering wheel on apparent mass (medians of 12 subjects with the steering wheel at horizontal position S_{H3} and footrest at F_{H4}): S_{V1} (——), S_{V3} (. . .) and S_{H5} (—.—) at 1.0 ms^{-2} r.m.s. (Toward and Griffin, 2010).

The presence of a footrest has also been reported to affect the dynamic response (e.g., Fairley and Griffin 1989; Nawayseh and Griffin 2003; Martin and Griffin, 2010). The eeffect of four different footrest heights (i.e., different thigh contacts) on apparent mass with vertical random vibration in the frequency range 0.25-20 Hz has been investigated (Nawayseh and Griffin, 2003; Figure 2.17). At each magnitude, peaks in the vertical apparent mass decreased when thigh contact was reduced, indicating that reducing thigh contact reduced the mass supported on the seat but increased the mass supported on the footrest (Figure 2.18). No significant difference in resonance frequency due to the different mass distribution with different thigh contact conditions was found. The dynamic response at the seat showed one resonance at 5 Hz with maximum thigh contact posture, while the average thigh contact showed two resonances, at 5 and 11 Hz respectively. The minimum thigh contact showed a third resonance at around 7.5 Hz. The authors suggested that: (i) the resonance frequency of apparent mass on the seat was mainly dependent on the motion of upper-body; (ii) changing thigh contact not only varied the mass distribution but also changed the thigh stiffness which might have

maintained the same proportional contribution of the mass and the stiffness to the resonance frequency in the four postures.

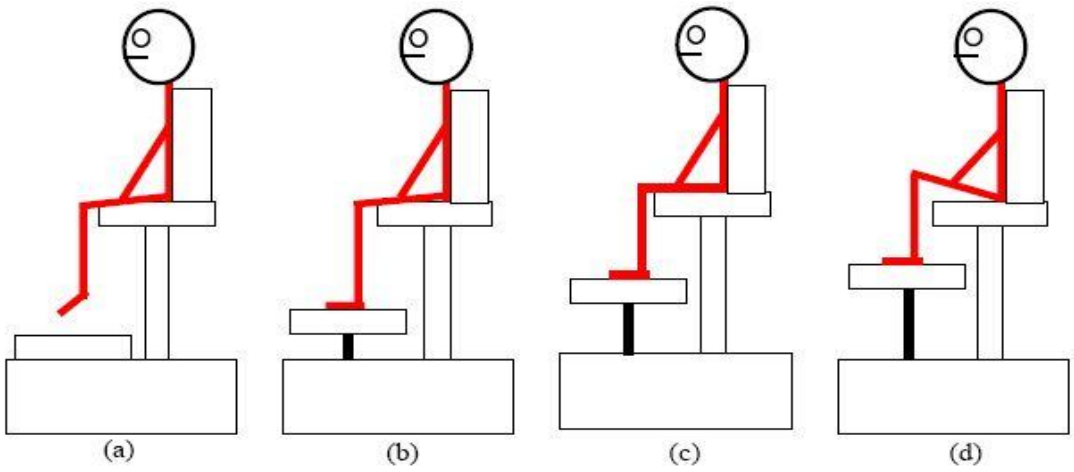

Figure 2.17 Schematic diagrams of the four sitting postures: (a) feet hanging; (b) maximum thigh contact; (c) average thigh contact and (d) minimum thigh contact (Nawayseh and Griffin 2003).

Increasing the horizontal distance between the footrest and the seat was reported to increase the apparent mass at the primary resonance frequency and at 0.4 Hz (Toward and Griffin, 2010) but had little effect on the resonance frequency. However, the effect of a footrest is quite different for a stationary footrest condition and a moving footrest. When a footrest was stationary, the apparent mass of a subject at 1 Hz was about 20% less than the static weight on the seat. When the footrest was moving in phase with the platform, the apparent mass at the lowest frequency was more or less the same as the static weight, as expected (Fairley and Griffin, 1989).

The sitting height (distance from the seat pan to the floor) or the height of the lower leg has also been reported to have a significant influence on the peak magnitudes of the apparent mass (e.g., Fairley and Griffin, 1989; Wang *et al.*, 2004). Higher seat height was reported to result in greater body mass supported on the seat and yield higher peak magnitudes of apparent mass: a 10% difference in body mass was expected to arise when there was 100 mm difference in seat height (Wang *et al.*, 2004).

Whatever the body support is (e.g., back support, thigh contact or foot contact), variability in the apparent mass, especially the resonance in the apparent mass seems to be associated with a change in the mass supported by the seat. Therefore, Changing

the mass supported on the seat by adding body support and changing stiffness by changing sitting posture prove effective ways to change apparent mass on the seat, especially the resonance frequency. This is consistent with the fundamental theory that the natural frequency of the system could be represented with the square root of the ratio of stiffness and mass of the system.

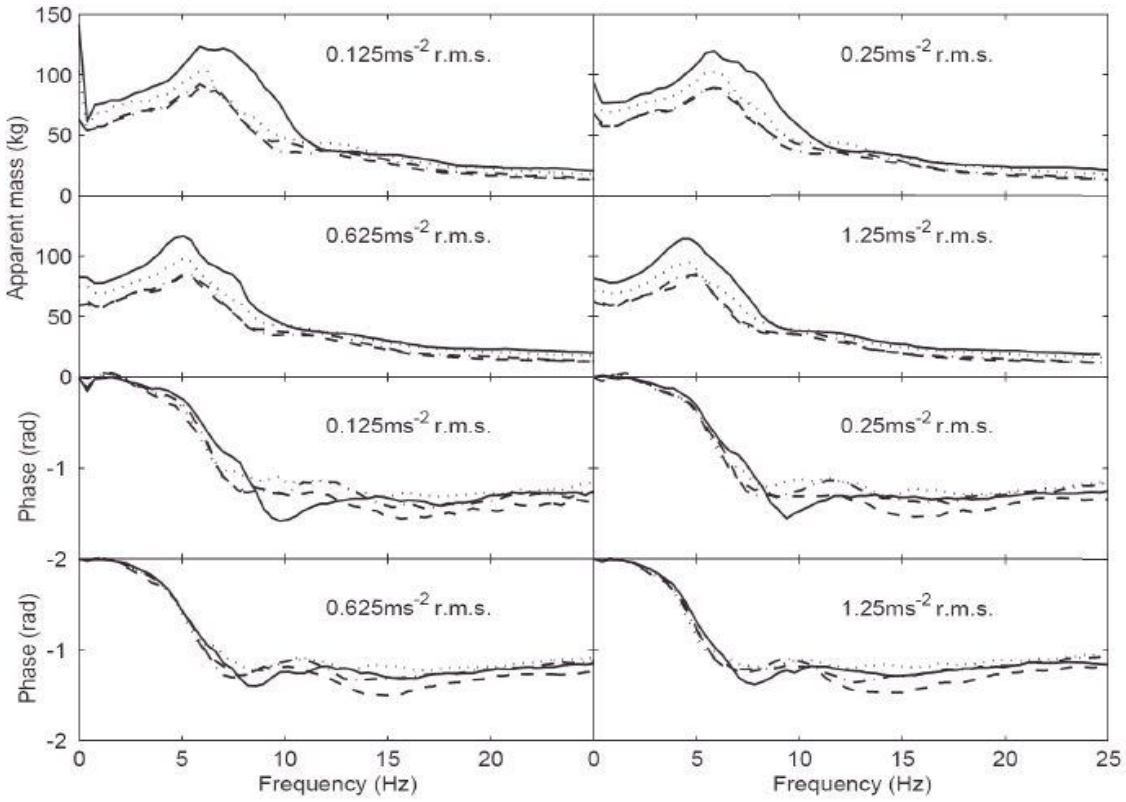

Figure 2.18 Median vertical apparent mass and phase angle of 12 subjects exposed to vertical random vibration (0.25-20 Hz) at 0.125 ms^{-2} r.m.s., 0.25 ms^{-2} r.m.s., 0.625 ms^{-2} r.m.s., and 1.25 ms^{-2} r.m.s. in four different thigh contact conditions. ——, feet hanging; …., maximum thigh contact; —.—, average thigh contact; — —, minimum thigh contact (Nawayseh and Griffin, 2003).

2.3 Apparent mass of the seated human body with horizontal vibration

The biodynamic responses of the seated human body with horizontal vibration show a resonance at lower frequency, compared to the biodynamic response with vertical excitation (e.g., Fairley and Griffin, 1990; Mansfield and Lundström, 1999a; Hinz *et al.*, 2006a; Qiu and Griffin, 2010).

The apparent mass in the fore-and-aft and lateral directions with eight subjects and broadband vibration (0.25-20 Hz) in both horizontal directions with and without a backrest have been investigated (Fairley and Griffin, 1990). When there was no backrest,

the first resonance at 0.7 Hz and a second less evident resonance were found for the response in both the fore-and-aft and the lateral directions (Figure 2.19). It was suggested that peak moduli in the fore-and-aft apparent mass arise from rotation of the whole upper-body. When the pitching motion of the upper-body was reduced, the peak modulus of the apparent mass was reduced. Only one mode was observed for backrest contact condition, with the resonance frequency in the region of 3 Hz for fore-and-aft apparent mass and 1.5 Hz for lateral apparent mass.

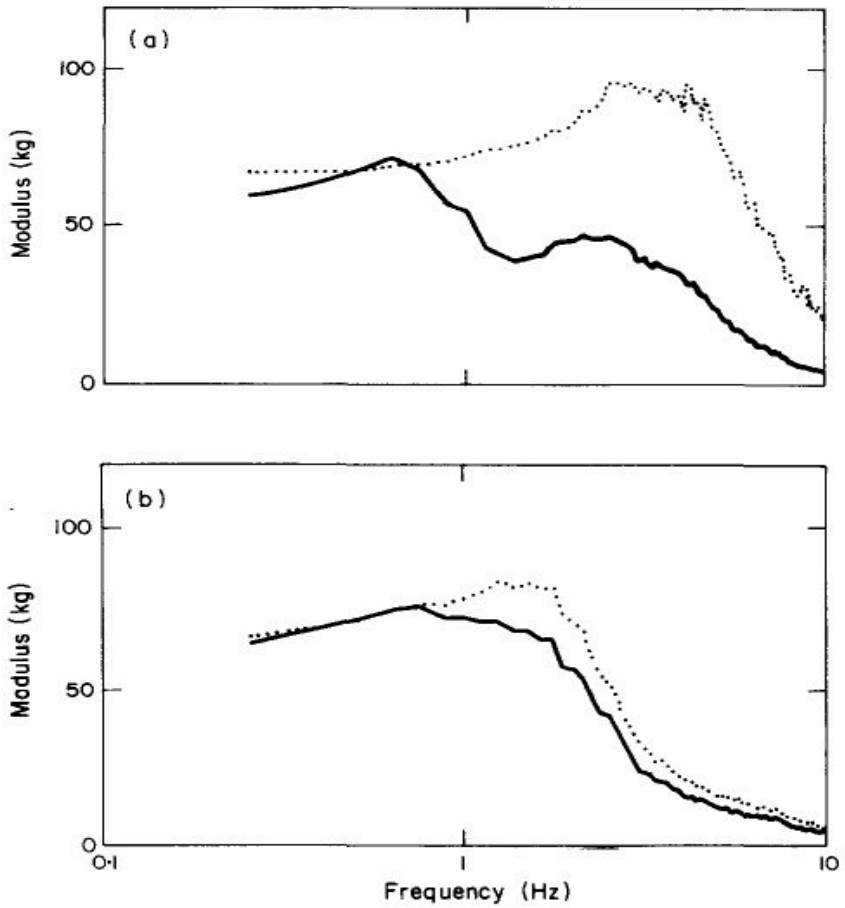

Figure 2.19 Mean apparent mass of eight subjects exposed to horizontal vibrations at 1.0 ms^{-2} r.m.s. (a) Fore-and-aft ; (b) lateral: - - -, with backrest; ——, without backrest (Fairley and Griffin 1990).

The horizontal apparent masses of 13 subjects exposed to various combinations of vibrations were determined (Hinz *et al.*, 2006a). There was single-axis excitation in each of the three translational directions, combined fore-aft and lateral excitation, and combined vertical, fore-aft and lateral excitation. The magnitude of vibration in each axis was 0.25 ms^{-2} r.m.s., 1.0 ms^{-2} r.m.s., and 2.0 ms^{-2} r.m.s. A primary peak in the fore-and-

aft apparent mass was found in the region of 2.18 and 2.94 Hz, but was not observed with all subjects or at all vibration magnitudes. Peaks in the apparent mass increased with increasing body mass and decreased with increasing chest circumference in the subjects. Two modes of lateral apparent mass were registered: one below 1 Hz and another between 1.61 and 2.19 Hz. With vibration in the lateral direction (i.e. *y*-axis), the upper-body was observed to sway from side to side and the buttocks moved out of phase with the upper-body and shoulders.

The dynamic responses of 12 male subjects exposed to fore-and-aft random vibration (0.25–20 Hz, at 0.125 ms^{-2} r.m.s., 0.25 ms^{-2} r.m.s., 0.625 ms^{-2} r.m.s., and 1.25 ms^{-2} r.m.s.) on the seat and footrest was investigated with and without backrest (Nawayseh and Griffin, 2005). Subjects sat on a rigid seat with and without backrest with different thigh contact conditions (Figure 2.17). Three vibration modes in the fore-and-aft apparent mass on the seat at frequencies below 10 Hz in all postures (around 1 Hz, between 1 and 3 Hz, and between 3 and 5 Hz) were found (Figure 2.20). At the feet, the fore-and-aft forces showed a resonance between 3 and 5 Hz, which increased in frequency and magnitude when a backrest was used.

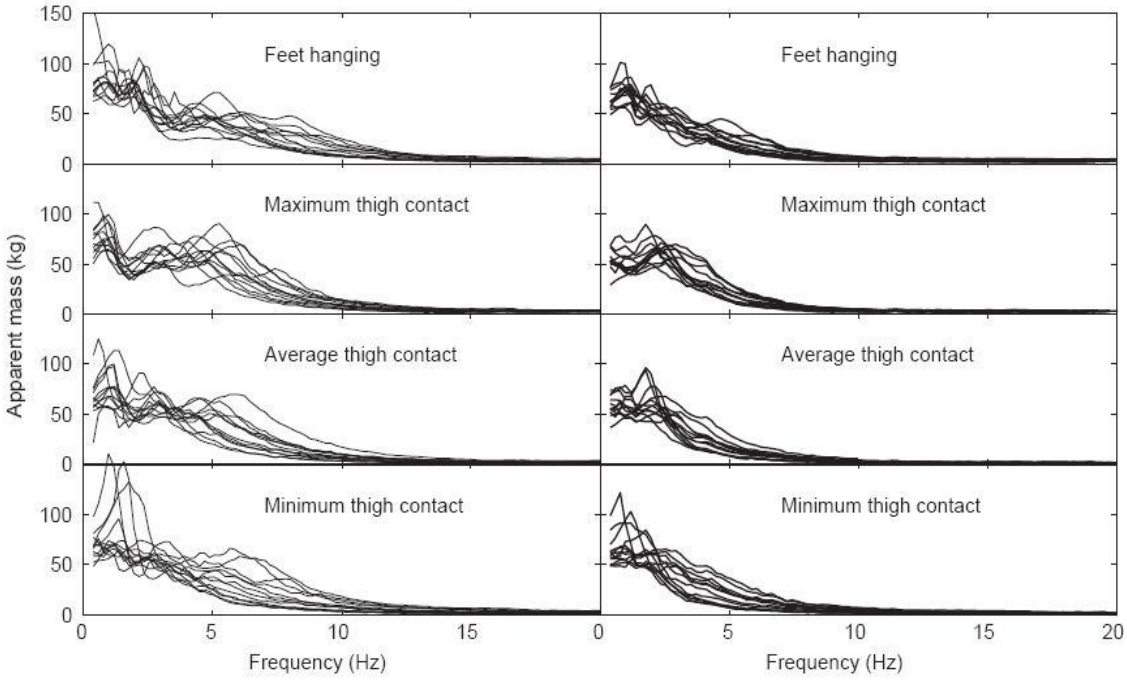

Figure 2.20 Fore-and-aft apparent mass on the seat of 12 male subjects exposed to fore-and-aft random vibration (0.25–20 Hz) at two vibration magnitudes. ——, 0.125 ms^{-2} r.m.s., ——, 1.25 ms^{-2} r.m.s. (Nawayseh and Griffin, 2005).

Little effect of thigh contact on the fore-and-aft inline apparent mass at frequencies less than 3 Hz or greater than 10 Hz was observed (Nawayseh and Griffin, 2005). However, the peak modulus of the fore-and-aft inline apparent mass at the back increased when thigh contact was increased. The feet hanging posture and the minimum thigh contact induced maximum forces at the seat in the fore-and-aft direction.

Considerable vertical forces were found on the seat and the footrest when there was fore-aft excitation (Nawayseh and Griffin, 2005). The effect of thigh contact on the vertical cross-axis apparent mass on the seat was not consistent across the frequency range (Figure 2.21). A significant difference was found in the vertical cross-axis apparent masses measured with and without a backrest at 0.78, 2.15, 6.05, 8.0, and 12 Hz. Greater vertical forces on the feet below 4 Hz was observed with subjects without a backrest.

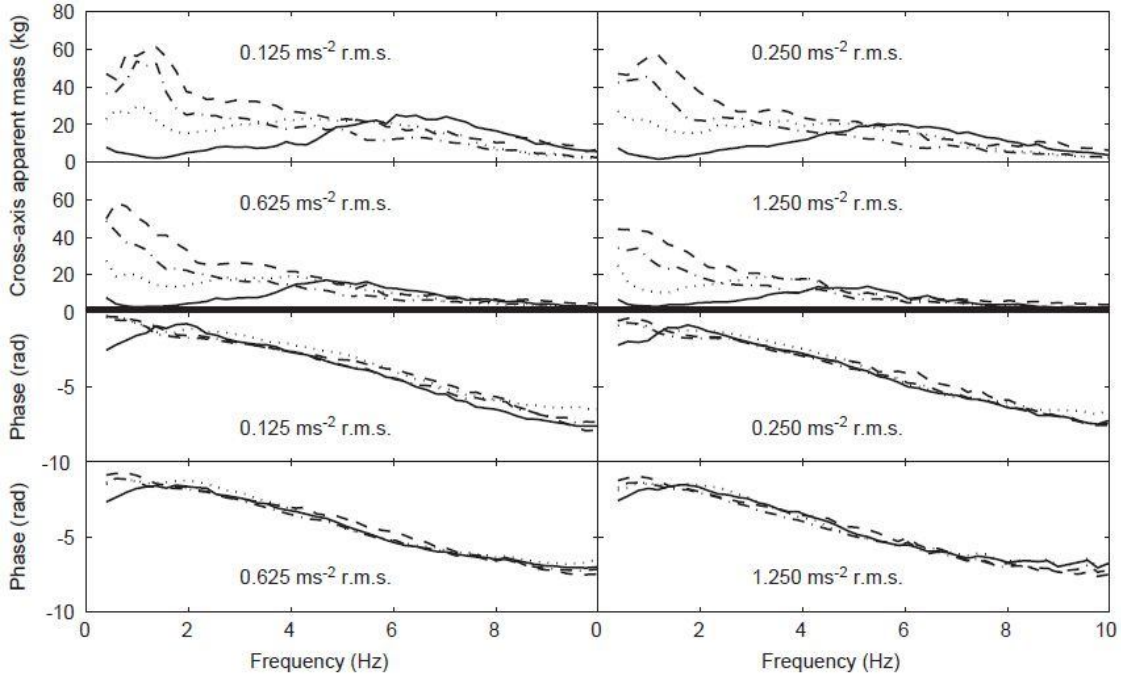

Figure 2.21 Median vertical cross-axis apparent mass and phase angle at the seat of 12 subjects exposed to fore-and-aft whole-body vibration: effect of posture (i.e., thigh contact). ——, feet hanging; - - -, maximum thigh contact; —.—, average thigh contact; — —, minimum thigh contact (Nawayseh and Griffin, 2005).

2.4 Non-linearity in human response to vibration

A shift in the resonance frequency of the apparent mass on the seat, forces on the back and the feet when vibration characteristics are changed has been reported extensively (e.g., Fairley and Griffin, 1989; Smith, 1994; Lundström and Holmlund, 1998; Mansfield

and Lundström, 1999a; Mansfield and Griffin, 2000; Matsumoto and Griffin 2002a; Matsumoto and Griffin, 2002b; Mansfield *et al.*, 2005a; Mansfield *et al.*, 2005b; Qiu and Griffin, 2010). Although the mechanism causing the non-linearity has not been unequivocally determined, it is observed to be closely related to factors such as the vibration magnitude and the vibration spectrum, and might be caused by thixotropy of soft human tissue.

2.4.1 Effects of vibration magnitude

Many studies have been carried out to investigate the effect of vibration magnitudes on the apparent mass. The resonance of the apparent mass was constantly found to shift to a lower frequency with an increase in the vibration magnitude (e.g., Figure 2.22).

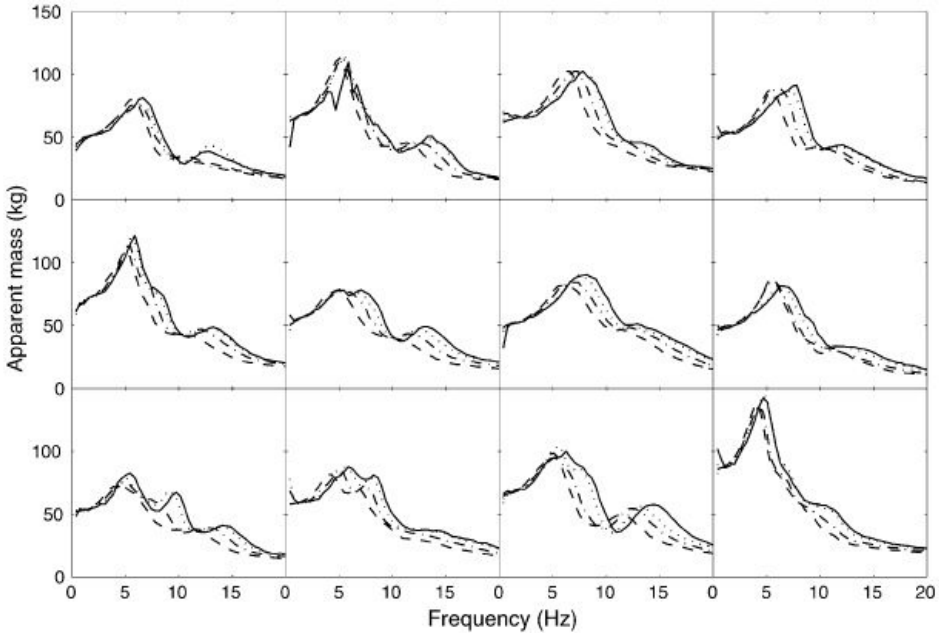

Figure 2.22 The individual vertical apparent masses of 12 subjects measured in the average thigh contact posture at four vibration magnitudes. ——, 0.125 ms^{-2} r.m.s.; - - -, 0.25 ms^{-2} r.m.s.; —.—, 0.625 ms^{-2} r.m.s.; — —, 1.25 ms^{-2} r.m.s. (Nawayseh and Griffin, 2004).

The effect of vibration magnitude is expected to be influenced by muscle tension. With increases in the magnitude of random vibration from 0.35 to 1.4 ms^{-2} r.m.s., the apparent mass resonance frequency decreased from 5.25 to 4.25 Hz with a normal muscle tension, from 5.0 to 4.38 Hz with the buttocks muscles tensed, and from 5.13 to 4.5 Hz with the abdominal muscles tensed (Matsumoto and Griffin, 2002; Figure 2.23). The non-linear response of the human body shown by a reducing resonance frequency with increasing vibration magnitudes was reported to be reduced with minimum thigh contact

– a posture that increased pressure on the tissue under the buttocks (Nawayseh and Griffin, 2003). The fore-and-aft cross-axis apparent mass on the seat and forces on the back have also been found to be nonlinear with changing vibration magnitudes (e.g., Figure 2.24).

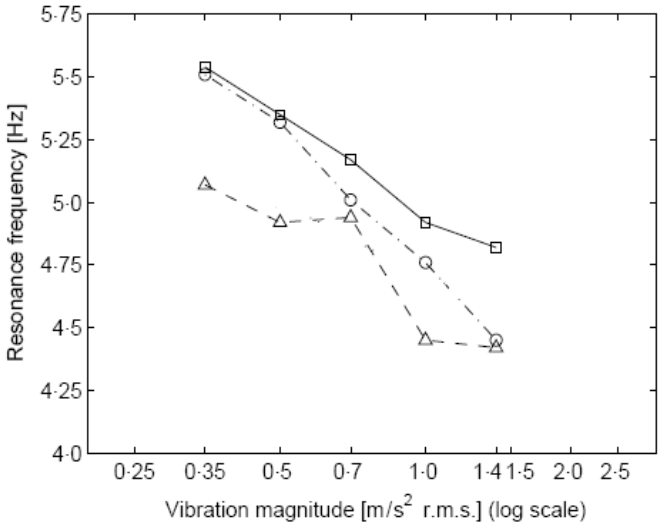

Figure 2.23 Mean resonance frequencies of the apparent mass of eight subjects exposed to random vibration from 0.35 to 1.4 ms^{-2} r.m.s., in three conditions. —.O. —, condition 1: comfortable, upright posture with normal muscle tension. —Δ—, condition 2: with the muscles of the buttocks tensed; —□—, condition 3: with the volume of the abdomen minimized (Matsumoto and Griffin, 2002).

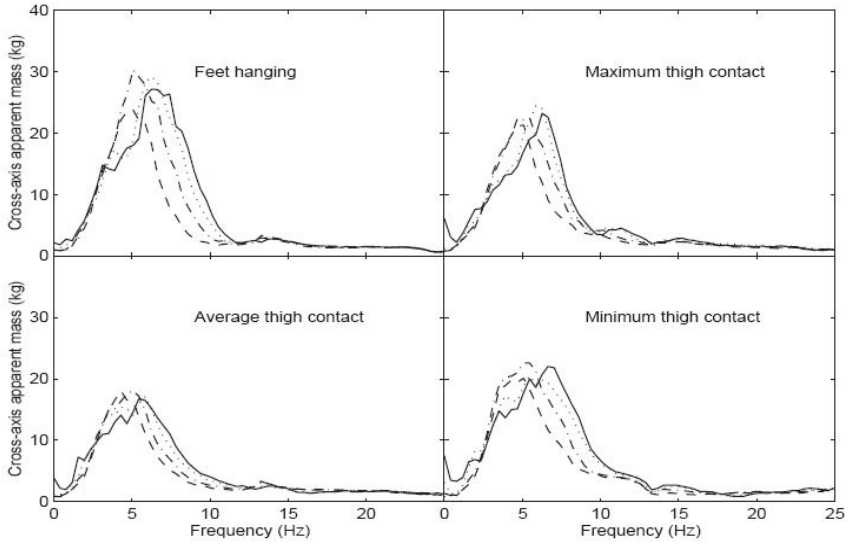

Figure 2.24 Median fore-and-aft cross-axis apparent masses of 12 subjects exposed to broadband (0.25 to 25 Hz) random vertical whole-body vibration: effect of vibration magnitude: ——, 0.125 ms^{-2} r.m.s.; — —, 0.25 ms^{-2} r.m.s.; —.—, 0.625 ms^{-2} r.m.s.; - - -, 1.25 ms^{-2} r.m.s. (Nawayseh and Griffin, 2003).

2.4.2 Effect of vibration spectrum

Many studies have reported driving point impedance or transmissibility with random vibration while some dynamic responses have been measured with sinusoidal vibration (e.g., Mansfield and Maeda, 2005b). Random vibration contains all frequencies with energy distributed equally. Sinusoidal vibration is composed of a single frequency and measurements have to be made many times if the dynamic response at more than one frequency is of interest.

Apart from change in vibration magnitudes, difference in vibration spectra has also been observed to induce nonlinearity in biodynamic response (e.g., Toward, 2003; Mansfield *et al*., 2006). The effect of vibration spectra and waveform on the primary resonance frequency in the vertical apparent masses of 12 seated subjects exposed to three groups of stimuli have been investigated (Mansfield *et al*., 2006): Group A comprised three repeats of random vertical vibration at 0.5, 1.0, and 1.5 ms^{-2} r.m.s. with subjects sitting in a relaxed upright posture. Group B used the same vibration stimuli as Group A, but with subjects sitting in a "tense" posture. Group C used vibration where the vibration spectrum was dominated by either low-frequency vibration (the stimulus comprised the 0.5 ms^{-2} random signal low-pass filtered at 7.0 Hz added to the 1.5 ms^{-2} random signal high-pass filtered at 7.0 Hz), high-frequency vibration (the stimulus comprised of the 1.5 ms^{-2} r.m.s. random signal low-pass filtered at 7.0 Hz added to the 0.5 ms^{-2} random signal high-pass filtered at 7.0 Hz), or 1.0 ms^{-2} r.m.s. sinusoid at the frequency of the second peak in apparent mass (about 10–14 Hz) added to 0.5 ms^{-2} r.m.s. random vibration. The resonance frequency was lower with "low frequency" vibration than with "higher frequency" and "sine" vibration (Figure 2.25). The peaks of apparent mass were lower for "low frequency" stimulus than the "high frequency" and "sine" stimulus.

The apparent mass of 12 seated subjects exposed to random broadband vibration from 0.125 to 25 Hz (at 0.25 ms^{-2} r.m.s.) on which nine ½-octave narrow-band inputs were superimposed at four magnitudes (0.25, 0.4, 0.63, and 1.0 ms^{-2} r.m.s.) were determined (Toward, 2002). Vibration below 4 Hz had the greatest effect on the apparent mass at the resonance frequency and the peak modulus of apparent mass decreased with increasing magnitudes. This trend was generally reversed above 4 Hz (Figure 2.26). Vibration at frequencies less than 8 Hz had the greatest effect on the nonlinearity while the nonlinear response tended to be less evident at higher frequencies (Figure 2.27).

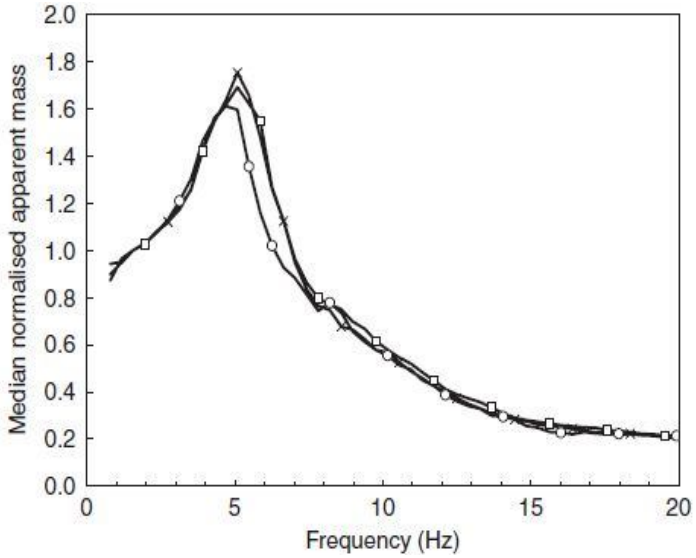

Figure 2.25 Median normalized apparent masses of 12 subjects exposed to random vibration: effect of vibration spectrum in a relaxed upright posture. —□—: 'high frequency', —o—: 'low frequency', —×—: 'sine' (Mansfield *et al*., 2006).

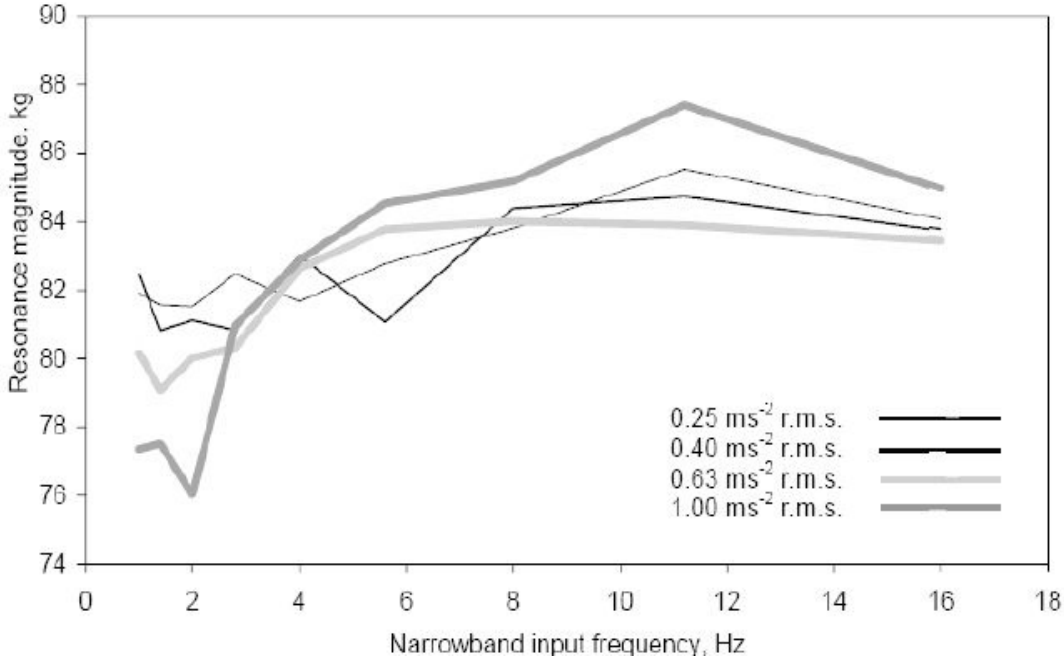

Figure 2.26 Median apparent mass at resonance measured with narrowband inputs at nine $^1/_2$-octave input frequencies (centred at: 1.0, 1.4, 2.0, 2.8, 4.0, 5.6, 8.0, 11.2, 16.0 Hz) and four input magnitudes superimposed on 0.25 ms^{-2} r.m.s. broadband 0.125–25 Hz vibration (Toward, 2002).

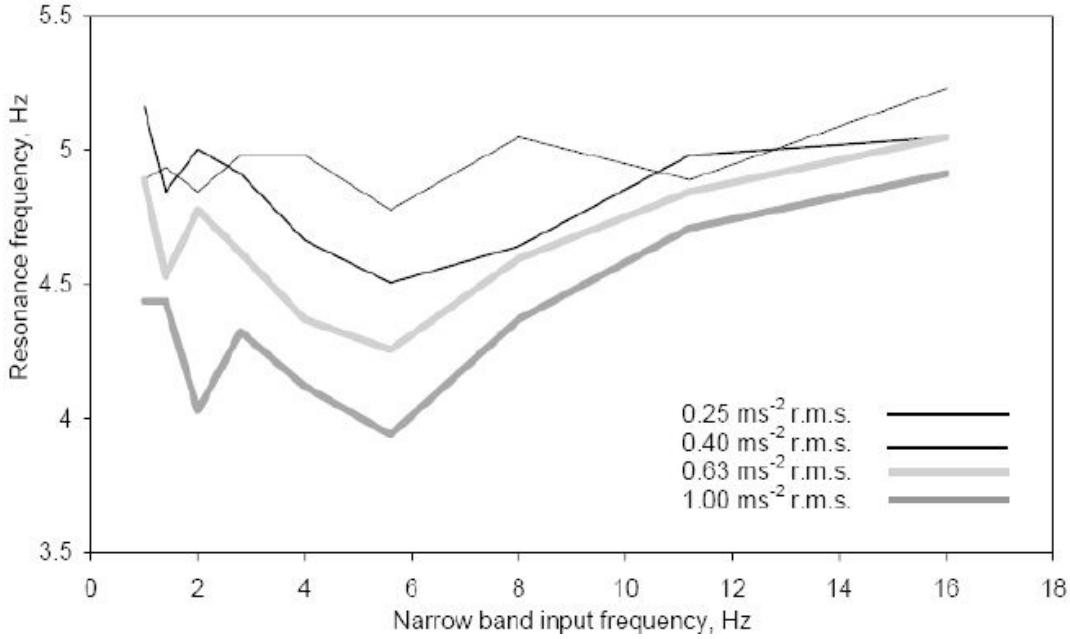

Figure 2.27 Median apparent mass resonance frequency measured with narrow-band inputs at nine ½-octave input frequencies (centred at: 1.0, 1.4, 2.0, 2.8, 4.0, 5.6, 8.0, 11.2, 16.0 Hz) and four input magnitudes superimposed on 0.25 ms^{-2} r.m.s. broadband 0.125–25 Hz vibration (Toward, 2002).

2.4.3 Thixotropy: tonic and phasic tissue activity

Thixotropy refers to the recovery behavior of colloidal materials after the breakdown of structural linkages (Tanner, 1985). It was also suggested to be a passive property of human tissues (i.e., the stiffness of tissues increases with prior stillness or low magnitude stimuli but decreases with prior perturbation). The passive tissue performance has been observed with the human wrist (Lakie *et al*., 1979), finger flexor (Hagbarth *et al*., 1985; Lakie, 1986), finger extensor (Lakie, 1986) and the rib cage respiratory muscles (Homma and Hagbarth, 2000).

The nonlinearity in the apparent mass associated with the change in vibration magnitudes has also been observed to be largely dependent on the passive thixotropic behaviour apart from the voluntary muscle tension mentioned in Section 2.2.1. It was found that the reduction in the resonance frequency of vertical apparent mass of seated subjects with vibration magnitudes increasing from 0.25 ms^{-2} r.m.s. to 2.0 ms^{-2} r.m.s. was 0.1 Hz with voluntary periodic upper-body movement whereas the reduction was 1.1 Hz when there was no voluntary movements (Huang and Griffin, 2006).

With 12 semi-supine subjects exposed to vertical continuous random vibration and intermittent vibration (alternately 1.0 and 0.25 ms^{-2} r.m.s.; Huang and Griffin, 2008,

Figure 2.28), the resonance frequency at the low magnitude (0.25 ms^{-2} r.m.s.) was observed to be lower with intermittent vibration than with the continuous vibration, whereas the resonance frequency at a high magnitude (1.0 ms^{-2} r.m.s.) was higher with intermittent vibration than with continuous vibration (Huang and Griffin, 2008). The authors attributed the lower resonance frequency at lower vibration magnitude with intermittent vibration to be the effect of prior high magnitude "perturbation". Similarly, the higher resonance frequency at high vibration magnitude with intermittent vibration was attributed to be the effect of prior low magnitude "perturbation". The effect of intermittent vibration on the horizontal cross-axis apparent mass was not significant, possibly due to the low magnitude of the response in the cross-axis direction. It was also observed that the absolute difference between the resonance frequencies of vertical apparent mass (*x*-axis) at 0.25 and 1.0 ms^{-2} r.m.s. was significantly less with intermittent random vibration than with the continuous random vibration. However, absolute differences between the peak frequencies of horizontal (z-axis) cross-axis apparent mass at 0.25 and 1.0 ms^{-2} r.m.s. were not significantly different between the intermittent random vibration and the continuous random vibration.

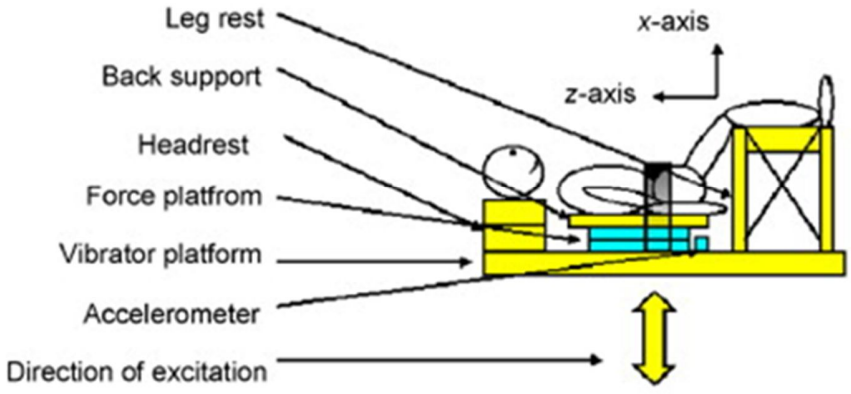

Figure 2.28 Schematic diagram of experimental set-up for semi-supine subjects (Huang and Griffin, 2008).

The resonance frequencies of horizontal (*z*-axis) apparent masses of 12 subjects with intermittent longitudinal random vibration at 0.25 ms^{-2} r.m.s. were found to be significantly lower than those with continuous random vibration at the same magnitude (Huang and Griffin, 2008). The absolute difference between the resonance frequencies

at 0.25 and 1.0 ms^{-2} r.m.s. was less with intermittent random vibration than with the continuous random vibration for all 12 subjects.

The peak frequency of vertical cross-axis apparent mass with intermittent random vibration was also significantly lower than the peak frequency with continuous random vibration at 0.25 ms^{-2} r.m.s. (Huang and Griffin, 2008). The absolute differences between the peak frequencies with 0.25 and 1.0 ms^{-2} r.m.s. were significantly less with the intermittent random vibration than with the continuous random vibration. The authors concluded that the passive thixotropic properties of the body could be the principal cause of the nonlinearity seen in measures of the apparent mass and transmissibility of the human body.

2.5 Apparent mass of seated human body with multi-axis vibration

When subjects were exposed to dual-axis and multi-axis excitation, the apparent mass distribution over frequency seemed to be quite similar to the case of single-axis input (Hinz *et al*., 2006a; Mansfield and Maeda 2006; Qiu and Griffin, 2010).

2.5.1 Apparent mass with dual-axis excitation

With vibration in both vertical and fore-and-aft directions, resonance of vertical apparent mass and fore-and-aft cross-axis apparent mass shifted to lower frequency compared to those with single-axis vertical excitation (Qiu and Griffin, 2010; Figure 2.29 and Figure 2.30). Apart from the decrease in the peak frequency, the coherency between the vertical acceleration and the vertical force was lowered by the addition of fore-and-aft excitation but raised by increasing the magnitude of the vertical excitation (Figure 2.31). The coherence between fore-and-aft forces and vertical acceleration was reduced compared to that with single-axis vertical vibration (Figure 2.30). With increasing vibration magnitudes in the fore-and-aft direction, the coherence was found to be further decreased (Figure 2.30).

A similar trend was observed for vertical cross-axis apparent mass (Figure 2.31). Peaks in the vertical cross-axis apparent mass with dual-axis vibration were less clear than that with single axis vibration (Figure 2.31).

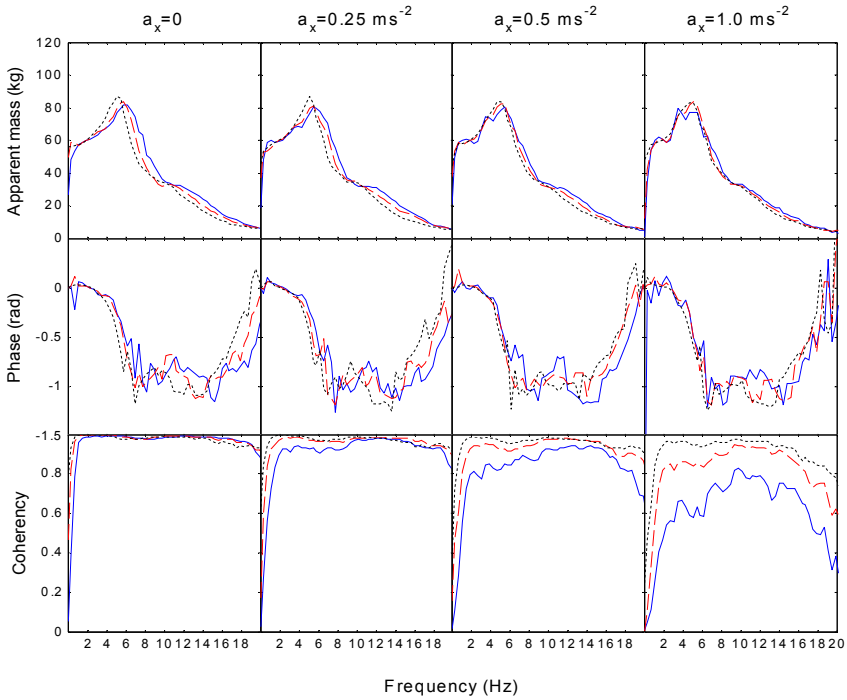

Figure 2.29 Median vertical apparent mass of 12 subjects with single-axis and dual-axis excitation. ——, a_z = 0.25 ms^{-2} r.m.s.; — —, a_z = 0.5 ms^{-2} r.m.s.; - - -, a_z = 1.0 ms^{-2} r.m.s. (Qiu and Griffin, 2010).

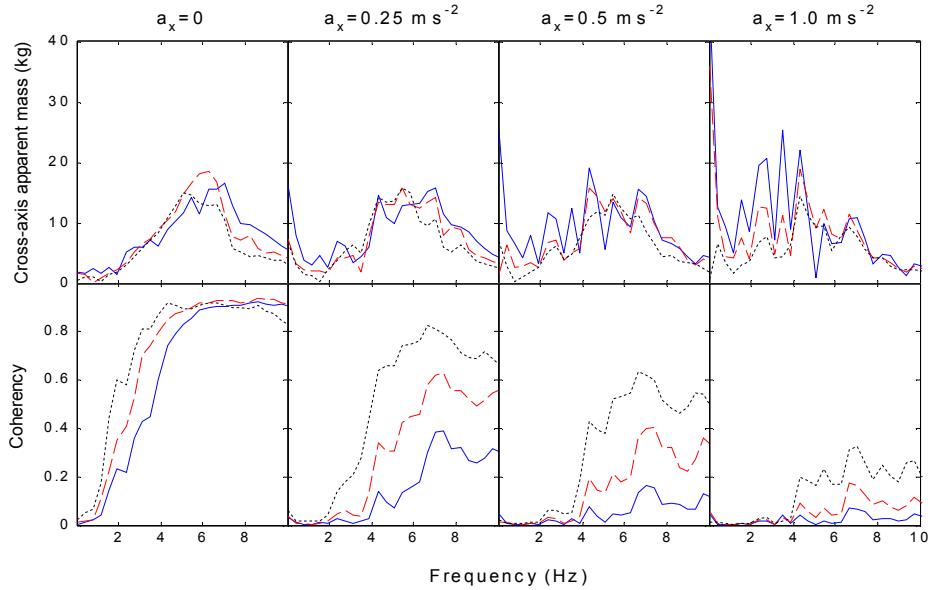

Figure 2.30 Median fore-and-aft cross-axis apparent mass of 12 subjects with single-axis and dual-axis excitation. ——, a_z = 0.25 ms^{-2} r.m.s.; — —, a_z = 0.5 ms^{-2} r.m.s.; - - -, a_z = 1.0 ms^{-2} r.m.s. (Qiu and Griffin, 2010).

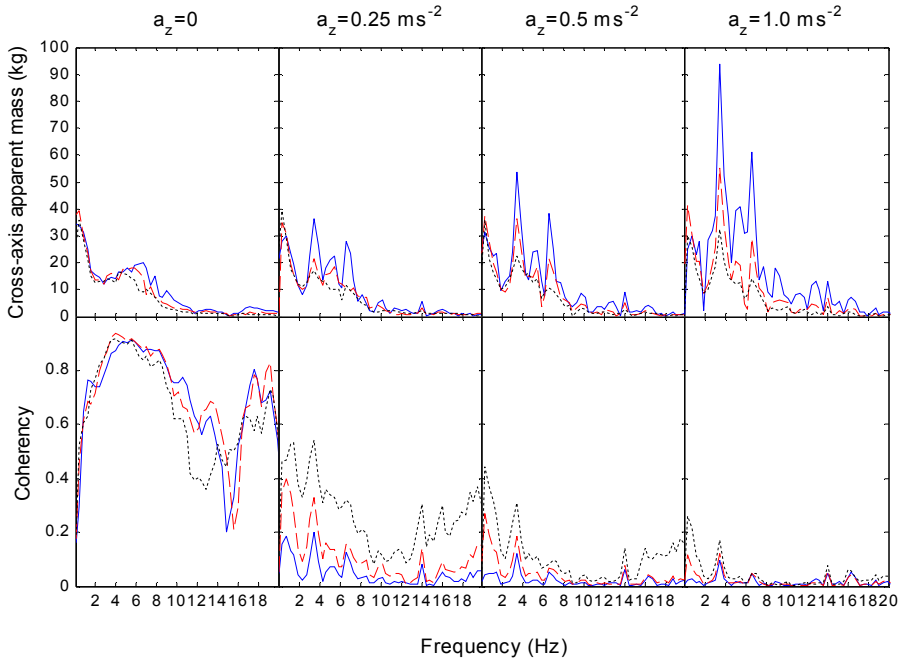

Figure 2.31 Median vertical cross-axis apparent mass 12 subjects expose to during single-axis and dual-axis random (0.2-20 Hz) excitation without a backrest. ——, a_x = 0.25 ms^{-2} r.m.s.; — —, a_x = 0.5 ms^{-2} r.m.s.; - - -, a_x = 1.0 ms^{-2} r.m.s. (Qiu and Griffin, 2010).

2.5.2 Apparent mass with tri-axial excitation

With tri-axial fore-and-aft, lateral and vertical excitation, the maximum moduli and resonance frequency in the vertical apparent mass were reduced compared to those with single-axis excitation (Hinz *et al*., 2006a; Figure 2.32(a)). The resonance frequency was also reduced with increasing the magnitude of vertical excitation while the magnitude of fore-and-aft and lateral excitation kept constant.

Similar nonlinearity was observed with the fore-and-aft apparent mass (Figure 2.32(b), Hinz *et al*., 2006a): the resonance frequencies (between 2 to 4 Hz) were reduced when the input was changed from single-axis to three-axis vibration. However, when the number of input axes was increased from two to three (i.e., from combined fore-and-aft and lateral excitation to combined fore-and-aft, lateral and vertical excitation), the maximum moduli of the fore-and-aft apparent increased during low magnitude exposure (magnitude here was represented with the vector sum of magnitude of vibration in three axes) but remained constant during high magnitude exposure.

The maximum moduli of the lateral apparent mass were significantly lower when the numbers of axes were increased from one to two and from two to three (Figure 2.32(c);

Hinz *et al.*, 2006a). The peak frequencies shifted towards higher frequencies when a second axis was added. When the third axis was supplemented, the peak frequency increased with low magnitude lateral excitation and decreased with high magnitude lateral excitation.

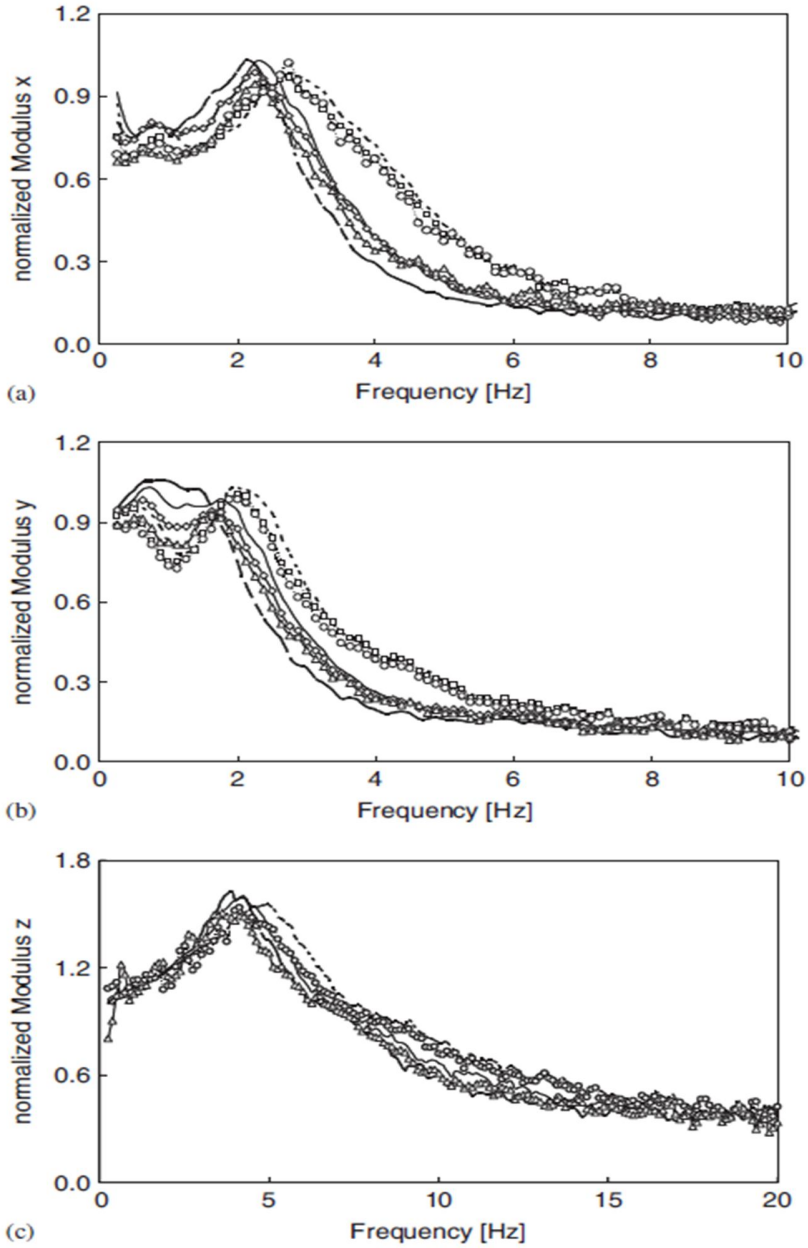

Figure 2.32 Mean values of the normalized moduli of the apparent mass function: (a) in x-direction, (b) in y-direction, (c) in z-direction. ……, vibration magnitude E1, ——, vibration magnitude E2, —.—, vibration magnitude E3, 'no marker' single-axis excitation X, Y, Z, □, dual-axis excitation XY E1, o, three-axis excitation E1, ◊, dual-axis excitation XY E2, Δ, three-axis excitation XYZ E2.

It is shown in Sections 2.4 and 2.5 that nonlinearity in apparent mass could be caused by changing the characteristics of the vibration (e.g., vibration magnitudes) or with the addition of an orthogonal vibration. A clear understanding of the nonlinearity in biodynamic response (e.g., a resonance shift to lower frequencies) would assist the evaluation of seats' ride comfort and improve the seat design. In particular, research on the effect of the orthogonal vibrations on apparent mass has a desirable application prospect as exposure of drivers and passengers of vehicles to vibration usually involves multi-axis excitation.

2.6 Body transmissibility

Body transmissibility reflects how much of the vibration on the seat is transmitted to the pelvis, spine, abdomen wall, or the head (e.g., Griffin, 1975; Paddan and Griffin 1988a; Paddan and Griffin 1988b; Messenger and Griffin, 1989; Matsumoto and Griffin, 1998a; Kitazaki and Griffin, 1998; Paddan and Griffin 1998; Mansfield and Griffin, 2000).

The translational vibration (fore-and-aft, lateral and vertical) and the rotational motion (roll, pitch, and yaw) of the head were measured with a gripped bite-bar (Paddan and Griffin, 1988a). With vertical seat motion, the head motion up to 25 Hz occurred principally in the fore-and-aft, vertical and pitch axes of the head. With fore-and-aft seat motion, the head motion up to 16 Hz also occurred principally in the fore-and-aft, vertical and pitch axes of the head. The resonance in the fore-aft head motion located around 2 Hz. With lateral seat motion, the principal head motion occurred in the lateral direction with peak transmissibility also around 2 Hz. This study also showed that backrest contact increased the magnitude of head vibration during vertical seat vibration and fore-and-aft seat vibration but had little effect on the head motion with lateral seat vibration.

With the head pitched down by 40º or 60º, vertical seat-to-head transmissibility was reduced compared to that with the head horizontal (Messenger and Griffin, 1989). Rotating the head in yaw or roll also increased the modulus of the yaw transmissibility or the roll transmissibility. Posterior tilting of the pelvis tended to increase the vertical head transmissibility in the frequency range 6 to 35 Hz while anterior tilting of the pelvis reduced the transmissibility in the same frequency range. Increasing forward inclination of the upper back reduced the vertical transmissibility to the head at frequencies greater than 6 Hz but increased the transmissibility at frequencies less than 6 Hz.

The motions of the head, spine, pelvis and viscera in the mid-sagittal plane of eight subjects exposed to vertical random vibration from 0.5 to 30 Hz at a magnitude of 1.7 ms^{-2} r.m.s. were measured in three different postures (Kitazaki and Griffin, 1998). Eight modes of body deformation were extracted from the median transfer functions of the subjects in a normal sitting posture below 10 Hz (Figure 2.33).

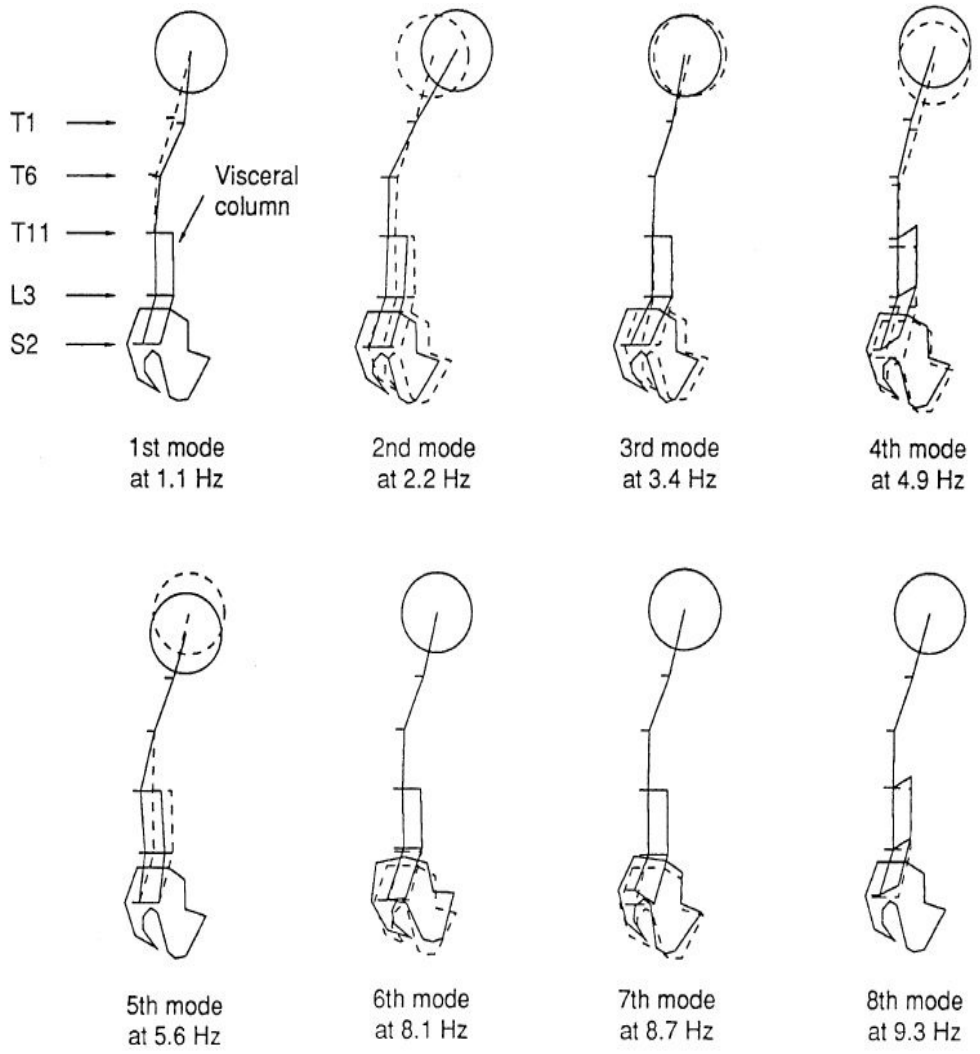

Figure 2.33 Vibration mode shapes below 10 Hz in the normal posture extracted from the mean transfer functions of the eight subjects exposed to vertical random vibration from 0.5 to 30 Hz at a magnitude of 1.7 ms^{-2} r.m.s. — —, the initial position of body parts; ——, vibration modes (Kitazaki and Griffin ,1998).

It was clear that the extracted mode shapes below 10 Hz were various combinations of bending deformations of the spine, vertical motion of the viscera, axial and shear

deformations of the buttocks tissue, pitching motion of the pelvis and pitching motion of the head. The fourth mode at 4.9 Hz, particularly, consisted of an entire body mode, in which the head, spinal column and the pelvis moved vertically due to axial and shear deformations of the buttocks tissue, in phase with a vertical visceral mode, and a bending mode of the upper thoracic and the cervical spine. This mode was suggested to correspond to the principal resonance of the apparent mass which was measured in that study with the same subjects. The sixth mode at 8.1 Hz and the seventh mode at 8.7 Hz contained pitching modes of the pelvis with different locations of the pivot. The eighth mode at 9.3 Hz was the second visceral mode. The sixth, seventh and eighth modes was suggested to correspond to the second principal resonance of the apparent mass.

The transmissibility from vertical seat motion to vertical, fore-and-aft, and pitch motion of the head, to six locations along the spine (T1, T5, T10, L1, L3, and L5) and to the pelvis was measured with eight male subjects exposed to vertical random vibration at 1.0 ms^{-2} r.m.s. (Matsumoto and Griffin, 1998a). The force on the seat was also measured and then used to calculate the apparent mass. Most of the vertical transmissibilities (Figure 2.34) showed a peak in the region of 5 Hz which was the principal resonance frequency of the apparent mass. The peaks of the vertical transmissibilities were found to decrease at higher measurement locations except for T1. The authors suggested that the head motion might have an effect on the transmissibility to T1.

The fore-and-aft cross-axis transmissibility to each location for each subject was much smaller than those in the vertical directions except to the head and T1 (Figure 2.35). The transmissibility to the head and T1 showed a peak around 6 and 7 Hz while the resonance was not evident at other locations up to 10 Hz. The pitch transmissibility to each measurement location showed a resonance around 5 Hz. The pitch transmissibility to the head was higher than that to T1 (Figure 2.36). The transmissibility to the head and T1 were larger than those to locations along the spine and pelvis.

Calculated movement of the upper body at the principal resonance frequency of the apparent mass indicated that bending or rocking motions of the spine appeared to be dominant at resonance frequency of the apparent mass (Figure 2.37). The bending motion of the lower thoracic spine and the lumbar spine region was more significant than the upper thoracic spine. The pitch motion of pelvis was also observed to contribute to the resonance accompanied with the axial and shear deformation of the tissue beneath the pelvis.

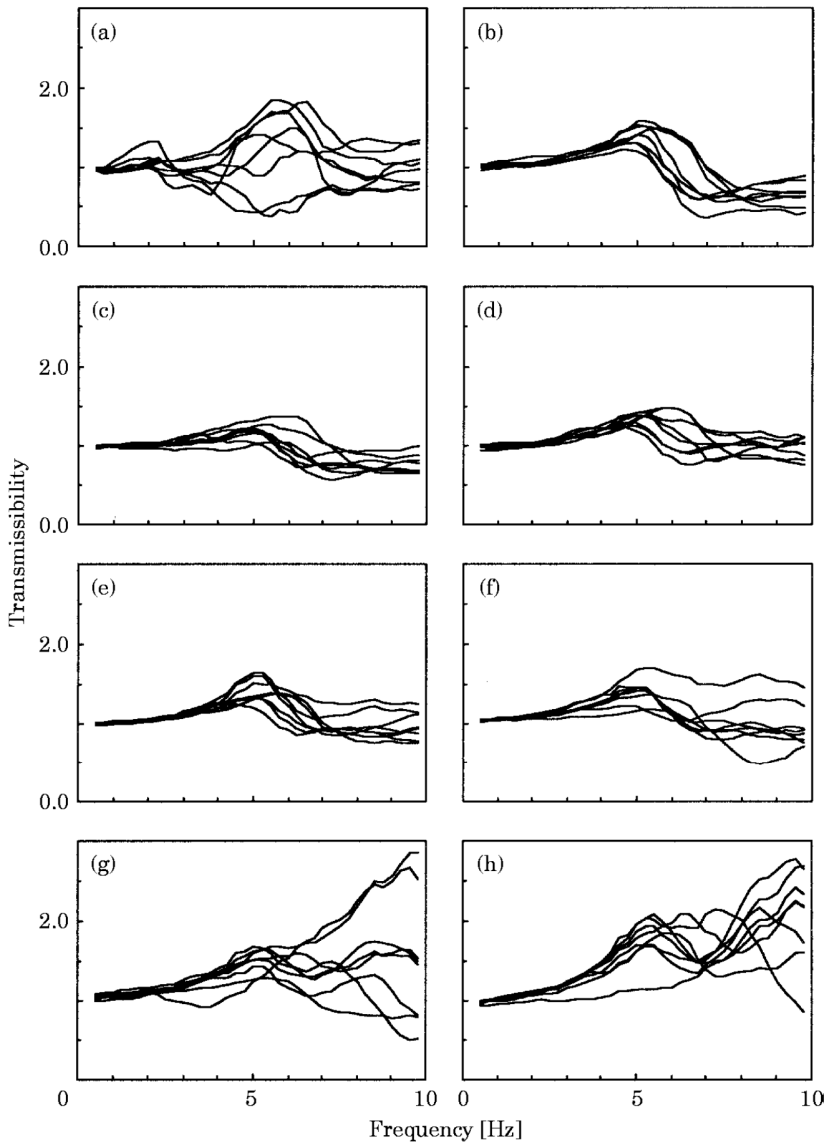

Figure 2.34 Vertical transmissibility to (a) head; (b) T1; (c) T5; (d) T10; (e) L1; (f) L3; (g) L5; (h) pelvis for the eight subjects exposed to vertical random vibration up to 10 Hz at 1.0 ms^{-2} r.m.s. (Matsumoto and Griffin, 1998a).

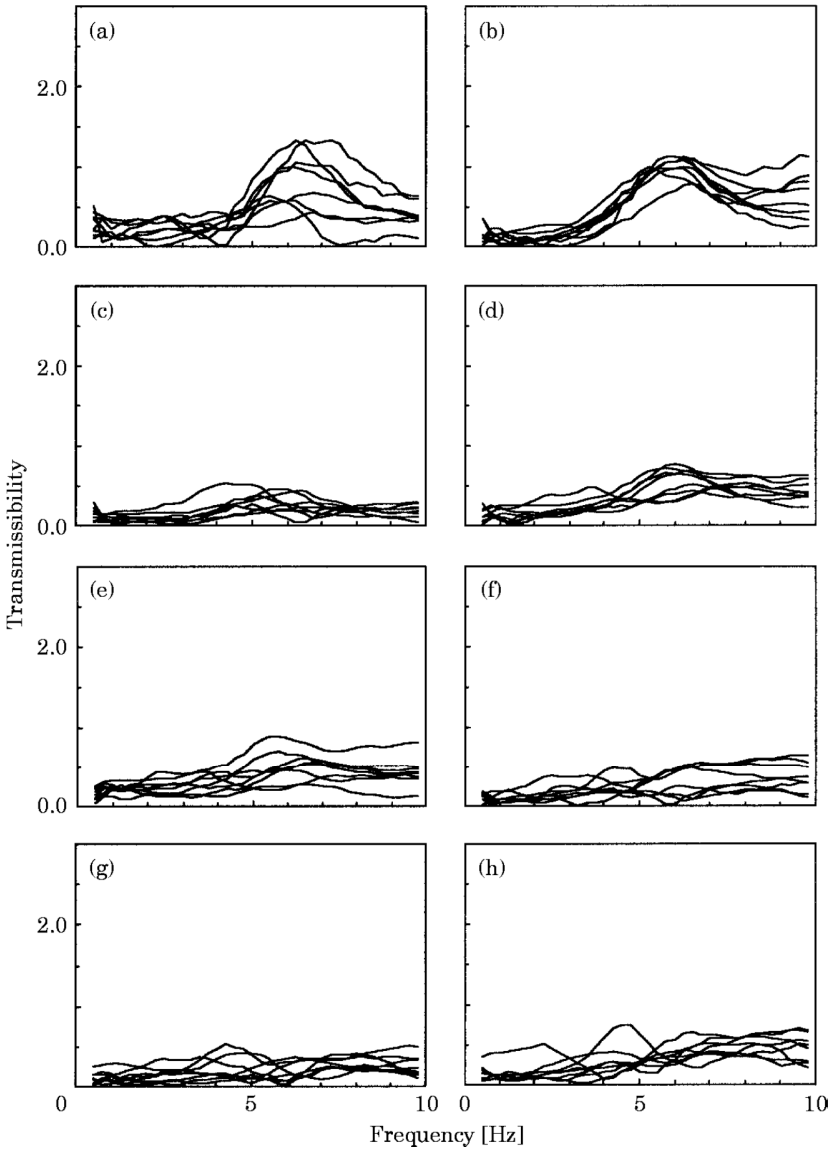

Figure 2.35 Fore-aft transmissibility to (a) head; (b) T1; (c) T5; (d) T10; (e) L1; (f) L3; (g) L5; (h) pelvis for the eight subjects exposed to vertical random vibration up to 10 Hz at 1.0 ms^{-2} r.m.s.(Matsumoto and Griffin, 1998a).

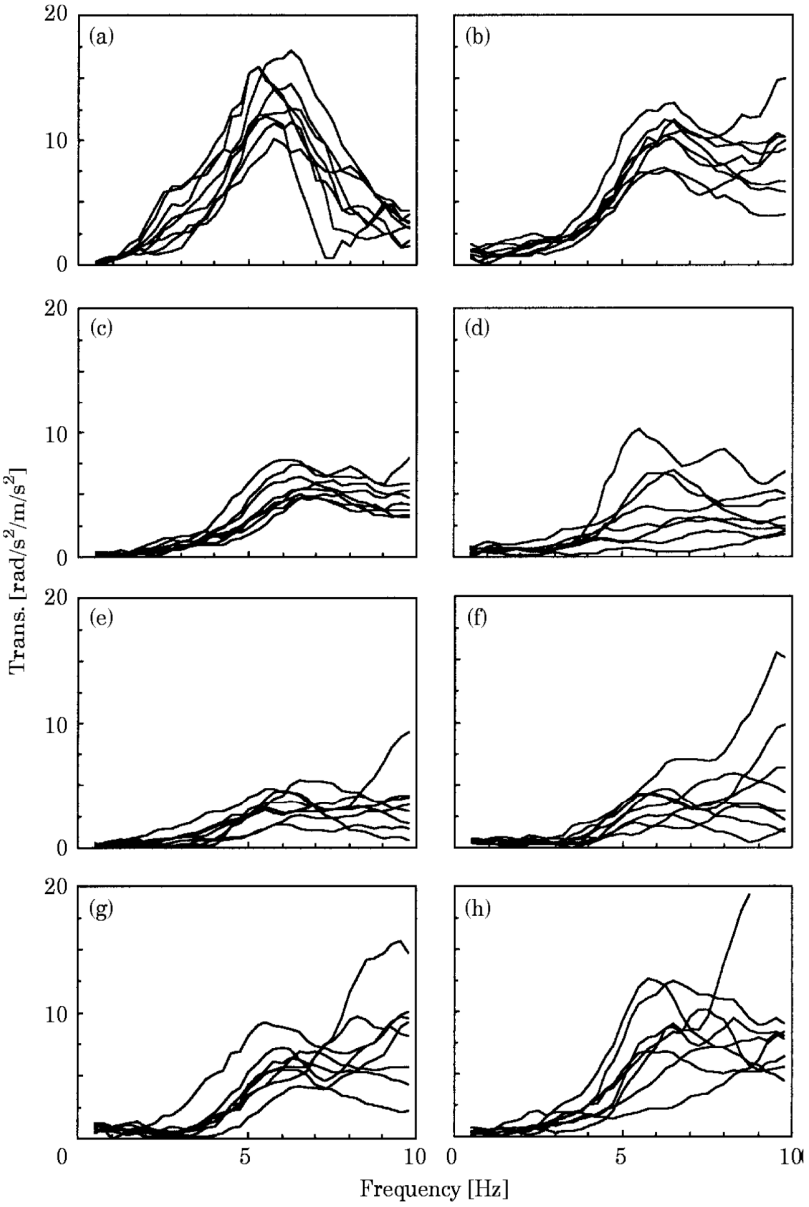

Figure 2.36 Pitch transmissibility to (a) head; (b) T1; (c) T5; (d) T10; (e) L1; (f) L3; (g) L5; (h) pelvis for the eight subjects exposed to vertical random vibration up to 10 Hz at 1.0 ms^{-2} r.m.s. (Matsumoto and Griffin, 1998a).

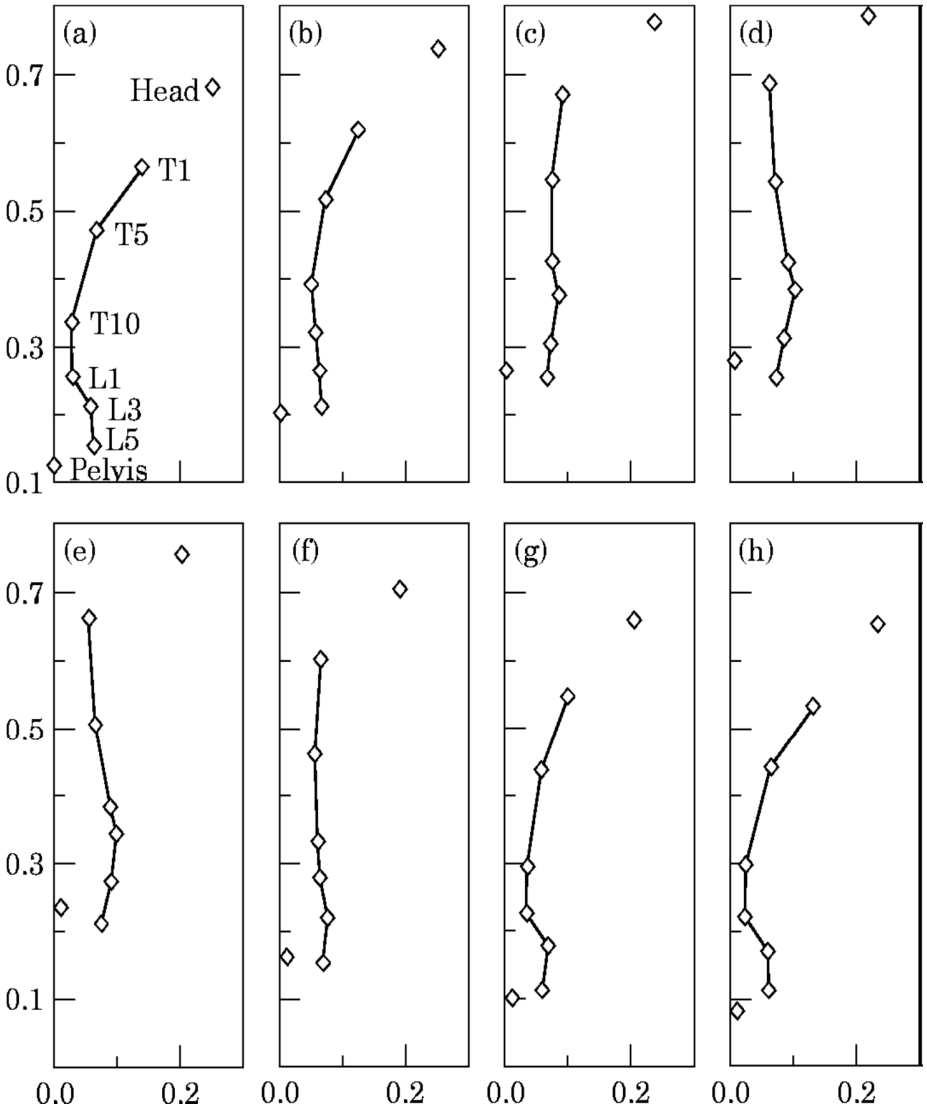

Figure 2.37 Movement of the upper body at the principal resonance frequency of the apparent mass of a single subject at 5.25 Hz when the seat moved upward. The units for both axes are metres, and the scale of the movement is exaggerated for clarity (Matsumoto and Griffin, 1998a).

A nonlinearity in body transmissibility associated with a change in vibration magnitude has also been reported. By exposing twelve subjects to vertical random vibration at 0.25, 0.5, 1.0, 1.5, 2.0, 2.5 ms^{-2} r.m.s. and in the frequency range 0.2-20 Hz, the apparent mass and the transmissibility of the subjects were measured from the seat to various locations on the body surface (i.e., the upper and lower abdominal wall, at L3, over the posterior superior iliac spine and the iliac crest) (Figure 2.38; Mansfield and Griffin, 2000). Resonance frequencies of transmissibility from vertical seat motion to vertical motion at the spine and pelvis (Figure 2.38(f), (g) and (h)) decreased with the increasing

vibration magnitudes. The first resonance frequency was reduced from 6 to 4 Hz and the second resonance frequency from 10 to 7 Hz when the vibration magnitudes increased from 0.25 to 2.5 ms^{-2} r.m.s. The authors found that the extent of nonlinearity was greater for the seat-to-spine and seat-to-abdomen transmissibility.

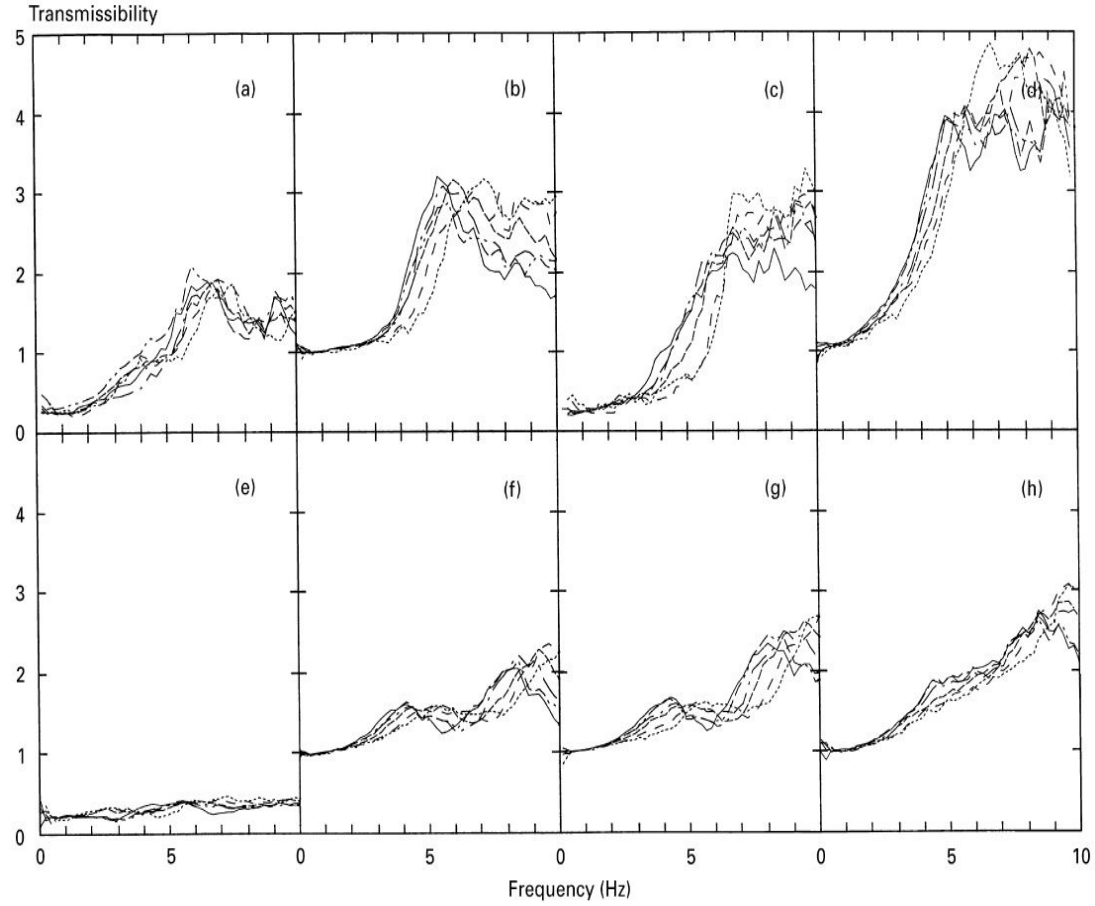

Figure 2.38 Median seat to abdomen transmissibility of twelve subjects exposed to vertical random vibration at magnitudes of 0.25 (……), 0.5 (- - -), 1.0 (— —), 1.5 (—.—), 2.0 (- -.- -), 2.5 ms^{-2} r.m.s. (——). Seat to lower abdominal wall: (a) fore-and-aft, (b) vertical. Seat to upper abdominal wall: (c) fore-and-aft, (d) vertical. Seat to lumbar spine: (e) fore-and-aft, (f) vertical, (g) posterior superior iliac spine, (h) iliac crest (Mansfield and Griffin, 2000).

Knowledge of body transmissibility is helpful for the evaluation of the discomfort or potential injury on the local body parts. Understanding of the nonlinearity in transmissibility will also improve understanding of the mechanism contributed to the nonlinearity in apparent mass. Both the apparent mass and transmissibility with vertical excitation has been reported by a few studies as reviewed above. However, body

transmissibility with horizontal vibration remains unpublished although apparent mass with horizontal vibration have been studied.

2.7 Biodynamic modelling

2. 7.1 One-dimensional lumped-parameter models

Lumped-parameter models are widely used as they are easy to develop by fitting experiment data. In this type of model the human body is represented by several masses which are not necessarily anatomically representative. Masses are interconnected by springs and dampers and generally limited to move in just one direction. Some models include rotational degrees-of-freedom to investigate the pitch motion.

Many lumped-parameter models have been established based on certain experimental data and specific testing conditions. Some of these models are reviewed here for convenience.

A single-degree-of freedom lumped-parameter model was proposed to reproduce the vertical apparent masses of 60 seated subjects (Fairley and Griffin, 1989; Figure 2.39). The body mass that moved relative to the seat and the body mass that did not move relative to the seat were represented by sprung mass, m_1, and unsprung mass, m_2, respectively. The interaction between legs and stationary footrest was simulated by the spring mass m_3.

Alternative mathematical models were later developed to represent the vertical apparent masses of the 60 seated subjects exposed to vertical broadband random vibration (0.2-20 Hz) at 1.0 ms^{-2} r.m.s. (Wei and Griffin, 1998; Figure 2.40). Two of the models that provided the best fits to experimental phase data are shown in Figure 2.40(a) and Figure 2.40(b). Models were fitted to the individual data of 60 subjects and the average data of the whole group. The models were not anatomy-based but proposed to serve as mathematical tools to represent the modulus and phase of apparent mass. The two-degree-of-freedom model provided a better fit to the phase of the apparent mass at frequencies greater than about 8 Hz and a better fit to the modulus of the apparent mass at frequencies around 5 Hz than the single-degree-of-freedom model.

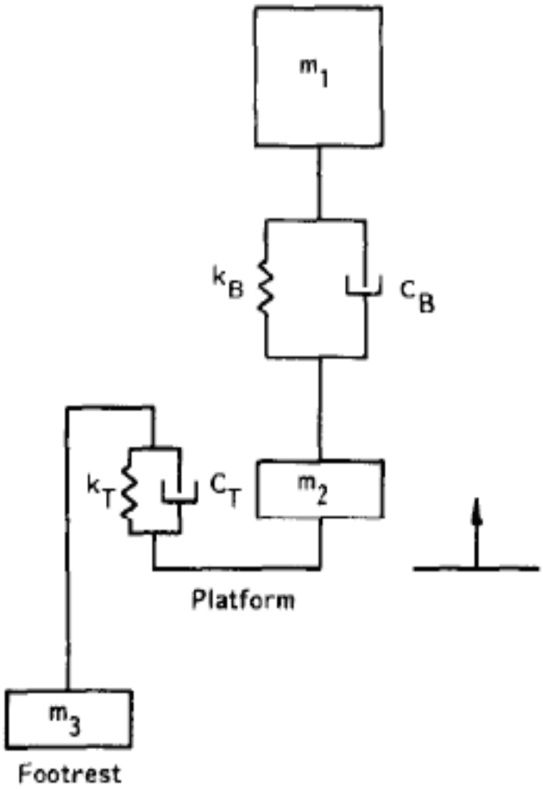

Figure 2.39 Simple lumped-parameters models representing the mean vertical apparent mass of 60 seated subjects (Fairley and Griffin, 1989).

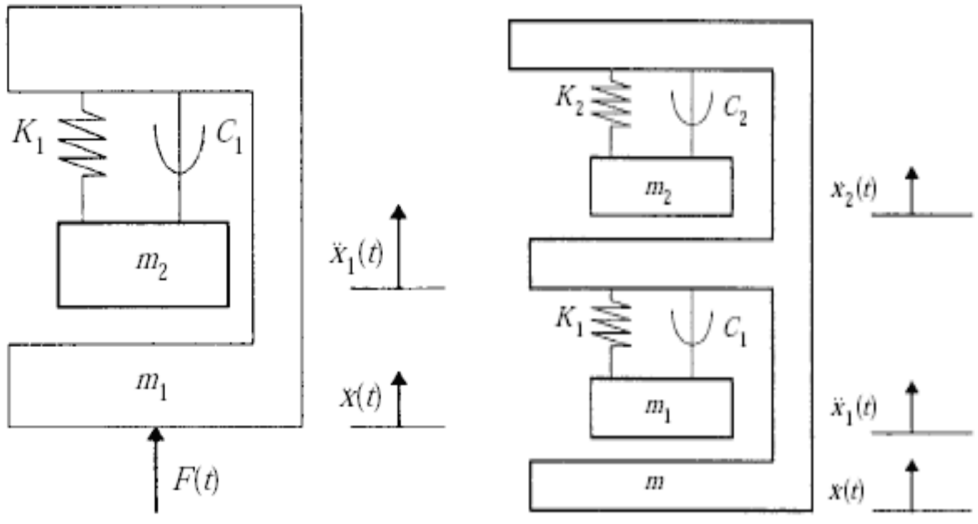

(a) (b)

Figure 2.40 Lumped-parameters models developed to represent the individual and mean modulus and phase of apparent mass. (a) single-degree-of-freedom model; (b) two-degree-of-freedom model (Wei and Griffin, 1998).

A three-degree-of-freedom model is recommended to represent the driving-point impedance, apparent mass and transmissibility in ISO 5982 (2001) (Figure 2.41). The model related to the data of 101 subjects with the masses in the range 49 to 93 kg who were exposed to both sinusoidal and random vibration (0.5 Hz to 20 Hz) with unweighted root-mean-square accelerations between 0.5 ms^{-2} r.m.s. and 3 ms^{-2} r.m.s. and frequency-weighted root-mean-square acceleration less than or equal to 2 ms^{-2} r.m.s. The subjects adopted an erect posture with back unsupported and feet vibrated by the same input as on the seat. An idealized range of values of driving-point impedance, apparent mass and transmissibility were defined. As discussed in Section 2.3.1, non-linearity in driving-point mechanical impedance and apparent mass responses may arise with variations in vibration amplitudes. The model parameters defined in the standard may not be able to represent the biodynamic response when the vibration magnitude is outside the range between 0.5 ms^{-2} and 3.0 ms^{-2} r.m.s. The masses, springs and dampers defined in the standard do not correspond to physiological structures within the human body.

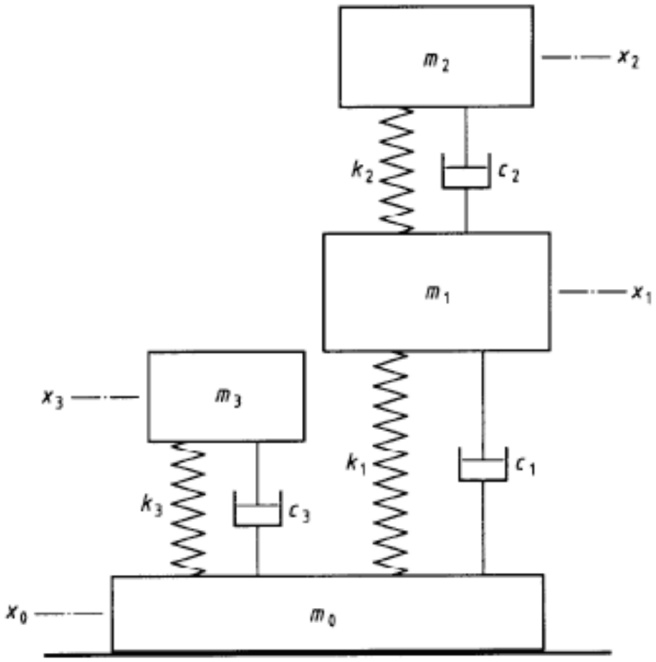

Figure 2.41 The three-degree-of-freedom model defined by the International Organisation for Standardization (ISO 5982, 2001) to represent the apparent mass, mechanical impedance and seat-to-head transmissibility of a seated person.

A five-degree-of-freedom lumped parameters model based on the measured driving-point impedance and transmissibility has been developed (Smith, 1994; Figure 2.42(a)).

The model was composed of five lumped masses that were assumed to anatomically represent the pelvis, spine, upper torso, lower torso and legs. The mechanical impedance on which the model was based was obtained by exposing four subjects to sinusoidal vibration from 3 to 20 Hz at 0.347, 0.694, and 1.734 ms^{-2} r.m.s. The model parameters were redistributed for impedance data obtained with different vibration magnitudes to take into account nonlinearity due to the change in vibration magnitudes. The most significant change in parameters was found in M_3, K_2, C_2 and C_5. The author suggested a combined vibration mode contributing to the nonlinearity with vibration magnitudes.

The model was later modified to simulate the different primary resonance frequency observed in the impedance and transmissibility to the chest (upper torso), the spine (the seventh cervical vertebrae C_7), the upper leg and the lower leg (Smith, 2000; Figure 2.42(b)). The effect of a seat cushion on the resonance behaviour was also evaluated with the model.

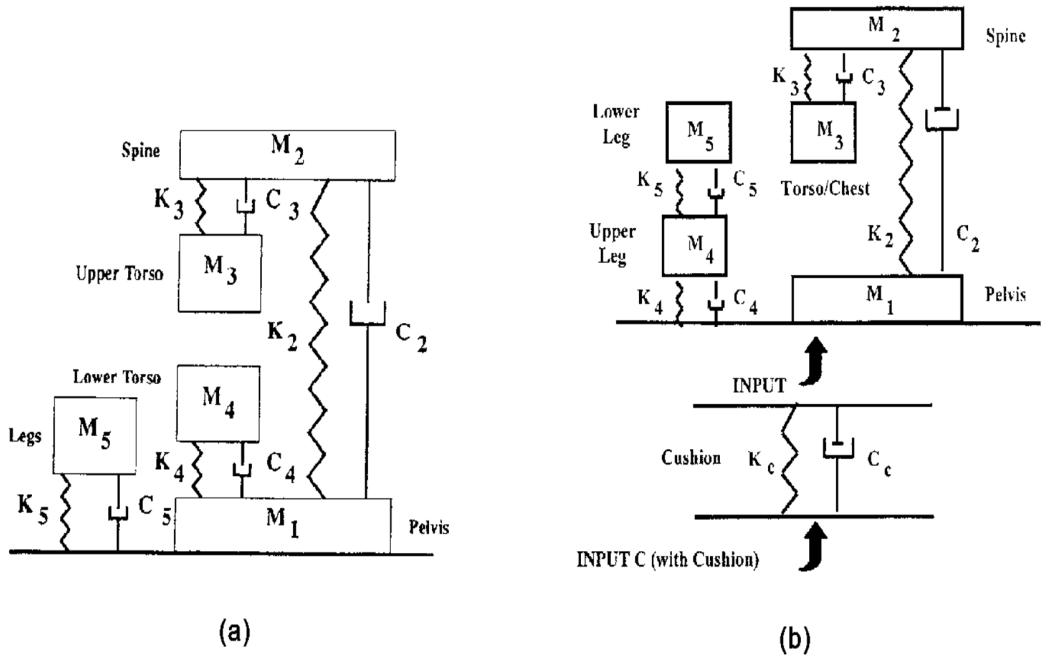

Figure 2.42 The five-degree-of-freedom models developed by: (a)8 Smith (1994) to represent the mechanical impedance of four subjects exposed to sinusoidal excitation from 3 to 20 Hz at three magnitudes at 0.347, 0.694, and 1.734 ms^{-2} r.m.s.; (b) Smith (2000) to simulate the major resonances in the mechanical impedance and transmissibility to the chest, spine (C7) and thighs with and without cushions.

To take into account of the effect of the backrest contact, backrest inclination, hand positions, foot positions and vibration magnitudes on the biodynamic response, the

modulus and the phase of experimental vertical apparent mass in various testing conditions were fitted to a single-degree-of-freedom lumped model (Toward and Griffin, 2010; Figure 2.43) with m_0 and m_1 representing a fixed frame and the mass moving relative to the seat respectively. The authors observed that the fitted moving mass was reduced while the associated stiffness k_1 was significantly increased, when there was backrest contact. The reduction in the moving mass was also suggested to be the main cause of the lower apparent mass at the resonance frequency when the rigid backrest was inclined from 0° to 30°. With a foam backrest, the decrease in the resonance frequency when the backrest was inclined from 15 to 30° was associated with a decrease in the stiffness of human tissue.

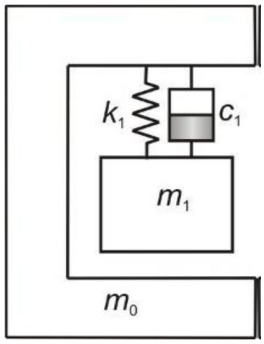

Figure 2.43 Single-degree-of-freedom model (Toward and Griffin, 2010).

Moving the hands from the lap to the steering wheel, a decrease in the moving mass and increase in the stiffness were observed (Toward and Griffin, 2010). The increase in the moving mass and a decrease in the stiffness were significantly associated with a decrease in the resonance frequency when the feet were moved forward (Toward and Griffin, 2010).

Increasing vibration magnitude was suggested to be associated with decrease in stiffness which caused the decrease in the resonance frequency while the moving mass was unaffected (Toward and Griffin, 2010).

2.7.2 Two-dimensional lumped-parameter models

To have a better representation of body motion, several studies have included rotational elements in the biodynamic models (e.g., Matsumoto and Griffin, 2001; Qiu, 2007; Nawayseh and Griffin 2009). These models were proposed with the hope of understanding cause-effect relationship which has not been fully published via experiment. They are therefore mechanism models to some extent.

Two models with four and five degrees of freedom respectively were developed to represent vertical apparent mass and transmissibility to the pelvis, spine, and viscera (Matsumoto and Griffin, 2001; Figure 2.44). Vertical spring and damper under mass 1 represents axis deformation of buttocks. Rotational degrees of freedom simulate pitch motion of pelvic (mass 2) and bending motion of spine (mass 3 for model 1 and mass 3, mass 5 for model 2). Mass 4, representing viscera was restricted to move only in the vertical direction. The upper-body was suggested to be constructed with at least two elements otherwise it would be very difficult to get properties parameters by match measured apparent mass and transmissibility. Modal analysis was performed, suggesting that the second mode with a natural frequency 5.66 Hz corresponded to the primary resonance. This mode consisted of vertical motion of the legs and viscera which was in phase of pitch motion of the pelvis. A parameter sensitivity study showed that both the apparent mass on the seat and the transmissibility from seat base to different locations of body in different directions were influenced by change of parameters in the vertical axis. However, rotational properties had little effect on the apparent mass.

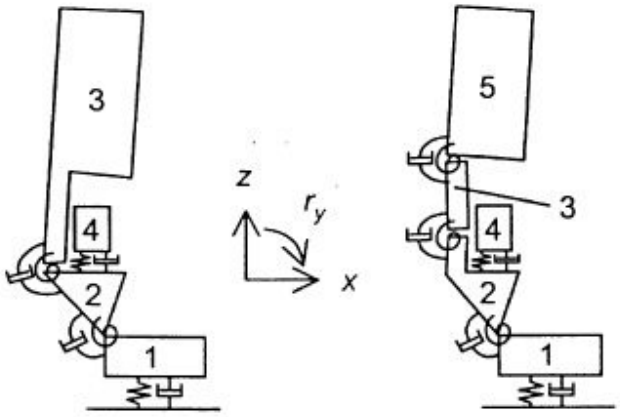

(a) Model 1 (b) Model 2

Figure 2.44 Models proposed to: (a) represent apparent mass up to 20 Hz and transmissibility to pelvis, upper body (T_5) and viscera up to 10 Hz; (b) represent apparent mass up to 20 Hz and transmissibility to pelvis, upper body (T_1, L_1)and viscera up to 10 Hz (Matsumoto and Griffin , 2001).

A combined seat-occupant model for vibration excitation in the fore-and-aft direction to predict the apparent mass and the seat transmissibility at the backrest has been reported (Qiu, 2007; Figure 2.45). The lower human body was represented by lumped mass m_1 and m_s while the upper body was modelled with lumped mass m_b and m_2. The seat and backrest was simulated with m_{0b} and m_{0s} respectively. A total of 24 parameters

were involved in the model, 23 of which were optimized by curving fitting. The model was calibrated with the apparent mass measured by Nawayseh and Griffin (2005) and seat transmissibility obtained by Qiu and Griffin (2003).

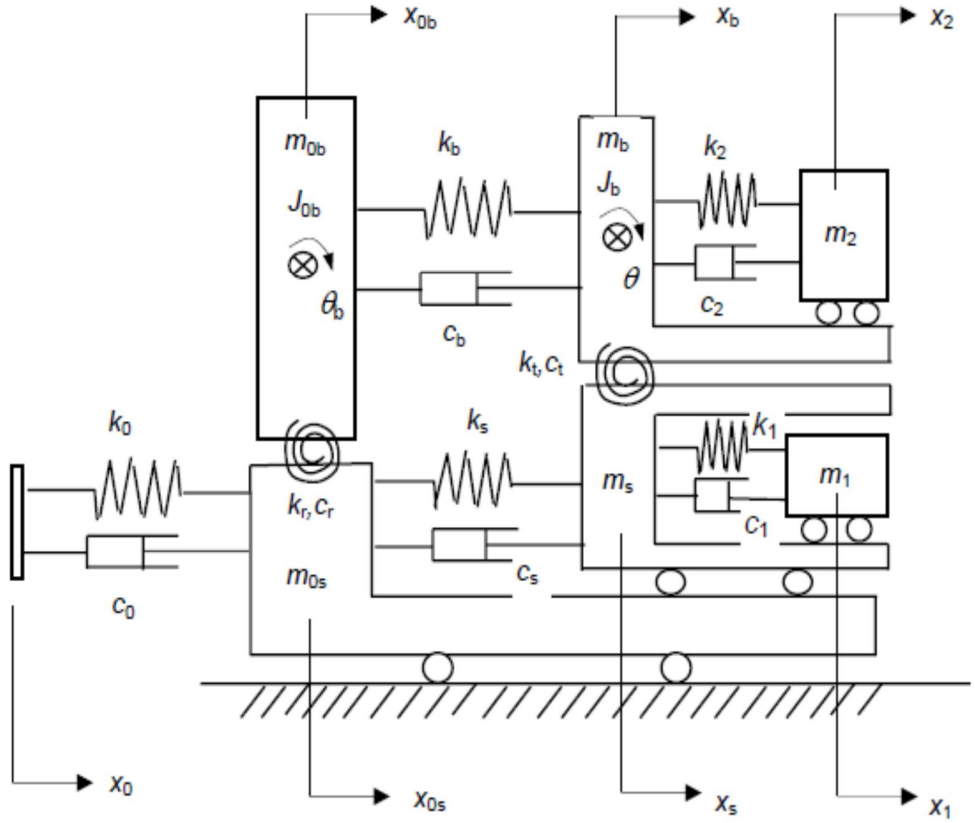

Figure 2.45 the combined seat-occupant model to predict apparent mass and the seat transmissibility at the backrest (Qiu, 2007).

2.7.3 Multi-body dynamic models

Multi-body dynamic models comprise several rigid bodies interconnected by revolute joints (i.e. rotational springs and dampers). These bodies are expected to be anatomically representative and each of them has three degrees of freedom in the sagittal plane, namely vertical, fore-and-aft, and rotational. Therefore motion of each body segment is predictable with a multi-body model.

A five-degree-of-freedom model to evaluate ride comfort in terms of transmissibility to the head, back and hip with vertical vibration was proposed (Cho and Yoon, 2001; Figure 2.46). The whole human was simplified into three rigid bodies in 2-D sagittal plane (i.e. lower body incorporating sacrum, thighs and legs, upper body with arms, heads and so on). Backrest support was taken into account in light of its contribution to

maintain posture and decrease muscle tension. However, foot support was ignored. Each body of the model was interconnected by linear translational springs and dampers together with rotational springs and dampers. Three vertical and horizontal spring-damper units representing the mechanical properties of seat and backrest cushions are serially connected to lower bodies and upper bodies. The mean mass properties of each segment were from literature with standard deviations while the centre of each body was assumed to be at the middle of two joints. The joints and contact positions were measured. Seat cushion parameters were extracted from measured seat transmissibility and the other parameters of model were identified by matching predicted transmissibility to experiment value. The five-degree-of-freedom of model can describe not only vertical motion of hip and head but also fore-and-aft motion of back which a lumped parameter model cannot generally do.

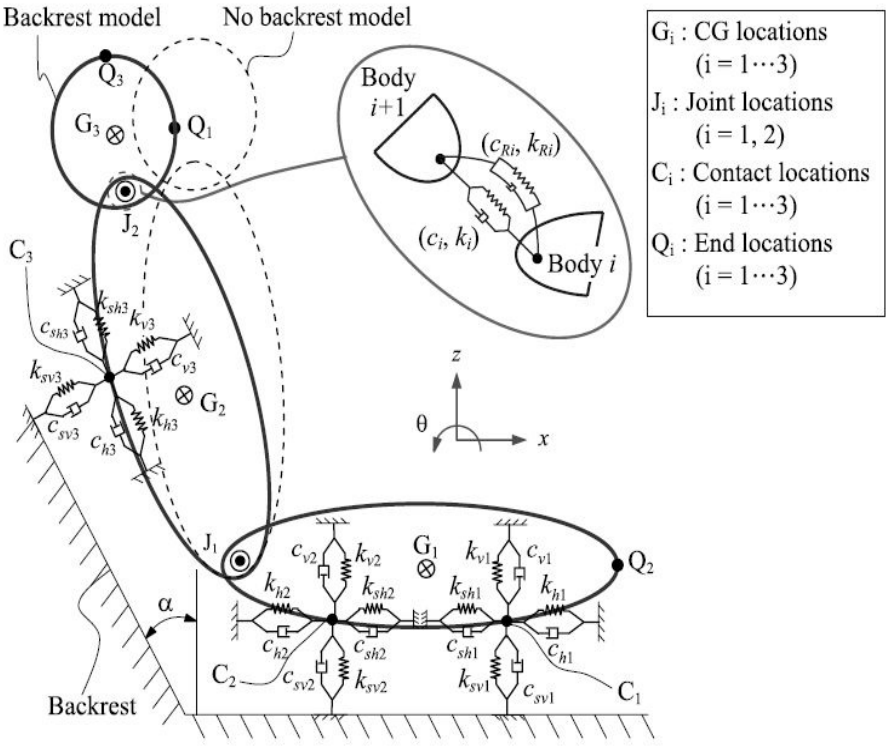

Figure 2.46 The model proposed to represent mean transmissibility to the head, back and hip of 5 subjects exposed to vertical random vibration (1-25 Hz) at 1.0 ms^{-2} r.m.s. (Cho and Yoon, 2001).

An eight-degree-of-freedom multi-body dynamic model expanding the one proposed by Kim *et al*. (2005) was developed to simulate the transmissibility to the hip, back and head (Liang and Chiang, 2008). The model was composed of five rigid segments,

representing thighs, pelvis, upper-body, head and viscera respectively (Figure 2.47). Mechanical properties were obtained by matching simulated seat to head transmissibility and apparent mass to individual measured data while other model properties were from anthropometric literature.

Calibration was carried out for models with and without backrest, both results of which were consistent with experiment data in terms of seat to head transmissibility. Apparent masses with different postures were evaluated. Results showed that apparent mass was closely related to body mass but it was not discussed in detail. Hand positions were also ignored, the influence of which on human biodynamic response was worthy of further study as author suggested.

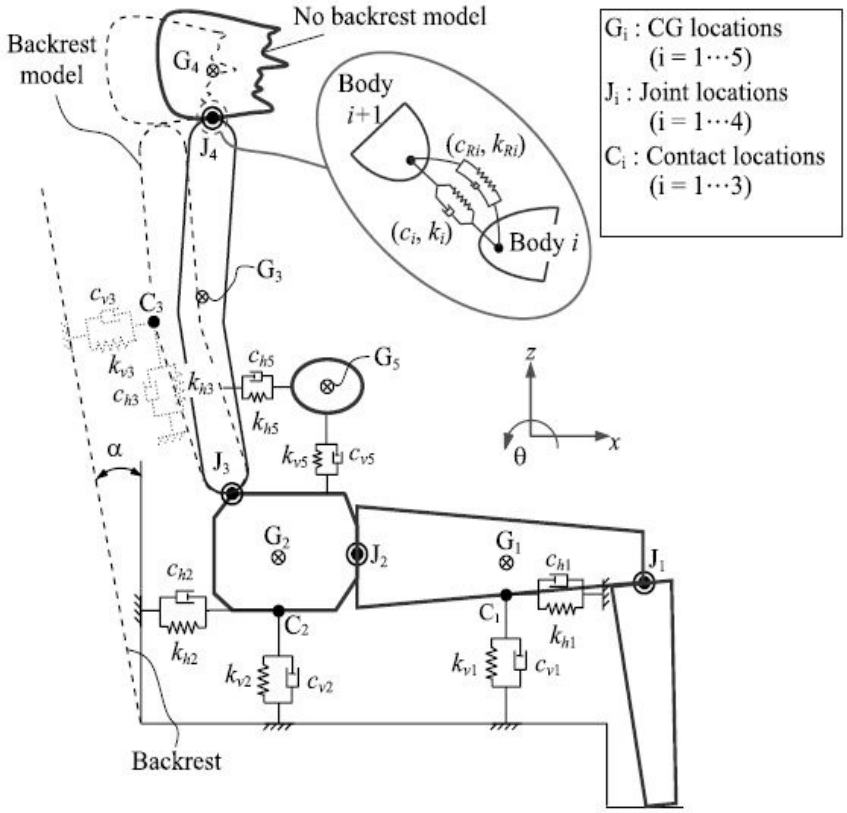

Figure 2.47 The model developed to represent the transmissibility to the hip, back and head with and without backrest (Liang and Chiang, 2008).

A multi-body model was developed to predict the static equilibrium of a seated occupant and showed how the equilibrium was influenced by seat parameters (Ippili *et al*., 2007; Figure 2.48). The model incorporated the non-linear viscoelastic character of flexible foam. Firstly, compression force–deflection (CFD) tests of a type A foam and type D

foam were conducted on cube foam blocks, the results of which were shown in Figure 2.49 and Figure 2.50. Secondly, quasi-static unidirectional compression behaviour of foam was assumed to be sum of nonlinear elastic force and the linear viscoelastic force. The interaction force between occupant and seat were modelled, consisting of a Coulomb friction force and tangible force which few researchers had considered before.

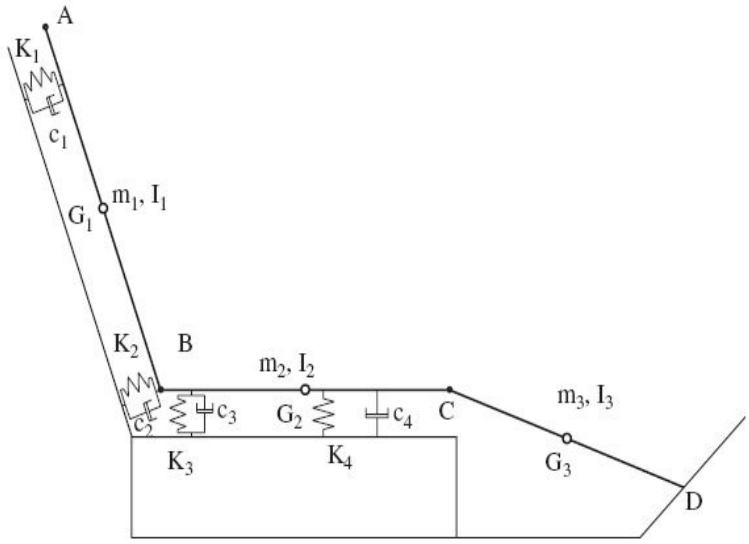

Figure 2.48 The mannequin–seat model proposed to predict the static equilibrium of a seated car seat occupant and how the equilibrium was influenced by seat parameters (Ippili *et al.*, 2007).

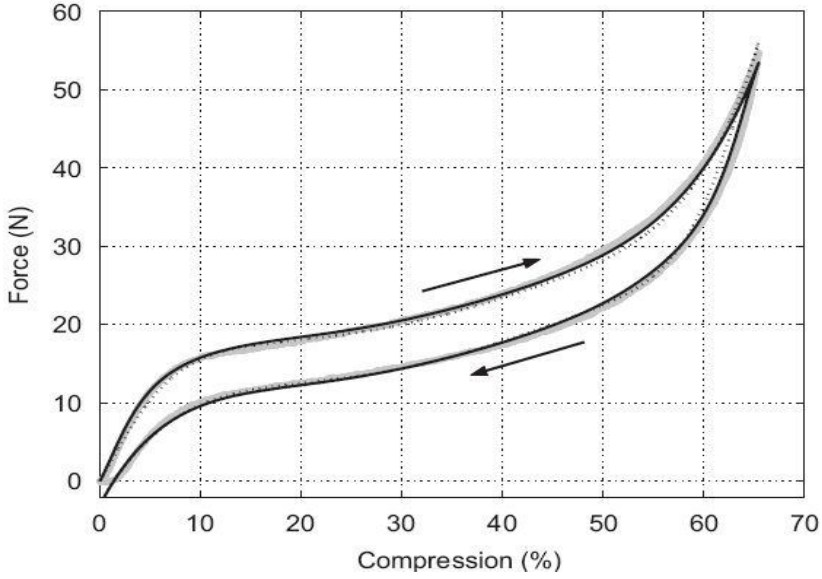

Figure 2.49 The force–strain response of foam type A (Ippili *et al.,* 2007).

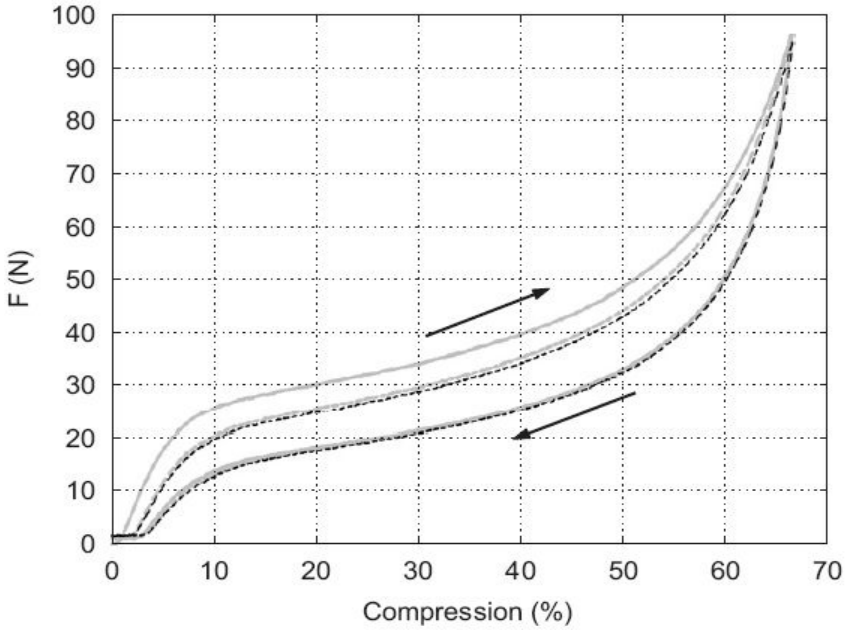

Figure 2.50 The force–strain response of foam type D (Ippili *et al.,* 2007).

Foam model and interaction forces were all incorporated into a seat-occupant model with some assumptions (i.e. motion of seat back did not have significant role on static settling behaviour). Feet were constrained to move along footrest, so a constrained function was needed in addition of equations of motion derived by using Lagrange equation method. Parametric studies were performed in terms of variation of foam type, contact area, spring locations, interfacial force coefficients, initial sitting posture, and dimensions of occupant. It was found that static equilibrium positions were most sensitive to stiffness and location of spring under pelvis which carried most of occupant weight.

2.7.4 Finite element models

Finite element model of the human body and seat consist of numerous of elements interconnected by nodes (e.g., Verver, 2004; Pankoke *et al*., 2008) or lumped spring-damper (e.g., Kitazaki and Griffin, 1997; Pankoke *et al*., 1998). Such a model is usually accurately anatomically depicted with detailed skeleton structure and muscle in regions of interest such as spine, back, pelvic and thigh. This type of model can be developed to predict not only body motion but also internal forces contributing to injury. Various commercial finite element human body models were developed for different applications, which were summarised by Verver (2004). However, properties of elements are difficult

to obtain and validate. Furthermore, finite element models of human body are generally complex and computationally inefficient.

Some models were developed to investigate relationships between mode shapes and human response. For instance, a modal analysis using finite element methods was performed and extracted seven modal shapes below 10 Hz (Kitazaki and Griffin, 1997; Figure 2.51). The results showed that the fourth calculated mode shape which consisted of entire body mode with vertical and fore-and-aft pelvic motion due to deformation of tissue beneath pelvis and in phase with vertical viscera motion corresponded to the primary resonance. The second resonance was found to be related to second viscera mode and pelvic rotation which was dominant in the sixth and seventh predicted mode shape respectively.

Resonance shift due to posture change was also investigated with the finite element model. Changing from erect to normal posture with pelvis rotation backward, contact area was assumed to move to parts of buttocks posterior to ischial tuberosities which led to an increase of the axial stiffness of buttocks tissue and a higher resonance frequency. Changing from normal to slouched posture, head and spine tended to incline forward, increasing contact between thigh and seat. Tissue also became softer and resonance frequency was decreased.

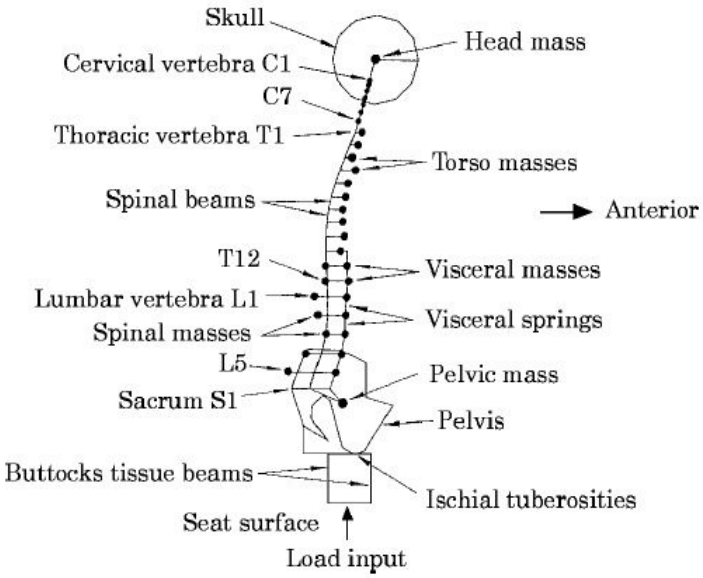

Figure 2.51 Planar finite element model of human body with normal posture developed to investigate modes relating to vibration response up to 10 Hz (by Kitazaki and Griffin, 1997).

A finite element model of a sitting man consisting of rigid bodies representing lower lumbar spine particularly, upper torso, neck, head, arm, viscera, pelvis and leg was proposed (Pankoke *et al*., 1998). The connectors between the rigid bodies were linear springs. The model provided a reasonable prediction of the resonance frequency and the peak magnitude of the mechanical impedance of seated subject in standard posture but underestimated the response above the peak frequency. It was reported the model was able to predict the dynamic response in different postures by adjusting the static force and moment on the pelvis relative to the values in the standard posture, and for different subjects by adjusting the body weight parameters as well as the body height parameters relative to the 50^{th} percentile male. The predicted transmissibility from vertical seat motion to the fore-and-aft motion of the head was in agreement with the experimental value in the frequency range of 0 to 5 Hz but underestimated the head motion above 5 Hz. The predicted peak magnitude of the impedance was higher for the heavier subject occurring at lower frequency, but the prediction was not calibrated.

A buttocks finite element model, the geometry of which was based on a 78 year old male was developed to predict the pressure distribution on the various seat surfaces (Figure 2.52, Verver, 2004).

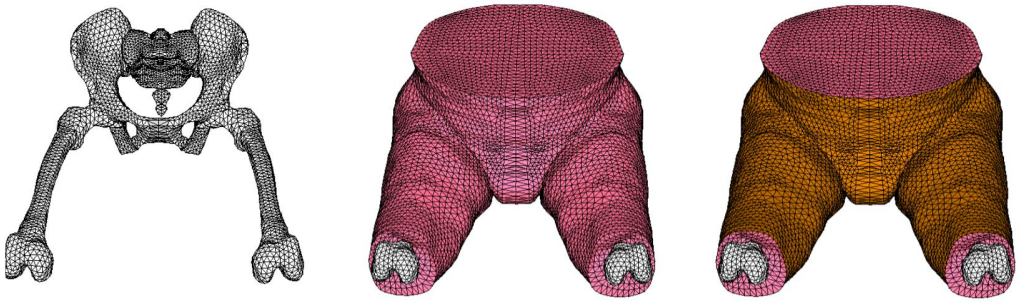

(a) (b) (c)

Figure 2.52 Finite element model of the pelvis and thighs: (a) the bony structures. (b) the bony structures and the human soft tissues. (c) the complete model-bony structures, human tissues and skin (Verver, 2004).

The bony structure was assumed to be rigid and the skin was elastic. A Mooney-Rivlin hyperelastic isotropic material model was included in the soft tissue. The FE model predicted the maximum pressure located under the bony structure, which was also observed with the volunteer subject. The predicted average pressure on a cushion seat was comparable to the experimental value while the predicted contact area was smaller

than the measured data. The model overestimated the stress at the front of the cushion beneath the thighs.

A finite element model was proposed to predicting seating comfort and the H-point (Pankoke *et al.*, 2008*)*. The seat structure was firstly modeled, including supporting components, joints which were defined in forms of kinematics coupling, controlling and adjusting components, suspension and back support. Cushion and cover were then added to structure, properties of which were tested according to corresponding test standard (Figure 2.53). An H-point-manikin model was developed afterwards, reproducing manikin's kinematics, mass and mechanical properties, surface contour, geometry, load, friction between manikin and seat surface and so on in virtual environment.

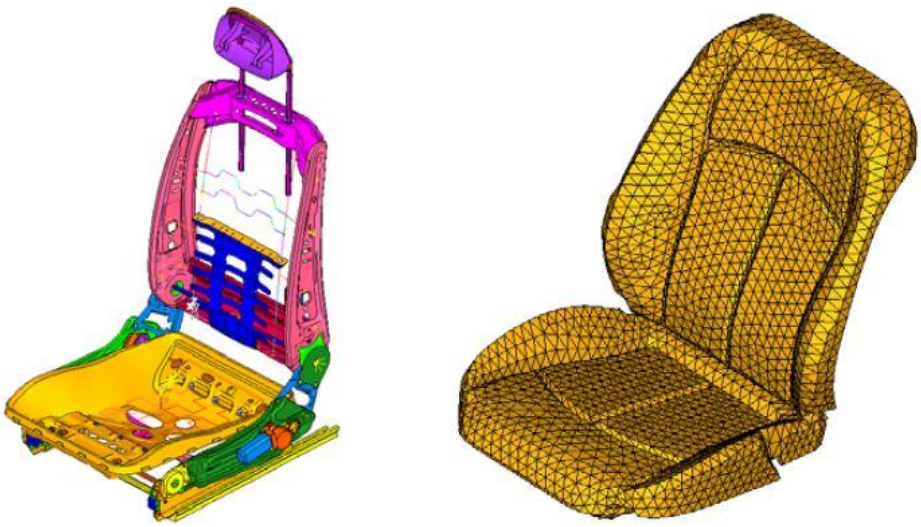

Figure 2.53 Seat structure and cushion model (Pankoke *et al.*, 2008).

A CASIMIR occupant model, which included detailed geometry and dynamic characteristic of lumbar spine, abdominal and dorsal musculature, abdominal cavity, upper torso and arms, pelvic, legs, neck and head was adopted (Figure 2.54). It was adaptable in terms of both percentile and posture. Static seating simulation was conducted after modelling using ABAQUS solver, yielding pressure distribution, and location of hip-joint, which are commonly used as criteria for seat design.

Dynamic comfort is investigated by performing modal analysis of both seat structure and occupied seat. The results suggested that the seat occupant had a significant effect on not only the natural frequencies but also the mode shape of the seat. The response of

seat-occupant under vertical excitation was predicted in the frequency domain in terms of a seat transfer function and a seat backrest transfer function. The predicted results were in good agreement with measurement values.

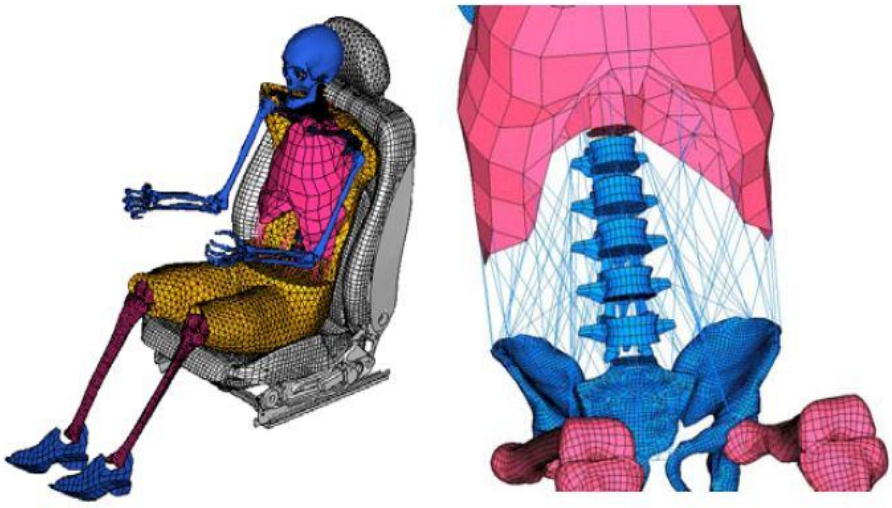

Figure 2.54 CASIMIR, lumbar spine and muscle model to predict seating comfort and H-point as well as backrest pressure (Pankoke *et al.*, 2008).

2. 8 Discussions and Conclusions

2.8.1 Biodynamic response of human body

The resonance frequency in the apparent mass and transmissibility associated with vertical excitation is decreased with increasing vibration magnitude (Section 2.4.1 and Section 2.6). A few studies have reported a similar softening effect on the resonance in the vertical apparent mass with the addition of an orthogonal excitation (Section 2.5.1). However, whether the body transmissibility with combined vertical and fore-and-aft excitation also exhibits a softening effect has not yet been investigated.

The fore-and-aft apparent mass and the vertical cross-axis apparent mass have been reported to show a primary resonance around 1 Hz and a second resonance between 2 and 3 Hz when there is no backrest (Section 2.3). The fore-and-aft head motion produced by fore-and-aft seat motion exhibits a principal peak in the vicinity of 2 Hz (e.g., Paddan and Griffin, 1988b). However, the motion of the spine and the pelvis with fore-and-aft excitation is unknown. The resonance frequency in the fore-and-aft apparent mass around 2 Hz is reduced with increasing the magnitude of fore-and-aft excitation and with the addition of vertical excitation (Section 2.5.1), but little is known about the

effect of vibration magnitude or the addition of an orthogonal excitation on the resonance in the motion of the upper body (the pelvis and the spine) associated with fore-and-aft excitation.

Sitting posture has been reported to change the biodynamic response with both vertical excitation (Section 2.2) and fore-and-aft excitation (Section 2.3). It is of interest to investigate whether changing sitting posture has a similar effect on the dynamic response with dual-axis excitation (e.g., an erect posture increases the resonance frequency in the vertical apparent mass). It remains unexplored whether sitting posture affects the association between the apparent mass and the transmissibility with dual-axis excitation.

2.8.2 Mathematical models

Models may be grouped into three types in terms of the methods employed to develop models (Section 2.7). A model like that proposed by Nawayseh and Griffin (2009) may not be regarded as a lumped-parameter model in a strict sense in this thesis. To author's knowledge, lumped-parameter models are usually used to represent motion of particles. Any similar models with geometric dimension involved might not simply be considered as lumped-parameter ones but combination of particles and rigid (or flexible) bodies. Finite element models are not only able to represent the global dynamic response such as apparent mass or transmissibility but also have the capacity of the predicting local biodynamic response, e.g., pressure distribution on the seat surface, spinal force between vertebrae, and muscle tension. In this sense, finite element is advantageous over the lumped-parameter model and multi-body model. But it is obvious that finite element model is computationally costly. Efforts should be made to reduce the complexity of the finite element model and retain the structures which are necessary to achieve the objective of the modelling.

Alternatively, models can also be categorized as quantitative models, mechanistic models and effect models in terms of the purpose of the models as suggested by Griffin (2001). Most models constructed with lumped-parameter technique are in the category of quantitative models. Development of mechanistic models and effect models needs in-depth understanding of mechanisms of how human body segments move under various vibration environments and often needs utilising multi-body dynamics and/or finite element method.

Linear biodynamic models may generally be viewed as quantitative models, irrespective of the form and the application. These models were formed with the mechanical properties of the human body (e.g., the dynamic stiffness of the tissue, muscle kept unchanged during the vibration time history and frequency). The determination of these parameters was largely dependent on the response that the model was proposed to represent. Although some of these models (e.g., Kitazaki and Griffin, 1997; Pankoke *et al.*, 1998) adopted part of the tissue properties estimated from anthropometric measurement, parameter identification with various curve fitting methods was widely used. In this sense, models are more quantitative than mechanistic.

For some instances a quantitative model could be also mechanistic or effect ones. Although parameters were often determined via curve fitting, linear models are also able to help improve the understanding of the vibration modes or the properties-response relationship. Multi-body models (e.g., Matsumoto and Griffin, 2001; Kim *et al*., 2003) and the simple finite element models (e.g., Kitazaki and Griffin, 1997) which extracted the vibration modes of the human body helped identify the contribution of the movement of the torso to the driving point impedance. By fitting a lumped-parameter model to the apparent mass with vertical excitation at various magnitudes (Mansfield, 1998), the vertical stiffness connecting the human body and the seat surface was found to be decrease, implying the softening effect of the human tissue. Similarly, the fitting of a single degree-of–freedom model to the vertical apparent masses of seated subjects suggested that the increasing stiffness of the supporting tissue was responsible for the increase in the peak magnitude of the apparent mass with backrest contact compared to that without backrest (e.g., Toward and Griffin, 2010). In this sense, quantitative models could be mechanistic models or effect models.

The multi-body biodynamic models developed so far have been based solely on the apparent mass in the direction of excitation (Session 2.7.3). There are no known multi-body models representing both the in-line apparent mass and the cross-axis apparent mass of the seated human body.

From the reviewed literature, it is also known that published models for seat-occupant system are limited to a single input (Section 2.7). This is different from the actual case where passengers and drivers in vehicles are normally exposed to multi-axis vibration. Therefore, models developed in the reported studies so far cannot meet the requirements of analysis of ride dynamics, for example, prediction of the vibration

transmitted to a driver or passengers through seats in a car travelling on a road. Some studies have measured the apparent mass when the human body was exposed to vertical and horizontal vibration. However, models with dual-axis excitation have not been seen.

Nonlinear models were proposed with the intention of representing the mechanism of the observed nonlinearity (e.g., Section 2.7.3 and Section 2.7.4). These models were developed with the assumption that the tissue properties (e.g., stiffness and damping) are frequency-dependent or magnitude-dependent (e.g., dependent on the displacement or velocity). Displacement-dependent stiffness has been reported for a compressed sample of foam (e.g., Ippili *et al.*, 2008) and muscle (e.g., Saraf *et al.*, 2007). Sensible predictions of the pressure distribution on an occupied soft seat were provided with a finite element model of the buttocks which included linear skin, rigid bony structure and nonlinear hyperelastic isotropic soft tissue (Verver, 2004). However, it is not known that whether the nonlinear force-deflection properties of tissue based on the quasi-static compression (i.e., the loading is so slow that the inertial effects could be ignored) is efficient in representing the variation in the resonance in the dynamic response (e.g., vertical apparent mass) with dynamic excitation at different magnitudes.

2.8.3 The research scope of the thesis

In the light of the state of knowledge summarised in this chapter, the research undertaken for this thesis was conducted to answer the following questions:

(1) What are the effects of vibration magnitude and the addition of an orthogonal excitation on the principal resonance in the apparent mass, the transmissibility of the body, and the association between the apparent mass and the transmissibility?

(2) By what mechanism does sitting posture affect the resonance in the apparent mass and transmissibility and their association with single-axis and dual-axis vibration excitation?

(3) Can a multi-body model characterize the vertical in-line apparent mass, the fore-and-aft cross-axis apparent mass, and the body transmissibility with dual-axis vibration excitation?

(4) What necessary complexity of a finite element model is needed in order to predict the apparent mass and the transmissibility of the body, the pressure distribution at the seat and the nonlinearities in the biodynamic responses?

CHAPTER 3: AN ANALYTIC MODEL OF THE IN-LINE AND CROSS-AXIS APPARENT MASS OF THE SEATED HUMAN BODY EXPOSED TO VERTICAL VIBRATION WITH AND WITHOUT BACKREST

3.1 Introduction

Exposure to whole-body vibration can affect the health, performance, and comfort of seated people, with most problems caused by low frequency vibration (e.g. less than 30 Hz). Understanding of biodynamic responses to whole-body vibration (e.g., the apparent mass and transmissibility of the body) can assist understanding of the effects of vibration on health, performance, and comfort, and the optimisation of seating dynamics.

The biodynamic responses of the seated human body to vertical vibration excitation have been measured experimentally and some of the results summarised in International Standard 5982 (2001). Factors responsible for differences in the biodynamic responses of different people (i.e., inter-subject variability) and variations within a person (i.e., intra-subject variability) have also been investigated. Experimental studies suggest that the main factors influencing the vertical apparent mass of the body (i.e., the complex ratio of the vertical force and the vertical acceleration measured at the supporting seat surface) are body weight (Fairley and Griffin, 1989; Toward and Griffin, 2010), sitting posture (Fairley and Griffin, 1989; Mansfield and Griffin, 2002), vibration magnitude (Fairley and Griffin, 1989; Qiu and Griffin, 2010), vibration spectra (Toward, 2002; Mansfield and Maeda, 2005), and age (Fairley and Griffin, 1989; Toward and Griffin, 2010). Some studies have found that support for the feet (Nawayseh and Griffin, 2004; Toward and Griffin, 2010) and holding a steering wheel (Wang *et al*., 2004; Toward and Griffin, 2010) can also influence the forces measured at the seat.

The vertical apparent mass of the seated human body is greatest around 5 Hz. The apparent mass is approximately proportional to subject mass, and so inter-subject variability in apparent mass can be greatly reduced by dividing the apparent mass by the sitting mass, to produce what is called the “normalized apparent mass” (Fairley and Griffin, 1989). In ISO 5982 (2001) the effect of body mass on apparent mass is acknowledged by grouping data according to body mass (i.e., 55 kg, 75 kg and 90 kg).

In addition to a vertical (i.e., in-axis) response to vertical excitation, there is also a fore-and-aft (i.e., cross-axis) response, evident in fore-and-aft forces at the seat and the backrest during vertical excitation (Nawayseh and Griffin, 2004).

Backrests affect biodynamic responses to whole-body vibration, with several possible explanations: (i) because they influence sitting posture and the geometry of the spine, (ii) because they support some of the weight of the upper-body, (iii) because they constrain the movement of the upper-body, and (iv) because they provide an additional vibration input to the body (Fairley and Griffin, 1990). The principal resonance frequency in the vertical apparent mass of the body tends to increase when the back is supported by a backrest, and the apparent mass is increased at frequencies greater than the resonance frequency but reduced at lower frequencies, consistent with some of the body weight being supported by the backrest (Fairley and Griffin, 1989; Nawayseh and Griffin, 2004, Toward and Griffin, 2010). A backrest may constrain a vibration mode around 1 Hz: the first resonance in the fore-and-aft cross-axis apparent mass observed without a backrest can be eliminated by a backrest (Qiu and Griffin, 2010).

Various forms of biodynamic model have been developed to represent the driving point apparent mass and the transmissibility of the body. The types of models can be roughly classified as lumped-parameter models, multi-body models, and finite-element models. Simple lumped-parameter models are capable of predicting the modulus and phase of the in-line vertical apparent mass, and provide reasonable agreement to measured values up to about 20 Hz when using only a single degree-of-freedom, and very close agreement when using two degrees-of-freedom (Wei and Griffin, 1998). Although easy to develop and calibrate, lumped-parameter models are limited to one dimensional analysis, and so they do not allow the representation of the motion of body segments.

To accommodate the rotation of body segments during vertical excitation, combined lumped-mass and rigid body models have been developed with rotational degrees-of-freedom (Matsumoto and Griffin, 2001; Nawayseh and Griffin, 2009; Qiu and Griffin, 2010). These models do not represent all the motions of body segments but they can simulate both the pitch movement of the upper torso and the translational movement of the lower body. Multi-body dynamic models have been developed with rigid bodies interconnected by rotational joints so as to reflect attributes of the anatomical segments of the human body and simulate vertical, fore-and-aft, and rotational body motion (Kim *et al*., 2003; Liang *et al*., 2008). The multi-body models developed so far have been based solely on the apparent mass in the direction of excitation. There are no known multi-body models representing both the in-line apparent mass and the cross-axis apparent mass of the seated human body.

The objective of this study was to develop a multi-body dynamic model of the vertical and fore-and-aft responses of the human body exposed to vertical excitation while sitting in a normal upright posture on a rigid seat with or without a backrest. The purpose was to identify the characteristics of a model needed to reflect both the vertical in-line apparent mass and the fore-and-aft cross-axis apparent mass on the seat and consider the contributions of the principal body segments to the dynamic responses, especially the primary resonance.

The calibration of the model in this study was based on previously reported experimental data (Nawayshe and Griffin, 2004; Qiu and Griffin, 2010). Nawayseh and Griffin (2004) exposed 12 subjects with four different thigh contact conditions to random vertical vibration at four magnitudes in the frequency range 0.25 to 20 Hz. The subjects adopted a normal upright sitting posture and leaned against a rigid flat vertical backrest. The median apparent mass at the seat and at the backs of the 12 subjects sitting with average thigh contact was used for model calibration. Qiu and Griffin (2010) exposed 12 subjects to random vertical vibration (0.2 to 20 Hz) in all 15 possible combinations of four vibration magnitudes of fore-and-aft excitation (0, 0.25, 0.5, 1.0 ms^{-2} r.m.s.) and the same four magnitudes of vertical excitation. The subjects sat in a normal upright posture with hands on their laps and average thigh contact on a rigid horizontal seat without backrest. Force and acceleration were measured on the seat in both the vertical and fore-and-aft directions. The median vertical apparent mass and the median fore-and-aft apparent mass of the 12 subjects were used to calibrate the model developed here.

3.2 The human body model without backrest

3.2.1 Model description

A dynamic model of the body with the capacity of being extended to simulate the effect of backrest contact must include segments representing appropriate anatomical parts of the back and be capable of accommodating both translational and rotational movements of these segments. The body developed in this study was represented by five rigid bodies based on the body segments defined by Dempster (1967): upper body, middle body, pelvis, thighs, and legs. Although simplified, the model is intended to represent the gross anatomy of the body.

The upper body was associated with the thoracic spine and combined the thorax, head, neck, and upper limbs. The motions of the head and seat-to-head transmissibility were

not of primary interest, so the head and the neck were not included as separate entities in the model. The middle body was associated with the lumbar spine and can be considered to include the abdomen with the viscera. The pelvis was associated with the segment starting from the fifth lumbar vertebrae to the ischial tuberosities.

Three inter-connected rigid bodies represented the thoracic spine (upper body), lumbar spine (middle body), and pelvis. The spinal curvature represented by the initial inclination of these three segments was based on measurements by Kitazaki and Griffin (1997) for a normal upright posture. Between the joints, the spine was assumed to be straight, assuming bending deformation between individual vertebrae was small and could be represented by rotation between the three rigid bodies. The vertebrae and disks were not modelled because the model was not designed to predict spinal forces.

The mass and mass moment of inertia of the thighs was adjusted to account for the inertia of the hands and forearms that were assumed to rest on the thighs. The feet were included with the segment representing the legs.

The five rigid bodies were inter-connected by pin joints, assuming no translational movements between the bodies. The axial and the shear deformations of the pelvis and thigh tissue at the seat-occupant interface were simulated using linear springs and dampers. Friction force on the seat-occupant interface was neglected assuming that there was no relative motion between the seat and the human body. The model is shown in Figure 3.1.

3.2.2 Geometry and inertial properties

The length of each segment of the model was expressed as a percentage of stature and based on data from Dempster *et al.* (1967) and a NASA Reference Publication (1978). The mass of each rigid body was assumed to be uniform, so that the mass was located at the centre of the body. The location of each centre of mass, expressed as the distance from the proximal end to the centre of mass, was also based on Dempster *et al.* (1967). The length and centre of mass of each body segment are listed in Table 3.1, where H is the body stature (assumed to be 1.73 m, the median stature of the 12 subjects in the experiment by Qiu and Griffin (2010).

The mass of each segment expressed as a percentage of total body mass was mainly based on data in the NASA Reference Publication (1978). No data are available for the individual moments of inertia of the lumbar region or the upper torso.

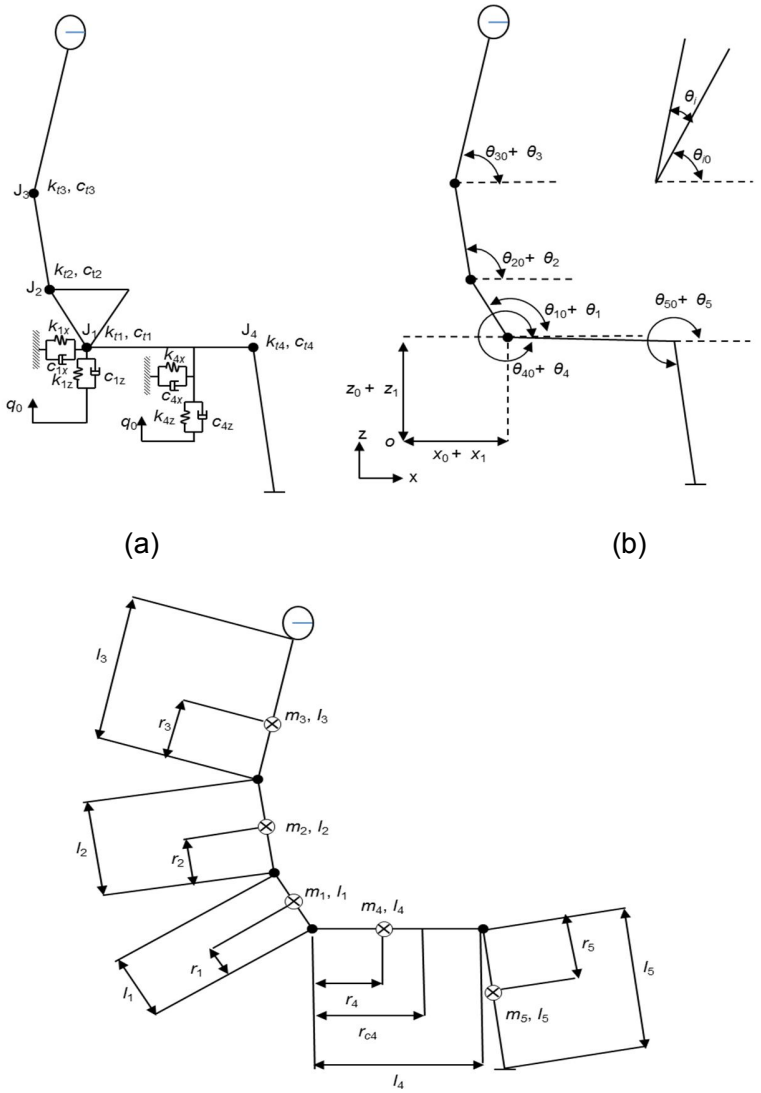

Figure 3.1 A two-dimensional multi-body biomechanical model of the human body in the normal upright posture: (a) mechanical properties; (b) motion description in arbitrary position. J_i, i = 1, 2, 3, and 4: pin joint simulated with rotational spring k_{ti} and damper c_{ti}; k_{1x}, c_{1x}, shear stiffness and damping of pelvis tissue; k_{1z}, c_{1z}, axial stiffness and damping of pelvis tissue; k_{4x}, c_{4x}, shear stiffness and damping of thigh tissue; k_{4z}, c_{4z}, axial stiffness and damping of thigh tissue; q_0; vertical vibration. θ_{i0}, i=1, 2, 3, 4, 5, initial inclination of each body segment; θ_i, small oscillation of each segment with respect to initial position; the thighs were inclined down at the front by 10° and the lower legs were inclined at 10° to the vertical; (c) geometry and inertia properties, l_i and r_i, i=1, 2, 3, 4, 5, are the lengths and centres of mass of each segment , r_{c4} is the contact p point at the thigh to be determined, m_i, I_i, i=1, 2, 3, 4, 5, are the masses and moments of inertia of each rigid body.

The initial values of the moments of inertia for these segments were estimated from reported values for the total torso, head and neck (Dempster *et al.*, 1967). The data were

then adjusted by comparing the predicted and the measured values of the apparent mass and the cross-axis apparent mass.

The assumed mass ratios and moments of inertia of each segment are listed in Table 3.2, where *M* is the total body mass (assumed to be 68.6 kg), and the median total mass of the 12 subjects in the experiment by Qiu and Griffin (2010).

Table 3.1 Initial lengths of body parts and centres of mass.

	Length (m)	centre of mass
Pelvis (l_1)	0.08*H*	0.71l_1
Middle body (l_2)	0.17*H*	0.55l_2
Upper body (l_3)	0.23*H*[a]	0.50l_3
Thighs (l_4)	0.20*H*	0.43l_4
Legs (l_5)	0.21*H*	0.43l_5

[a], length of craniocervical link and thoracic link.

Table 3.2 Initial masses and second moments of inertia.

	Mass (*M*=68.6 kg)		moment of inertia (kg m^2)
Pelvis (m_1)	0.13*M*	8.900	0.025
Middle body (m_2)	0.16*M*	10.97	0.12
Upper body (m_3)	0.33*M* [b]	22.63	1.28 [d]
Thighs (m_4)	0.26*M* [c]	17.56	0.45
Legs (m_5)	0.12*M*	8.51	0.13

[b], mass including upper arms;

[c], mass including forearms and hands;

[d], moments of inertia taking into account of additional effect of forearms and hands.

3.2.3 Equations of motion

It was assumed that all springs and dampers were linear and that the human body vibrated with small oscillation around the equilibrium position. The model has seven-degrees-of-freedom: x_1, the horizontal displacement of the pelvis joint; z_1, the vertical displacement of the pelvis joint; θ_1, the absolute rotational deflection of the pelvis; θ_2, the absolute rotational deflection of the middle body; θ_3, the absolute rotational deflection of the upper-body; θ_4, the absolute rotational deflection of the thigh; θ_5, the absolute rotational deflection of the leg.

The equations of motion of the model were derived using the Lagrange formulation. The kinetic energy, T, potential energy, U, dissipation function, D, and generalized forces, Q, of the system are:

$$T = \frac{1}{2}\sum_{i=1}^{5} m_i(\dot{x}_{ri}^2 + \dot{z}_{ri}^2) + \frac{1}{2}\sum_{i=1}^{5} I_i\dot{\theta}_i^2,$$

$$U = \frac{1}{2}(k_{1x}x^2{}_1 + k_{4x}x^2{}_{r_{c4}}) + \frac{1}{2}(k_{1z}(z_1 - q_0)^2 + k_{4z}(z_{r_{c4}} - q_0)^2) + \frac{1}{2}k_{t1}(\theta_1 + \theta_4)^2 + \frac{1}{2}k_{t2}(\theta_1 - \theta_2)^2 + \frac{1}{2}k_{t3}(\theta_2 - \theta_3)^2 + \frac{1}{2}k_{t4}(\theta_4 + \theta_5)^2$$

,

$$D = \frac{1}{2}(c_{1x}\dot{x}_1^2 + c_{4x}\dot{x}_{r_{c4}}^2) + \frac{1}{2}(c_{1z}(\dot{z}_1 - \dot{q}_0)^2 + c_{4z}(\dot{z}_{r_{c4}} - \dot{q}_0)^2) + \frac{1}{2}c_{t1}(\dot{\theta}_1 + \dot{\theta}_4)^2 + \frac{1}{2}c_{t2}(\dot{\theta}_1 - \dot{\theta}_2)^2 + \frac{1}{2}c_{t3}(\dot{\theta}_2 - \dot{\theta}_3)^2 + \frac{1}{2}c_{t4}(\dot{\theta}_4 + \dot{\theta}_5)^2$$

G_i=0, i=1, 2, 3, 4,5,6,7. (3.1)

Where, m_i i=1, 2, 3, 4, 5, are the masses of each rigid body and x_{ri} and z_{ri}, i=1, 2, 3, 4, 5, are the position vectors of the centres of gravity of each rigid body.

$x_{r_1} = x_1 + r_1\cos\theta_1$, $z_{r_1} = z_1 + r_1\sin\theta_1$;

$x_{r_2} = x_1 + l_1\cos\theta_1 + r_2\cos\theta_2$, $z_{r_2} = z_1 + l_1\sin\theta_1 + r_2\sin\theta_2$;

$x_{r_3} = x_1 + l_1\cos\theta_1 + l_2\cos\theta_2 + r_3\cos\theta_3$, $z_{r_3} = z_1 + l_1\sin\theta_1 + l_2\sin\theta_2 + r_3\sin\theta_3$;

$x_{r_4} = x_1 + r_4\cos\theta_4$, $z_{r_4} = z_1 + r_4\sin\theta_4$;

$x_{r_5} = x_1 + l_4\cos\theta_4 + r_5\cos\theta_5$, $z_{r_5} = z_1 + l_4\sin\theta_4 + r_5\sin\theta_5$;

$x_{r_{c4}} = x_1 + r_{c4}\cos\theta_4$, $z_{r_{c4}} = z_1 + r_{c4}\sin\theta_4$. (3.2)

Where k_{ti}, i=1, 2, 3, 4, are rotational springs; c_{ti}, i=1, 2, 3, 4, are rotational dampers; k_{1x} and c_{1x} are the horizontal stiffness and damping of the pelvis tissue; k_{1z} and c_{1z} are the vertical stiffness and damping of the pelvis tissue; k_{4x} and c_{4x} are the horizontal stiffness and damping of the thigh tissue; k_{4z} and c_{4z} are the vertical stiffness and the damping of the thigh tissue (Figure 3.1); l_i and r_i, i=1, 2, 3, 4, 5, are the lengths and centres of mass of each segment (Table 3.1); r_{c4} is the contact point at the thigh to be determined. The nonlinearity due to the nonlinear geometry shown in the equations above was simplified by performing Taylor's expansion with respect to the static equilibrium position assuming that there was only small oscillation during vibration. The linearization was carried out on the basis of the approximation below:

$$\sin\theta = \sin(\theta_0 + \theta') \approx \sin\theta_0 + \cos\theta_0 * \theta', \cos\theta = \cos(\theta_0 + \theta') \approx \cos\theta_0 - \sin\theta_0 * \theta'. \quad (3.3)$$

Where θ_{i0}, i=1, 2, 3, 4, 5, are the initial inclinations of each rigid body.

Equation (3.2) was reproduced as follows:

$$x_{r_1} = x_1 + r_1\cos\theta_{10} - \theta'_1 r_1 \sin\theta_{10},\ z_{r_1} = z_1 + r_1\sin\theta_{10} + \theta'_1 r_1\cos\theta_{10};$$

$$x_{r_2} = x_1 + l_1\cos\theta_{10} + r_2\cos\theta_{20} - \theta'_1 l_1\sin\theta_{10} - \theta'_2 r_2\sin\theta_{20};$$

$$z_{r_2} = z_1 + l_1\sin\theta_{10} + r_2\sin\theta_{20} + \theta'_1 l_1\cos\theta_{10} + \theta'_2 r_2\cos\theta_{20};$$

$$x_{r_3} = x_1 + l_1\cos\theta_{10} + l_2\cos\theta_{20} + r_3\cos\theta_{30} - \theta'_1 l_1\sin\theta_{10} - \theta'_2 l_2\sin\theta_{20} - \theta'_3 r_3\sin\theta_{30};$$

$$z_{r_3} = z_1 + l_1\sin\theta_{10} + l_2\sin\theta_{20} + r_3\sin\theta_{30} + \theta'_1 l_1\cos\theta_{10} + \theta'_2 l_2\cos\theta_{20} + \theta'_3 r_3\cos\theta_{30};$$

$$x_{r_4} = x_1 + r_4\cos\theta_{40} - \theta'_4 r_4\sin\theta_{40},\ z_{r_4} = z_1 + r_4\sin\theta_{40} + \theta'_4 r_4\cos\theta_{40};$$

$$x_{r_5} = x_1 + l_4\cos\theta_{40} + r_5\cos\theta_{50} - \theta'_4 l_4\sin\theta_{40} - \theta'_5 r_5\sin\theta_{50};$$

$$z_{r_5} = z_1 + l_4\sin\theta_{40} + r_5\sin\theta_{50} + \theta'_4 l_4\cos\theta_{50} + \theta'_5 r_5\cos\theta_{50};$$

$$x_{r_{c4}} = x_1 + r_{c4}\cos\theta_{40} - \theta'_4 r_{c4}\sin\theta_{40},\ z_{r_{c4}} = z_1 + r_{c4}\sin\theta_{40} + \theta'_4 r_{c4}\cos\theta_{40}. \qquad (3.4)$$

The Equation (3.4) was written in the matrix format as follows:

$$\begin{bmatrix} x_{r1} \\ z_{r1} \\ x_{r2} \\ z_{r2} \\ x_{r3} \\ z_{r3} \\ x_{r4} \\ z_{r4} \\ x_{r4} \\ z_{r4} \\ x_{r_{c4}} \\ z_{r_{c4}} \end{bmatrix} = \begin{bmatrix} 1 & 0 & -r_1\sin\theta_{10} & 0 & 0 & 0 & 0 \\ 0 & 1 & r_1\cos\theta_{10} & 0 & 0 & 0 & 0 \\ 1 & 0 & -l_1\sin\theta_{10} & -r_2\sin\theta_{20} & 0 & 0 & 0 \\ 0 & 1 & l_1\cos\theta_{10} & r_2\cos\theta_{20} & 0 & 0 & 0 \\ 1 & 0 & -l_1\sin\theta_{10} & -l_2\sin\theta_{20} & -r_3\sin\theta_{30} & 0 & 0 \\ 0 & 1 & l_1\cos\theta_{10} & l_2\cos\theta_{20} & r_3\cos\theta_{30} & 0 & 0 \\ 1 & 0 & 0 & 0 & 0 & -r_4\sin\theta_{40} & 0 \\ 0 & 1 & 0 & 0 & 0 & r_4\cos\theta_{40} & 0 \\ 1 & 0 & 0 & 0 & 0 & -l_4\sin\theta_{40} & -r_5\sin\theta_{50} \\ 0 & 1 & 0 & 0 & 0 & l_4\cos\theta_{40} & r_5\cos\theta_{50} \\ 1 & 0 & 0 & 0 & 0 & -r_{c4}\sin\theta_{40} & 0 \\ 0 & 1 & 0 & 0 & 0 & r_{c4}\cos\theta_{40} & 0 \end{bmatrix} \begin{bmatrix} x_1 \\ z_1 \\ \theta'_1 \\ \theta'_2 \\ \theta'_3 \\ \theta'_4 \\ \theta'_5 \end{bmatrix} + \begin{bmatrix} r_1\cos\theta_{10} \\ r_1\sin\theta_{10} \\ l_1\cos\theta_{10} + r_2\cos\theta_{20} \\ l_1\sin\theta_{10} + r_2\sin\theta_{20} \\ l_1\cos\theta_{10} + l_2\cos\theta_{20} + r_3\cos\theta_{30} \\ l_1\sin\theta_{10} + l_2\sin\theta_{20} + r_3\sin\theta_{30} \\ r_4\cos\theta_{40} \\ r_4\sin\theta_{40} \\ l_4\cos\theta_{40} + r_5\cos\theta_{50} \\ l_4\sin\theta_{40} + r_5\sin\theta_{50} \\ r_{c4}\cos\theta_{40} \\ r_{c4}\sin\theta_{40} \end{bmatrix} \qquad (3.5)$$

The equations of motion for every generalized coordinate were obtained by substituting Equations (3.1) and (3.4) into Lagrange formulation and performing partial differentiation individually:

$$\frac{d}{dt}\left(\frac{\partial T}{\partial \dot{q}_r}\right)-\frac{\partial T}{\partial q_r}+\frac{\partial U}{\partial q_r}+\frac{\partial D}{\partial \dot{q}_r}=0\,. \tag{3.6}$$

It is noted that only small oscillations of human body with respect to its equilibrium position are considered. The change in the height of centre of gravity is thus very small. The potential energy associated with gravity is ignored in the potential energy U in Equation (3.1).

Laplace transformation was performed to yield the equations of motion in the s-domain. The ratio of the Laplace transforms of each fore-and-aft, vertical and pitch displacement corresponding to the generalized coordinates of the model and the base displacement in the s-domain were obtained, and denoted as $Q_1(s)$, $Q_2(s)$, $Q_3(s)$, $Q_4(s)$, $Q_5(s)$, $Q_6(s)$ and $Q_7(s)$ (see Appendix A).

The apparent mass, the complex ratio of the resultant force to the acceleration on the seat surface, was then derived.

The vertical apparent mass of the model was formulated as follows:

$$M_z(s)=\frac{F_z(s)}{A_0(s)}=\frac{(k_{1z}+c_{1z}s)(Q_2-1)+(k_{4z}+c_{4z}s)(Q_2+\cos\theta_{40}r_{c4}Q_6-1)}{s^2}\,. \tag{3.7}$$

where F_z(s) is the vertical force on the seat surface, $A_0(s)$ is the base acceleration.

The fore-and-aft cross-axis apparent mass of the model was formulated as follows:

$$M_z(s)=\frac{F_x(s)}{A_0(s)}=\frac{(k_{1x}+c_{1x}s)Q_1+(k_{4x}+c_{4x}s)(Q_1-\sin\theta_{40}r_{c4}Q_6)}{s^2}\,. \tag{3.8}$$

where $F_x(s)$ is the fore-and-aft force on the seat surface.

3.2.4 Identification of the parameters of the nominal model

The parameters shown in Table 3.3 to Table 3.5 were identified by optimisation using the 'fmincon' function in MATLAB (version 2009b). The optimization procedure identified the model parameters that minimized the mean square errors between the computed and measured median modulus and phase of the vertical apparent mass and the computed and measured modulus and phase of median fore-and-aft cross-axis apparent mass at the seat over the frequency range of 0.3 to 20 Hz. The measured apparent mass data were those obtained by Qiu and Griffin (2010).

$$E(\lambda)=\min(E_{M_z}(\lambda)+E_{M_x}(\lambda)+w_1*E_{pM_z}(\lambda)+w_2*E_{pM_x}(\lambda))^{1/2}\,, \tag{3.9}$$

where $E_{M_z}(\lambda)$ and $E_{M_x}(\lambda)$ are sums of squared-errors of modulus of vertical apparent mass and fore-and-aft cross-axis apparent mass; $E_{pM_z}(\lambda)$ and $E_{pM_x}(\lambda)$ are sums of squared-errors of phase of vertical apparent mass and fore-and-aft cross-axis apparent mass ; w_1 and w_2 are weighting factors for the phase.

$$E_{M_z}(\lambda) = \frac{1}{N}\sum_{i=1}^{N}\left(\left|M_{z_c}(f_i)\right| - \left|M_{z_t}(f_i)\right|\right)^2 ,$$

$$E_{M_x}(\lambda) = \frac{1}{N}\sum_{i=1}^{N}\left(\left|M_{xi_c}(f_i)\right| - \left|M_{xi_t}(f_i)\right|\right)^2 ,$$

$$E_{pM_z}(\lambda) = \frac{1}{N}\sum_{i=1}^{N}\left(pM_{z_c}(f_i) - pM_{z_t}(f_i)\right)^2 ,$$

$$E_{pM_z}(\lambda) = \frac{1}{N}\sum_{i=1}^{N}\left(pM_{x_c}(f_i) - pM_{x_t}(f_i)\right)^2 . \qquad (3.10)$$

where:

$M_{z_c}(f_i)$ is the calculated vertical apparent mass at vibration frequency f_i

$M_{z_t}(f_i)$ is the median measured vertical apparent mass at vibration frequency f_i

$M_{x_c}(f_i)$ is the calculated fore-and-aft cross-axis apparent mass at vibration frequency f_i

$M_{x_t}(f_i)$ is the median measured fore-and-aft cross-axis apparent mass at vibration frequency f_i

$pM_{z_c}(f_i)$ is the calculated phase of vertical apparent mass at vibration frequency f_i

$pM_{z_t}(f_i)$ is the median measured phase of vertical apparent mass at vibration frequency f_i

$pM_{x_c}(f_i)$ is the calculated phase of fore-and-aft cross-axis apparent mass at vibration frequency f_i

$pM_{x_t}(f_i)$ is the median measured phase of fore-and-aft cross-axis apparent mass at vibration frequency f_i

N is the number of data samples containing the measured apparent mass in the frequency range 0.3 to 20 Hz.

$\boldsymbol{\lambda}$ is the vector of the mechanical parameters of the model to be optimized. A total of 21 parameters were involved in the optimization procedure, with $\boldsymbol{\lambda}$ given by:

$$\boldsymbol{\lambda}=[m_1, m_2, m_3, m_4, m_5, k_{1z}, c_{1z}, k_{1x}, c_{1x}, k_{4z}, c_{4z}, k_{4x}, c_{4x}, k_{t1}, c_{t1}, k_{t2}, c_{t2}, k_{t3}, c_{t3}, k_{t4}, c_{t4}]^{T}. \quad (3.11)$$

The error in the vertical in-line apparent mass and the error in the fore-and-aft cross-axis apparent mass were assigned the same weighting factors, so that they contributed equally to the total error. Although the measured vertical apparent mass was greater than the measured cross-axis fore-and-aft apparent mass, varying the weighting factors had little effect on the outcome. Weighting factors for the phase (w_1 and w_2) are always greater than 1 because the values of the phase are much less than the apparent mass.

Appropriate guesses for the initial parameters were required for the optimization program to converge. A set of mechanical parameters was chosen by referring to reported studies and adjusted after each optimization run. The optimization of mass was commenced with the initial values listed in Table 3.2. Limits for each variable were adjusted during optimization. The optimized mechanical parameters obtained for the nominal model are shown in Table 3.3 and Table 3.4.

Table 3.3 Translational stiffness and damping.

Stiffness (N m^{-1})			Damping (Ns m^{-1})		
	Initial	optimized		initial	optimized
k_{1z}	117000	125000	c_{1z}	42	83
k_{1x}	65	48	c_{1x}	34	41
k_{4z}	19000	14000	c_{4z}	2500	1010
k_{4x}	58	95	c_{4x}	44	52

The adjusted mass is listed in Table 3.5. A large increase in the mass of thighs m_4, and a reduction in the mass of upper body, m_3, was observed. This indicates that the centre of gravity of the upper body (i.e., body 3) locates above the thighs so much of the weight of the arms and a portion of the weight of the thoracic cavity may have been supported on the thighs.

The modulus and phase of the predicted in-line vertical apparent mass and the cross-axis fore-and-aft apparent mass are compared with the median measured values in Figure 3.2.

Table 3.4 Rotational stiffness and damping.

Stiffness (Nm rad^{-1})			Damping (Nms rad^{-1})		
	initial	optimized		initial	optimized
k_{t1}	1000	1400	c_{t1}	368	250
k_{t2}	110	180	c_{t2}	124	82
k_{t3}	930	830	c_{t3}	306	130
k_{t4}	150	140	c_{t4}	2004	2050

Table 3.5 Adjusted mass of each segment for the human body model without backrest.

m^e_1 (kg)	m^e_2 (kg)	m^e_3 (kg)	m^e_4 (kg)	m^e_5 (kg)
8.00	11.30	15.70	27.00	6.60

^{e}, Adjusted mass of each segment.

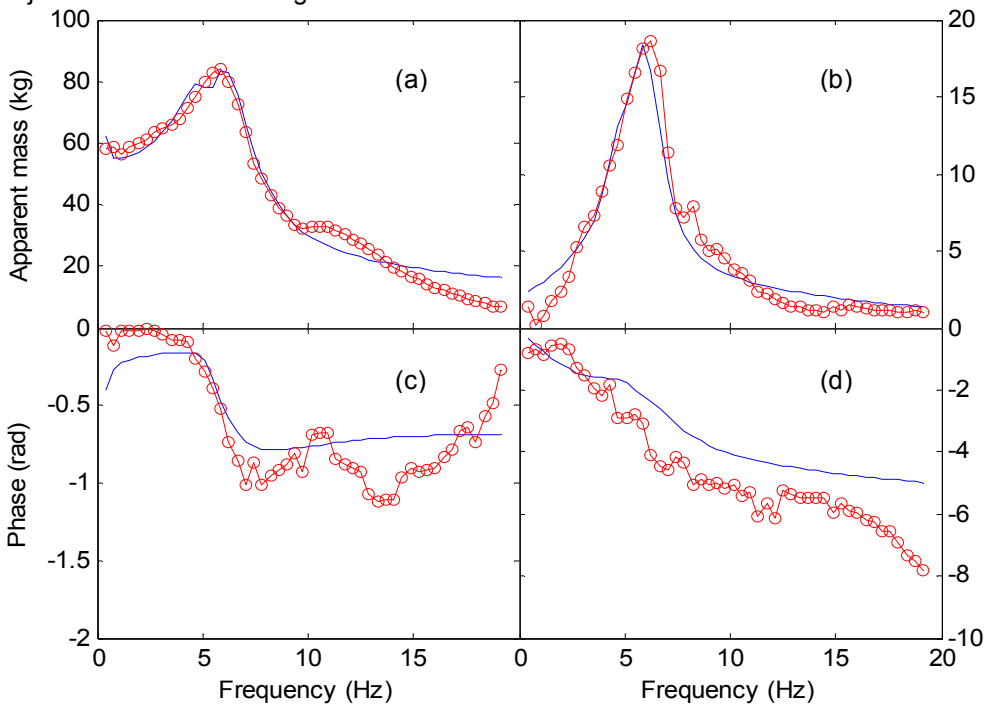

Figure 3.2 Comparisons between the predicted and measured vertical apparent mass and fore-and-aft cross-axis apparent mass of the human body without backrest: ——, predicted value; —O—, measured value. (a) Modulus of the vertical apparent mass on the seat; (b) modulus of the fore-and-aft cross-axis apparent mass on the seat; (c) phase of the vertical apparent mass on the seat; (d) phase of the fore-and-aft cross-axis apparent mass on the seat.

The first peaks in the predicted vertical apparent mass and the fore-and-aft cross-axis apparent mass are in the region of 5 Hz, similar to the measured apparent values. Although the modulus and phase of the vertical apparent mass are in reasonable agreement with the experimental data, they do not show a second resonance around 13 Hz evident in the experiment data. The primary resonance frequency of predicted cross-axis apparent mass was 5.47 Hz, slightly lower than the measured value 5.86 Hz, but the fore-and-aft cross-axis apparent mass was generally consistent with the experimental values over the frequency range up to 20 Hz.

3.2.5 Parameter sensitivity of the human body model

A matrix for the parameter sensitivity analysis of the body model was adopted (Ju *et al*., 1987):

$$P_{ij} = \frac{\Delta R_i / R_i}{\Delta {}^{j}\psi \ / {}^{j}\psi} \ , \qquad (3.12)$$

where, $\mathbf{\Psi}=[k_{1z}, c_{1z}, k_{1x}, c_{1x}, k_{4z}, c_{4z}, k_{4x}, c_{4x}, k_{t1}, c_{t1}, k_{t2}, c_{t2}, k_{t3}, c_{t3}, k_{t4}, c_{t4}, m_1, m_{2,} m_3, m_4, m_5]^{\mathrm{T}}$ is the vector of the mass properties and mechanical parameters as introduced in Section 3.2.1; ${}^{j}\psi$ and $\Delta {}^{j}\psi$ represent the *j*th (*j*=1, 2, …, 21) parameter of the vector $\mathbf{\psi}$ at its nominal value and a small perturbation of that parameter; R_i represents the responses to be examined, with *i*=1 being the peak modulus of the vertical apparent mass, *i*=2 the corresponding resonance frequency, *i*=3 the peak of fore-and-aft cross-axis apparent mass, and *i*=4 the corresponding resonance frequency computed with the set of model parameters at their nominal values (the set obtained by optimisation to match the median experimental data in Qiu and Griffin, 2010); ΔR_i are the differences of the above responses between using the nominal set and the new set of parameters with the perturbation. If α is the perturbation factor (α=30% was used in this study), then $\Delta {}^{j}\psi = \alpha {}^{j}\psi$ and the new set of parameters with the perturbation is formed with ${}^{j}\psi^{new} = {}^{j}\psi + \Delta {}^{j}\psi$ whilst other parameters keep their nominal values. With this new set of model parameters, the peak apparent masses and the corresponding peak frequencies can be computed as R_i^{new} and hence ΔR_i can be calculated as $\Delta R_i = R_i^{new} - R_i$. The greater the value of P_{ij} the more sensitive the response R_i to the parameter ${}^{j}\psi$.

The resultant sensitivity matrix was:

$$\mathbf{P} = \left[\mathbf{P_{tr}} \quad \mathbf{P_{rot}} \quad \mathbf{P_m}\right]_{4\times 21}, \qquad (3.13)$$

where, $\mathbf{P_{tr}}$, $\mathbf{P_{rot}}$, and $\mathbf{P_m}$ represent the sensitivity matrices of the translational stiffness and damping of the tissue beneath the pelvis and the thighs (k_{1z}, c_{1z}, k_{1x}, c_{1x}, k_{4z}, c_{4z}, k_{4x}, c_{4x}), rotational stiffness and damping of each rigid body (k_{t1}, c_{t1}, k_{t2}, c_{t2}, k_{t3}, c_{t3}, k_{t4}, c_{t4}), and the mass of each body segment (m_1, m_2, m_3, m_4, m_5), respectively:

$$\mathbf{P_{tr}} = \begin{bmatrix} 0.359 & 0.009 & -0.002 & 0.003 & -0.056 & -0.095 & 0.000 & 0.001 \\ 0.143 & 0.000 & 0.000 & 0.000 & 0.000 & 0.071 & 0.000 & 0.000 \\ 0.019 & 0.010 & 0.021 & 0.228 & 0.038 & -0.067 & 0.004 & 0.257 \\ 0.143 & 0.000 & 0.000 & 0.000 & 0.000 & 0.071 & 0.000 & 0.000 \end{bmatrix}_{4\times 8}, \qquad (3.14)$$

In $\mathbf{P_{tr}}$, it was found that the peak magnitude of the vertical apparent mass and the corresponding resonance frequency on the seat were sensitive to parameters k_{1z} and c_{4z}.

The fore-and-aft cross-axis apparent mass on the seat was sensitive to parameters c_{4x} and c_{1x}, and the frequency at which the peak modulus of the fore-and-aft cross-axis apparent mass occurred was sensitive to parameters k_{1z} and c_{4z}, in that order. The peak of the fore-and-aft cross-axis apparent mass was increased and occurred at a higher frequency when k_{1z} was increased, while the peak of the vertical apparent mass was decreased and occurred at a higher frequency when c_{4z} was increased.

$$\mathbf{P_{rot}} = \begin{bmatrix} 0.292 & -0.030 & 0.002 & -0.271 & 0.002 & -0.064 & 0.000 & 0.017 \\ 0.071 & 0.000 & 0.000 & 0.071 & 0.000 & -0.071 & 0.000 & 0.000 \\ 0.400 & -0.017 & 0.000 & -0.018 & 0.001 & -0.019 & 0.000 & 0.038 \\ 0.071 & 0.000 & 0.000 & 0.071 & 0.000 & -0.071 & 0.000 & 0.000 \end{bmatrix}_{4\times 8}, \qquad (3.15)$$

In $\mathbf{P_{rot}}$, the peak magnitude of the vertical apparent mass and the corresponding vertical resonance frequency were sensitive to parameters k_{t1} and c_{t2}. The fore-and-aft cross-axis apparent mass on the seat and the corresponding resonance frequency were both sensitive to parameter k_{t1}.

$$\mathbf{P_m} = \begin{bmatrix} 0.090 & 0.162 & 0.102 & 0.368 & 0.109 \\ 0.000 & 0.000 & -0.071 & -0.071 & -0.071 \\ 0.008 & 0.016 & 0.000 & 0.015 & 0.297 \\ 0.000 & 0.000 & 0.000 & -0.073 & -0.143 \end{bmatrix}_{4\times 5}, \qquad (3.16)$$

In $\mathbf{P_m}$, it was found that the vertical apparent mass at the resonance frequency was sensitive to parameter m_4, and the frequency at which the peak modulus of the apparent mass occurred was equally sensitive to parameters m_3, m_4, and m_5. The fore-and-aft

cross-axis apparent mass and the corresponding resonance frequency were sensitive to parameter m_5.

3.2.6 Modal analysis of the human body model without backrest.

Mathematical modal analysis of the seated human body was performed to investigate the vibration modes that contributed to the resonance appearing in the apparent mass response.

Equations of motion can be rewritten as:

$$\mathbf{M}\ddot{\mathbf{X}} + \mathbf{C}\dot{\mathbf{X}} + \mathbf{K}\mathbf{X} = \mathbf{F}, \qquad (3.17)$$

where, $\mathbf{X}$, $\dot{\mathbf{X}}$, and $\ddot{\mathbf{X}}$ are the displacement, velocity and acceleration vectors, respectively, with seven degrees of freedom for the human body model in this study. The variables **M**, **K**, and **C** are the mass, stiffness, and damping matrices of the human body system with a size 7 X 7. The external force, **F***,* is a vector with a size 7 X1. The undamped natural frequencies of the system can be determined by calculating the eigenvalues of the matrix $\mathbf{M}^{-1}\mathbf{K}$, and the mode shape can be generated according to the eigenvectors of the matrix. Undamped mode analysis was performed for the seated human body model exposed to vertical vibration. With no damping, two modes were found in the frequency range less than 10 Hz with the single vertical input. The natural frequencies and the corresponding modal vectors are shown in Table 3.6.

Table 3.6 Undamped natural frequencies and mode shapes of model with vertical vibration.

Mode[f]	1	2
natural frequency(Hz)	1.42	5.68
pelvis horizontal	-0.050	0.122
pelvis vertical	0.006	0.172
pelvis pitch	0.752	1.000
lumbar spine pitch	-1.000	0.993
thoracic spine pitch	0.074	-0.400
thigh pitch	0.051	-0.819
leg pitch	0.147	-0.151

[f], The human body was exposed to vertical vibration at 0.5 ms^{-2} r.m.s., with feet supported on the moving footrest.

The mode shapes are illustrated in Figure 3.3. The positive mode vector values were taken as the forward and upward motion for translational degrees-of-freedom and counter-clockwise rotation for rotational degrees-of-freedom. The centre of the leg rotation was assumed to be at the feet as the feet were constrained on the footrest surface. The first mode at 1.42 Hz (Figure 3.3(a)) mainly involved a pitching motion of the pelvis out of phase with a bending mode of the lumbar spine, with axial and shear deformation of tissue beneath the pelvis.

The second mode at 5.29 Hz (Figure 3.3(b)) is assumed to be the main contributor to the primary resonance and involved body motion in both the vertical and fore-aft direction with pitch motions of the pelvis and the upper body.

By performing modal analysis of a finite element model, Kitazaki and Griffin (1997) identified seven modes of the human body seated without a backrest at frequencies less than 10 Hz. The fourth mode at 5.06 Hz appeared closely related to the primary resonance. From a human body model with five degrees-of-freedom, Matsumoto and Griffin obtained three modes at frequencies less than 10 Hz (Matsumoto and Griffin, 2001): at 2.53 Hz, 5.66 Hz and 8.62 Hz. Considering the mode shapes and natural frequencies, the modes found in this study may correspond to the second and fourth mode in the study by Kitazaki and Griffin (1997) and the first and second mode in the study by Matsumoto and Griffin (2001). The greater number of modes obtained by Kitazaki and Griffin (1997) is chiefly because the finite element method was employed. A third mode at 8.62 Hz was observed by Matsumoto and Griffin (2001) but not in the current study, possibly because different object functions were adopted in the two studies: vertical apparent mass and body transmissibility were used in the error function by Matsumoto and Griffin while vertical and fore-and-aft cross-axis apparent mass were used in this study. The viscera were ignored in the present model, although a visceral mode was found in the study by Matsumoto and Griffin (2001).

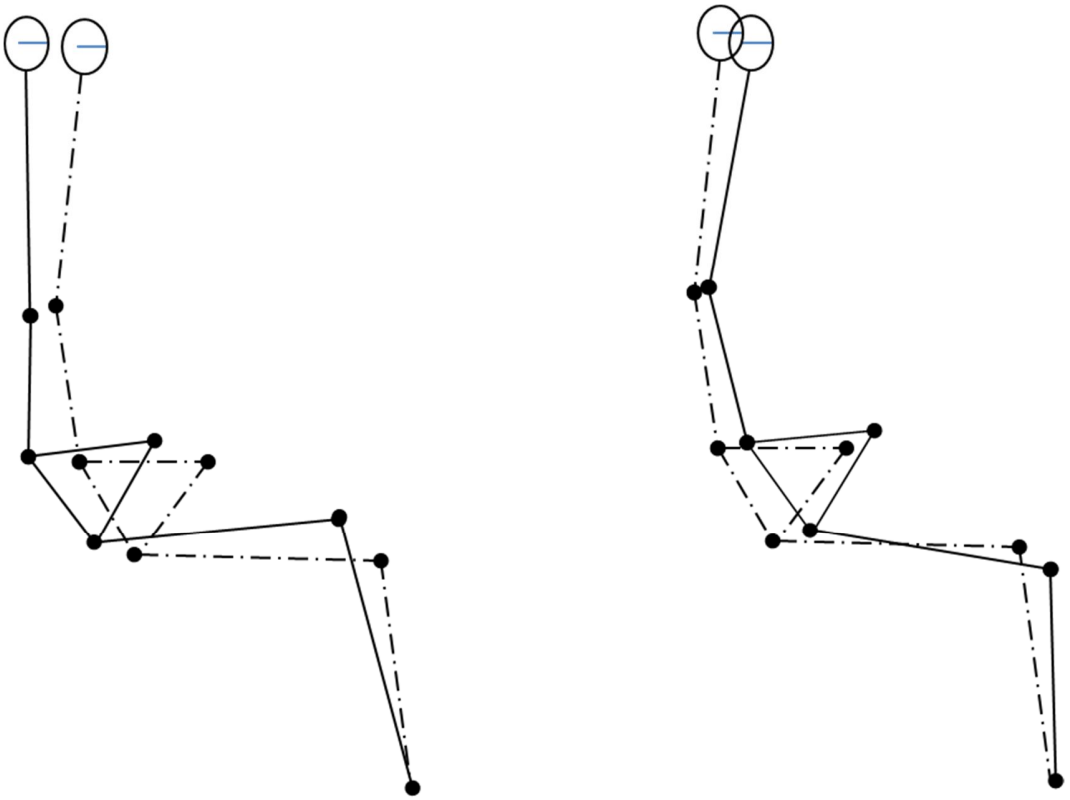

(a) (b)

Figure 3.3 Mode shapes of the human body :(a) the first mode at 1.42 Hz; (b) the second mode at 5.29 Hz; —.—, initial shape; ——, deformed shape. The scale of the mode vector values in Table 6 are exaggerated for clarity.

3.3 Human body model with a backrest

3.3.1 Model description

When supported by a backrest, the body may make contact with the back support at the lower back (e.g., pelvis and lower lumbar spine), the middle back (e.g., upper lumbar spine and lower thoracic spine), or the upper back (e.g., upper thoracic spine and shoulders). The principal contact point may depend on the posture: at the upper back with an erect posture, the middle back with a normal posture, and the lower back with a slouched posture. If the backrest is sufficiently high (or shaped or compliant), the body may make contact at several locations (e.g., lower, middle, and upper back simultaneously). In this study, the contact point was assumed to be located at the middle back.

A set of vertical and horizontal springs and dampers was used to simulate the interaction between the back and the backrest, as shown in Figure 3.4.

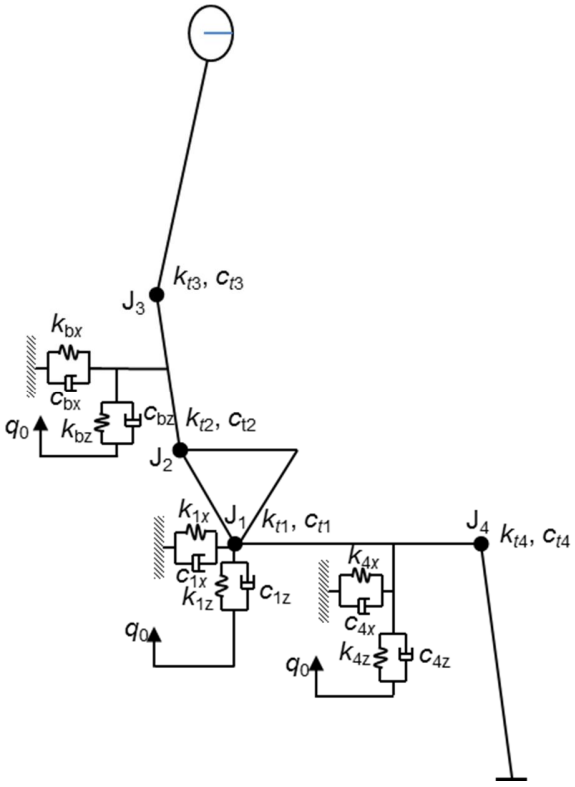

Figure 3.4 The human body model with backrest.

The spring k_{bx} and the damper c_{bx} represent the horizontal stiffness and damping of the back tissues, while k_{bz} and c_{bz} represent the vertical stiffness and damping of the back tissues. Friction forces on the seat and the backrest were neglected assuming that there was no relative motion between the seat and human body and between the backrest and the human body.

The formation of the equations of motion of the human body with the backrest was similar to the method adopted in Section 3.2.3. The kinetic energy, T, potential energy, U, dissipation function, D, and generalized forces, Q of the system are:

$$T = \frac{1}{2}\sum_{i=1}^{5} m_i(\dot{x}_{ri}^2 + \dot{z}_{ri}^2) + \frac{1}{2}\sum_{i=1}^{5} I_i\dot{\theta}_i^2$$

$$U=\frac{1}{2}(k_{1x}x^2{}_1+k_{4x}x^2{}_{r_{c4}}+k_{bx}x^2{}_{rcb})+\frac{1}{2}(k_{1z}(z_1-q_0)^2+k_{4z}(z_{r_{c4}}-q_0)^2+k_{bz}(z_{rcb}-q_0)^2)$$
$$+\frac{1}{2}k_{t1}(\theta_1+\theta_4)^2+\frac{1}{2}k_{t2}(\theta_1-\theta_2)^2+\frac{1}{2}k_{t3}(\theta_2-\theta_3)^2+\frac{1}{2}k_{t4}(\theta_4+\theta_5)^2$$
$$D=\frac{1}{2}(c_{1x}\dot{x}_1^2+c_{4x}\dot{x}_{r_{c4}}^2+c_{bx}\dot{x}_{rcb}^2)+\frac{1}{2}(c_{1z}(\dot{z}_1-\dot{q}_0)^2+c_{4z}(\dot{z}_{r_{c4}}-\dot{q}_0)^2+c_{bz}(\dot{z}_{rcb}-\dot{q}_0)^2)$$
$$+\frac{1}{2}c_{t1}(\dot{\theta}_1+\dot{\theta}_4)^2+\frac{1}{2}c_{t2}(\dot{\theta}_1-\dot{\theta}_2)^2+\frac{1}{2}c_{t3}(\dot{\theta}_2-\dot{\theta}_3)^2+\frac{1}{2}c_{t4}(\dot{\theta}_4+\dot{\theta}_5)^2$$

Q_i=0, i=1, 2, 3, 4, 5, 6, 7, (3.18)

where x_{rcb} and z_{rcb} represent the back contact location.

$$x_{rcb}=x_1+l_1\cos\theta_1+r_{cb}\cos\theta_2,\ z_{rcb}=z_1+l_1\sin\theta_1+r_{cb}\sin\theta_2. \quad (3.19)$$

Equation (3.19) was simplified by performing Taylor's expansion.

$$x_{rcb}=x_1+l_1\cos\theta_{10}+r_{cb}\cos\theta_{20}-\theta'_1 l_1\sin\theta_{10}-\theta'_2 r_{cb}\sin\theta_{20},$$
$$z_{rcb}=z_1+l_1\sin\theta_{10}+r_{cb}\sin\theta_{20}+\theta'_1 l_1\cos\theta_{10}+\theta'_2 r_{cb}\cos\theta_{20}. \quad (3.20)$$

where r_{cb} is the distance between the back contact and the lumbar joint (i.e. joint 2).

The definitions of independent coordinates (i.e., the degrees of freedom and the centres of gravity of each body segment) were the same as Equations (3.2-3.4). The analytical solutions of the apparent mass of the human body at the seat with backrest were the same as Equations (3.7-3.8), but with different expressions for $Q_1(s)$, $Q_2(s)$, $Q_3(s)$, $Q_4(s)$, $Q_5(s)$, $Q_6(s)$ and $Q_7(s)$.

3.3.2 Parameter identification

The parameter vector of the model was defined as: λ=[m_1, m_2, m_3, m_4, m_5, k_{1z}, c_{1z}, k_{1x}, c_{1x}, k_{4z}, c_{4z}, k_{4x}, c_{4x}, k_{bz}, c_{bz}, k_{bx}, c_{bx}, k_{t1}, c_{t1}, k_{t2}, c_{t2}, k_{t3}, c_{t3}, k_{t4}, c_{t4}]^T. The optimization procedure was carried out with respect to the median values of the vertical apparent mass and fore-and-aft cross-axis apparent mass on the seat, the ratio of the vertical force to the vertical acceleration on the backrest, and the ratio of the fore-and-aft force to the vertical acceleration on the back, as measured by Nawayseh and Griffin (2004). The values for the mechanical parameters determined by the optimisation are listed in Table 3.7 and Table 3.8.

Table 3.7 Translational stiffness and damping of human body with backrest.

Stiffness (N m^{-1})			Damping (Ns m^{-1})		
	initial	optimized		initial	optimized
k_{1z}	106275	97900	c_{1z}	32	80
k_{1x}	636	952	c_{1x}	31	15
k_{4z}	14191	20700	c_{4z}	3021	1010
k_{4x}	105	301	c_{4x}	1036	1740
k_{bz}	3800	4050	c_{bz}	296	170
k_{bx}	2500	4000	c_{bx}	650	800

Table 3.8 Rotational stiffness and damping of human body with backrest.

Stiffness (Nm rad^{-1})			Damping (Nms rad^{-1})		
	initial	optimized		initial	optimized
k_{t1}	100	77	c_{t1}	50	16
k_{t2}	2000	1540	c_{t2}	80	54
k_{t3}	1000	890	c_{t3}	1000	1370
k_{t4}	8	12	c_{t4}	80	50

The masses of the body segments which were optimised to match the experimental values were listed in Table 3.9. The mass of the upper body, m_3, was increased compared to the initial value in Table 3.2. It was assumed that a larger portion of the weight of arms moved with the upper body when subjects were supported by a backrest.

Table 3.9 Adjusted mass of each segment for the human body model with backrest.

$m^g{}_1$ (kg)	$m^g{}_2$ (kg)	$m^g{}_3$ (kg)	$m^g{}_4$ (kg)	$m^g{}_5$ (kg)
8.0	12.0	24	18	6.6

^{g}, adjusted mass of each segment.

It is noted that the identified parameters in Tables 3.7-3.9 (also in Tables 3.3 -3.5) are for a particular testing condition. Parameters are likely to vary a little for other testing conditions (e.g., a different vibration magnitude) or a different subject. On the other hand, the identified parameter values are those that minimise the cost function, there is no guarantee that they are physically representative values. The predicted vertical apparent mass and fore-and-aft apparent mass were shown in Figure 3.5.

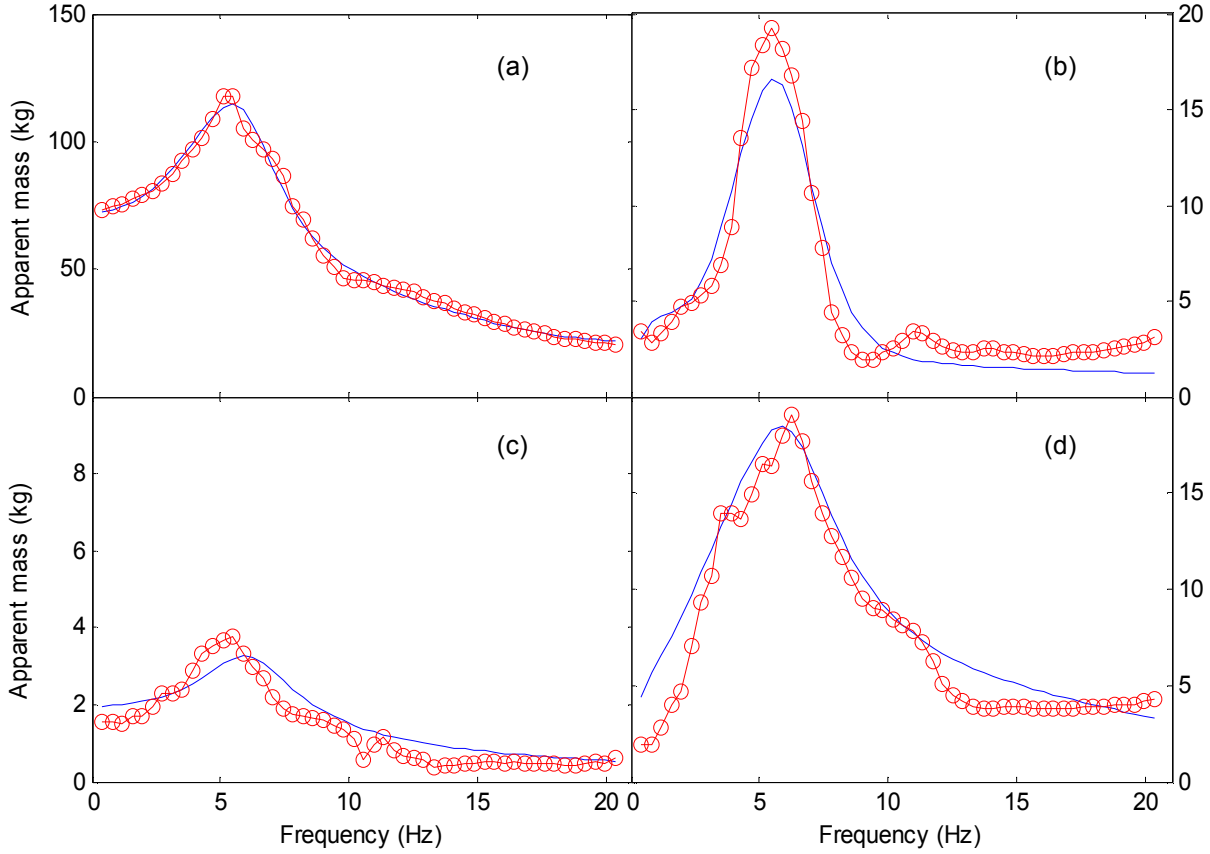

Figure 3.5 Comparisons between the predicted and measured vertical apparent mass and fore-and-aft cross-axis apparent mass of the human body with backrest: ——, predicted value (with contact on the upper lumbar spine); —O—, measured value. (a) Vertical apparent mass on the seat; (b) fore-and-aft cross-axis apparent mass on the seat; (c) vertical apparent mass at the back; (d) fore-and-aft cross-axis apparent mass on the back.

The distance between the back contact point and the lumbar joint was included in the optimization. The optimised distance was 0.25 m, accounting for 85% of the length of the lumbar segment.

3.3.3 Parameter sensitivity of the human body model with backrest

Similar to the human body model without backrest, the sensitivity of the peak modulus and the resonance frequency of the apparent mass on the seat and the back in both the vertical and fore-and-aft directions to the parameters of human body model with backrest was analysed using the sensitivity matrix method (Equation (3.12)) and:

$\boldsymbol{\psi}^{T}$

$=[k_{1z}, c_{1z}, k_{1x}, c_{1x}, k_{4z}, c_{4z}, k_{4x}, c_{4x}, k_{bz}, c_{bz}, k_{bx}, c_{bx}, k_{t1}, c_{t1}, k_{t2}, c_{t2}, k_{t3}, c_{t3}, k_{t4}, c_{t4}, m_1, m_2, m_3, m_4, m_5]_{1 \text{ X } 25}$. (3.21)

The responses to be examined, R_i, were the peak modulus of the vertical apparent mass on the seat (i=1), the corresponding resonance frequency (i=2), the peak of fore-and-aft cross-axis apparent mass on the seat (j=3) and the corresponding resonance frequency (j=4), the peak modulus of the vertical apparent mass at the back (i=5) and the corresponding resonance frequency (i=6), the peak of fore-and-aft cross-axis apparent mass at the back (j=7) and the corresponding resonance frequency (j=8). A perturbation factor, α=30%, was used. The resultant sensitivity matrix was:

$$\mathbf{P_b} = \left[\mathbf{P_{tr\text{-}b}} \quad \mathbf{P_{rot\text{-}b}} \quad \mathbf{P_{m\text{-}b}}\right]_{8\times 25}, \tag{3.22}$$

where $\mathbf{P_{tr\text{-}b}}$, $\mathbf{P_{rot\text{-}b}}$, and $\mathbf{P_{m\text{-}b}}$ represent sensitivity values of translational stiffness and damping, rotational stiffness and damping, and the mass of each body segment respectively.

$$\mathbf{P_{tr\text{-}b}} = \begin{bmatrix}
-0.148 & -0.011 & 0.000 & 0.000 & -0.056 & -0.061 & 0.000 & 0.059 & -0.010 & 0.040 & -0.004 & -0.002 \\
0.259 & 0.000 & 0.000 & 0.000 & 0.000 & 0.000 & 0.000 & 0.000 & 0.000 & 0.000 & 0.000 & 0.000 \\
-0.350 & -0.015 & 0.000 & 0.000 & 0.128 & -0.127 & 0.000 & 0.494 & 0.015 & -0.028 & -0.001 & -0.041 \\
0.134 & -0.133 & 0.000 & 0.000 & 0.000 & 0.000 & 0.000 & 0.000 & -0.133 & 0.000 & 0.000 & 0.000 \\
-0.358 & -0.008 & 0.000 & 0.000 & 0.002 & 0.044 & 0.000 & 0.002 & 0.265 & 0.380 & -0.004 & -0.009 \\
0.143 & 0.000 & 0.000 & 0.000 & 0.000 & 0.000 & 0.000 & 0.000 & 0.000 & 0.000 & 0.000 & 0.000 \\
-0.080 & 0.017 & 0.000 & 0.000 & -0.312 & 0.036 & 0.000 & 0.004 & 0.063 & -0.066 & 0.003 & 0.631 \\
0.267 & 0.000 & 0.000 & 0.000 & 0.000 & 0.000 & 0.000 & 0.000 & 0.000 & 0.000 & 0.000 & 0.000
\end{bmatrix} \tag{3.23}$$

In $\mathbf{P_{tr\text{-}b}}$, the vertical apparent mass on the seat was sensitive to parameters k_{1z} and $c_{4z,}$ and the resonance frequency of the apparent mass was sensitive to parameter k_{1z}.

The fore-and-aft cross-axis apparent mass on the seat was sensitive to parameter c_{4x}, followed by k_{1z}, with the resonance frequency of the fore-and-aft cross-axis apparent mass sensitive to parameter k_{1z}.

The vertical apparent mass on the back was sensitive to parameters c_{bz} and k_{1z}, and the resonance frequency of the apparent mass was only sensitive to parameter k_{1z}.

The fore-and-aft cross-axis apparent mass at the back was sensitive to parameter c_{bx}, with the corresponding resonance frequency sensitive to parameter k_{1z}.

$$\mathbf{P}_{\text{rot-b}} = \begin{bmatrix} 0.000 & 0.346 & 0.059 & 0.007 & 0.000 & 0.006 & 0.000 & -0.002 \\ 0.000 & 0.143 & 0.000 & 0.143 & 0.000 & 0.000 & 0.000 & 0.000 \\ 0.014 & 0.090 & 0.089 & 0.041 & 0.000 & 0.014 & 0.000 & -0.006 \\ -0.133 & 0.000 & 0.000 & 0.000 & 0.000 & 0.000 & 0.000 & 0.000 \\ 0.054 & 0.070 & 0.020 & -0.084 & 0.000 & 0.002 & 0.000 & 0.000 \\ 0.000 & 0.143 & 0.143 & 0.000 & 0.000 & 0.000 & 0.000 & 0.000 \\ 0.022 & -0.215 & -0.077 & -0.102 & 0.000 & -0.015 & 0.000 & 0.002 \\ 0.000 & 0.134 & 0.000 & 0.000 & 0.000 & 0.000 & 0.000 & 0.000 \end{bmatrix}, \quad (3.24)$$

In $\mathbf{P}_{\text{rot-b}}$, the vertical apparent mass on the seat and the corresponding resonance frequency were both sensitive to parameters c_{t1} and c_{t2}. The fore-and-aft cross-axis apparent mass on the seat and the corresponding resonance frequency were sensitive to parameters c_{t1} and k_{t1}, respectively.

The vertical apparent mass and the fore-and-aft cross-axis apparent mass at the back were sensitive to parameters c_{t2}, c_{t1}, k_{t1} and k_{t2}, in that order. The resonance frequency of the fore-and-aft cross-axis apparent mass was only sensitive to parameter c_{t1} when 30% was used for the perturbation factor.

$$\mathbf{P}_{\text{m-b}} = \begin{bmatrix} 0.122 & -0.031 & -0.066 & 0.337 & 0.220 \\ 0.000 & -0.143 & -0.286 & 0.142 & 0.000 \\ 0.071 & 0.021 & -0.070 & 0.301 & 0.221 \\ -0.133 & -0.133 & -0.267 & 0.000 & -0.133 \\ 0.082 & 0.029 & 0.080 & 0.163 & 0.103 \\ 0.000 & -0.143 & -0.286 & 0.000 & 0.000 \\ 0.065 & 0.029 & 0.168 & 0.160 & 0.055 \\ 0.000 & -0.133 & -0.133 & 0.000 & 0.000 \end{bmatrix}, \quad (3.25)$$

In $\mathbf{P}_{\text{m-b}}$, the vertical apparent mass and the fore-and-aft cross-axis apparent mass on the seat were sensitive to parameters m_4 and m_5. The corresponding resonance frequency was sensitive to parameters m_3 and m_2.

The vertical apparent mass at the back was sensitive to parameters m_4 and m_5, with the resonance frequency of the apparent mass equally sensitive to parameters m_3 and m_2. The fore-and-aft cross-axis apparent mass at the back was sensitive to parameters m_3, m_4, and m_1, with the resonance frequency equally sensitive to parameters m_3 and m_2.

3.4 Discussion

3.4.1 The human body model without backrest

3.4.1.1 Proposed model

The model developed in this study has simplified the human body to five rigid bodies, with the head, neck, and arms incorporated within the upper-body segment. Because seat-to-head transmissibility was not of interest and head motion has little influence on the response at the driving point, it seemed reasonable to combine the head and neck with the upper trunk, unlike some previous multi-body dynamic models (Cho *et al.*, 2001; Kim *et al.*, 2005). For the same reason, the viscera and the arms were not simulated individually. The upper-body was divided into the upper-trunk and middle-trunk, assuming these two parts move relative to each other during whole-body vibration and contribute differently to the apparent mass at the seat. The five segment model appears to present a reasonable trade-off between simplicity and accuracy: including a greater number of body segments in the model will make it appear more realistic but a more complicated model is not necessarily a more accurate model or a more useful model.

The stiffness and damping elements located beneath the pelvis and thighs were used to represent the forces induced by deformation of tissues beneath the pelvis and thighs rather than the deformation of a compliant seat. By adding serial springs and dampers representing the deflection forces from a seat cushion, the interaction with a seat might be investigated (Cho *et al.*, 2001). The properties of a cushion (e.g. the dynamic stiffness in axial and shear directions) can be measured in the laboratory (Fairley and Griffin, 1986; Wei and Griffin, 1998; Cho *et al.*, 2001; Kim *et al.*, 2005; Ippili *et al.*, 2008) or determined by the optimization of a suitable model. Alternatively, the interaction between a compliant seat and a seat occupant may be modelled using finite element methods and a model combining flexible and rigid bodies. A finite element description of the interface between the occupant and a seat may also have the capacity to predict the pressure distribution over the interface.

Although non-linearity in human responses has been reported, in this thesis the translational and rotational stiffness and damping are assumed to be linear. Non-linearity can occur in both human tissues (Nawayseh and Griffin, 2004) and in seat cushions (Ippili *et al.*, 2008). The properties of human tissues and seat cushions may be expected to vary with many factors including the contact area. Some biodynamic models

incorporate non-linear springs, the stiffness of which depends on the relative displacement between adjacent parts (Liu *et al*., 1998), or nonlinear spring and viscous damping, the forces of which are due to relative displacements and velocities and their cubic terms (Muksian *et al*., 1974), but the optimisation of non-linear models awaits improved understanding of the mechanisms involved in the nonlinear responses of the body.

3.4.1.2 Use of median apparent mass

The medians of the modulus and phase of the apparent mass were used assuming there could exist a virtual subject with a response similar to the median values of a group of subjects. Although some inter-subject variability is smeared out in the median data it appears that for vertical in-line apparent mass and fore-and-aft cross-axis apparent mass the median value reflects the overall trend and behaviour of the principal resonance that dominates the modulus and phase (e.g., Nawayshe and Griffin, 2004; Qiu and Griffin, 2010). Parameters optimized to fit the model to the median data might therefore be adjusted to predict the responses of individuals by suitable changes to the inertial properties, stature, and other parameters, such as the vertical stiffness of the pelvis.

3.4.1.3 Parameter sensitivity

The sensitivity analysis indicated that at the primary resonance both the vertical apparent mass and the fore-and-aft apparent mass were most affected by the vertical degree-of-freedom (i.e., the vertical motion of the whole body). This is reasonably consistent with previous studies (Kitazaki and Griffin, 1997; Matsumoto and Griffin, 2001). The modulus of the fore-and-aft cross-axis apparent mass was primarily determined by the shear damping of the thighs (i.e., c_{4x}).

The high sensitivity to k_{t1} and c_{t2} implies that rotational motion of the pelvis and bending motion of lumbar spine made a large contribution to the apparent mass at resonance. As the shear property of tissue seems to influence the pitch motion, sensitivity to k_{t1} and c_{t2} indicates that pitch motion played a significant role in producing the fore-and-aft forces at the seat-occupant interface. The vertical and fore-and-aft movement induced by rotation of the pelvis and the lumbar spine may influence the apparent mass in both the vertical and the fore-and-aft directions. The low sensitivity to c_{t1} and k_{t2} suggest that the pelvis

joint may behave more like a spring while the lumbar joint (i.e., inter-brae disk) may behave more like a damper.

3.4.2 The human body model with backrest

3.4.2.1 The backrest contact point

The point of contact with the backrest was simulated by reaction forces on the thoracic spine, or by forces on both the lumbar and the thoracic spine (as shown in Figure 3.6(a) and Figure 3.6(b), respectively) so that parameter identification could be carried out to investigate the appropriateness of these contact locations as alternatives to contact on the upper lumbar spine.

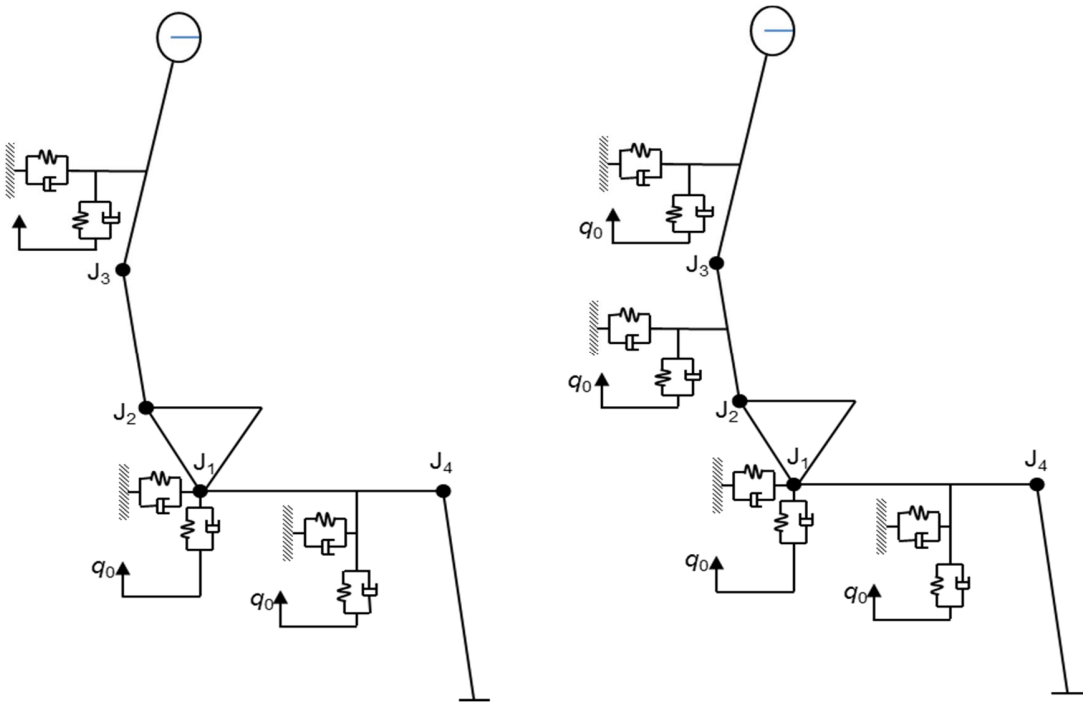

(a) (b)

Figure 3.6 The human body model with alternative contact locations: (a) contact at the thoracic spine; (b) contact at both the lumbar and thoracic spine.

The least-square-error between the analytical apparent mass and the measured apparent mass on the seat and on the back was calculated. The error values obtained for the model used in this study (contact on the upper lumbar spine), a model with contact on the thoracic spine, and a model with contact on both the lumbar spine and the thoracic spine were, respectively, 2.7 kg, 3.4 kg and 4.9 kg. The smaller error with contact on the upper lumbar spine, as used in the main study, suggests this was an

effective contact point providing the best representation of backrest contact in the experiment that provided the measured biodynamic responses. It is also noted that the initial parameters (e.g., k_{1x}) needed for the model with contact on the thoracic spine than are smaller the model with contact on the lumbar spine to get a sensible curve fitting.

To further investigate the effect of varying the point of contact from the upper lumbar spine (as assumed to develop the model), the modulus of the apparent mass at the seat and the back were also calculated with contact points located on the middle of the lumbar spine (r_{cb}=0.5l_2) and the lower lumbar spine (r_{cb}=0.2l_2). To accommodate the change in geometry with the lower contact position, the pelvis and lumbar back were rotated forward by 10° and 4°, respectively. For contact at the middle of the lumbar spine, the pelvis and the lumbar spine were rotated forward by 5° and 2°, respectively. The moduli of the apparent masses calculated with the three different contact locations are compared in Figure 3.7.

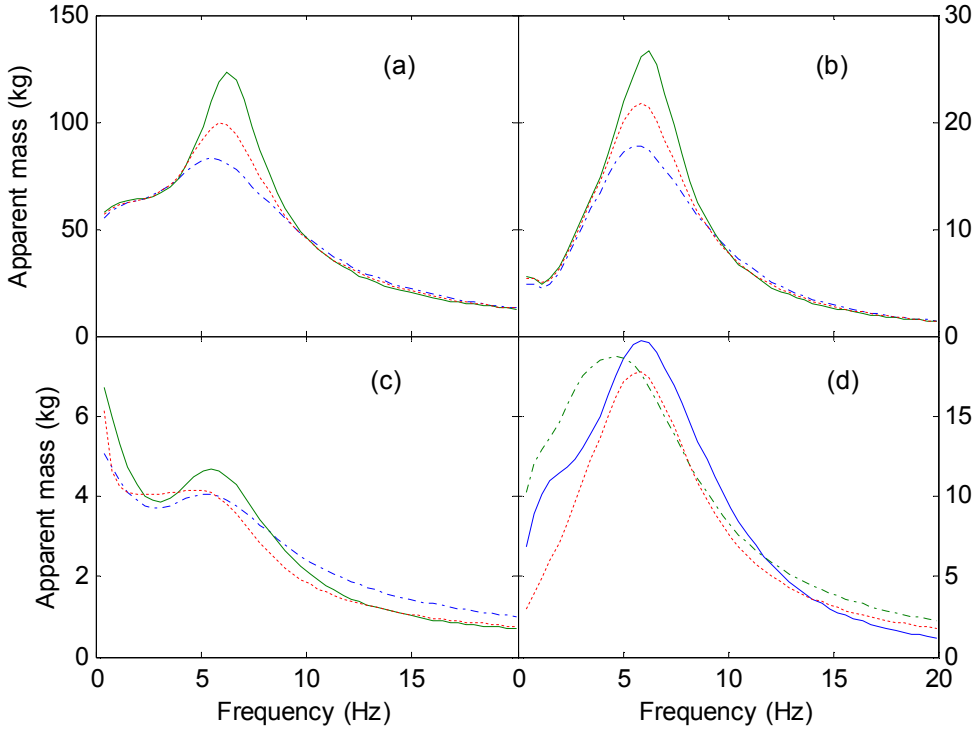

Figure 3.7 Calculated apparent mass with different positions of contact with backrest: ——, contact with lower lumbar spine; - - -, contact with middle lumbar spine; —.—, contact with upper lumbar spine. (a) vertical apparent mass on the seat; (b) fore-and-aft cross-axis apparent mass on the seat; (c) vertical apparent mass at the back; (d) fore-and-aft cross-axis apparent mass at the back.

Around the resonance frequency, the vertical apparent mass and the cross-axis apparent mass on the seat increased as the vertical contact position became lower, but

there were less consistent changes in the vertical apparent mass and fore-and-aft cross-axis apparent mass at the back.

3.4.2.2 Parameter sensitivity

Similar to the human body model without backrest, the vertical apparent mass on the seat when the body was supported by a backrest was sensitive to k_{1z}, c_{4z}, c_{t2} and m_4, while the fore-and-aft cross-axis apparent mass was sensitive to c_{4x}, k_{1z}, c_{t1}, k_{t2}. Changes to the stiffness and damping of tissues at the back did not result in evident variation in either the vertical apparent mass or the fore-and-aft cross-axis apparent mass at the seat. The vertical apparent mass at the back was largely dependent on parameters c_{bz}, k_{1z}, c_{t2}, c_{t1} and m_4, while the fore-and-aft cross-axis apparent mass was primarily determined by c_{bx}, k_{4z}, k_{1z}, c_{t1}, c_{t2} and m_4.

The vertical pelvis stiffness, k_{1z}, was the parameter most influencing the vertical apparent mass of human body on the seat, both with and without the backrest. This is understandable as the ischial tuberosities, where the spring k_{1z} is located, support most of the body weight. The stiffness k_{1z} was lower with the backrest than without the backrest. This might be attributed to a nonlinear compression-stiffness relationship of the interface tissue: the weight supported at the seat-occupant interface, m_4, was reduced when there was backrest (Table 3.5 and Table 3.8) and the reduced compression resulted in a lower axial stiffness.

Increasing the axial stiffness and damping of the back tissues reduced the vertical and fore-and-aft apparent mass on the seat and the vertical apparent mass at the back. A stiffer axial spring on the back meant that coupling between the back and backrest was enhanced, limiting the motion of the upper body. The reaction forces on the seat and the vertical reaction force on the back were thus reduced.

When the total body mass is constant, increasing the mass of the lumbar and thoracic spine decreased the apparent mass on the seat but increased the apparent mass at the back. This suggests the apparent mass on the seat was negatively correlated with the mass of the upper body while the apparent mass at the back was positively correlated with the mass of the upper body (when the back was supported by a backrest). There was an opposite trend when there was no backrest: an increase in the mass of the upper body (lumbar and thoracic regions) would obviously increase the mass supported on the seat when the back was unsupported.

Increasing the mass of the thighs increased both the apparent mass on the seat and the apparent mass at the back, possibly because the thighs supported a significant proportion of the body weight. Increasing the mass of each body segment reduced the resonance frequency, as expected.

3.5 Conclusion

A seven degree-of-freedom multi-body model has been developed to represent the dynamic response of the human body when seated with or without a backrest and exposed to vertical vibration excitation. When sitting without a backrest, the model represents both the vertical apparent mass and the fore-and-aft cross-axis apparent mass on the seat. When sitting with a backrest, the model also represents the vertical apparent mass and the fore-and-aft cross-axis apparent mass at the back.

Sensitivity analysis showed that the vertical apparent mass and the fore-and-aft cross-axis apparent mass on the seat and the backrest were all highly sensitive to the axial stiffness of the tissue beneath pelvis. Pitch motion of the upper-body contributed to the vertical apparent mass and the fore-and-aft cross-axis apparent mass on the seat. The apparent mass at the back was more sensitive to the stiffness and damping of the lower back than the properties of the upper back.

CHAPTER 4: VERTICAL VIBRATION OF THE SEATED HUMAN BODY: NONLINEARITY, CROSS-AXIS COUPLING AND ASSOCIATIONS BETWEEN RESONANCES IN TRANSMISSIBILITY AND APPARENT MASS

4.1 Introduction

Human exposures to whole-body vibration usually involve excitation in more than one axis, and yet most experimental studies of human responses to vibration have been restricted to a single axis of excitation. The biodynamic responses to vertical and fore-and-aft vibration are coupled, so the response to vibration in one of these directions can be modified by excitation in the orthogonal direction. This coupling may influence effects of whole-body vibration on comfort, performance, and health, but is more easily understood in the biodynamic responses. Increased understanding of the biodynamic responses to multiple-axis excitation (e.g., apparent mass and transmissibility) should also assist the development of improved biodynamic models of the body.

The vertical apparent mass of the human body exhibits a primary resonance at about 5 Hz, with the resonance frequency decreasing with increasing magnitude of vibration excitation (Fairley and Griffin, 1989; Nawayseh and Griffin, 2003). The transmissibility of the body has a more complex response, but shows broadly similar changes with increasing magnitude of vibration excitation (Matsumoto and Griffin, 1998b; Mansfield and Griffin, 2000).

There have been various attempts to relate the response measured at the seat-occupant interface (e.g., the driving point apparent mass) to the movements of the pelvis, spine, viscera, and head. From X-ray film of the lumbar spine during vertical excitation at about 1.0 ms^{-2}, bending of the order of ±1° between adjacent lumbar vertebrae has been reported at the principal resonance around 4 Hz (Sandover *et al*., 1987). The analysis indicated phase differences in the bending along the spine and possibly a rocking motion of the pelvis. Complex modes of the spine and pelvis were also observed by Kitazaki and Griffin (1998) who extracted eight modes from median transfer functions between vertical seat motion and motions of the head, spine, pelvis, and viscera in the mid-sagittal plane. It was suggested that the fourth mode at 4.9 Hz (involving bending of the upper thoracic spine, motion of the entire body in which the head, spinal column and pelvis move vertically due to axial and shear deformations of the buttocks tissue in phase with vertical motion of the viscera) might correspond to the principal resonance of

the apparent mass. The relation between resonances in the apparent mass and the body transmissibility (from vertical seat motion to the head, the first (T1), the fifth (T5), and the tenth (T10) thoracic vertebrae, the first (L1), the third (L3) and the fifth (L5) lumbar vertebrae and to the pelvis) has been reported (Matsumoto and Griffin, 1998a). Most of the vertical transmissibilities showed a peak in the region of 5 Hz at the principal resonance of the apparent mass. It was suggested that at this resonance the dominant motion was a bending of the lumbar spine and probably the lowest thoracic spine, possibly coupled with a rocking motion of the upper thoracic spine about the lower thoracic spine.

Nonlinearity has been observed in the resonance frequencies of both the apparent mass and transmissibility to various locations on the body. In standing subjects, the resonance frequencies in the apparent mass at the seat and transmissibilities to T1, T8, and L4, the iliac crest and the knee were lower with higher magnitudes of vibration (Matsumoto and Griffin, 1998b). In seated subjects, vertical transmissibilities to the spine, posterior superior iliac spine and the iliac crest all show a resonance similar to the apparent mass resonance (i.e. around 4 Hz) and decrease with increasing magnitude of vertical vibration excitation (Mansfield and Griffin, 2000).

Human bodies are often exposed to vibration involving multi-axis excitation. Previous studies with single-axis excitation have shown biodynamic responses are cross-axis coupled (e.g., Nawayseh and Griffin, 2003). Response of human body to vibration exhibits nonlinear characteristics such that the superposition principle is not adequate (e.g., Qiu and Griffin, 2010). It is therefore desirable to study how the cross-axis coupling and nonlinearity of human body change the apparent mass with dual-axis excitation. The few studies of the vertical apparent mass of the human body with the additional orthogonal excitation suggest the vertical apparent mass is similar to that with single-axis excitation (Hinz *et al*., 2006a; Mansfield and Maeda, 2006; Qiu and Griffin, 2010). However, the addition of vibration in an orthogonal direction tends to soften the dynamic response, similar to increasing the magnitude of vibration in the direction of single-axis excitation (Hinz *et al*., 2006a; Mansfield and Maeda, 2006; Qiu and Griffin, 2010). The transmissibility of the upper body (the pelvis and spine) exposed to dual-axis vibration has not yet been reported. How the vibration modes of the upper body contribute to the resonance seen in the apparent mass during dual-axis excitation remains unknown.

The experiment reported here was primarily designed to investigate the effect of the magnitude of vertical excitation and the addition of fore-and-aft excitation on the principal resonance evident in the apparent mass and the transmissibility of the seated human body. It was desired to understand the association between the principal resonances in the apparent mass and the vibration modes of the pelvis and spine during dual-axis vibration. It was hypothesised that the transmission of vertical seat vibration to the pelvis and the upper-body would be similar with single-axis vertical excitation and dual-axis vertical and fore-and-aft excitation, and that the resonance frequencies evident in transmissibilities from vertical seat vibration to various locations on the body would decrease with the addition of fore-and-aft excitation.

4.2 Experiment method

4.2.1 Apparatus

A rigid seat was secured to a 6-axis motion simulator capable of 1-m vertical displacement, 0.5-m fore-and-aft and lateral displacement, ±10 degrees of roll and pitch, and ±10 degrees of yaw. A force plate (Kistler 9281 B) consisting of four tri-axial quartz transducers at the four corners of a rectangular aluminium plate was secured to the supporting surface of the seat to allow the measurement of forces in the vertical and fore-and-aft directions. Signals from the four force transducers orientated to be sensitive to vertical force were summed and amplified by a charge amplifier (Kistler 5001). Signals from the four force transducers orientated to be sensitive to fore-and-aft force were summed and amplified by a similar charge amplifier. A tri-axial SIT-pad was used to measure acceleration in the fore-and-aft and vertical directions at the centre of the force platform. The signals were recorded using an *HVLab* data acquisition system (issue 1.0, 2009).

4.2.2 Subjects and stimuli

Twelve male subjects with median age 26.5 years (range 23 to 36 years), weight 68.5 kg (range 60.4 to 80 kg), and stature 1.74 m (range 1.65 to 1.82 m), participated in the study that was approved by the Human Experimentation Safety and Ethics Committee of the Institute of Sound and Vibration Research at the University of Southampton. During the experiment, subjects sat with their upper body in a comfortable upright position and looked straight ahead. Their feet were supported by a footrest that moved with the simulator platform.

Subjects were exposed to random vibration with approximately flat constant-bandwidth acceleration spectra (0.2 to 20 Hz) in six combinations of four magnitudes of fore-and-aft vibration (0, 0.25, 0.5, or 1.0 ms^{-2} r.m.s.) and four magnitudes of vertical vibration (0, 0.25, 0.5, or 1.0 ms^{-2} r.m.s.) (Table 4.1). All stimuli were of 60-s duration, with motions in the fore-and-aft and vertical directions uncorrelated with each other.

Table 4.1 Vertical (*z*-axis) and fore-and-aft (*x*-axis) excitations experienced by subjects.

		x-axis excitation (ms^{-2} r.m.s.)			
		0	0.25	0.5	1.0
z-axis excitation (ms^{-2} r.m.s.)	0	-	-	-	-
	0.25	a_z	-	-	-
	0.5	a_z	-	-	-
	1.0	a_z	$a_x + a_z$	$a_x + a_z$	$a_x + a_z$

4.2.3 Motion measurement locations on the body

Acceleration was measured in the fore-and-aft and vertical directions on the body surface over the first, fifth, and twelfth thoracic vertebrae, the third lumbar vertebra, and the pelvis (at the iliac crest). The pitch motion of the pelvis was also estimated from the difference between two vertical accelerations mounted at 25-mm separation on a single block located at the iliac crest.

The vibration on the body surface was measured with two miniature accelerometers (Entran EGA(X)) attached orthogonally to T-shaped balsa wood blocks. The weight of each block was about 1 g and similar to that of each miniature accelerometer. The block was attached to the body surface with double-side adhesive tape with a contact area similar to that of a vertebral body. The experimental set-up and the mounting of the accelerometer block are shown in Figure 4.1.

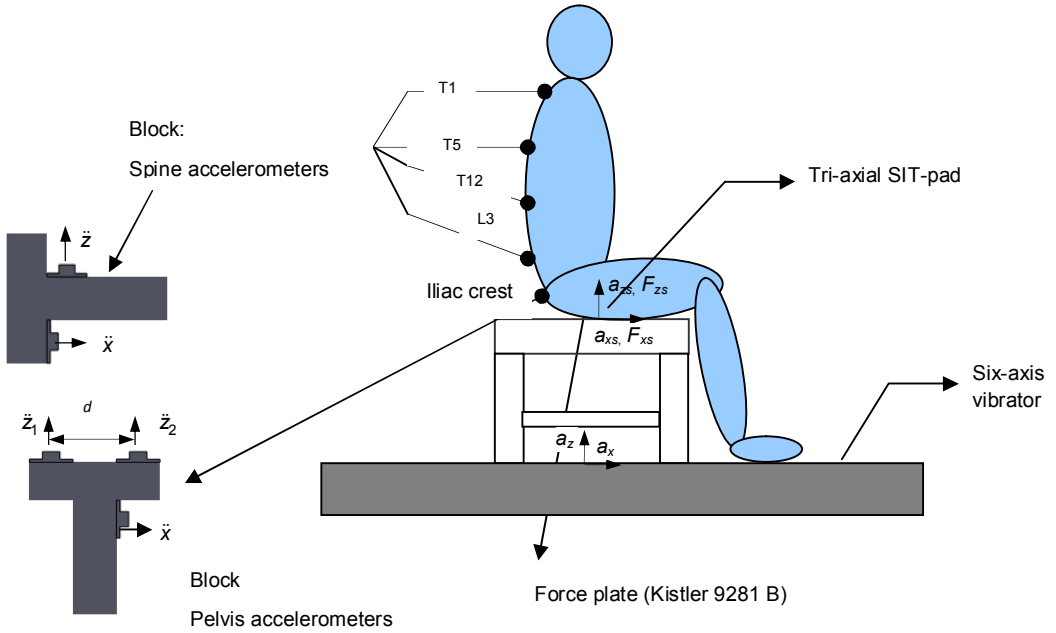

Figure 4.1 Experiment set-up and the body transmissibility measurement locations.

4.2.4 Calibrations of transducers

The force plate was calibrated in the vertical and fore-and-aft directions respectively (Figure 4.2).

The vertical force was calibrated with placing inert mass (i.e., lead bag) of 10 kg on the middle of the top plate. The fore-and-aft force was calibrated by applying a pulling force of 100 N to a spring scale. The scale on Figure 4.2(b) is just above the force plate so the distance between the scale and the force plate could be neglected. A steel bar was inserted to a bolt hole in the platform. The diameters of the hole and the bar are similar. The steel bar stood against the edge of the top plate and the spring was attached to the bar.

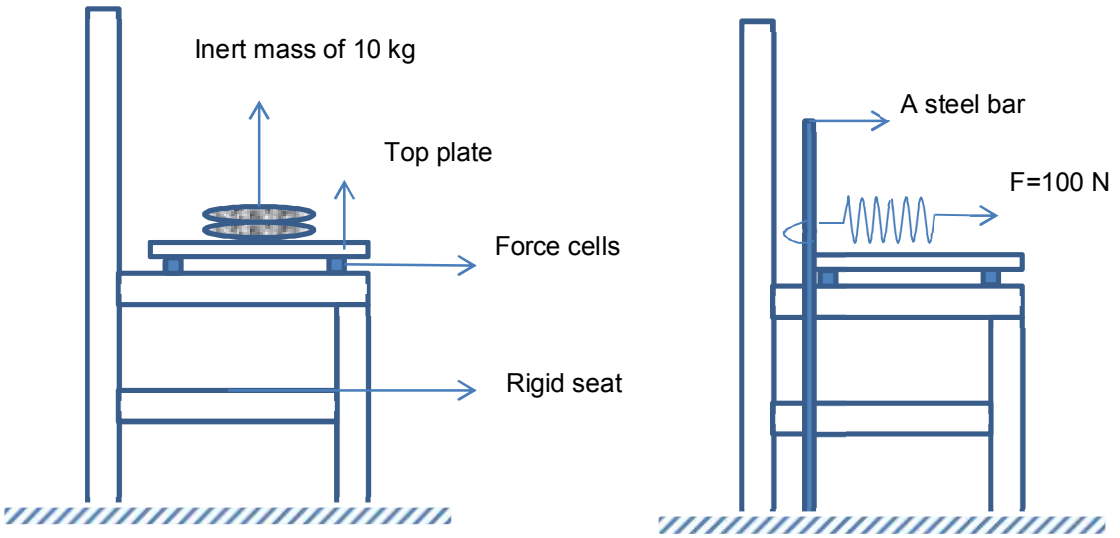

Figure 4.2 Calibration of the force plate in (a) vertical direction; (b) fore-and-aft direction.

Each accelerometer was calibrated so as to make sure the acceleration difference before and after turning it over was 2 g (g is the gravity acceleration, 9.81 ms^{-2} was used). A further dynamic calibration was carried out for these accelerometers to estimate the inter-channel transfer functions (Figure 4.3).

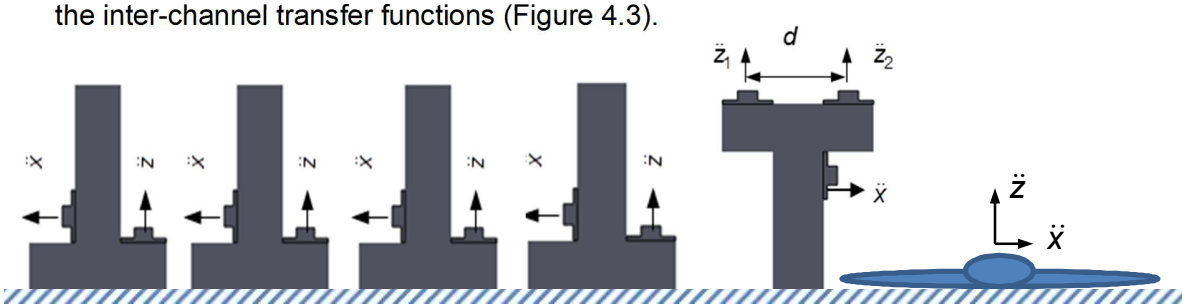

Figure 4.3 The set-up for the dynamic calibration of accelerometers (Cables were not shown).

The accelerometers were exposed to single-axis vertical excitation at 0.5 ms^{-2} r.m.s., single-axis fore-and-aft excitation at 0.5 ms^{-2} r.m.s. respectively. The vertical acceleration measured with the SIT-PAD was chosen as the nominal input when the vertical excitation was applied. The transfer functions between the vertical acceleration measured with the miniature accelerometers and the nominal input were estimated. Similarly, the transfer functions between the fore-and-aft acceleration measured with the miniature accelerometers and the nominal input (i.e., fore-and-aft acceleration measured with the SIT-PAD) were estimated. The passing criterion was that the modulus of the

transfer functions was between 0.95 and 1.05 and the phase lag was not greater than 0.05 rad.

4.2.5 Mass cancellation

Mass cancellation was performed in the time domain to remove the influence of the mass of the top plate above the force transducers from the measured force.

Masses of the top plate in the vertical and fore-and-aft directions were estimated firstly. The force plate together with the rigid seat (Figure 4.1) without any other preload was exposed to vertical excitation at 0.5 ms^{-2} r.m.s., fore-and-aft excitation at 0.5 ms^{-2} r.m.s., combined vertical excitation at 0.5 ms^{-2} r.m.s. and fore-and-aft excitation at 0.5 ms^{-2} r.m.s. sequentially. Forces and accelerations were acquired with a sampling rate of 512 samples per second via anti-aliasing filters at 50 Hz. Signal processing was conducted with a frequency resolution of 0.25 Hz. The auto-spectral density was calculated using Pwelch method and the cross- spectral density was calculated using cpsd method. Both Pwelch and cpsd methods are available in MATLAB. A Hanning window was used with an overlap of 50%. About 30 averagings were then conducted for the signal of 60-s duration. A longer duration of stimuli may cause fatigue to subjects.

Assuming that a_x and a_z represented the fore-and-aft and vertical accelerations and f_{xp} and f_{zp}, the fore-and-aft and vertical forces, the vertical apparent mass M_{zp} and the fore-and-aft apparent mass M_{xp} of the force plate was calculated with equations below:

$$M_{zp} = \frac{G_{a_z f_{zp}}}{G_{a_z}}, \quad M_{xp} = \frac{G_{a_x f_{xp}}}{G_{a_x}} \quad (4.1)$$

Where,

G_{a_z} , is the auto spectrum of a_z,

G_{a_x} , is the auto spectrum of a_x,

$G_{a_z f_{zp}}$, is the cross-spectrum of a_z and f_{zp},

$G_{a_x f_{xp}}$, is the cross-spectrum of a_x and f_{xp}.

The apparent mass of the force plate estimated with single-axis and dual-axis excitation was in good agreement with each other, i.e., around 29.5 kg for vertical apparent mass, 31.5 kg for fore-and-aft apparent mass over the frequency range 0 to 20 Hz (Figure 4.4).

The phase between the excitation and the force was below 0.06 rad in this frequency range. The seat and the force plate could be regarded as rigid structure.

With f_{zm} and f_{xm} representing measured vertical force and fore-and-aft force when the subjects sit on the seat, f_z and f_x representing the actual vertical force and fore-and-aft force between the human body and the seat, mass cancellation was performed as follows:

$$f_z = f_{zm} - 29.5*a_z;\ f_x = f_{xm} - 31.5*a_x. \quad (4.2)$$

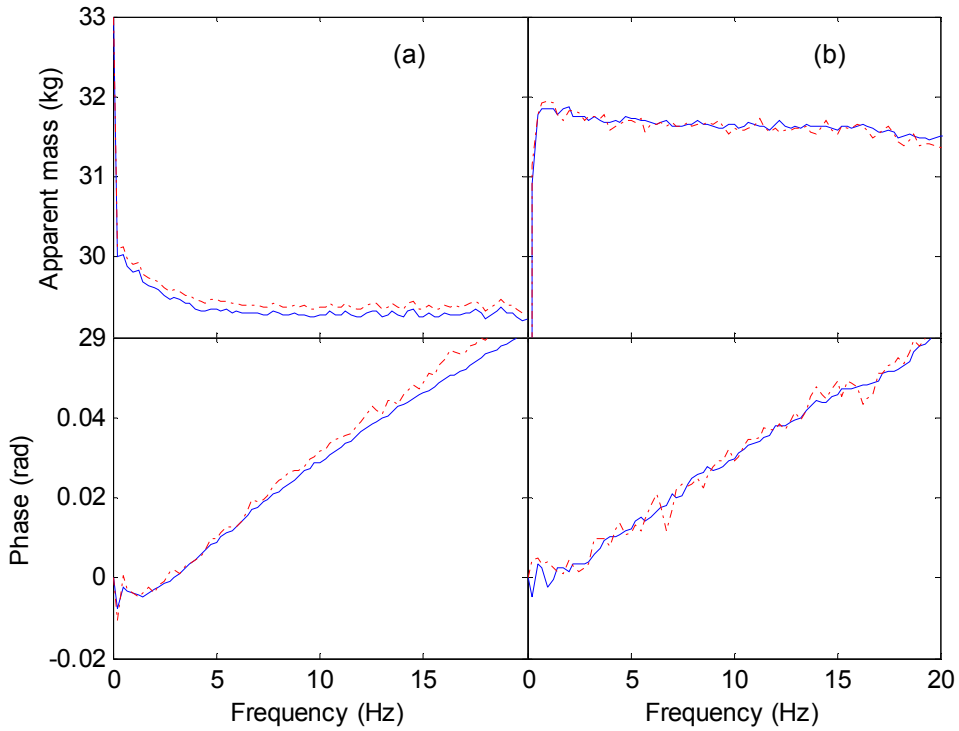

Figure 4.4 Apparent mass of the force plate: (a) vertical apparent mass; (b) fore-and-aft apparent mass. ——, estimated with single-axis excitation; —.—, estimated with dual-axis excitation.

4.2.6 Data analysis

The vertical apparent mass and the fore-and-aft cross-axis apparent mass of the human bodies and the corresponding coherency were calculated using cross-spectra density method (CSD).

$$M_{zz} = \frac{G_{a_z f_z}}{G_{a_z}}, \qquad \gamma^2_{zz} = \frac{\left|G_{a_z f_z}\right|^2}{G_{a_z} G_{f_z}}$$
$$M_{zx} = \frac{G_{a_z f_x}}{G_{a_z}}, \qquad \gamma^2_{zx} = \frac{\left|G_{a_z f_x}\right|^2}{G_{a_z} G_{f_x}} \quad . \tag{4.3}$$

Where,

G_{f_x} and G_{f_z} are the auto spectra of f_x and f_z,

$G_{a_z f_z}$, is the cross-spectrum of a_z and f_z, and

$G_{a_z f_x}$, is the cross-spectrum of a_z and f_x.

The vertical transmissibility and the fore-and-aft cross-axis transmissibility were calculated with a_{tx} and a_{tz} representing the fore-and-aft and vertical acceleration measured on the body surface.

$$T_{zz} = \frac{G_{a_z a_{tz}}}{G_{a_z}}, \qquad \gamma^2_{T_{zz}} = \frac{\left|G_{a_z a_{tz}}\right|^2}{G_{a_z} G_{a_{tz}}}$$
$$T_{zx} = \frac{G_{a_z a_{tx}}}{G_{a_z}}, \qquad \gamma^2_{T_{zx}} = \frac{\left|G_{a_z a_{tx}}\right|^2}{G_{a_z} G_{a_{tx}}} \quad . \tag{4.4}$$

Where,

G_{a_z} , is the auto spectrum of a_z,

$G_{a_{tz}}$ and $G_{a_{tx}}$ are the auto spectra of $a_{tz,}$ and a_{tx},

$G_{a_z a_{tz}}$, is the cross-spectrum of a_z and a_{tz}.

$G_{a_z a_{tx}}$, is the cross-spectrum of a_z and a_{tx}.

The pitch motion of the pelvis was defined as ratio of the difference in the two vertical vibrations to the distance between the two transducers (Figure 4.1):

$$\ddot{\theta} = \frac{\ddot{z}_1 - \ddot{z}_2}{d} \quad . \tag{4.5}$$

The pitch transmissibility of the pelvis was calculated as

$$T_{pch} = \frac{G_{a_z \theta}}{G_{a_z}}, \qquad \gamma^2_{T_{pch}} = \frac{\left|G_{a_z \theta}\right|^2}{G_{a_z} G_{\theta}} \tag{4.6}$$

.

Where,

$G_{a_z\theta}$, is the cross-spectrum of a_z and θ,

G_{θ} , is the auto spectrum of θ.

Equations (4.3-4.6) were used to calculate the transfer functions with both single-axis and dual-axis excitation, because they are appropriate when the two inputs are independent (Bendat and Piersol, 1986).

The inclination of the body surface was taken into account by using the angle between the body surface and the vertical as shown in Figure 4.5. If $\ddot{z}$ and $\ddot{x}$ are the measured accelerations along the body surface and normal to the body surface, respectively, the time history of the vertical acceleration, a_{tz}, and fore-and-aft acceleration, a_{tx}, were corrected:

$a_{tx} = \ddot{x} \cos \Psi - \ddot{z} \sin \Psi$,

$a_{tz} = \ddot{z} \cos \Psi + \ddot{x} \sin \Psi$. (4.7)

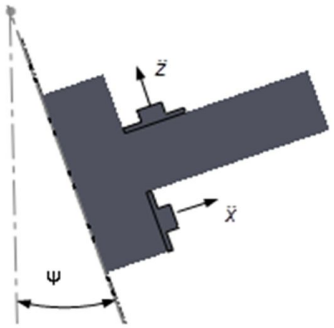

Figure 4.5 The inclination of the body surface

The transmissibility to the spine $T_s(f)$ was estimated based from the transmissibility $T(f)$ between the seat and the body surface after applying a correction function, $C(f)$, to take into account the effect of the tissue between the accelerometer and the bone (Kitazaki and Griffin, 1995):

$$T_s(f) = T(f)C(f) . \quad (4.8)$$

where $T(f)$ is T_{zz} or T_{zx} in Equation (4.2).

$C(f)$ is the inverse of the transfer function of the local tissue-accelerometer system:

$$C(\delta) = \frac{1-\delta^2 + 2i\varsigma\delta}{1+2i\varsigma\delta} . \quad (4.9)$$

Where, $\delta = \frac{f}{f_0}$ is the frequency ratio (with f and f_0 the excitation frequency and the natural frequency, respectively) and ς is the damping ratio.

A cotton thread was attached to the accelerometer block mounted at the location where body motion was measured. The thread was then pulled in the direction normal to the body surface and the cotton cut to produce a transient response in the local system (Figure 4.6). This was repeated with the cotton pulled parallel to the surface of the body.

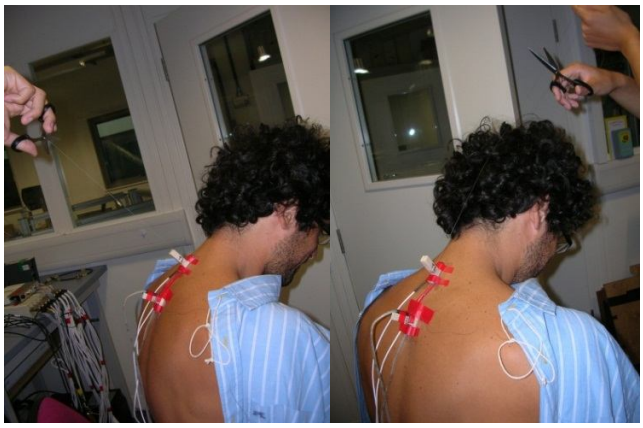

(a) (b)

Figure 4.6 Measurement of the transient response of local human body-blocks system: (a) normal direction; (b) shear direction.

The time histories of the responses in the two directions were recorded for 2 seconds at a sampling rate of 512 samples per second. The natural frequency f_0 was obtained from the modulus of the Fast Fourier Transform of the acquired time history. The damping ratio was determined from the difference between the natural frequency and the frequency corresponding to the half power points in the peak of the modulus curve. The corrections function was determined with the obtained natural frequency and the damping ratio. The correction function for the transmissibility at T1 of subject 11, as an example, is shown in Figure 4.7. The transmissibility to T1 of the same subject before and after data correction is shown in Figure 4.8.

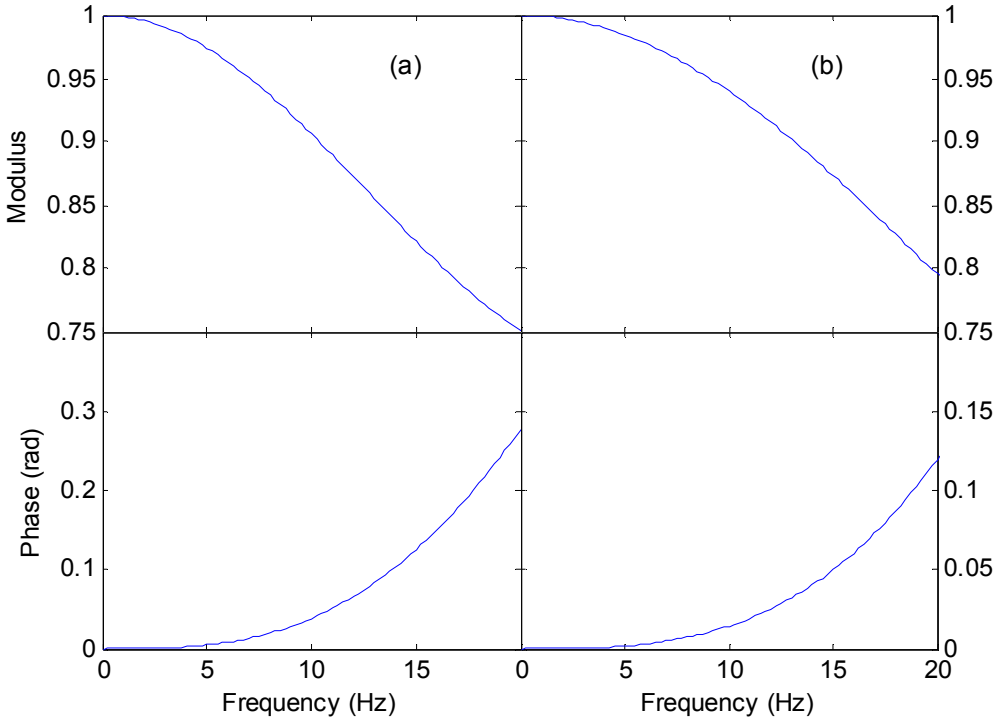

Figure 4.7 Median data correction function obtained with the repeated local transient response at the first thoracic spine of subject 11: (a) normal direction; (b) shear direction.

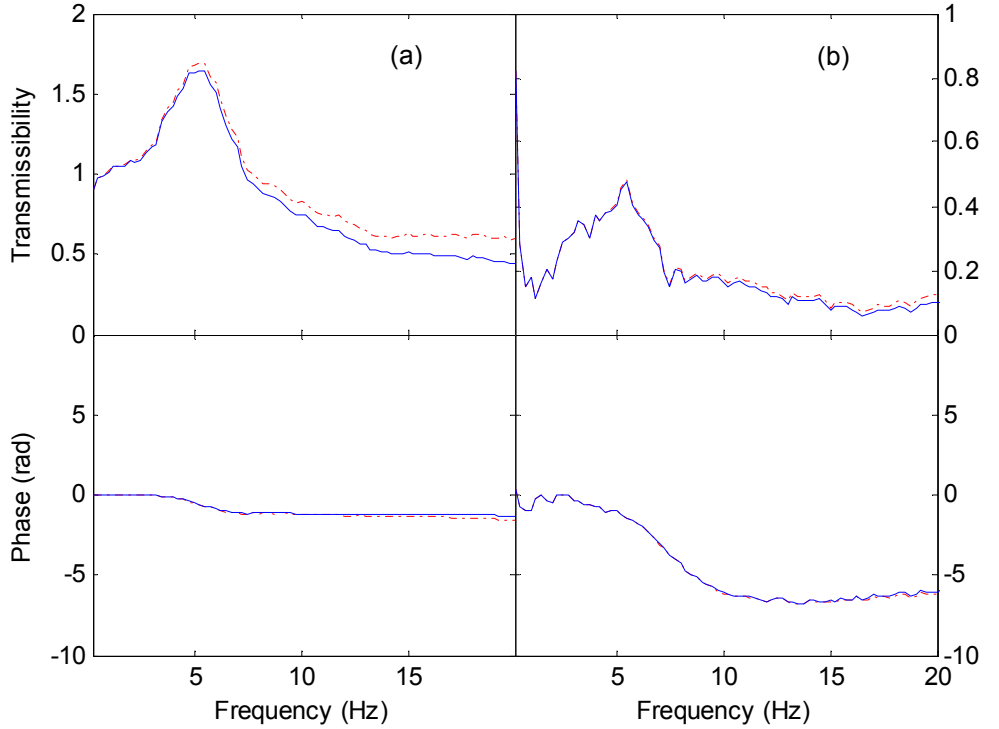

Figure 4.8 Transmissibility from the vertical seat base motion to: (a) the vertical motion; (b) fore-and-aft motion over the first thoracic spine level of subject 2. ——, data before correction, i.e., motion on the body surface; —.—, data after correction, i.e., motion of the spine.

The tissue-correction had more effect in the vertical direction than in the fore-and-aft direction, implying the tissue is stiffer in the normal direction than in the shear direction. The transmissibility presented below was corrected separately for each subject.

4.3 Results

4.3.1 Apparent mass

With single-axis and dual-axis excitation, both the vertical apparent mass and the fore-and-aft cross-axis apparent mass showed a primary resonance at about 5 Hz, consistent with previous studies (Figure 4.9). A second resonance in the vertical apparent mass was observed around 8 Hz in subject 5 and in the region of 10 to 12 Hz with subjects 6 and 12.

With single-axis vertical excitation, the resonance frequency evident in the median vertical apparent mass decreased from 5.25 Hz to 4.75 Hz as the vibration magnitude increased from 0.25 to 1.0 ms^{-2} r.m.s. (p=0.002, Wilcoxon; Figure 4.10 (a)). With both vertical and fore-and-aft excitation, the resonance frequency in the vertical apparent mass reduced from 4.5 Hz with fore-and-aft vibration at 0.25 ms^{-2} r.m.s. to 4.25 Hz with fore-and-aft excitation increased to 1.0 ms^{-2} r.m.s. (p=0.007, Wilcoxon; Figure 4.11(a)).

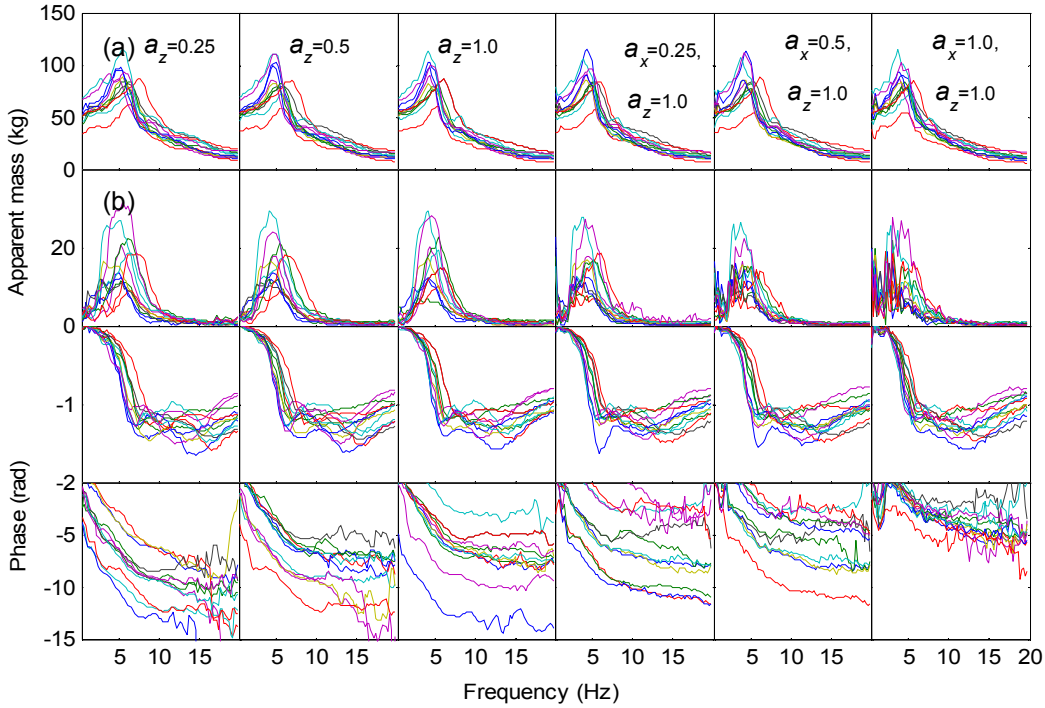

Figure 4.9 Individual apparent masses of 12 subjects: (a) the vertical apparent mass and phase; (b) the fore-and-aft cross-axis apparent mass and phase.

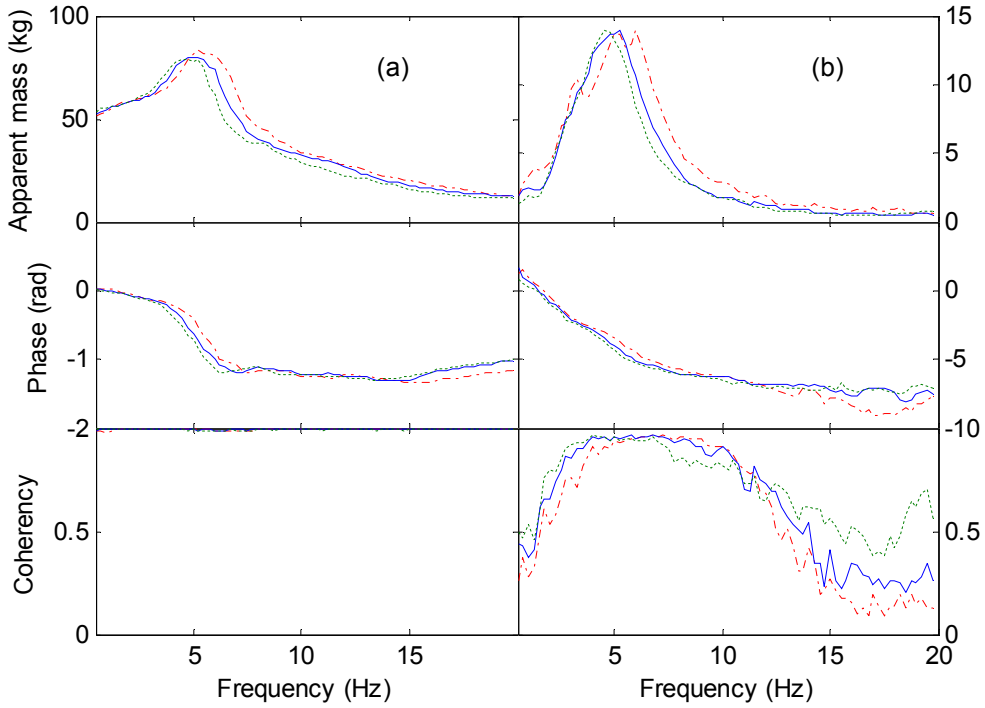

Figure 4.10 Effect of magnitude of the single-axis vertical excitation on: (a) vertical apparent mass; (b) fore-and-aft cross-axis apparent mass. —.—, a_z=0.25 ms^{-2} r.m.s.; — —, a_z=0.5 ms^{-2} r.m.s.; - - -, a_z=1.0 ms^{-2} r.m.s. (medians of 12 subjects).

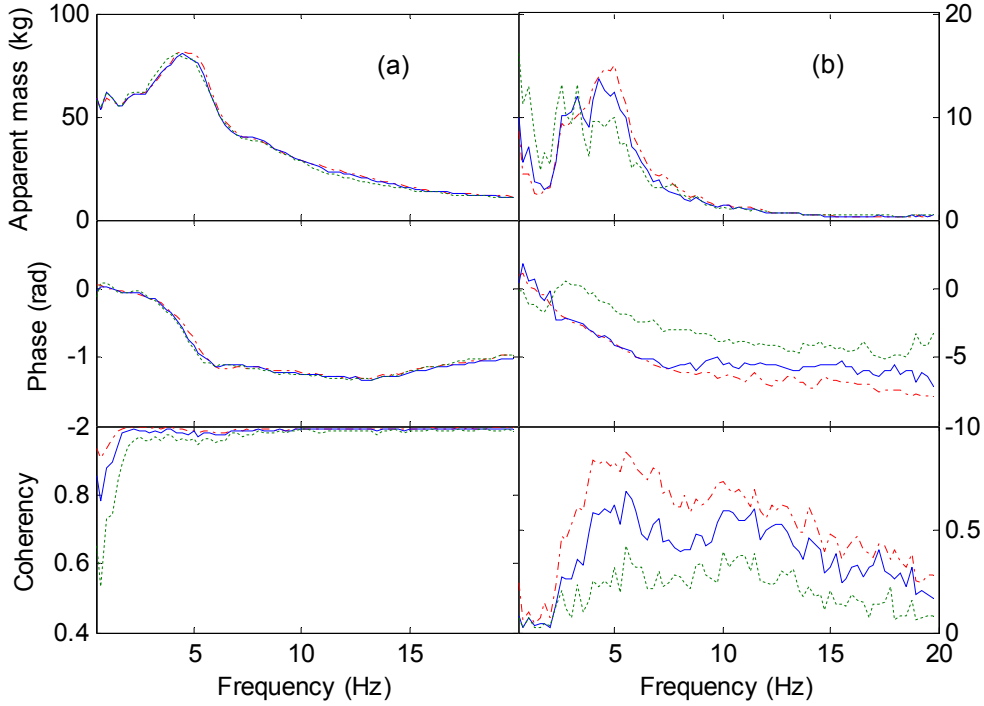

Figure 4.11 Effect of magnitude of the additional fore-and-aft excitation on: (a) vertical apparent mass; (b) fore-and-aft cross-axis apparent mass. —.—, a_x=0.25 ms^{-2} r.m.s., a_z=1.0 ms^{-2} r.m.s.; ——, a_x=0.5 ms^{-2} r.m.s., a_z=1.0 ms^{-2} r.m.s.; - - -, a_x=1.0 ms^{-2} r.m.s., a_z=1.0 ms^{-2} r.m.s.

The fore-and-aft cross-axis apparent mass exhibited a similar nonlinear characteristic: the resonance frequency decreased with increasing magnitude of vertical excitation and with the addition of fore-and-aft excitation (Figure 10(b) and Figure 11(b)). The coherency between the fore-and-aft force and vertical acceleration dropped as the magnitude of the fore-and-aft excitation increased.

4.3.2 Transmissibility

4.3.2.1 Vertical transmissibility

With both single-axis and dual-axis excitation, the vertical transmissibility to T1 had a primary resonance in the vicinity of 5 Hz, similar to the principal resonance in the vertical apparent mass (Figure 4.12).

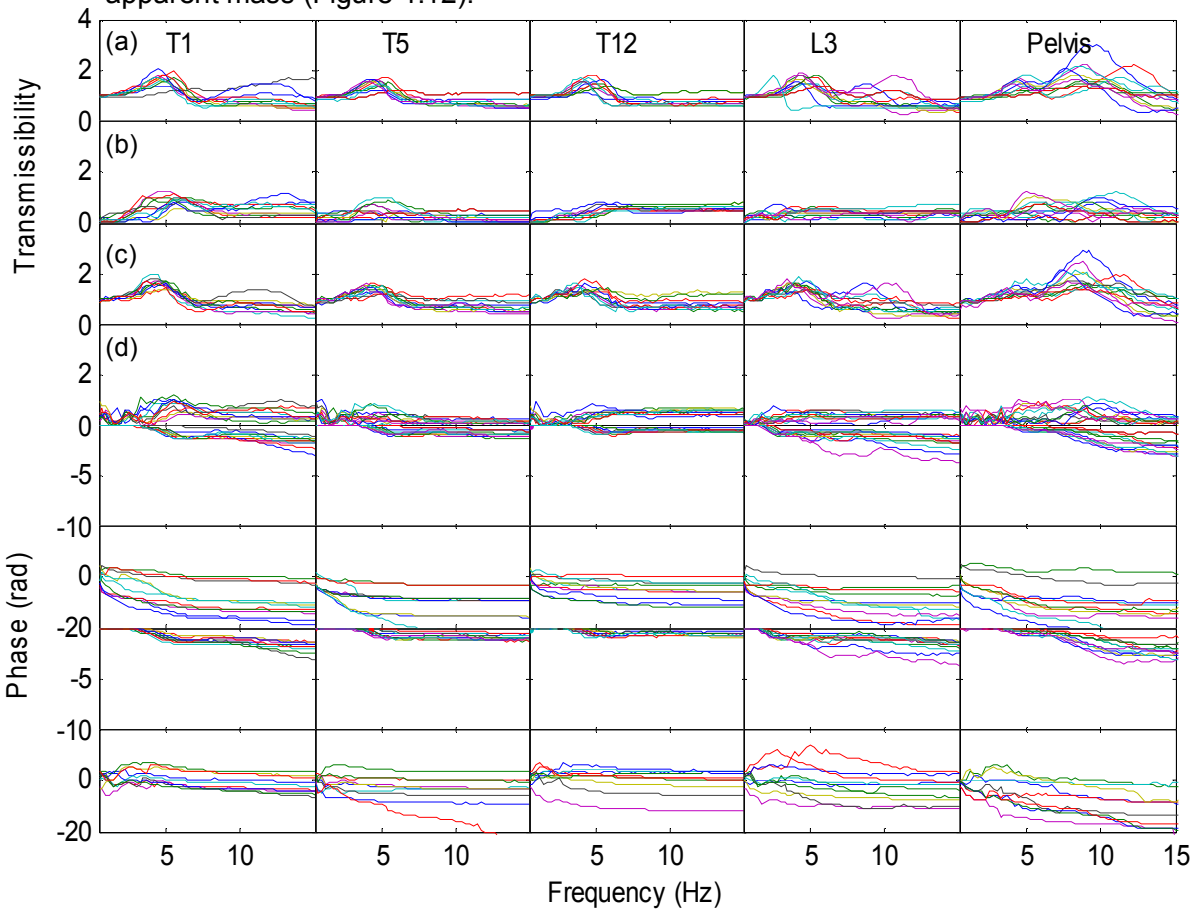

Figure 4.12 Individual transmissibility from vertical seat motion to upper body motion of 12 subjects: (a) vertical transmissibility and phase with single-axis vibration (a_z=1.0 ms^{-2} r.m.s.); (b) fore-and-aft cross-axis transmissibility and phase with single-axis vibration (a_z=1.0 ms^{-2} r.m.s.); (c) vertical transmissibility and phase with dual-axis vibration (a_x=1.0 ms^{-2} r.m.s., a_z=1.0 ms^{-2} r.m.s.); (d) fore-and-aft cross-axis transmissibility and phase with dual-axis vibration (a_x=1.0 ms^{-2} r.m.s., a_z=1.0 ms^{-2} r.m.s.). (The individual transmissibility at other vibration magnitudes is shown in Appendix B.)

The vertical transmissibility to T5, T12, and L3 showed trend similar to the transmissibility to T1 with a similar resonance (row (a) and row (c) in Figure 4.12).

The resonance frequencies to the different locations along the spine differed between locations (Friedman, p<0.05). The resonance frequency to T1 was higher than the resonance to T12 (Wilcoxon, p=0.036) and T5 (Wilcoxon, p=0.026). The resonance frequency to L3 was lower than that to T1 (Wilcoxon, p=0.003), T5 (Wilcoxon, p=0.002), and T12 (Wilcoxon, p=0.002) with 1.0 ms^{-2} r.m.s. single-axis vertical excitation, and also with combined 1.0 ms^{-2} r.m.s. vertical excitation and 1.0 ms^{-2} r.m.s. fore-and-aft excitation (Wilcoxon, p=0.003 for T1, T5, and T12). For these excitation conditions the resonance frequency in the transmissibility to the pelvis was significantly higher than the resonance frequencies in the transmissibilities to T1, T5, T12, and L3 (Wilcoxon, p<0.05).

The peak modulus in the vertical transmissibility to the thoracic spine differed between the three measurement locations (Friedman, p<0.05 for all excitations). The peak modulus in the vertical transmissibility to T1 was greater than the peak modulus in the vertical transmissibility to T5 and T12 (Wilcoxon, p<0.05 with all six combinations of exposure).

4.3.2.2 Fore-and-aft cross-axis transmissibility

The fore-and-aft transmissibility to all locations along the spine showed a primary peak at 5 Hz (row (b) and row (d) in Figure 4.12). The fore-and-aft transmissibility to the pelvis had peaks at about 3, 8 and 12 Hz, but with great variability among subjects (row (b) and row (d) in Figure 4.12).

The peak modulus in the fore-and-aft cross-axis transmissibility to the thoracic spine differed between measurement locations (Friedman, p<0.05). The peak modulus in the fore-and-aft cross-axis transmissibility was greater to T1 than to T5 with single-axis vertical excitation at 1.0 ms^{-2} r.m.s. (Figure 4.12; Wilcoxon, p<0.001). The peak modulus in the fore-and-aft cross-axis transmissibility was also greater to T1 than to T12 with all six combinations of excitations (Wilcoxon, p<0.05).

4.3.2.3 Pitch transmissibility to the pelvis

The transmissibility from vertical seat vibration to pitch of the pelvis had a similar trend to the transmissibility from vertical seat vibration to fore-and-aft vibration of the pelvis, with similar resonance frequencies but much inter-subject variability (Figure 4.13). The pitch transmissibility with either single-axis or dual-axis excitation has a primary resonance

between 8-10 Hz. The main difference may be due to the inter-subject variability with dual-axis excitation being larger with single-axis excitation. With the addition of fore-aft excitation, pitch motion is generated with fore-and-aft excitation apart from vertical excitation. Noise may be introduced when the subject involve more volunteered muscle tension to keep their body in balance.

There was a correlation between the primary resonance frequencies in the pitch transmissibility to the pelvis and the fore-and-aft cross-axis transmissibility to the pelvis with single-axis vertical excitation at 0.25 ms^{-2} r.m.s. (Spearman, ρ = 0.529, p=0.077).

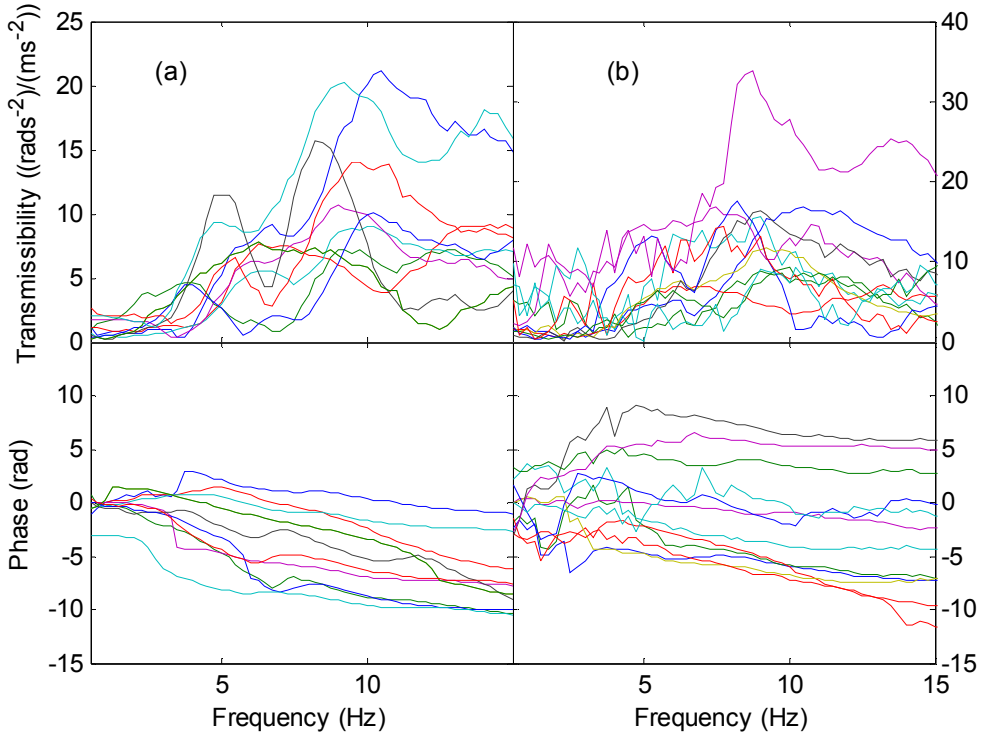

Figure 4.13 Individual transmissibility from vertical seat motion to pitch of the pelvis of 12 subjects: (a) pitch transmissibility with 1.0 ms^{-2} r.m.s. vertical vibration (a_z=1.0 ms^{-2} r.m.s.); (b) pitch transmissibility with dual-axis vibration (a_x=1.0 ms^{-2} r.m.s., a_z=1.0 ms^{-2} r.m.s.). (The individual transmissibility at other vibration magnitudes is shown in Appendix B.)

4.3.2.4 Nonlinearity in vertical transmissibility

With single-axis excitation, the primary resonance frequencies in the vertical transmissibility to each measurement location decreased with increasing vibration magnitude (Friedman, p=0.001 for all measurement locations; Figure 4.14). With dual-axis excitation, the resonance frequency in the vertical transmissibilities decreased as the magnitude of fore-and-aft excitation increased with constant magnitude of vertical

excitation (Friedman, p=0.001 for the pelvis and L3, p=0.003 for T12; p=0.029 for T5 and T1; Figure 4.15).

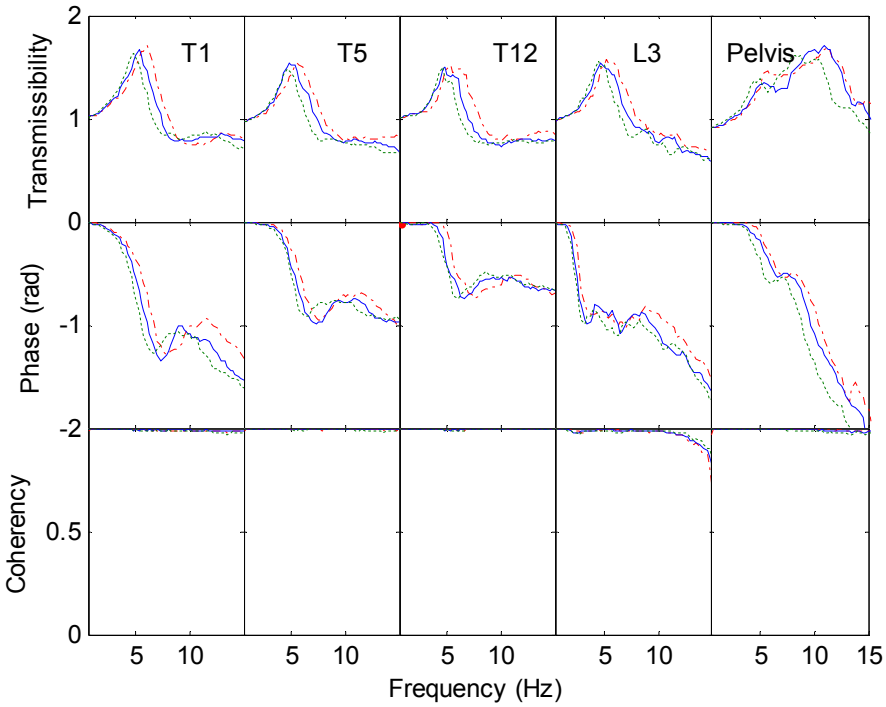

Figure 4.14 Effect of magnitude of the single-axis vertical excitation on the vertical transmissibility to each measurement location: —.—, a_z=0.25 ms^{-2} r.m.s.; ——, a_z=0.5 ms^{-2} r.m.s.; - - -, a_z=1.0 ms^{-2} r.m.s. (medians of 12 subjects).

The extent of the nonlinearity in the vertical transmissibility from the seat to each location on the body was quantified as the percentage reduction in the resonance frequency when: (i) the magnitude of single-axis vertical vibration excitation increased from 0.25 to 1.0 ms^{-2} r.m.s., and (ii) when single-axis vertical vibration excitation (a_z =1.0 ms^{-2} r.m.s.) was replaced by dual-axis vibration excitation (a_x=1.0 and a_z =1.0 ms^{-2} r.m.s.). With single-axis vertical excitation, there was no statistically significant difference in the extent of nonlinearity at the different measurement locations on the body (Friedman, p=0.184). With dual-axis excitation, the extent of the nonlinearity differed between locations (Friedman, p=0.019). The nonlinearity to L3 was less than the nonlinearity to the pelvis (Wilcoxon, p=0.034) and to T1 (Wilcoxon, p=0.005), and the nonlinearity to T5 was less than the nonlinearity to T1 (Wilcoxon, p=0.047).

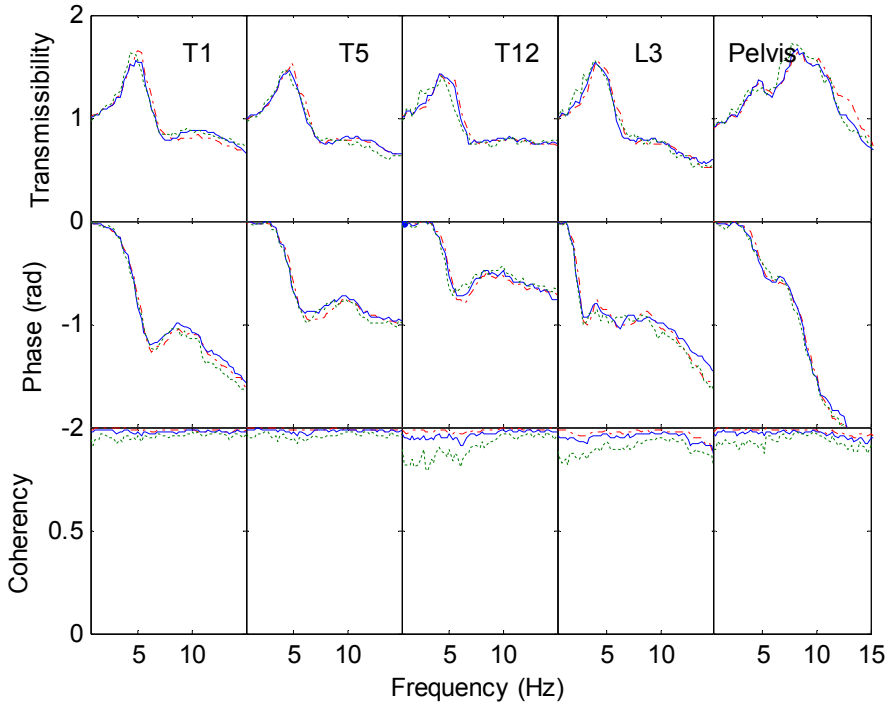

Figure 4.15 Effect of magnitude of the additional fore-and-aft excitation on the vertical transmissibility to each measurement location. —.—, a_x=0.25 ms^{-2} r.m.s., a_z=1.0 ms^{-2} r.m.s.; ——, a_x=0.5 ms^{-2} r.m.s., a_z=1.0 ms^{-2} r.m.s.; - - -, a_x=1.0 ms^{-2} r.m.s., a_z=1.0 ms^{-2} r.m.s. (medians of 12 subjects).

4.3.2.5 Nonlinearity in cross-axis transmissibility

Increasing the magnitude of vertical excitation reduced the resonance frequency in the fore-and-aft cross-axis transmissibility to T5 (Friedman, p<0.001) and T1 (Friedman, p=0.006; Figure 4.16), but not to T12 or L3. However, the resonance frequency in the fore-and-aft motion of the pelvis reduced with increasing magnitude of vertical excitation (Friedman, p<0.001; Figure 4.16) and the addition of fore-and-aft excitation (Friedman, p<0.001; Figure 4.17). The resonance frequency in the pitch motion of the pelvis reduced with increasing magnitude of single-axis excitation (Friedman, p<0.001; Figure 4.18(a)), but not with increasing magnitude of the additional fore-and-aft excitation (Friedman, p=0.068; Figure 4.18(b)). The transmissibility at resonance in the fore-and-aft directions at each measurement location were unaffected by vibration magnitude, except at T1 where the fore-and-aft transmissibility decreased with increasing vertical excitation magnitude (Friedman, p=0.002; Figure 4.16).

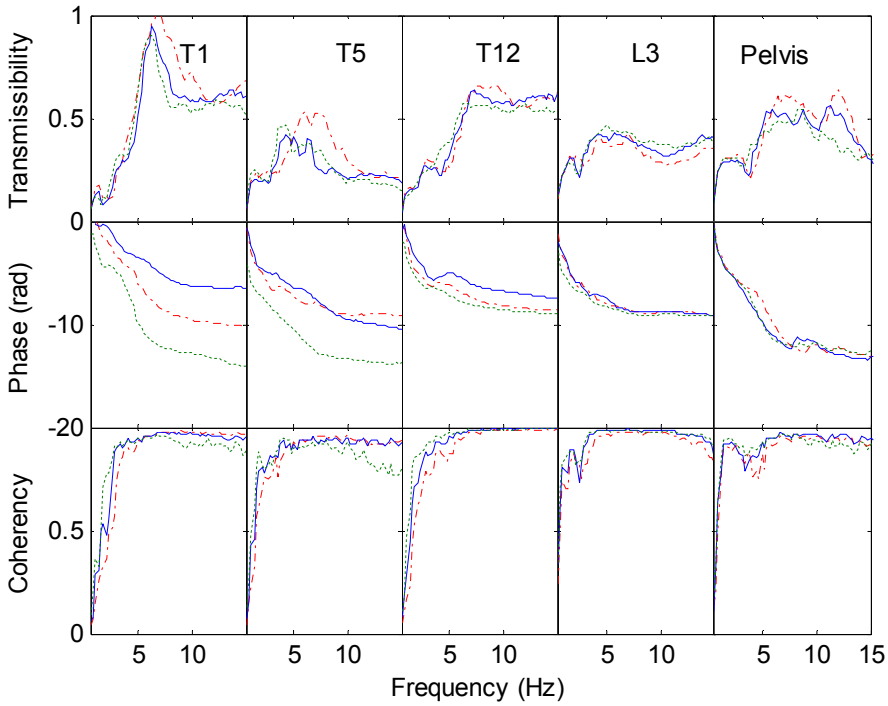

Figure 4.16 Effect of magnitude of the single-axis vertical excitation on the fore-and-aft cross-axis transmissibility to each measurement location: —.—, a_z=0.25 ms^{-2} r.m.s.; ——, a_z=0.5 ms^{-2} r.m.s.; - - -, a_z=1.0 ms^{-2} r.m.s. (medians of 12 subjects).

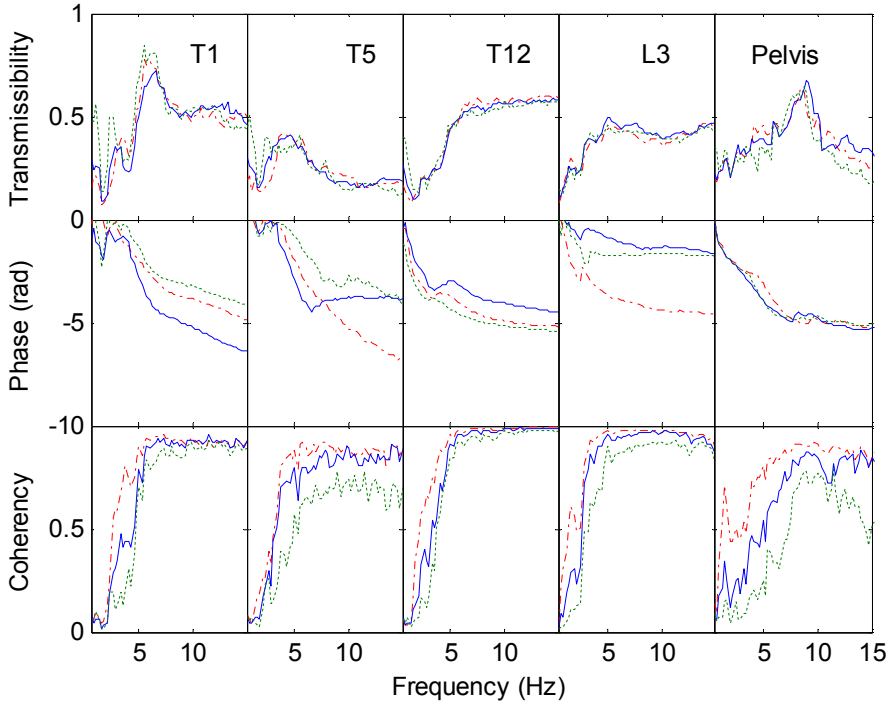

Figure 4.17 Effect of magnitude of the additional fore-and-aft excitation on the fore-and-aft cross-axis transmissibility to each measurement location: —.—, a_x=0.25 ms^{-2} r.m.s., a_z=1.0 ms^{-2} r.m.s.; ——, a_x=0.5 ms^{-2} r.m.s., a_z=1.0 ms^{-2} r.m.s.; - - -, a_x=1.0 ms^{-2} r.m.s., a_z=1.0 ms^{-2} r.m.s. (medians of 12 subjects).

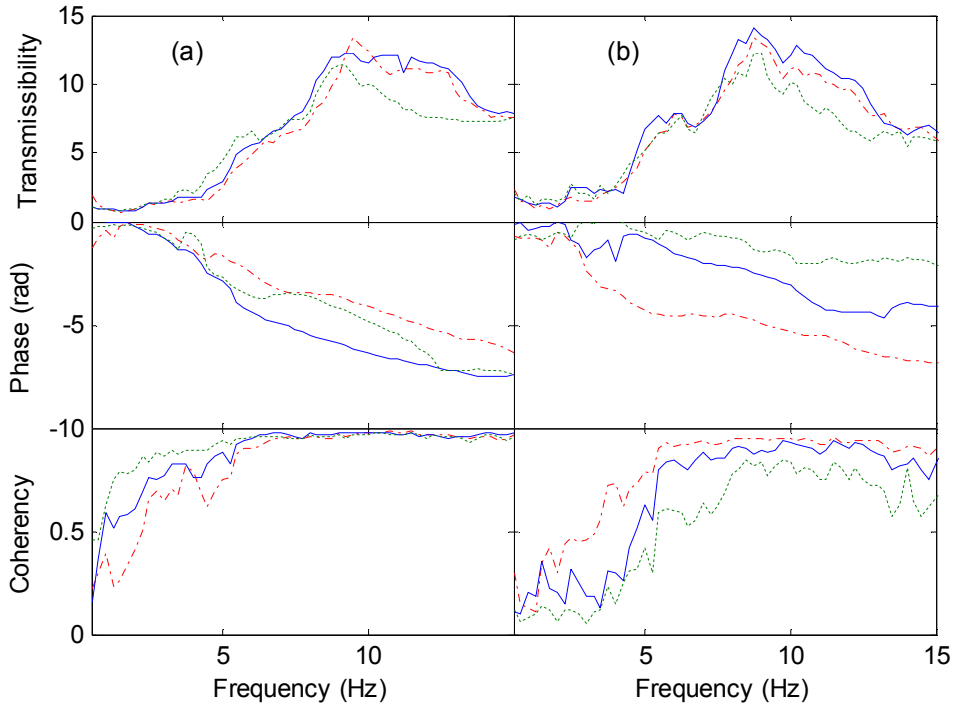

Figure 4.18 Median pitch transmissibility of pelvis of 12 subjects exposed to: (a) single-axis vibration, —.—, a_z=0.25 ms^{-2} r.m.s.; ——, a_z=0.5 ms^{-2} r.m.s.; - - -, a_z=1.0 ms^{-2} r.m.s.; (b) dual-axis vibration, —.—, a_x=0.25 ms^{-2} r.m.s., a_z=1.0 ms^{-2} r.m.s.; ——, a_x=0.5 ms^{-2} r.m.s., a_z=1.0 ms^{-2} r.m.s.; - - -, a_x=1.0 ms^{-2} r.m.s., a_z=1.0 ms^{-2} r.m.s.

The pitch transmissibility at resonance was also unchanged with changes in the magnitude of single-axis vertical vibration or dual-axis excitation. The coherency between vertical excitation and pitch motion of the pelvis was low during dual-axis excitation, because the fore-and-aft excitation caused much of the pelvis pitch motion.

4.3.2.6 Relative displacement between measurement locations

To investigate how the pelvis and each part of the spine moved relative to each other, the relative vertical and fore-and-aft displacements were calculated: the difference in the acceleration measured during single-axis vertical excitation was high-pass filtered (Bessel filter at 0.5 Hz) and then double-integrated to obtain the time history of the relative displacement between adjacent locations. The power spectral densities of these relative displacements are shown in Figure 4.19.

For each pair of adjacent locations, the relative displacements are much greater in the fore-and-aft direction than in the vertical direction, suggesting bending of the spine, pitch motion of the pelvis, and sheer motion of tissues beneath the ischial tuberosities. During vertical excitation, the greatest fore-and-aft relative displacement occurred between L3 and the iliac crest, even though their vertical separation was less than between the other

five pairs of adjacent locations. This suggests bending of the lower lumbar spine relative to the pelvis. The greatest relative displacement in the vertical direction was also observed at this location. However, it was not possible to determine from the measurements whether the centre of rotation of the pelvis was at the ischial tuberosities or the lower lumbar spine. Relative displacements at the upper thoracic spine (from T1 to T5) were smaller than at the lower thoracic spine (from T5 to T12), implying the lower thoracic spine tended to bend more than the upper thoracic spine.

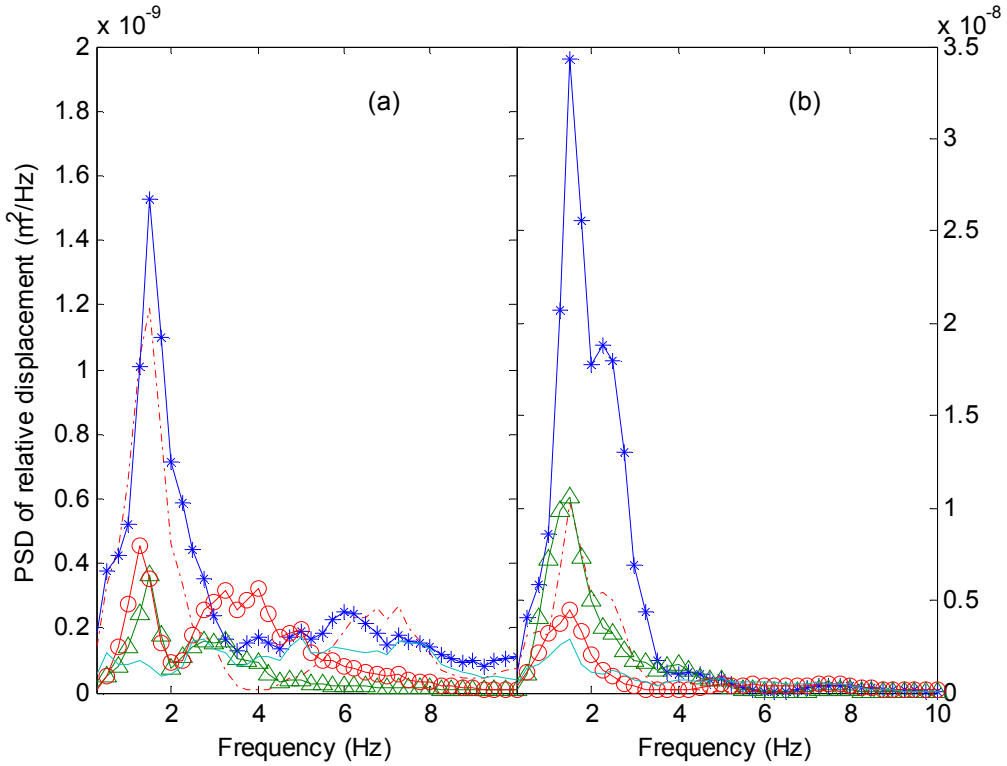

Figure 4.19 Example power spectral densities of (a) vertical relative displacement; (b) fore-and-aft relative displacement between: —.—, pelvis and seat; —*—, L3 and pelvis; —Δ—, T12 and L3; —O—, T5 and T12; ——, T1 and T5 (subject 8).

4.4 Discussion

4.4.1 Apparent mass

The vertical apparent mass and the fore-and-aft cross-axis apparent mass exhibited a primary resonance at about 5 Hz, similar to that reported previously (Fairley and Griffin, 1989; Nawayseh and Griffin, 2003). Previous studies with single-axis vertical excitation have found that the resonance frequency in the vertical apparent mass is correlated with the resonance frequency in the fore-and-aft cross-axis apparent mass (Nawayseh and Griffin, 2003; Qiu and Griffin, 2010). In the present study, the highest correlation

between the primary resonance frequencies in the vertical apparent mass and the fore-and-aft cross-axis apparent mass was obtained with single-axis vertical excitation at 1.0 ms^{-2} r.m.s. (Spearman, ρ=0.676, p=0.016). The resonance frequency in both the vertical apparent mass and the fore-and-aft cross-axis apparent mass were reduced as the excitation magnitude increased, consistent with a softening of the body tissues found in many previous studies (Fairley and Griffin, 1989; Qiu and Griffin, 2010).

With dual-axis excitation, the vertical in-line apparent mass and the fore-and-aft cross-axis apparent mass were similar, but not identical, to the apparent masses measured with single-axis excitation, as reported in previous studies (Hinz *et al*., 2006a; Mansfield and Maeda, 2006; Qiu and Griffin, 2010). The resonance in the apparent mass shifted to lower frequencies with the addition of fore-and-aft excitation. This may be because the addition of a fore-and-aft excitation increased the movement within the body, similar to increasing the magnitude of single-axis vertical excitation. However, to produce an equivalent resonance shift required a greater increase in the magnitude of fore-and-aft excitation than an increase in the magnitude of vertical vibration: a statistically significant decrease in the resonance frequency of the vertical apparent mass required an increase of 0.25 ms^{-2} r.m.s. in the magnitude of vertical vibration but an increase of 0.5 ms^{-2} r.m.s. in the magnitude of fore-and-aft excitation. The same increase in the magnitude of excitation in both axes tended to introduce a greater softening effect in the fore-and-aft cross-axis apparent mass than in the vertical inline apparent mass (see Section 4.3.1). With dual-axis excitation, the vertical force would have been generated by both the vertical excitation and the pitch motion of the upper-body produced by the fore-and-aft excitation. Similarly, the fore-and-aft force would have been generated by both the fore-and-aft excitation and the pitch motion of the upper-body produced by the vertical excitation. The non-linearity in the vibration modes will have been influenced by the combined effect of excitation in the two perpendicular directions, but the excitation had more effect on the inline response than the cross-axis response.

4.4.2 Transmissibility

A primary resonance in the vertical transmissibility to T1, T5, T12 and L3 at about 5 Hz, and in the vertical transmissibility to the pelvis at about 5 Hz and 8 to 10 Hz is consistent with findings in Matsumoto and Griffin (1998a) and Mansfield and Griffin (2000).

The resonance frequencies evident in the transmissibilities reduced when either the in-line vertical vibration excitation increased or, with constant vertical excitation, the fore-

and-aft excitation increased (Figures 4.14 and 4.15, Section 4.3.2.4). This non-linearity was also apparent in transfer functions between adjacent measurement locations (Figure 4.20). Such widespread nonlinearity could be influenced by nonlinearity at one location (e.g. tissue beneath the ischial tuberosities, as discussed in Section 4.4.1) but the biodynamic characteristics of other parts, including elements in the spine, may also have contributed. The simultaneous presence of fore-and-aft excitation might alter the geometry of the spine and pelvis, compared to that with single-axis vertical excitation. A change in the sitting posture may shift the resonance in the body transmissibility. However, the extent of the nonlinearity with dual-axis excitation differed between locations (Section 4.3.2.4), implying that the pelvis and the different segments of the spine were not equally affected by the addition of fore-and-aft excitation.

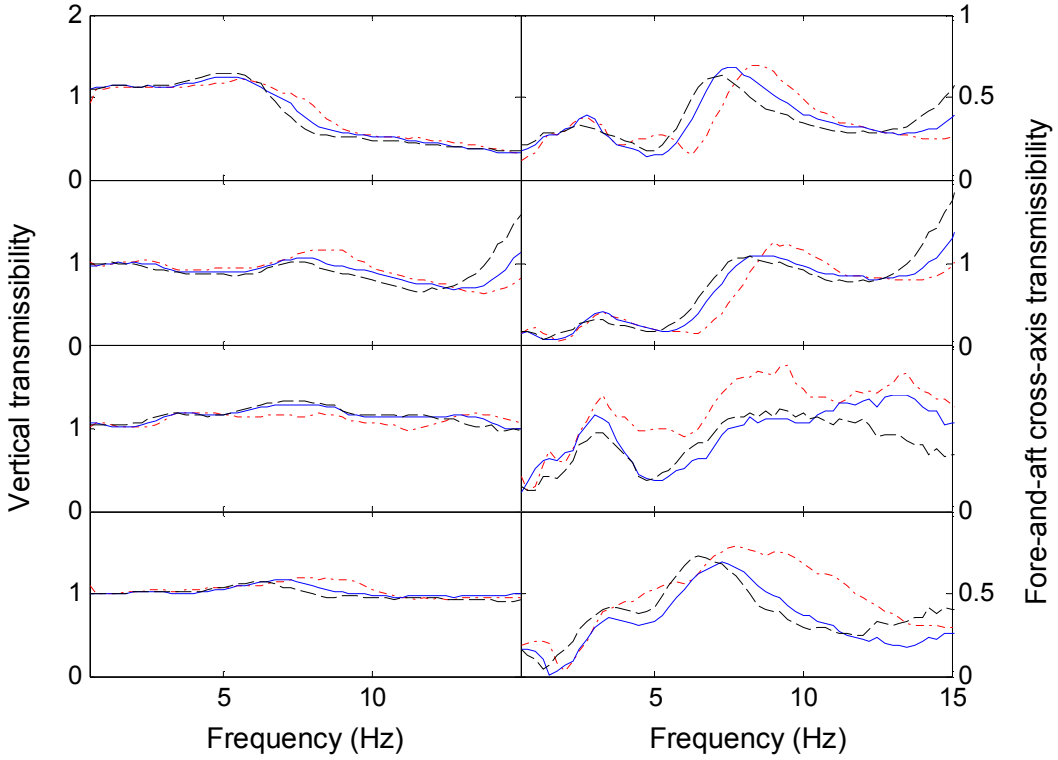

Figure 4.20 Nominal transfer functions of motions of two adjacent measurement locations of subject 1: (a) from pelvis to L3; (b) from L3 to T12; (c) from T12 to T5; (d) from T5 to T1. —.—, a_z=0.25 ms^{-2} r.m.s.; ——, a_z=0.5 ms^{-2} r.m.s.; - - -, a_z=1.0 ms^{-2} r.m.s.

4.4.3 Relation between transmissibility and apparent mass

Pitch motion of the upper thoracic spine about the lower thoracic spine is thought to contribute to the resonance in the vertical apparent mass (Matsumoto and Griffin, 1998a). In all conditions of the present study, the resonance frequency in the vertical transmissibility to T1 and T5 was significantly associated with the resonance frequency in the vertical apparent mass (Table 4.2). At this resonance, the vertical motion of the upper thoracic spine showed greater transmissibility to T1 than to T5, consistent with pitch motion contributing to the primary resonance of the vertical apparent mass. The resonance in the vertical transmissibility to T12 and was not significantly associated with resonance in the vertical apparent mass with any vibration excitation, implying that the vertical motion of the lower thoracic spine did not contribute to the mode responsible for the vertical apparent mass resonance.

Table 4.2 Correlation (Spearman test) between the resonance frequency of the vertical apparent mass and the resonance frequency in the vertical transmissibility.

a_z (ms^{-2} r.m.s.)	a_x (ms^{-2} r.m.s.)		Pelvis	L3	T12	T5	T1
0.25	0	Correlation coefficient	0.387	0.752	0.169	0.760	0.934
		p value	0.214	0.005	0.599	0.004	<0.001
0.5	0	Correlation coefficient	0.662	0.545	0.101	0.889	0.904
		p value	0.019	0.067	0.749	<0.001	<0.001
1,0	0	Correlation coefficient	0.476	0.515	0.228	0.980	0.982
		p value	0.116	0.087	0.475	<0.001	<0.001
1.0	0.25	Correlation coefficient	0.809	0.895	0.04	0.950	0.967
		p value	<0.001	<0.001	0.903	<0.001	<0.001
1.0	0.5	Correlation coefficient	0.771	0.928	0.291	0.989	0.944
		p value	0.003	<0.001	0.358	<0.001	<0.001
1.0	1.0	Correlation coefficient	0.223	0.814	0.255	0.922	0.732
		p value	0.487	<0.001	0.425	<0.001	<0.001

The correlation between the movement of the lumbar spine and the pelvis changed according to the vibration excitation. With the three dual-axis excitations, the resonance frequency in the vertical transmissibility to L3 was associated with the resonance frequency in the vertical apparent mass. With single-axis vertical excitation, a significant correlation was only found with the lowest magnitude of excitation (0.25 ms^{-2} r.m.s.). With dual axis excitation (a_z=1.0 ms^{-2} with a_x=0.25 ms^{-2} r.m.s., and a_z=1.0 ms^{-2} with a_x=0.5 ms^{-2} r.m.s.) and with single-axis excitation at a_z=0.5 ms^{-2} r.m.s., the resonance frequency of the vertical motion of the pelvis was correlated to the vertical apparent mass. The findings suggest that the vertical apparent mass of the body at resonance is influenced by the vibration modes of several body segments, especially those with longitudinal motion of the lumbar spine and pelvis, with contributions that vary according to the magnitude of the vibration excitation in the vertical and fore-and-aft directions.

The resonance frequency evident in the pitch motion of the pelvis was not closely related to the resonance frequency of the vertical apparent mass with any of the six vibration excitations. This is consistent with Matsumoto and Griffin (1998a) who concluded that pitch motion of the pelvis did not make a major contribution to the principal resonance in the vertical apparent mass.

The resonance frequencies in the fore-and-aft cross-axis transmissibility to each measurement locations did not show correlations with the resonance frequency of the vertical apparent mass during either single-axis or dual-axis excitation, possibly because fore-and-aft motion was low compared to the vertical motion.

4.5 Conclusion

The resonance frequencies evident in the vertical apparent mass, the fore-and-aft cross-axis apparent mass, and the transmissibilities between vertical seat vibration and vibration of the spine and pelvis in the fore-and-aft and vertical directions (and pitch motion at the pelvis) reduced as the magnitude of vertical vibration increased. There were similar reductions with constant magnitude vertical vibration but increasing magnitude of fore-and-aft excitation.

With single-axis vertical excitation, a softening of the tissues with increasing vibration magnitude may explain the non-linearity. With dual-axis excitation, the nonlinear behaviour may be explained by coupling between the mode associated with vertical excitation and the cross-axis influence of the fore-and-aft excitation.

A complex combination of vibration modes (with pitch of the upper thoracic spine, bending of the lumbar spine, and longitudinal deformation of the buttocks tissues) appear to contribute to the principal resonance in the vertical apparent mass. It seems that the involvement of different body segments in the resonance varies with the magnitude of the vibration and the number of vibration axes.

CHAPTER 5: FORE-AND-AFT VIBRATION OF THE SEATED HUMAN BODY: NONLINEARITY, CROSS-AXIS COUPLING AND ASSOCIATIONS BETWEEN RESONANCES IN TRANSMISSIBILITY AND APPARENT MASS

5.1 Introduction

The vibration exposure in the field usually involves multi-axis excitation. The excitation in each axis is coupled so that the response in one axis may be changed by the excitation in an orthogonal direction. Understanding of the biodynamic response with dual-axis excitation will improve the dynamic modelling so as to advance prediction of occupant ride comfort. The principal resonance of the seated human body excited by fore-and-aft vibration is at a much lower frequency than the 5-Hz principal resonance associated with vertical excitation. In eight males sitting without a backrest during fore-and-aft random vibration, a first resonance in the apparent mass around 0.7 Hz and a less-pronounced second resonance between 1.5 to 3 Hz have been reported (Fairley and Griffin, 1990). In 12 males exposed to fore-and-aft random vibration over the range 0.25 to 20 Hz, three resonances (around 1 Hz, between 1 and 3 Hz, and between 3 and 5 Hz) have been seen in the fore-and-aft apparent mass measured on a seat without backrest (Nawayseh and Griffin, 2005). With sinusoidal excitation, the fore-and-aft apparent mass has been reported to be greatest around 2.5 Hz (Subashi *et al.*, 2009).

With single-axis vertical excitation, the principal resonance in the driving point apparent mass has been related to movements of the pelvis, the spine and the viscera (Sandover *et al.*, 1987; Kitazaki and Griffin, 1998; Matsumoto and Griffin, 1998a; Mansfield and Lundström, 1998). It has been shown that fore-and-aft vibration of a seat can affect the transmission of vertical seat vibration to the pelvis and the upper-body (Chapter 4), but there are no published studies of the motion of the pelvis or upper-body during fore-and-aft excitation, so the modes associated with resonances in the fore-and-aft apparent mass are unknown.

During fore-and-aft excitation, both the fore-and-aft apparent mass and the vertical cross-axis apparent mass (i.e. the ratio of vertical force to fore-and-aft acceleration) depend on the vibration magnitude. It has been reported that the resonance frequency of the second mode of the fore-and-aft apparent mass (in the range 1.5 to 3 Hz) decreased as the magnitude of fore-and-aft vibration excitation increased (Fairley and Griffin, 1990). It was also reported that with increasing magnitude of fore-and-aft vibration, the fore-

and-aft apparent mass increased at a resonance around 2 or 3 Hz but decreased at a resonance around 5 or 6 Hz (Mansfield and Lundström, 1998). At frequencies greater than 6 Hz, both the fore-and-aft apparent mass and the vertical cross-axis apparent mass reduced progressively as the magnitude of the fore-and-aft vibration increased from 0.125 to 1.25 ms^{-2} r.m.s. (Nawayseh and Griffin, 2005). The frequencies of the principal resonance in the fore-and-aft apparent mass around 2 Hz and in the vertical cross-axis apparent mass around 4 to 8 Hz have also been observed to decrease with increasing the magnitude of the fore-and-aft excitation (Qiu and Griffin, 2010).

A few studies have investigated the apparent mass of the human body with dual-axis excitation and found that the apparent mass is similar to that with single-axis excitation. Nonetheless, additional excitation in an orthogonal direction tends to reduce the modulus of the primary peak in the fore-and-aft apparent mass (Hinz *et al*., 2006a; Mansfield and Maeda, 2006; Qiu and Griffin, 2010). The transmissibility of the human body exposed to dual-axis vibration has not previously been investigated systematically. How the vibration modes of the upper body contribute to the resonances seen in the apparent mass during dual-axis excitation is unknown.

In Chapter 4, how biodynamic response to the vertical excitation depends on the magnitude of vertical excitation and the addition of fore-and-aft excitation was identified, but the transmission of vibration to the spine and pelvis during fore-and-aft excitation has not previously been reported. As a parallel study, the research presented in this chapter was designed to examine how the apparent mass and the transmissibility of the human body sitting without a backrest depends on the magnitude of fore-and-aft vibration excitation and the addition of vertical excitation. It was hoped to advance understanding of the association between the fore-and-aft apparent mass and vertical cross-axis apparent mass and the transmission of vibration to the pelvis and the spine during dual-axis excitation. It was hypothesised that the transmission of fore-and-aft vibration to the pelvis and the upper-body would be similar with single-axis fore-and-aft excitation and dual-axis fore-and-aft and vertical excitation, but that the addition of vertical excitation would tend to reduce the resonance frequencies.

5.2 Experiment method

5.2.1 Apparatus

Subjects sat in a rigid seat mounted on the ISVR 6-axis motion simulator capable of ±0.5 m vertical displacement, ±0.25 m fore-and-aft and lateral displacement, ±10 degrees of roll and pitch, and ±10 degrees of yaw. A force plate capable of measuring forces in the fore-and-aft and vertical directions simultaneously was secured to the supporting surface of the seat. The force plate (Kistler 9281 B) consisted of four tri-axial quartz transducers at the four corners of a rectangular aluminium plate. Signals from the four force transducers orientated to be sensitive to fore-and-aft force were summed and amplified by a charge amplifier (Kistler 5001). Signals from the four force transducers orientated to be sensitive to vertical force were summed and amplified by a similar charge amplifier. A tri-axial SIT-pad was used to measure the fore-and-aft and vertical acceleration on the seat surface at the centre of the force platform.

5.2.2 Subjects and stimuli

Twelve male subjects with median age 26.5 years (range 23 to 36 years), weight 68.5 kg (range 60.4 to 80 kg), and stature 1.74 m (range 1.65 to 1.82 m), participated in the study that was approved by the Human Experimentation Safety and Ethics Committee of the Institute of Sound and Vibration Research at the University of Southampton. During the experiment, subjects sat with their upper body in a comfortable upright position and looked straight ahead. Their feet were supported by a footrest that moved with the simulator platform.

Subjects were exposed to random vibration with approximately flat constant-bandwidth acceleration spectra (0.2 to 20 Hz) in six combinations of four magnitudes of fore-and-aft vibration (0, 0.25, 0.5, or 1.0 ms^{-2} r.m.s.) and four magnitudes of vertical vibration (0, 0.25, 0.5, or 1.0 ms^{-2} r.m.s.) (Table 5.1). All stimuli were of 60-s duration, with motions in the fore-and-aft and vertical directions uncorrelated with each other.

Table 5.1 Vertical (*z*-axis) and fore-and-aft (*x*-axis) excitations experienced by subjects.

		x-axis excitation (ms^{-2} r.m.s.)			
		0	0.25	0.5	1.0
z-axis excitation (ms^{-2} r.m.s.)	0		a_x	a_x	a_x
	0.25	-	-	-	$a_x + a_z$
	0.5	-	-	-	$a_x + a_z$
	1.0	-	-	-	$a_x + a_z$

5.2.3 Motion measurement locations on the body

Acceleration was measured in the fore-and-aft and vertical directions on the body surface over the first, fifth, and twelfth thoracic vertebrae, the third lumbar vertebra, and the pelvis (at the iliac crest). The pitch motion of the pelvis was also estimated from the difference between two vertical accelerations mounted at 25-mm separation on a single block located at the iliac crest.

The vibration on the body surface was measured with two miniature accelerometers (Entran EGA(X)) attached orthogonally to T-shaped balsa wood blocks. The weight of each block was about 1 g and similar to that of each miniature accelerometer. The block was attached to the body surface with double-side adhesive tape with a contact area similar to that of a vertebral body.

The experimental set-up and the mounting of the accelerometer block are shown in Figure 5.1.

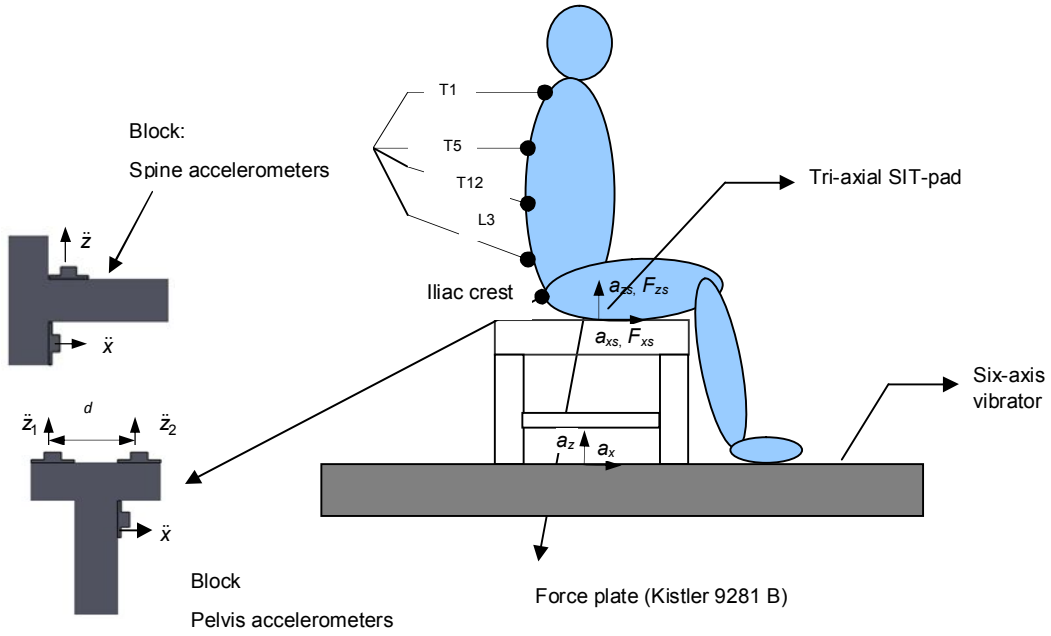

Figure 5.1 Experiment set-up and the body transmissibility measurement locations.

5.2.4. Data analysis

Forces and accelerations were acquired with a sampling rate of 512 samples per second via anti-aliasing filters at 50 Hz. Mass cancellation was performed in the time domain to remove the influence of the mass of the top plate above the force transducers from the

measured fore-and-aft force (Qiu and Griffin, 2010). Signal processing was conducted with a frequency resolution of 0.25 Hz.

Assuming that a_x and a_z represent the fore-and-aft and vertical accelerations and f_x and f_z, the fore-and-aft and vertical forces, the fore-and-aft apparent mass and the vertical cross-axis apparent mass and the corresponding coherency were calculated using the *HVLab* Matlab Toolbox function using cross-spectra density method (CSD) .

$$\begin{aligned} M_{xx} &= \frac{G_{a_x f_x}}{G_{a_x}}, \quad \gamma^2_{xx} = \frac{\left|G_{a_x f_x}\right|^2}{G_{ax} G_{f_x}} \\ M_{xz} &= \frac{G_{a_x f_z}}{G_{a_x}}, \quad \gamma^2_{xz} = \frac{\left|G_{a_x f_z}\right|^2}{G_{a_x} G_{f_z}} \end{aligned} \quad . \tag{5.1}$$

Where,

G_{a_x} , is the auto spectrum of a_x,

G_{f_x} and G_{f_z} are the auto spectra of f_x and f_z,

$G_{a_x f_x}$, is the cross-spectrum of a_x and f_x, and

$G_{a_x f_z}$, is the cross-spectrum of a_x and f_z.

The fore-and-aft transmissibility and the vertical cross-axis transmissibility were calculated with a_{tx} and a_{tz} representing the fore-and-aft and vertical acceleration measured on the body surface.

$$\begin{aligned} T_{xx} &= \frac{G_{a_x a_{tx}}}{G_{a_x}}, \quad \gamma^2_{Txx} = \frac{\left|G_{a_x a_{tx}}\right|^2}{G_{a_x} G_{a_{tx}}} \\ T_{xz} &= \frac{G_{a_x a_{tz}}}{G_{a_x}}, \quad \gamma^2_{Txz} = \frac{\left|G_{a_x a_{tz}}\right|^2}{G_{a_x} G_{a_{tz}}} \end{aligned} \quad . \tag{5.2}$$

Where,

$G_{a_{tz}}$ and $G_{a_{tx}}$ are the auto spectra of a_{tz} and a_{tx},

$G_{a_x a_{tx}}$, is the cross-spectrum of a_x and a_{tx},

$G_{a_x a_{tz}}$, is the cross-spectrum of a_x and a_{tz}.

The pitch motion of the pelvis was defined as ratio of the difference in the two vertical vibrations to the distance between the two transducers (Figure 5.1):

$$\ddot{\theta} = \frac{\ddot{z}_1 - \ddot{z}_2}{d} \quad . \tag{5.3}$$

The pitch transmissibility of the pelvis was calculated as

$$T_{xpch} = \frac{G_{a_X\ddot{\theta}}}{G_{a_X}}, \qquad \gamma^2_{T_{xpch}} = \frac{\left|G_{a_X\ddot{\theta}}\right|^2}{G_{a_X} G_{\ddot{\theta}}} \tag{5.4}$$

.

Where,

$G_{a_x\ddot{\theta}}$, is the cross-spectrum of a_x and $\ddot{\theta}$,

$G_{\ddot{\theta}}$, is the auto spectrum of $\ddot{\theta}$.

Equations (5.1-5.4) were used to calculate the transfer functions with both single-axis and dual-axis excitation, because they are appropriate when the two inputs are independent (Bendat and Piersol, 1986).

The effect of inclination of the body surface was reduced using the angle between the body surface and the vertical axis (Chapter 4).

$$a_{tx} = \ddot{x}\cos\Psi - \ddot{z}\sin\Psi, \quad a_{tz} = \ddot{z}\cos\Psi + \ddot{x}\sin\Psi. \tag{5.5}$$

Where a_{tz} is the time history of the vertical acceleration and a_{tx} is the fore-and-aft acceleration; $\ddot{z}$ and $\ddot{x}$ are the measured accelerations along the body surface and normal to the body surface respectively; Ψ is the angle between the body surface and the vertical direction.

The motion of the spine, $T_s(f)$, was estimated from the transmissibility between the seat base and the body surface and a data correction function that takes into account the effect of the tissue and the skin between the bone and the accelerometer (Chapter 4).

5.3 Results

5.3.1 Apparent mass

5.3.1.1 Inter-subject variability

With single-axis and dual-axis excitation, the fore-and-aft apparent mass showed a first peak around 1 Hz. A second peak around 2 to 4 Hz can be observed for all 12 subjects (row (I) in Figure 5.2). All subjects except subjects 1 and 2 exhibited a third resonance in the range of 5 to 7 Hz. The vertical cross-axis apparent mass had a first peak in the frequency range 0.5 to 1.25 Hz (row (II) in Figure 5.2). A broad second peak was

apparent from 2 to 6 Hz in most subjects. Subjects 9 and 10 exhibited four peaks in the frequency range up to 10 Hz (around 1, 2.75, 5.25, and 7.5 Hz).

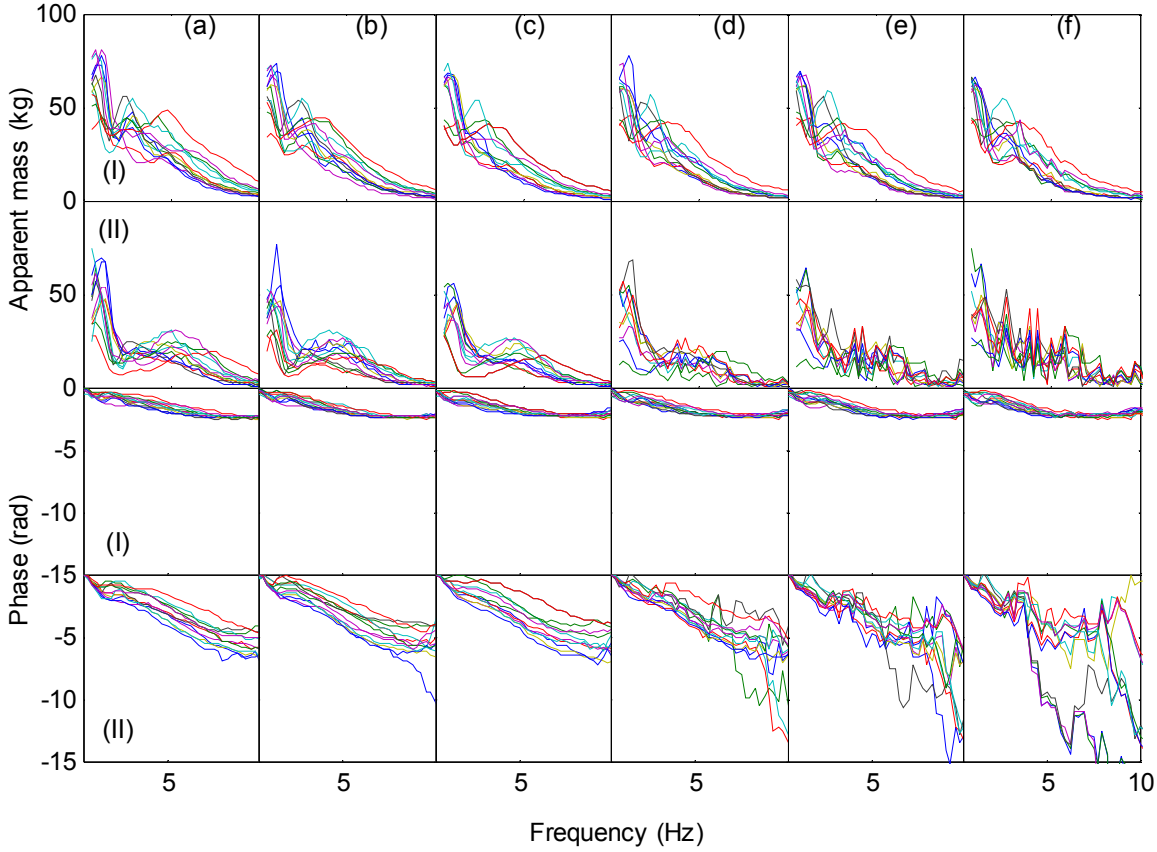

Figure 5.2 Individual apparent masses of 12 subjects: (I), the modulus and phase of the fore-and-aft apparent mass; (II), the modulus and phase of the vertical cross-axis apparent mass. (a) a_x=0.25 ms^{-2} r.m.s.; (b) a_x=0.5 ms^{-2} r.m.s.; (c) a_x=1.0 ms^{-2} r.m.s.; (d) a_x=1.0 ms^{-2} r.m.s., a_z=0.25 ms^{-2} r.m.s.; (e) a_x=1.0 ms^{-2} r.m.s., a_z=0.5 ms^{-2} r.m.s.; (f) a_x=1.0 ms^{-2} r.m.s., a_z=1.0 ms^{-2} r.m.s.

5.3.1.2 Nonlinearity in the apparent mass

With single-axis fore-and-aft excitation, the frequency of the first peak in the fore-and-aft apparent mass around 1 Hz was not changed significantly with a change in the magnitude of the single-axis fore-and-aft excitation or the additional vertical excitation. Nonlinearity was therefore examined by studying changes in the apparent mass at the resonance frequency.

Nonlinearity in the modulus of the fore-and-aft apparent mass was examined at the first resonance around 1 Hz, the second peak around 2.75 Hz, and the third peak around 5.25 Hz. Increasing the magnitude of single-axis fore-and-aft excitation reduced the fore-and-aft apparent mass at the first resonance (Friedman, p=0.006; Figure 5.3). The fore-

and-aft apparent mass also decreased as the additional vertical vibration increased in magnitude from 0.25 to 1.0 ms^{-2} r.m.s. when the fore-and-aft excitation was 1.0 ms^{-2} r.m.s. (Friedman, p=0.023; Figure 5.4). At 5.25 Hz, the fore-and-aft apparent mass was reduced with increasing magnitude of single-axis fore-and-aft excitation (Friedman, p<0.001; Figure 5.3) and with the addition of vertical excitation from 0.25 to 1.0 ms^{-2} r.m.s. during fore-and-aft excitation at 1.0 ms^{-2} r.m.s. (Friedman, p=0.005; Figure 5.4).

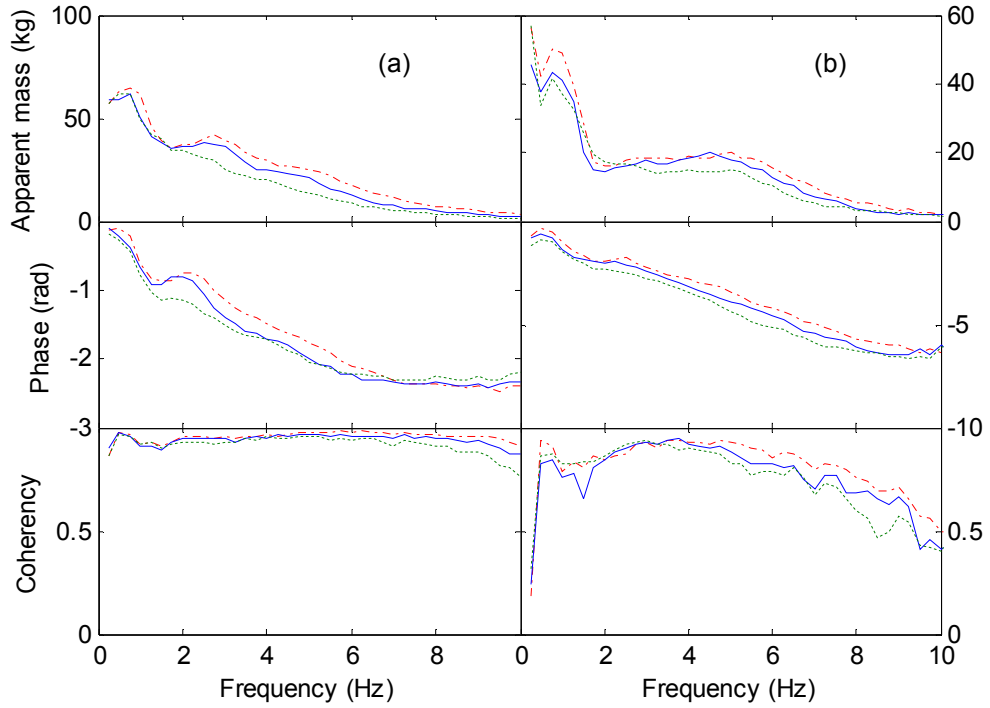

Figure 5.3 Effect of the magnitude of the single-axis fore-and-aft excitation on: (a) fore-and-aft apparent mass; (b) vertical cross-axis apparent mass. —.—, a_x=0.25 ms^{-2} r.m.s.; ——, a_x=0.5 ms^{-2} r.m.s.; - - -, a_x=1.0 ms^{-2} r.m.s. (medians of 12 subjects).

Nonlinearity in the modulus of the vertical cross-axis apparent mass was also examined at 1.0 Hz, 2.75 Hz, and 5.25 Hz. The vertical cross-axis apparent mass at 1.0 Hz reduced with increasing magnitude of single-axis fore-and-aft excitation (Friedman, p=0.001; Figure 5.3). A similar change was observed as the magnitude of the additional vertical vibration increased from 0.25 to 1.0 ms^{-2} r.m.s. while maintaining the fore-and-aft vibration magnitude at 1.0 ms^{-2} r.m.s. (Friedman, p=0.039; Figure 5.4). At 2.75 Hz, there was no significant reduction in the vertical cross-axis apparent mass with either increasing magnitude of the fore-and-aft excitation or the additional vertical excitation. At 5.25 Hz, the vertical cross-axis apparent mass was reduced with increasing magnitude of fore-and-aft excitation (Friedman, p=0.009; Figure 5.3) and with increasing magnitude

of the additional vertical excitation from 0.25 to 1.0 ms^{-2} r.m.s. (Friedman, p<0.001; Figure 5.4)

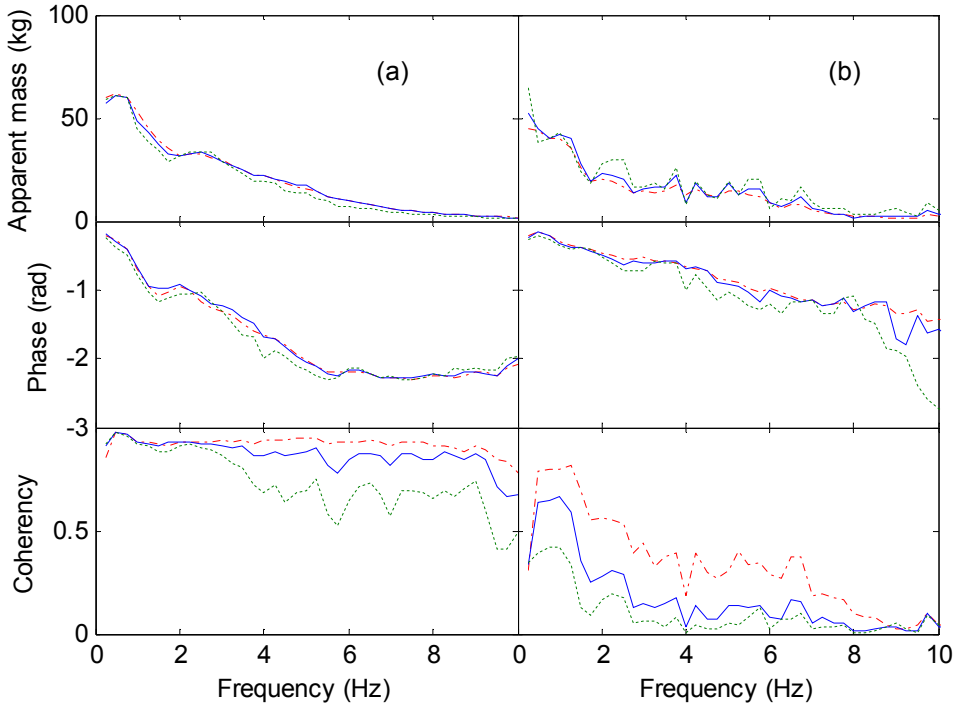

Figure 5.4 Effect of the magnitude of the additional vertical excitation on: (a) fore-and-aft apparent mass; (b) vertical cross-axis apparent mass. —.—, a_z=0.25 ms^{-2} r.m.s., a_x=1.0 ms^{-2} r.m.s.; ——, a_z=0.5 ms^{-2} r.m.s., a_x=1.0 ms^{-2} r.m.s.; - - -, a_z=1.0 ms^{-2} r.m.s., a_x=1.0 ms^{-2} r.m.s. (medians of 12 subjects).

5.3.2 Transmissibility

5.3.2.1 Fore-and-aft transmissibility

There was large inter-subject variability in the fore-and-aft inline transmissibility to the spine and the pelvis (Figure 5.5(a) and Figure 5.5(c)). The transmissibility from fore-and-aft seat motion to fore-and-aft motion at T1 showed a first peak over the frequency range 0.5 to 1.25 Hz in all subjects. Second and third peaks were present around 2.25 and 4.5 Hz but were smaller and observed in only 8 of the 12 subjects. The transmission of fore-and-aft vibration to T5 and T12 was similar to T1. The transmissibility to L3 showed a first peak in the frequency range 0.5 to 1.75 Hz and a second peak around 2.5 Hz. A third peak around 7.5 Hz was observed in subject 12. There was greater inter-subject variability in transmissibility to the pelvis than to other locations. The primary peak occurred in the range 0.5 to 1.75 Hz for seven subjects, with other subjects exhibiting higher primary resonance frequencies (2 Hz for subject 7; 2.25 Hz for subject 12; 3 Hz for subject 9; 3.25 Hz for subject 11; 4.25 Hz for subject 10).

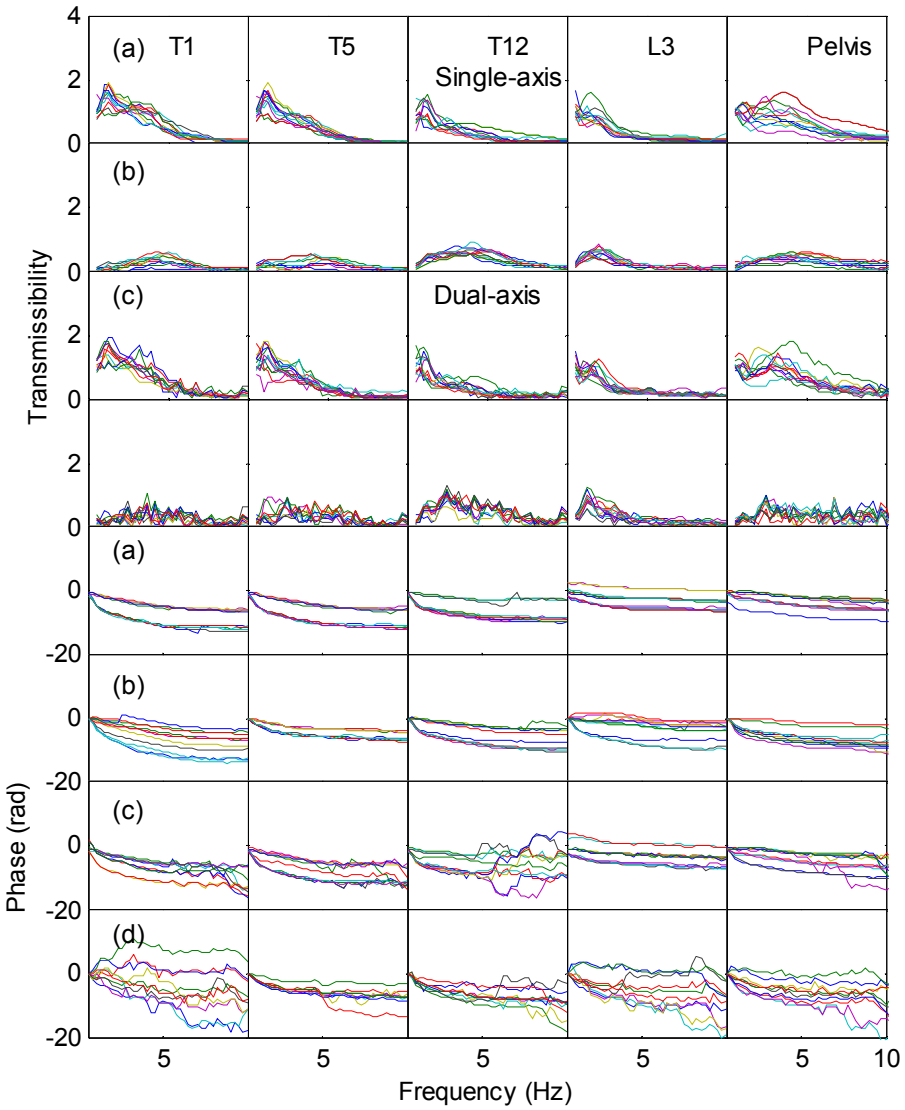

Figure 5.5 Individual transmissibility from fore-and-aft seat motion to upper body motion of 12 subjects: (a) fore-and-aft transmissibility with single-axis fore-and-aft vibration (a_x=1.0 ms^{-2} r.m.s.); (b) vertical cross-axis transmissibility with single-axis fore-and-aft vibration (a_x=1.0 ms^{-2} r.m.s.); (c) fore-and-aft transmissibility with dual-axis vibration (a_x=1.0 ms^{-2} r.m.s, a_z=1.0 ms^{-2} r.m.s.); (d) vertical cross-axis transmissibility with dual-axis vibration (a_x=1.0 ms^{-2} r.m.s., a_z =1.0 ms^{-2} r.m.s.). (The individual transmissibility at other vibration magnitudes is shown in Appendix C.)

The first resonance in the fore-and-aft transmissibility differed between the five measurement locations (Friedman, p<0.05). With lowest single-axis fore-and-aft vibration level, i.e., a_x=0.25 ms^{-2} r.m.s., the first resonance frequency of fore-and-aft transmissibility to L3 was significantly lower than that of fore-and-aft transmissibility to pelvis (Figure 5.5, Wilcoxon, p<0.05). The first resonance frequency of fore-and-aft

transmissibility to T12 was significantly lower than that of T5 and T1 (Wilcoxon, p<0.05). With highest dual-axis vibration level, i.e., a_x=1.0 ms^{-2} r.m.s., a_z=1.0 ms^{-2} r.m.s., the first resonance frequency of fore-and-aft transmissibility to L3 was also significantly lower than that of pelvis and T1 (Wilcoxon, p<0.05).

5.3.2.2 Vertical cross-axis transmissibility

The cross-axis transmissibility from fore-and-aft seat motion to vertical motion at each measurement location shows a first resonance in the range 2.25 to 5.25 Hz, with marked inter-subject variability (Figure 5.5(b), Figure 5.5(d)). The cross-axis vertical transmissibility to T1 had a resonance in the range 3.25 to 5.25 Hz for all except subject 1. The vertical transmissibility to T5 had a primary resonance in the range 2.25 to 5.5 Hz, for all except subjects 1, 2, and 8. The vertical transmissibility to T12 showed a primary resonance in the range 2.25 to 5 Hz for all except subject 2. The resonance in the vertical cross-axis transmissibility to L3 varied from 1.0 to 2.25 Hz, much lower than the vertical cross-axis transmissibility to other measurement locations but similar to the resonance in the fore-and-aft transmissibility to L3. The resonance frequencies in the vertical cross-axis transmissibility to the pelvis ranged from 3.25 to 5.25 Hz in nine of the 12 subjects, but with no evidence of a resonance in subjects 1, 7, or 9 over the frequency range 0.5 to 10 Hz.

The first resonance of the vertical cross-axis transmissibility were also found to be significantly varied among measurement locations (Friedman, p<0.05). The first resonance frequency of vertical cross-axis transmissibility to L3 was found to be significantly lower than those to all the other measurement locations with single-axis fore-and-aft vibration at a_x=1.0 ms^{-2} r.m.s (Wilcoxon, p<0.05). The first resonance frequency of vertical cross-axis transmissibility to T12 was significantly lower than that to pelvis (p<0.05). With the addition of vertical vibration also in the magnitude of 1.0 ms^{-2} r.m.s, the similar relationship between the first resonance frequency of vertical cross-axis transmissibility to L3 and other measurement locations was observed.

5.3.2.3 Pitch transmissibility to the pelvis

The transmissibility from fore-and-aft seat motion to pitch motion of the pelvis exhibited large inter-subject variability with both single-axis fore-and-aft excitation and dual-axis excitation (Figure 5.6). The primary resonance frequency in the pitch transmissibility ranged from 1 to 8.75 Hz with single-axis excitation and from 2.25 to 9.75 Hz with dual-

axis excitation. Similar to the fore-and-aft transmissibility to each measurement location, multiple peaks were observed with all subjects over the frequency range 0.5 to 10 Hz.

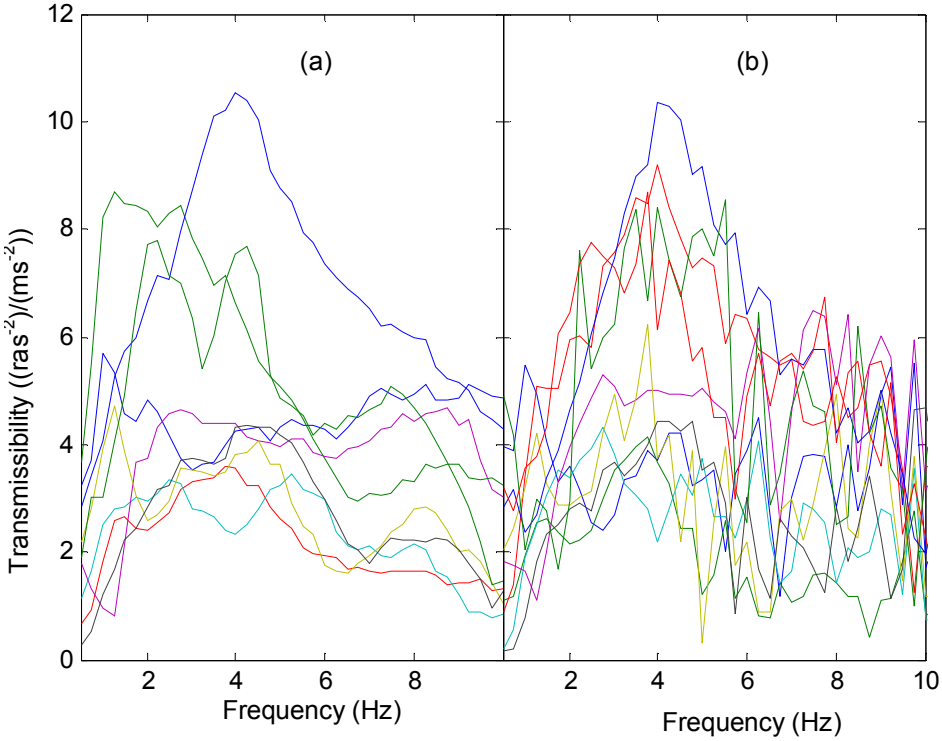

Figure 5.6 Individual transmissibility from fore-and-aft seat motion to pitch of the pelvis of 12 subjects: (a) pitch transmissibility with single-axis vibration (a_x=1.0 ms^{-2} r.m.s.); (b) pitch transmissibility with dual-axis vibration (a_x=1.0 ms^{-2} r.m.s., a_z =1.0 ms^{-2} r.m.s.). (The individual transmissibility at other vibration magnitudes is shown in Appendix C.)

5.3.2.4 Nonlinearity in the fore-and-aft transmissibility

The first resonance frequency of the fore-and-aft transmissibility to any of the measurement locations was not changed significantly with increasing magnitude of single-axis fore-and-aft excitation (Friedman, p>0.05 for all locations) or the addition of vertical excitation from 0.25 to 1.0 ms^{-2} r.m.s. (Friedman, p>0.05 for all locations). Nonlinearity was therefore examined by studying changes in the transmissibility at the resonance frequency.

The influence of the magnitude of fore-and-aft excitation and the addition of vertical excitation on the fore-and-aft transmissibility at the first resonance around 1 Hz, the second peak around 2.75 Hz, and the third peak around 5.25 Hz was examined for each measurement location (Figures 5.7 and 5.8).

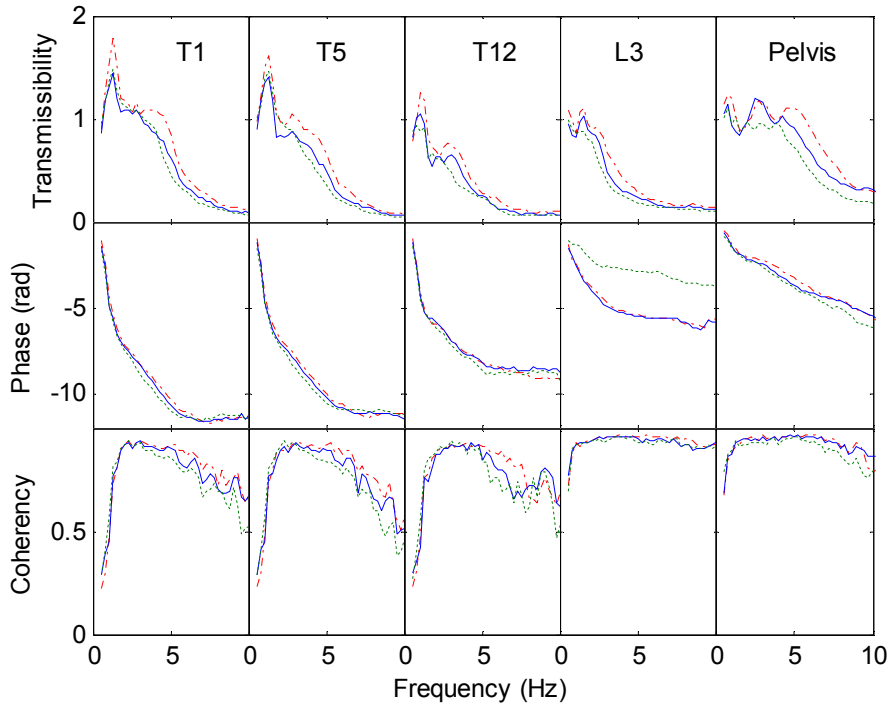

Figure 5.7 Effect of the magnitude of fore-and-aft excitation on the fore-and-aft transmissibility to each measurement location: —.—, a_x=0.25 ms^{-2} r.m.s.; ——, a_x=0.5 ms^{-2} r.m.s.; - - -, a_x=1.0 ms^{-2} r.m.s. (medians of 12 subjects).

The fore-and-aft transmissibility to the pelvis at the first resonance frequency reduced with increasing magnitude of the additional vertical excitation from 0.25 to 1.0 ms^{-2} r.m.s. (Friedman, p=0.017; Figure 5.8). However, a significant reduction in the fore-and-aft transmissibility to the pelvis at 2.75 Hz and 5 Hz was only found with increasing magnitude of single-axis fore-and-aft vibration (Friedman, p=0.005 at 2.75 Hz; p=0.015 at 5.25 Hz; Figure 5.7). The fore-and-aft transmissibility to L3 and T12 at the first resonance frequency was reduced with increasing magnitude of fore-and-aft vibration excitation (Friedman, p=0.006 for L3; p=0.039 for T12). The reductions at 2.75 Hz and 5.25 Hz were observed with both increasing magnitude of single-axis fore-and-aft excitation (Friedman, p<0.001) and increasing magnitude of the additional vertical excitation from 0.25 to 1.0 ms^{-2} r.m.s. (Friedman, p<0.001). A significant decrease in the fore-and-aft transmissibility to T5 was only observed at 5.25 Hz, but with both increasing magnitude of single-axis fore-and-aft vibration (p<0.001) and increasing magnitude of the additional vertical excitation from 0.25 to 1.0 ms^{-2} r.m.s. (Friedman, p=0.01). With increasing magnitude of single-axis fore-and-aft excitation there was a significant decrease in the fore-and-aft transmissibility to T1 at the first resonance frequency (Friedman, p=0.009) and at 5.25 Hz (Friedman, p<0.001).

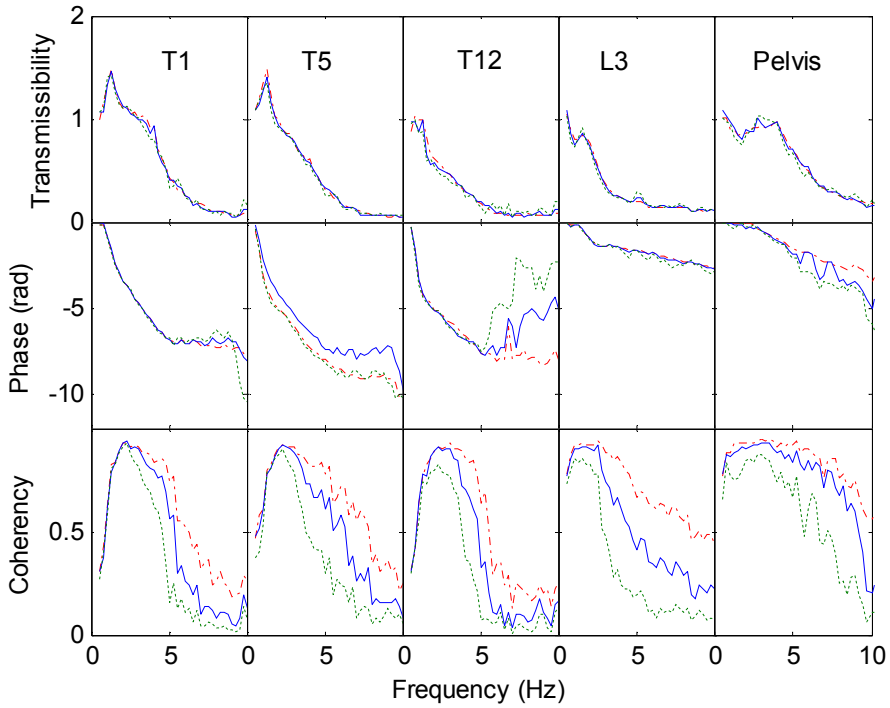

Figure 5.8 Effect of the magnitude of the additional vertical excitation on the fore-and-aft transmissibility to each measurement location: —.—, a_z=0.25 ms^{-2} r.m.s., a_x=1.0 ms^{-2} r.m.s.; ——, a_z=0.5 ms^{-2} r.m.s., a_x=1.0 ms^{-2} r.m.s.; - - -, a_z=1.0 ms^{-2} r.m.s., a_x=1.0 ms^{-2} r.m.s. (medians of 12 subjects).

5.3.2.5 Nonlinearity in the cross-axis transmissibility

With increasing magnitude of single-axis fore-and-aft excitation, there was a reduction in pitch transmissibility to the pelvis at 5.25 Hz (Friedman, p=0.017; Figure 5.9).

The nonlinearity in the vertical cross-axis transmissibility to each measurement location (Figures 5.10 and 5.11) at 1 Hz, 2.75 Hz and 5.25 Hz was also examined with changing magnitude of vibration excitation. The vertical cross-axis transmissibility to the pelvis at 2.75 Hz was reduced with increasing magnitude of vertical vibration from 0.25 to 1.0 ms^{-2} r.m.s. when the fore-and-aft excitation magnitude was at 1.0 ms^{-2} r.m.s. (Friedman, p=0.036). A significant reduction in transmissibility at 5.25 Hz was observed with increasing magnitude of single-axis fore-and-aft excitation (Friedman, p=0.013), and with increasing magnitude of additional vertical excitation from 0.25 to 1.0 ms^{-2} r.m.s. (Friedman, p=0.028). The vertical cross-axis transmissibility to L3 around 1 Hz decreased with increasing magnitude of the additional vertical excitation from 0.25 to 1.0 ms^{-2} r.m.s. (Friedman, p<0.001). The transmissibility at 2.75 Hz and at 5.25 Hz was also reduced with increasing magnitude of single-axis fore-and-aft excitation (Friedman,

p<0.001 at 2.75 Hz; p=0.005 at 5.25 Hz). The vertical cross-axis transmissibility to T12 and T5 around 1 Hz decreased with increasing magnitude of the additional vertical excitation from 0.25 to 1.0 ms^{-2} r.m.s. when the magnitude of the fore-and-aft excitation was constant at 1.0 ms^{-2} r.m.s. The transmissibility at 5.25 Hz also decreased with increasing magnitude of single-axis fore-and-aft excitation (Friedman, p=0.04). The vertical cross-axis transmissibility to T1 only decreased at 5.25 Hz, and only with increasing magnitude of single-axis fore-and-aft vibration (Friedman, p=0.028).

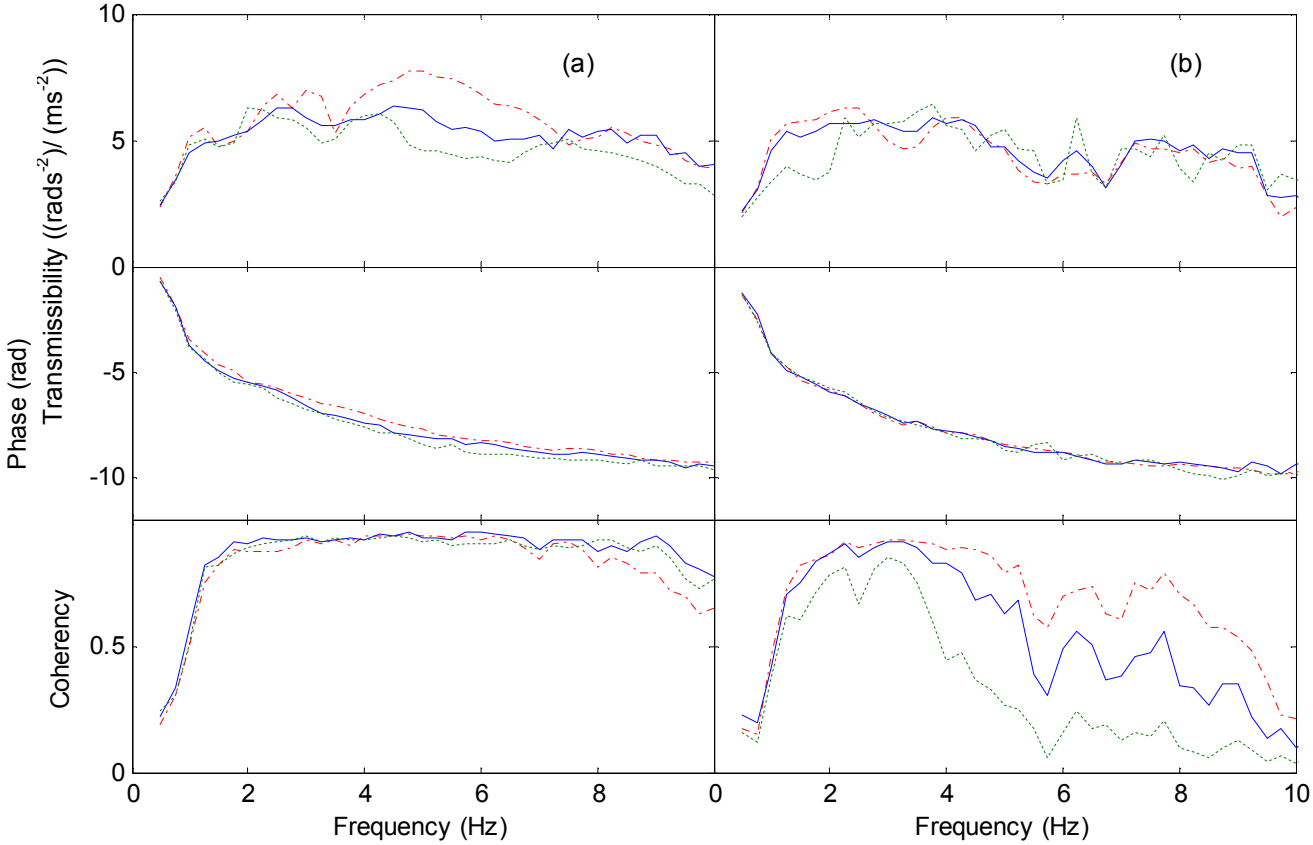

Figure 5.9 Median pitch transmissibility of the pelvis of 12 subjects exposed to: (a) single-axis vibration, —.—, a_x=0.25 ms^{-2} r.m.s.; ——, a_x=0.5 ms^{-2} r.m.s.; - - -, a_x=1.0 ms^{-2} r.m.s.; (b) dual-axis vibration, —.—, a_z=0.25 ms^{-2}r.m.s., a_x=1.0 ms^{-2} r.m.s.; ——, a_z=0.5 ms^{-2} r.m.s., a_x=1.0 ms^{-2} r.m.s.; - - -, a_z=1.0 ms^{-2} r.m.s., a_x=1.0 ms^{-2} r.m.s. (medians of 12 subjects).

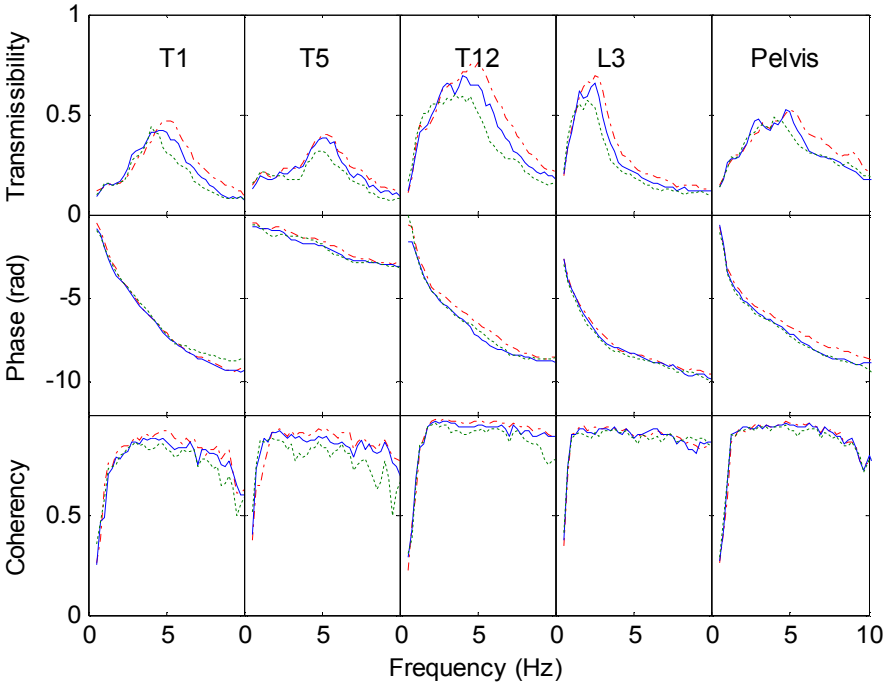

Figure 5.10 Effect of the magnitude of the fore-and-aft excitation on the vertical cross-axis transmissibility to each measurement location: —.—, a_x=0.25 ms^{-2} r.m.s.; ——, a_x=0.5 ms^{-2} r.m.s.; - - -, a_x=1.0 ms^{-2} r.m.s. (medians of 12 subjects).

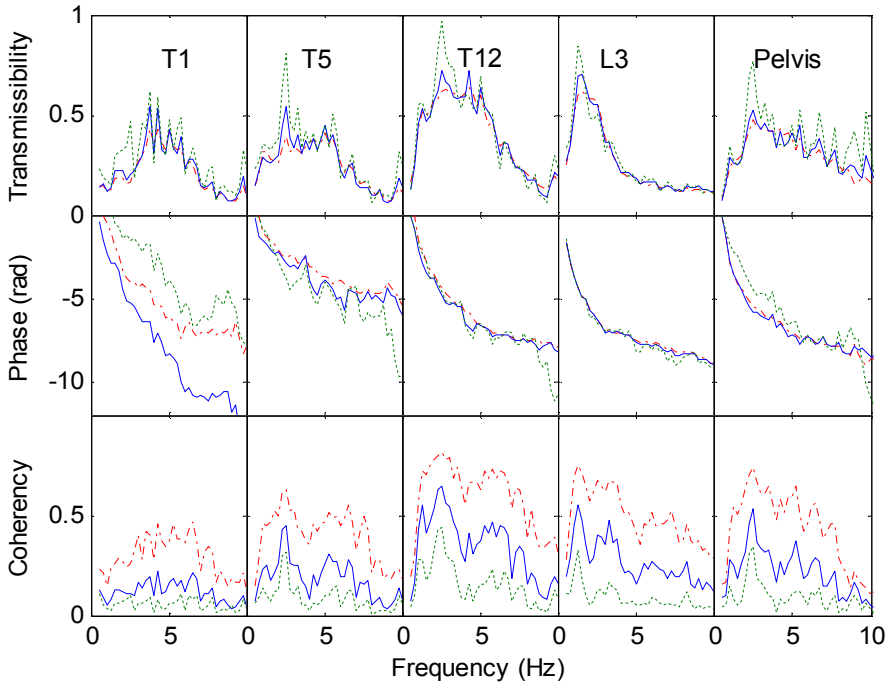

Figure 5.11 Effect of the magnitude of additional vertical excitation on the vertical cross-axis transmissibility of each measurement location: —.—, a_z=0.25 ms^{-2} r.m.s, a_x=1.0 ms^{-2} r.m.s.; ——, a_z=0.5 ms^{-2} r.m.s., a_x=1.0 ms^{-2} r.m.s.; - - -, a_z=1.0 ms^{-2} r.m.s., a_x=1.0 ms^{-2} r.m.s. (medians of 12 subjects).

5.3.2.6 Relative displacement between measurement locations

To investigate how the pelvis and each part of the spine moved relative to each other, the relative vertical and fore-and-aft displacements were calculated: the difference in the acceleration measured during single-axis fore-and-aft vibration at 1.0 ms^{-2} r.m.s. (subject 11) was high-pass filtered (Bessel filter at 0.5 Hz) and then double-integrated to obtain the time history of the relative displacement between adjacent locations. The power spectral density of the relative displacement from 0.25 to 5 Hz is shown in Figure 5.12.

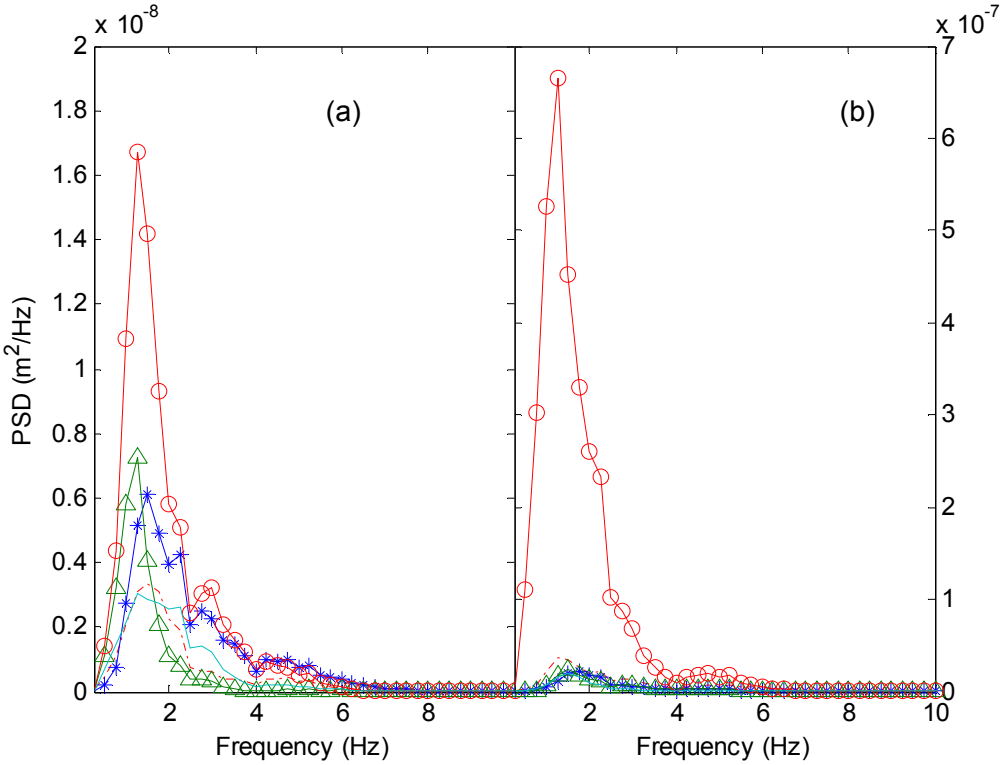

Figure 5.12 Example power spectral densities of (a) vertical relative displacement; (b) fore-and-aft relative displacement between: —.—, pelvis and seat; —O—, L3 and pelvis; —Δ—, T12 and L3; —*—, T5 and T12; ——, T1 and T5 (Subject 11 with single-axis fore-and-aft vibration at a_x=1.0 ms^{-2} r.m.s.).

The largest fore-and-aft relative displacement was found between L3 and the pelvis at the level of the iliac crest, followed by the relative displacement between the pelvis and the seat, between T12 and L3. The first few thoracic vertebrae between T1 and T5 showed the smallest relative fore-and-aft displacements.

The vertical relative displacements were much smaller than their fore-and-aft counterparts for each pair of adjacent locations. The largest vertical relative

displacement was also found between L3 and pelvis while the smallest vertical relative displacement was observed between T1 and T5.

5.4 Discussion

5.4.1 Apparent mass

The apparent mass measured in the present study exhibits similar characteristics to that published previously. The fore-and-aft apparent mass with single-axis fore-and-aft excitation showed the first peak in the vicinity of 1 Hz and a second mode between 2 and 4 Hz, consistent with previous findings (Mansfield and Lundström, 1999; Nawayseh and Griffin, 2005; Qiu and Griffin, 2010). The first peak in the vertical cross-axis apparent mass in the present study occurred in the frequency range 0.5 to 1.25 Hz and there was second wide peak between 2 and 6 Hz with most subjects, similar to results reported in Mansfield and Lundström (1999) and Nawayseh and Griffin (2005). With dual-axis excitation, the fore-and-aft apparent mass and the vertical cross-axis apparent mass exhibited similar resonant behaviour to that found with single-axis excitation (Figure 5.4), as suggested previously (Hinz *et al*., 2006a; Mansfield and Maeda, 2006; Qiu and Griffin, 2010).

Some previous studies have reported a decrease in the resonance frequency of the second mode in the fore-and-aft apparent mass between 2 to 3 Hz with increasing magnitude of excitation, but did not study the first mode around 1 Hz (Mansfield and Maeda, 2006; Qiu and Griffin, 2010). In the present study, the first resonance frequency in the fore-and-aft apparent mass was not found to depend on the magnitude of fore-and-aft excitation (as observed in Fairley and Griffin, 1990; Nawayseh and Griffin, 2005) or the magnitude of the additional vertical excitation. This does not necessarily mean the first resonance is unaffected by vibration magnitude: the 0.25-Hz frequency resolution of the analysis limited the ability to detect small changes in the resonance frequency. With no measurable change in the resonance frequency, the variation in the apparent mass modulus was used to quantify any nonlinearity evident with changing vibration magnitude.

The moduli at the first resonances in the fore-and-aft inline apparent mass and the vertical cross-axis apparent mass reduced with increasing magnitude of fore-and-aft excitation, as found previously (Fairley and Griffin, 1990; Nawayseh and Griffin, 2005; Qiu and Griffin, 2010). Similarly, with dual-axis excitation, the fore-and-aft inline apparent

mass and the vertical cross-axis apparent mass decreased when the magnitude of vertical excitation increased from 0.25 to 1.0 ms^{-2} r.m.s. while the fore-and-aft excitation was held constant at 1.0 ms^{-2} r.m.s. This implies coupling between the response to vertical and fore-and-aft excitation. To produce an equivalent reduction in the fore-and-aft apparent mass at resonance, a greater increase was required in the magnitude of the vertical excitation (0.5 ms^{-2} r.m.s., Section 5.3.1.2) than the magnitude of the fore-and-aft excitation (0.25 ms^{-2} r.m.s., Section 5.3.1.2).

5.4.2 Transmissibility

The fore-and-aft transmissibility to each measurement location exhibited a principal resonance frequency similar to the principal resonance in the fore-and-aft apparent mass (i.e., around 1 Hz), with a second mode around 2 to 4 Hz. The findings imply that the upper body moved like an inverted pendulum with a low resonance frequency. However, at frequencies greater than the first resonance, the upper body did not move like an inverted pendulum.

The effect of the magnitude of vibration on the first resonance in the fore-and-aft transmissibility of the body has not previously been reported. In the present study, similar to the apparent mass, the frequencies of the first resonances evident in the fore-and-aft transmissibilities to the pelvis and the spine were not significantly changed by changes in the magnitude of the fore-and-aft excitation. The absence of significant changes in the first resonance frequencies in the transmissibilities and the apparent masses implies that any changes are small relative to the frequency resolution employed in this study, but it does not exclude the possibility of real changes that may become apparent with further study using a finer frequency resolution.

The fore-and-aft transmissibility to the lumbar spine and the pelvis at the first resonance decreased when the magnitude of additional vertical vibration increased from 0.25 to 1.0 ms^{-2} r.m.s. while the magnitude of fore-and-aft excitation was held constant at 1.0 ms^{-2} r.m.s. (Section 5.3.2.4). The reduction might be attributed to increased damping of the pelvis tissue, but it could also be due to a change in stiffness with a variation in the resonance frequency expected with a change in stiffness not measurable with the 0.25-Hz frequency resolution. The addition of vertical excitation may also have moderated the transmission of fore-and-aft seat vibration to fore-and-aft motion of the upper body and the pelvis by encouraging a more erect posture of the upper body and the pelvis. It seems that different body segments are not equally sensitive to changes in the

magnitude of fore-and-aft excitation or the addition of vertical vibration: with increasing magnitude of fore-and-aft vibration, and increasing magnitude of additional vertical vibration, the fore-and-aft transmissibility to the pelvis, L3, T12 and T1was reduced at the first resonance but there was no reduction in transmissibility to T5 (Section 5.3.2.4).

5.4.3 Relation between the apparent mass and the transmissibility

Motions of the lumbar spine and the pelvis seem to contribute to the first resonance in the fore-and-aft apparent mass. The relative displacements in the fore-and-aft and vertical directions between adjacent measurement locations were greatest between L3 and the pelvis (Figure 5.12). The first resonance frequency in the fore-and-aft transmissibility to L3 was correlated with the first resonance in the fore-and-aft apparent mass (Table 5.2). The second greatest fore-and-aft and vertical relative displacement occurred between the pelvis and the seat, consistent with the first resonance in the fore-and-aft transmissibility to the pelvis being associated with the first resonance in the fore-and-aft apparent mass (Table 5.2).

Movements within the thoracic spine (i.e., T12, T5, and T1) do not seem to make a major contribution to the resonance seen in the driving point fore-and-aft apparent mass. The relative displacements between these locations along the thoracic spine were less than relative motions in the pelvis and lumbar spine (Figure 5.12). Furthermore, there was no significant correlation between the first resonance frequency in the fore-and-aft transmissibility to either T5 or T1 and the first resonance in the fore-and-aft apparent mass at the seat with any vibration excitation. There was a relation between the first resonance frequency in the fore-and-aft transmissibility to T12 and the first resonance in the fore-and-aft apparent mass, but only during dual-axis excitation (Table 5.2).

There was a high correlation between the first resonance frequency in the fore-and-aft transmissibility to the pelvis and the first resonance frequency in the fore-and-aft apparent mass. However, the pitch motion of the pelvis did not appear to contribute much to the first resonance in the fore-and-aft apparent mass: the first resonance frequency in the pitch transmissibility to the pelvis was not highly correlated with the resonance frequency in the fore-and-aft apparent mass (Table 5.2). This suggests that motion of the pelvis contributed to the resonance in the fore-and-aft apparent mass as a result of shear deformation of the tissues beneath the pelvis rather than pitch motion of the pelvis.

Table 5.2 Correlation (Spearman test) between the first resonance frequency in the fore-and-aft apparent mass and the resonance frequency in the fore-and-aft transmissibility to the spine and the pelvis for all six vibration exposures.

a_x (ms^{-2} r.m.s.)	a_z (ms^{-2} r.m.s.)		Pelvis	L3	T12	T5	T1	Pelvis pitch
0.25	0	Correlation coefficient	0.35	0.804	0.356	0.324	0.059	0.384
		p value	0.265	0.002	0.256	0.304	0.856	0.121
0.5	0	Correlation coefficient	0.359	0.633	0.562	0.005	0.021	0.408
		p value	0.251	0.027	0.057	0.988	0.949	0.142
1.0	0	Correlation coefficient	0.895	0.689	0.267	0.203	0.213	0.505
		p value	<0.001	0.013	0.401	0.527	0.507	0.094
1.0	0.25	Correlation coefficient	0.065	0.185	0.06	0.083	0.282	0.416
		p value	0.842	0.566	0.852	0.798	0.375	0.156
1.0	0.5	Correlation coefficient	0.525	0.646	0.755	0.455	0.182	0.107
		p value	0.08	0.023	0.005	0.137	0.872	0.896
1.0	1.0	Correlation coefficient	0.421	0.684	0.708	0.311	0.207	0.302
		p value	0.173	0.014	0.01	0.326	0.518	0.621

It seems logical to conclude that the combined movements of the lower thoracic spine, the lumbar spine, and the pelvis were the main contributors to the first resonance frequency in the fore-and-aft apparent mass. The motions of the middle and upper thoracic spine contributed little. This contrasts with the conclusion that movements of the upper thoracic spine (e.g., regions between T1 and T5) are associated with the first resonance in the vertical apparent mass of the body during vertical excitation (e.g., Kitazaki and Griffin, 1998).

5.5 Conclusion

The apparent mass and the transmissibility obtained with fore-and-aft excitation exhibited the primary resonance frequency around 0.7-1 Hz and the second mode between 2 to 3 Hz.

The primary resonance frequency of the fore-and-aft inline and vertical cross-axis apparent mass and transmissibility was independent of the fore-and-aft vibration magnitudes and the addition of vertical vibration. Resonances in the fore-and-aft inline apparent mass, the vertical cross-axis apparent mass, and the transmissibility to the spine decreased with increasing magnitude of fore-and-aft vibration and with the addition of vertical excitation. The nonlinear behaviour of the apparent mass and transmissibility during dual-axis excitation indicates coupling between the principal mode excited by fore-and-aft vibration and the cross-axis influence of vertical excitation.

It was suggested that the bending of the lower thoracic spine, the lumbar spine and possibly the shear deformation of the pelvis tissue, was a dominant mode at the primary resonance frequency excited by fore-and-aft vibration. The relative contributions to this mode from each body segment, especially the pelvis and the lower thoracic spine, depends on the vibration magnitude.

CHAPTER 6: TRANSMISSIBILITY AND APPARENT MASS OF SEATED HUMAN BODY WITH VERTICAL AND FORE-AFT VIBRATION: EFFECT OF SITTING POSTURE

6.1 Introduction

The biodynamic response of the seated human body exposed to vertical vibration excitation is dependent on many factors including posture (e.g., Fairley and Griffin, 1989; Kitazaki and Griffin, 1998; Matsumoto and Griffin, 2000; Mansfield and Griffin, 2002), backrest contact (e.g., Fairley and Griffin, 1989; Mansfield and Griffin, 2002; Nawayseh and Griffin, 2004; Wang *et al*., 2004; Qiu and Griffin, 2010; Toward and Griffin, 2009), support for the thighs and the feet (e.g., Fairley and Griffin, 1989; Nawayseh and Griffin, 2004; Toward and Griffin, 2010), and holding a steering wheel (e.g., Wang *et al*., 2004; Toward and Griffin, 2010). Knowledge of the effect of sitting posture on the biodynamic response with various excitations provides vital information for developing human body model. A human body model taking into account of factors like sitting postures would assist the evaluation of ride comfort of seat-occupant system and the development of vehicle seats.

Changes in sitting posture alter the geometry of the back, and this has been suggested as an explanation for the resonance frequency in the vertical apparent mass being at a greater frequency in both “erect” and “tense” postures than in a “normal” sitting posture (Fairley and Griffin, 1989; Lundström and Holmlund, 1998; Mansfield *et al*., 2005; Huang and Griffin, 2006). For example, the mean resonance frequency in the vertical apparent mass increased from 4.4 Hz in a slouched posture to 5.2 Hz in an “erect” posture (Kitazaki and Griffin, 1998), with the change attributed to stiffening in the erect posture.

For subjects sitting in nine conditions (i.e., “upright”, “anterior lean”, “posterior lean”, “kyphotic”, “back-on”, “pelvis support”, “inverted SIT-BAR”, “bead cushion”, “belt”, and “pelvis support”) the normalized vertical apparent mass at the resonance frequency was lowest in the “kyphotic” posture (Mansfield and Griffin, 2002). Compared to the “upright” posture, the resonance frequency increased in the “anterior lean” posture and decreased in the “bead cushion” condition. Pitch transmissibility to the pelvis reduced in the “belt” and the “pelvis support” conditions relative to the “normal” posture. During vertical excitation, the fore-aft force on a seat is also influenced by sitting posture: with reduced

thigh contact, the fore-and-aft forces (as reflected in the fore-and-aft cross-axis apparent mass) tend to reduce (Nawayseh and Griffin 2004).

The vertical transmissibility to various locations on the spine exhibits a primary resonance at about 5 Hz (e.g., Kitazaki and Griffin, 1998; Matsumoto and Griffin, 1998a). At the principal resonance of the vertical apparent mass, the natural frequency of the mode shapes of the pelvis and spine increase from 4.9 Hz in a normal upright posture to 5.2 Hz in an erect posture (Kitazaki and Griffin, 1998). Sitting posture also affects the transmission of vertical vibration from the seat to the head: posterior tilting of the pelvis increases vertical head motion in the frequency range 6 to 35 Hz while anterior tilting of the pelvis reduces the transmissibility in the same frequency range (e.g., Messenger and Griffin, 1989).

The fore-and-aft apparent mass of the seated human body exhibits a first resonance around 1 Hz and a second resonance in the range 2 to 3 Hz (e.g., Fairley and Griffin, 1990; Nawayseh and Griffin, 2004; Chapter 5). During fore-and-aft excitation, there is little effect of thigh contact on the fore-and-aft apparent mass measured at the seat at frequencies less than 3 Hz or greater than 10 Hz, but the peak fore-and-aft apparent mass measured at a backrest increases when there is increased contact between the thighs and the seat (Nawayseh and Griffin, 2004). With the feet hanging and minimum thigh contact, there are maximum forces in the fore-and-aft direction.

The resonance frequency in the vertical apparent mass (e.g., Nawayseh and Griffin, 2003) and vertical transmissibility to the spine (e.g., Chapter 4) decreased with increasing vibration magnitude. Increasing the magnitude of fore-aft excitation reduces the modulus of the first peak in the fore-and-aft apparent mass (e.g., Fairley and Griffin, 1990) and the fore-aft transmissibility to the spine and the pelvis (e.g., Chapter 5) but has no evident effect on the resonance frequency (e.g., Chapter 5).

The vertical and fore-and-aft apparent masses of the human body exhibit lower resonance frequencies with multi-axis excitation than with single-axis excitation (Hinz *et al*., 2006a; Mansfield and Maeda, 2006; Qiu and Griffin, 2010; Chapters 4 and 5), but the effect of sitting posture on apparent mass and transmissibility has not been studied with dual-axis vibration.

The research reported in this chapter was conducted to improve understanding of how sitting posture influences the principal resonances in the apparent mass and the

transmissibility of the body. It was hypothesised that the human body is stiffened in an erect posture compared to normal upright posture during vertical excitation, fore-aft excitation, and dual-axis excitation. It was also hypothesised that when a change of posture stiffens the body there will be less nonlinearity associated with changes in the magnitude of vibration in any direction.

6.2 Experiment design

6.2.1 Apparatus

A rigid seat was secured to a 6-axis motion simulator capable of 1-m vertical displacement, 0.5-m fore-and-aft and lateral displacement, ±10 degrees of roll and pitch, and ±10 degrees of yaw. A force plate (Kistler 9281 B) consisting of four tri-axial quartz transducers at the four corners of a rectangular aluminium plate was secured to the supporting surface of a rigid seat to allow the measurement of forces in the vertical and fore-and-aft directions. Signals from the four force transducers orientated to be sensitive to vertical force were summed and amplified by a charge amplifier (Kistler 5001). Signals from the four force transducers orientated to be sensitive to fore-and-aft force were summed and amplified by a similar charge amplifier. A tri-axial *HVLab* SIT-pad was used to measure acceleration in the fore-and-aft and vertical directions at the centre of the force platform. The signals were recorded using an *HVLab* data acquisition system (issue 1.0, 2009).

6.2.2 Subjects and stimuli

Twelve male subjects with median age 26.5 years (range 23 to 36 years), weight 68.5 kg (range 60.4 to 80 kg), and stature 1.74 m (range 1.65 to 1.82 m) participated in the study that was approved by the Human Experimentation Safety and Ethics Committee of the Institute of Sound and Vibration Research.

Subjects adopted three postures: normal upright, erect, and slouched. In the normal upright posture, subjects sat with their upper body in a comfortable upright position and looked straight ahead. In the erect posture, the pelvis and lumbar spine were rotated forward and the thoracic spine was rotated rearward to straighten the spine. In the slouched posture, the pelvis and lumbar spine were rotated rearward and the thoracic spine was rotated forward so subjects looked down with drooped shoulders. Subjects' hands rested on their laps and their feet rested on the vibrator table that moved with the seat. In each posture, the sitting weight was measured with electronic scales.

Subjects were exposed to 60-s random vibration with approximately flat constant-bandwidth acceleration spectra (0.2 to 20 Hz) in seven combinations of three magnitudes of fore-and-aft vibration and three magnitudes of vertical vibration (Table 6.1). The motions in the fore-and-aft and vertical directions were uncorrelated.

Table 6.1 Vertical (*z*-axis) and fore-and-aft (*x*-axis) excitations experienced by subjects.

		x-axis excitation (ms^{-2} r.m.s.)		
		0	0.25	1.0
z-axis excitation (ms^{-2} r.m.s.)	0	-	a_x	a_x
	0.25	a_z	-	$a_x + a_z$
	1.0	a_z	$a_x + a_z$	$a_x + a_z$

6.2.3 Motion measurement on the body

Acceleration was measured in the fore-and-aft and vertical directions on the body surface over the first, fifth, and twelfth thoracic vertebrae, the third lumbar vertebra, and the pelvis (at the iliac crest). Pitch motion of the pelvis was estimated from the difference between two vertical accelerations at 25-mm separation on a single block located at the iliac crest. Two miniature accelerometers (Entran EGA(X)) were attached orthogonally to T-shaped balsa wood blocks weighing about 1 g, similar to each accelerometer. The block was attached to the body surface with double-side adhesive tape with a contact area similar to that of a vertebral body (Figure 6.1). The inclinations of the spine and the pelvis in each sitting posture were measured. The measured angle was used for the data correction based on Equation (4.7).

6.2.4. Data analysis

Forces and accelerations were acquired at 512 samples/second via 50-Hz anti-aliasing filters. Mass cancellation in the time domain removed the influence of the mass above the force transducers from the measured forces (Chapters 4 and 5). Signal processing was conducted with a frequency resolution of 0.25 Hz. Details of signal processing have been addressed in Chapters 4 and 5.

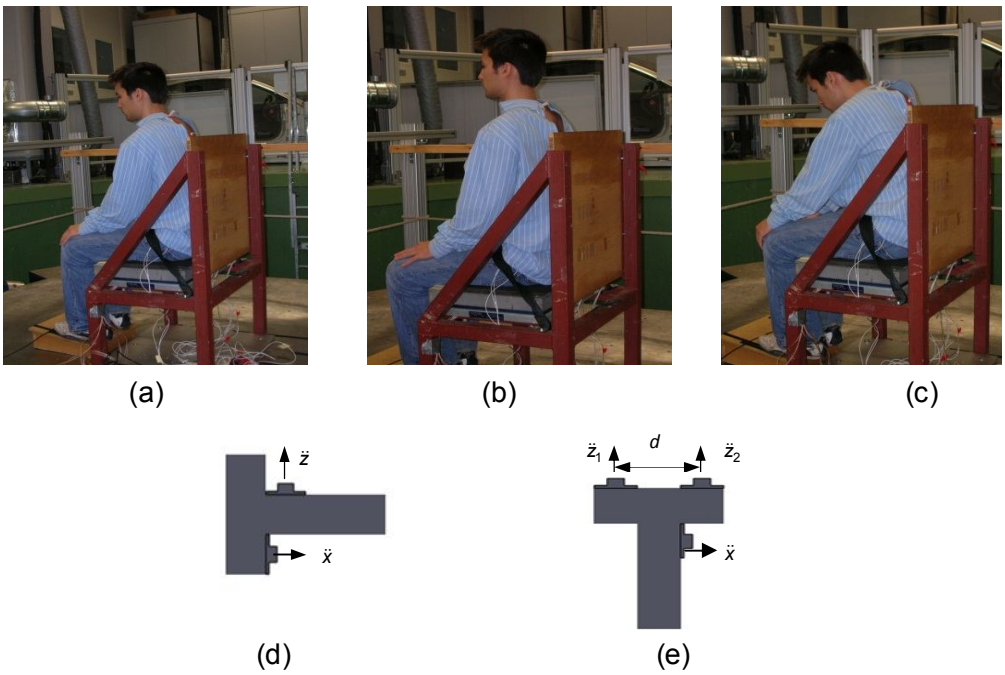

Figure 6.1 Experiment set-up and the sitting postures: (a) normal upright posture; (b) erect posture; (c) slouched posture; (d) accelerometers-blocks on the back; (e) accelerometers-block on the pelvis.

6.3 Results

6.3.1 Response to vertical excitation

6.3.1.1 Vertical apparent mass and fore-and-aft cross-axis apparent mass

In all three postures (normal upright, erect, and slouched), the median vertical apparent mass and the median fore-and-aft cross-axis apparent mass showed a primary resonance in the range 4 to 6 Hz (see Appendix D). The nonlinearity in the vertical apparent mass (reduction in resonance frequency when increasing the magnitude of vibration in either direction), did not differ among postures (Friedman, p>0.05 for the nonlinearity when increasing the magnitude of either the vertical excitation or the additional fore-aft excitation), but the nonlinearity in the fore-and-aft cross-axis apparent mass differed between postures (Friedman, p=0.03 when increasing the magnitude of vertical excitation), with a greater reduction in the resonance frequency when sitting in the slouched posture than in the normal upright posture (Wilcoxon, p=0.024), but no difference between the normal upright and the erect posture (Wilcoxon, p=0.180).

6.3.1.2 Effect of sitting posture on apparent mass

Sitting posture influenced the resonance frequency of the vertical apparent mass with single-axis vertical excitation at 1.0 ms^{-2} r.m.s. (Figure 6.2; Friedman, p=0.046) and with combined 1.0 ms^{-2} r.m.s. vertical excitation and 0.25 ms^{-2} r.m.s. fore-and-aft excitation (Figure 6.2; Friedman, p=0.013). Changing from normal upright to erect, the vertical apparent mass resonance frequency increased from 4.75 to 5.0 Hz with single-axis vertical excitation at 1.0 ms^{-2} r.m.s. (Figure 6.2; Wilcoxon, p=0.04) and from 4.25 to 4.75 Hz with dual-axis vibration (1.0 ms^{-2} r.m.s. vertical excitation with 0.25 ms^{-2} r.m.s. fore-and-aft excitation; Wilcoxon, p=0.007).

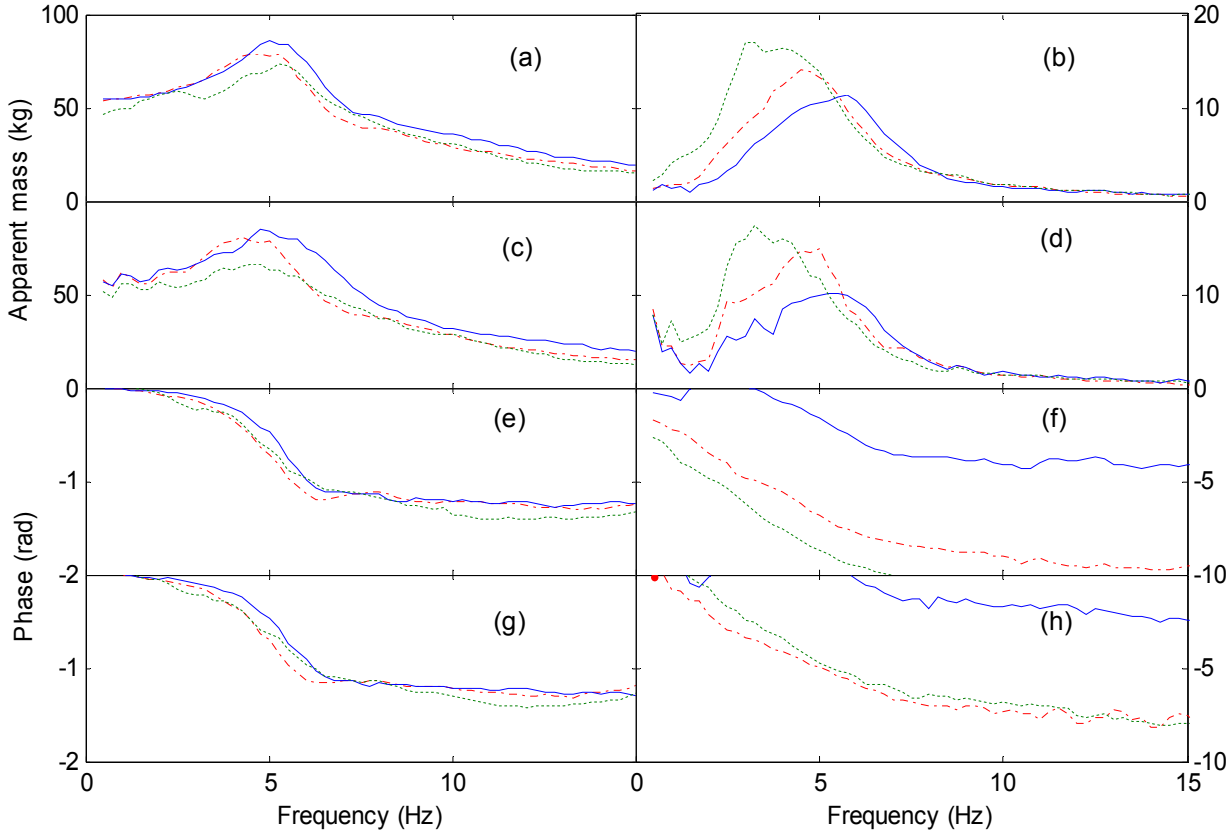

Figure 6.2 Effect of sitting posture on the modulus and the phase of the median vertical apparent mass (left column) and the fore-and-aft cross-axis apparent mass (right column): (a), (b), (e), (f), apparent mass and the phase at a_z =1.0 ms^{-2} r.m.s.; (c), (d), (g), (h), apparent mass and the phase at a_z =1.0, a_x =0.25 ms^{-2} r.m.s. —.—, normal upright posture; ——, erect posture; - - -, slouched posture.

The resonance frequency in the fore-and-aft cross-axis apparent mass differed between the three postures (Friedman, p<0.05). The resonance frequency was lower in the normal upright posture than in the erect posture (with single-axis vertical excitation at 1.0 ms^{-2} r.m.s.; Figure 6.2; Wilcoxon, p=0.007; with dual-axis excitation at a_z=1.0 ms^{-2} r.m.s.,

a_x=0.25 ms^{-2} r.m.s., Wilcoxon, p=0.01). The resonance frequency was higher in the normal posture than in the slouched posture (Figure 6.2, Wilcoxon, p<0.05 with single-axis vertical excitation at 1.0 ms^{-2} r.m.s. and with dual-axis excitation at a_z=1.0 ms^{-2} r.m.s., a_x=0.25 ms^{-2} r.m.s.).

6.3.1.3 Vertical transmissibility and fore-and-aft cross-axis transmissibility

In all three postures, the median vertical transmissibility to the spine, and the median fore-and-aft cross-axis transmissibility to the spine show a primary resonance around 5 Hz that reduced in frequency as the vibration magnitude increased (see Appendix D). With increased excitation, the reduction in the resonance frequency in the vertical transmissibility to T1 differed among sitting postures (Friedman, p=0.041), with a greater reduction in the erect posture than in the normal upright posture (Wilcoxon, p=0.02) but no difference between the normal upright posture and the slouched posture. The reduction in the resonance frequency in the vertical transmissibility to other measurement locations did not differ between postures (Friedman, p>0.05).

6.3.1.4 Effect of sitting posture on the translational transmissibility to the spine

Sitting posture influenced the resonance frequency in the vertical transmissibility to T1 (Figure 6.3; Friedman, p=0.048 with 0.25 ms^{-2} r.m.s. vertical excitation; p=0.04 with 1.0 ms^{-2} r.m.s. vertical excitation; p=0.01 with combined 1.0 ms^{-2} r.m.s. vertical and 1.0 ms^{-2} r.m.s. fore-and-aft excitation), to T5 with all vibration excitations (Friedman, p<0.05), and to T12 (Friedman, p=0.013 with 1.0 ms^{-2} r.m.s. vertical excitation). Sitting posture had no statistically significant effect on the resonance frequency in the vertical transmissibility to L3 and or the pelvis at any vibration magnitude (Friedman, p>0.05).

Changing from the normal upright posture to the erect posture, resonance frequency in the vertical transmissibility to T1 was increased (Figure 6.3; Wilcoxon, p=0.028 with vertical excitation at 0.25 ms^{-2} r.m.s., p=0.024 with vertical excitation at 1.0 ms^{-2} r.m.s., p=0.007 with combined 1.0 ms^{-2} r.m.s. vertical excitation and 1.0 ms^{-2} r.m.s. fore-and-aft excitation), to T5 (Wilcoxon, p<0.05), to T12 at 1.0 ms^{-2} r.m.s.(Wilcoxon, p=0.018). Changing from the normal upright posture to the slouched posture did not change the resonance frequency of the vertical transmissibility (Figure 6.3; Wilcoxon, p>0.05).

Sitting posture did not change the resonance frequency in the fore-and-aft cross-axis transmissibility to any measurement location (Figure 6.3; Friedman, p>0.05).

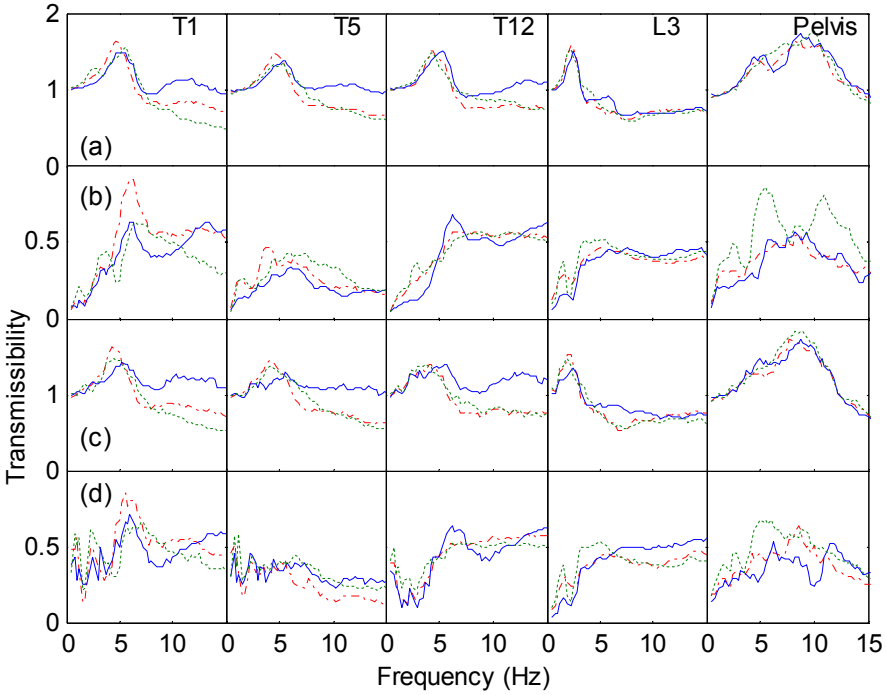

Figure 6.3 Transmissibility from vertical motion to each measurement location of 12 subjects: effect of sitting posture. —.—, normal upright posture; ——, erect posture; - - -, slouched posture. (a) vertical transmissibility at a_z=0.25 ms^{-2} r.m.s.; (b) fore-and-aft cross-axis transmissibility at a_x=0.25 ms^{-2} r.m.s.; (c) vertical transmissibility at a_z =1.0, a_x =0.25 ms^{-2} r.m.s.; (d) fore-and-aft cross-axis transmissibility at a_z =1.0, a_x =0.25 ms^{-2} r.m.s.

6.3.1.5 Pitch transmissibility to the pelvis

In all three postures, the transmissibility from the vertical seat acceleration to pitch acceleration of the pelvis had a primary resonance around 8 to12 Hz that reduced with increasing magnitude of vertical excitation and with the addition of fore-and-aft excitation (see Appendix D; Friedman, p<0.05).

6.3.1.6 Effect of sitting posture on pitch transmissibility to the pelvis

Sitting posture changed the resonance frequency in the pitch transmissibility with 1.0 ms^{-2} r.m.s. vertical excitation (Figure 6.4; Friedman, p=0.048) but not with other excitations. In the normal upright posture, the primary resonance frequency was lower than in the erect posture (Figure 6.4; Wilcoxon, p=0.035) but higher than in the slouched posture (Wilcoxon, p=0.033).

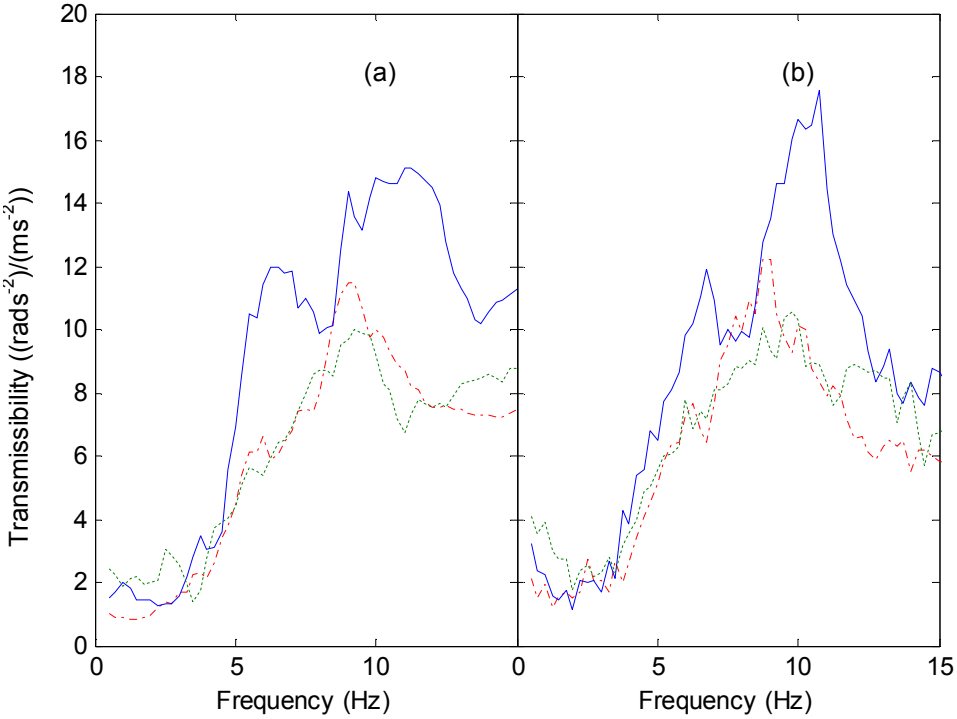

Figure 6.4 Transmissibility from vertical seat motion to pelvis pitch motion of 12 subjects: effect of sitting postures. —.—, normal upright posture; ——, erect posture; - - -, slouched posture. (a) single-axis vertical vibration at a_z=1.0 ms^{-2} r.m.s.; (b) dual-axis vibration at a_z =1.0, a_x =1.0 ms^{-2} r.m.s.

6.3.2 Response to fore-and-aft excitation

6.3.2.1 Fore-and-aft apparent mass and vertical cross-axis apparent mass

In all three postures, the median fore-and-aft apparent mass and the vertical cross-axis apparent mass showed a first peak around 1 Hz, second peak around 3 Hz, and a third peak in the range 5 to 7 Hz (see Appendix D).

6.3.2.2 Effect of sitting posture on apparent mass

Sitting posture influenced the frequency of the first resonance in the fore-and-aft apparent mass (Figure 6.5; Friedman, p=0.006) and the first resonance in the vertical cross-axis apparent mass (Figure 6.5, Friedman, p<0.05). Changing from the normal upright posture to the slouched posture increased the first resonance frequency in the fore-and-aft apparent mass (during dual-axis fore-and-aft and vertical excitation at 1.0 ms^{-2} r.m.s., Figure 6.5; Wilcoxon, p=0.018) and increased the first resonance frequency in the vertical cross-axis apparent mass (with single-axis fore-and-aft excitation at 0.25 ms^{-2} r.m.s., Wilcoxon, p=0.024; and with dual-axis fore-and-aft and vertical excitation at 1.0 ms^{-2} r.m.s., p=0.034).

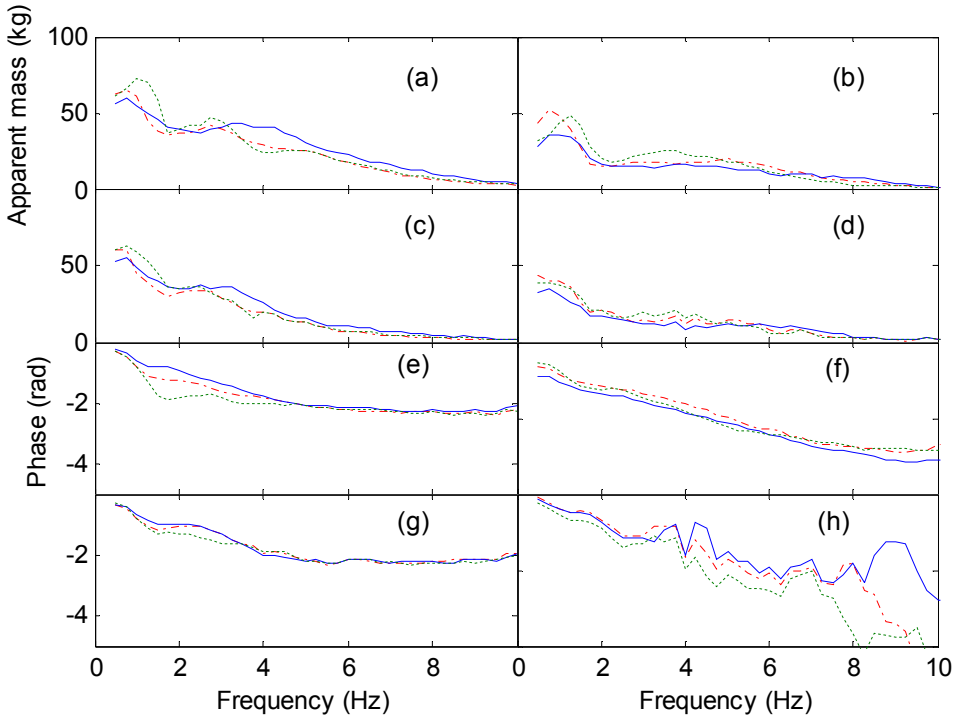

Figure 6.5 The modulus and the phase of the median fore-and-aft apparent mass (left column) and the vertical cross-axis apparent mass (right column): effect of sitting posture. (a), (b), (e), (f), apparent mass and the phase at a_x =0.25 ms^{-2} r.m.s.; (c), (d), (g), (h), apparent mass and the phase at a_x =1.0, a_z =1.0 ms^{-2} r.m.s. —.—, normal upright posture; ——, erect posture; - - -, slouched posture.

6.3.2.3 Fore-and-aft transmissibility and vertical cross-axis transmissibility

In all three sitting postures, the fore-and-aft transmissibility to the spine showed a first peak around 1 Hz and second peak between 2 and 3 Hz. The vertical cross-axis transmissibility to the spine had the primary peak around 4 Hz (see Appendix D).

6.3.2.4 Effect of sitting posture on the translational transmissibility to the spine

Sitting posture influenced the primary resonance frequency in the fore-and-aft transmissibility to T12 (Figure 6.6; Friedman, p=0.03 with 0.25 ms^{-2} r.m.s. fore-and-aft excitation), to L3 (Figure 6.6; Friedman, p<0.05 with all excitations), and to the pelvis (Figure 6.6; Friedman, p=0.048 with 1.0 ms^{-2} r.m.s. fore-and-aft excitation), but not to T1 or T5 (Figure 6.6; Friedman, p>0.05).

Changing from the normal upright posture to the slouched posture increased the primary resonance frequency in the fore-and-aft transmissibility to T12 (Wilcoxon, p=0.017). Changing from the normal upright posture to the erect posture increased the primary

resonance frequency in the fore-and-aft transmissibility to L3 (Wilcoxon, p<0.05) and to the pelvis (Wilcoxon, p=0.027).

Sitting posture influenced the primary resonance frequency in the vertical cross-axis transmissibility to T1 during fore-and-aft excitation at both 0.25 and 1.0 ms^{-2} r.m.s., and with combined 1.0 ms^{-2} r.m.s. fore-and-aft excitation and 0.25 ms^{-2} r.m.s. vertical excitation (Figure 6.6; Friedman, p<0.05). The primary resonance frequency to T1 reduced when changing from the normal upright posture to the slouched posture (Wilcoxon, p<0.05).

Sitting posture did not significantly affect the primary resonance frequency in the vertical cross-axis transmissibility to other measurement locations (Figure 6.6; Friedman, p>0.05).

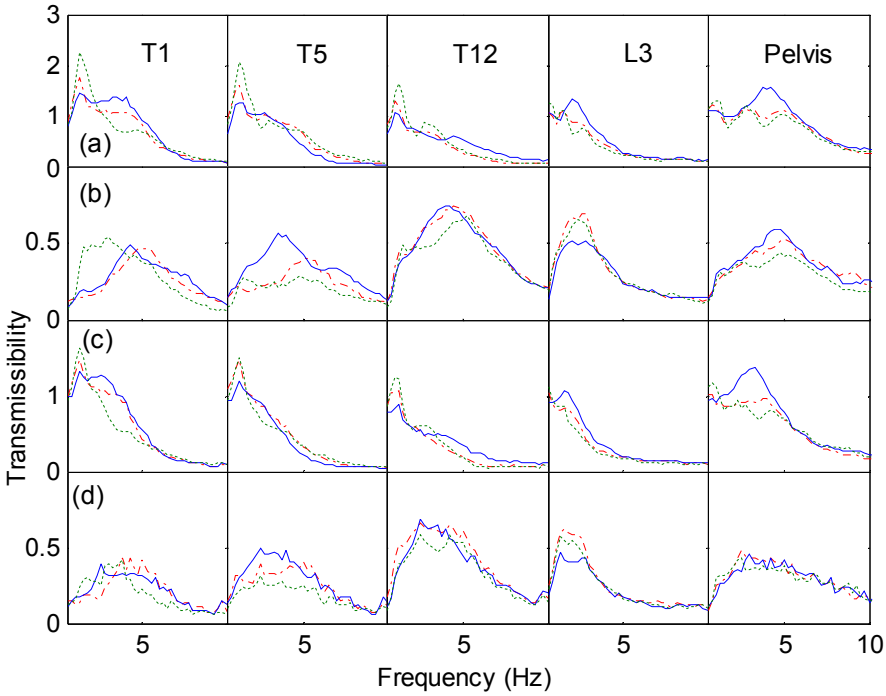

Figure 6.6 Transmissibility from fore-and-aft seat motion to each measurement location of 12 subjects: effect of sitting posture. —.—, normal upright posture; ——, erect posture; - - -, slouched posture. (a) fore-and-aft transmissibility at a_x=0.25ms^{-2} r.m.s.; (b) vertical cross-axis transmissibility at a_x=0.25 ms^{-2} r.m.s.; (c) fore-and-aft transmissibility at a_x =1.0, a_z =0.25 ms^{-2} r.m.s.; (d) vertical cross-axis transmissibility at a_x =1.0, a_z =0.25 ms^{-2} r.m.s.

6.3.2.5 Pitch transmissibility to the pelvis

In all three postures, the transmissibility from fore-and-aft seat motion to the pitch motion of the pelvis exhibited a primary resonance frequency in the range 3 to 6 Hz with single-

axis fore-and-aft excitation and with dual-axis excitation (see Appendix D). Although there is larger inter-subject variability and there are more than one peak in each transmissibility, a primary peak is easy to identify for each subject.

6.3.2.6 Effect of sitting posture on pitch transmissibility to the pelvis

There were no statistically significant changes in the primary resonance frequency of the pitch transmissibility to the pelvis, or the associated peak modulus, when changing sitting posture (Figure 6.7; Friedman, p>0.05).

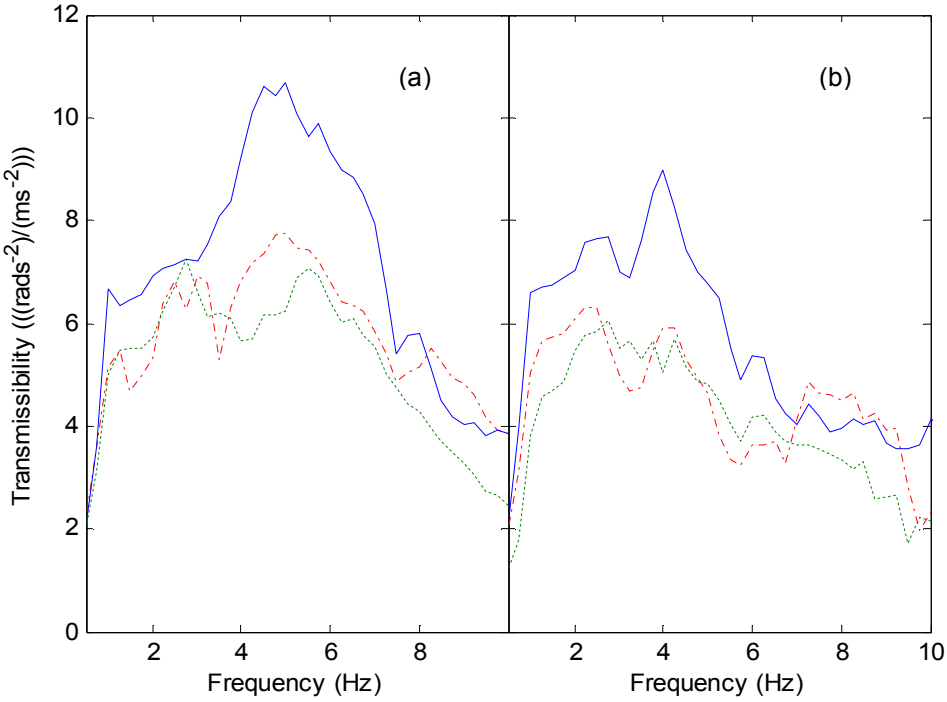

Figure 6.7 Transmissibility from fore-and-aft seat motion to pelvis pitch motion of 12 subjects: effect of sitting postures. —.—, normal upright posture; ——, erect posture; - - -, slouched posture. (a) single-axis fore-and-aft vibration at a_x=0.25 ms^{-2} r.m.s.; (b) dual-axis vibration at a_x =1.0, a_z =1.0 ms^{-2} r.m.s.

6.4 Discussion

6.4.1 Effect of the sitting posture on the apparent mass

Changing from the normal upright posture to the erect posture, the median sitting weight increased from 50.7 kg to 54.7 kg. This change was accompanied by a reduction in the contact area between the body and the seat surface, so that pressure at the ischial tuberosities was increased. The increased pressure at the ischial tuberosities can be expected to increase the axial stiffness of the local tissues. This is consistent with an increase in the resonance frequency when altering from the normal upright posture to the erect posture (Kitazaki and Griffin, 1998). The stiffer tissue might be partially

responsible for the increase in the resonance frequency of the vertical apparent mass with 1.0 ms^{-2} r.m.s. when changing from the normal upright posture to the erect posture, which was observed in the present study and previously (Fairley and Griffin, 1989).

Changing from the normal upright posture to the slouched posture increased the first resonance frequency of the fore-and-aft apparent mass. This might be associated with increased shear stiffness of buttocks tissue when the thigh contact was increased in the slouched posture.

6.4.2 Interaction between the effect of vibration magnitude and the effect of sitting posture on apparent mass

The extent of the nonlinearity, defined as the absolute change in the primary resonance frequency in the apparent mass due to the four-fold change of vibration magnitude from 0.25 to 1.0 ms^{-2} r.m.s., was posture-dependent. For example, when the magnitude of vertical excitation was increased, the absolute change in the resonance frequency in the fore-and-aft cross-axis apparent mass was greater in the slouched posture than in both the normal upright posture and the erect posture. The increased nonlinearity in the slouched posture is similar to the previous finding that the change in the resonance frequency of the vertical apparent mass with variations in the magnitude of vertical vibration was reduced when the stiffness of the pelvis tissue was increased (Nawayseh and Griffin, 2004).

6.4.3 Effect of sitting posture on the transmissibility

The resonance frequencies of the vertical transmissibility to the thoracic spine and to the pelvis, and the pitch transmissibility to the pelvis, were increased when changing from the normal upright posture to the erect posture. However, the resonance frequency of the vertical transmissibility to L3 was not changed significantly. This may have been because the curvature of the thoracic spine and the inclination of the pelvis contributed to the change of posture with the curvature of the lumbar spine varying somewhat less. The stiffening effect observed in the vertical transmissibility might be associated with an increase in the stiffness of pelvis tissue, which has previously been suggested as being partially responsible for the increase in the resonance frequency of the vertical apparent mass in an erect posture (Section 6.4.1). Changing from the normal upright posture to the erect posture increased the first resonance frequency of the fore-and-aft

transmissibility to L3 and the pelvis but not to the thoracic spine, implying that lumbar spine is more sensitive to fore-and-aft excitation than the thoracic spine.

6.4.4 Effect of sitting posture on the association between the resonance of the apparent mass and the transmissibility

With vertical excitation, the movement of the spine was seen to be associated with changes in the resonance in the apparent mass in the different postures employed in the present study. There was a correlation between the resonance frequency of the vertical transmissibility to T5 and T1 with the resonance frequency in the vertical apparent mass with 1.0 ms^{-2} r.m.s. in the normal upright posture but not in the erect posture. (Spearman, $p<0.05$ for both locations), while the resonance frequency of the vertical transmissibility to T12 and L3 was correlated with the resonance frequency in the vertical apparent mass in the erect posture but not in the normal upright posture (Spearman, $p<0.05$ for both locations in both postures). It seems that in the normal upright posture the motion of the upper thoracic spine contributed more to the resonance of the vertical apparent mass than the lower thoracic spine, whereas the opposite occurred in the erect posture. This might be because more vibration is transmitted to the head in the erect posture than in the normal upright posture. More pitch motion of the head is introduced in the erect posture and is coupled with the vertical motion of the thoracic spine. The association between the motion of the thoracic spine and the driving point dynamic response is reduced.

There were correlations between the resonance frequencies of the vertical transmissibilities to T1, T5, T12 and L3 with the resonance frequency in the vertical apparent mass in the slouched posture (Spearman, $p<0.05$), suggesting the motion of the whole spine contributed to the resonance of the vertical apparent mass in the slouched posture.

With fore-aft excitation, the first resonance frequencies of the fore-aft transmissibility of the pelvis, L3 and T12 were associated with the first resonance frequency of the fore-and-aft apparent mass (Spearman, $p<0.05$) in all three sitting postures. However, the first resonance frequencies of the fore-aft transmissibility of T5 and T1 was not correlated with the first resonance frequency of the fore-and-aft apparent mass (Spearman, $p>0.05$) in any sitting posture, suggesting that the resonance in the driving point apparent mass with fore-aft excitation was primarily contributed by the complex

motion of the lower thoracic spine, the lumbar spine and pelvis while the motion of the upper thoracic spine contributed little in any sitting posture.

6.5. Conclusion

With either vertical excitation or dual-axis excitation, an erect sitting posture tended to increase the resonance frequency of the vertical apparent mass, the vertical transmissibility to the thoracic spine and to the pelvis. With either fore-and-aft excitation or dual-axis excitation, an erect posture tended to increase the first resonance frequency of the fore-and-aft transmissibility to the lumbar spine and the pelvis. Changing from the normal upright posture to the slouched sitting posture tended to reduce the resonance frequency of the fore-and-aft cross-axis apparent mass but increase the first resonance frequency of the fore-and-aft apparent mass and the vertical cross-axis apparent mass. The nonlinearity evident when changing the magnitude of vibration tended to be less when sitting in an erect posture, and greater when sitting in a slouched posture, than when sitting in a normal upright posture.

The association between vibration modes of the upper body and the resonance of the vertical apparent mass differs between postures. In the normal upright posture, the resonance of the vertical apparent mass was more associated with the motion of upper thoracic spine than the lower thoracic spine. In the erect posture, the resonance of the vertical apparent mass was more associated with the motion of lower thoracic spine than the upper thoracic spine. In the slouched posture, the resonance of the vertical apparent mass was associated with the motion of the whole spine. The motions of the lower thoracic spine, the lumbar spine and the pelvis were associated with the first resonance in the fore-aft apparent mass irrespective of sitting postures.

CHAPTER 7: A MULTI-BODY DYNAMIC MODEL OF THE SEATED HUMAN BODY WITH COMBINED VERTICAL AND FORE-AND-AFT EXCITATIONS

7.1 Introduction

Various studies have measured the biodynamic responses of the seated human body to vertical vibration (e.g., Fairley and Griffin, 1989) and fore-and-aft vibration (e.g., Fairley and Griffin, 1990). The apparent mass, the complex ratio of force and acceleration at the same location, has often been used to characterise how the vibration is transmitted to the body. With vertical excitation, it is widely accepted that the vertical apparent mass has a primary resonance in the frequency range 4 to 6 Hz, with the resonance depending on the body weight, the vibration magnitude, and contact with a backrest, sitting posture, and other factors. With fore-and-aft excitation, the apparent mass shows a peak around 1 to 2 Hz if there is no backrest and a peak near 4 Hz with a backrest.

Exposures to whole-body vibration usually involve multi-axis excitation. Experimental studies with dual-axis excitation (Hinz *et al.*, 2006a, Mansfield and Maeda, 2006; Qiu and Griffin, 2010; Chapters 4-6) and tri-axial excitation (Hinz *et al.*, 2006a) have found that the apparent mass of the seated body is similar to that with single-axis excitation. However, consistent with the non-linearity found with single-axis excitation, the resonance frequency with dual-axis excitation is shifted to a lower frequency and the coherence is reduced between, for example, the vertical force and the vertical acceleration by the addition of fore-and-aft excitation (Qiu and Griffin, 2010).

Various lumped parameter models, multi-body dynamic models, and finite element models have been used to represent the apparent mass or transmissibility of the human body. Lumped parameter models (e.g., Wei and Griffin, 1998; Qiu, 2007) are easy to formulate and can provide a good fit to experimental data, but they are generally limited to one dimensional analysis. For example, a model with several masses and vertical springs and dampers only provides kinetic information in the vertical direction. Multi-body dynamic models (e.g., Matsumoto and Griffin, 2001; Yoshimura *et al.*, 2005; Chapter 3) are more anatomically representative than lumped parameter models and, with sufficient degrees-of-freedom, they can model the dynamic responses (e.g., force on the seat surface or the acceleration on the body surface) in the vertical, fore-and-aft, and pitch directions within the sagittal plane. Multi-body models are too simplified to predict spinal forces or represent the contact conditions between a compliant seat and the human body because contact is represented by a very limited number of springs and dampers,

such as one beneath the pelvis and another beneath the thighs. Finite element models (e.g., Kitazaki and Griffin, 1997; Siefert *et al*., 2008) can provide contact simulation closer to reality and, with an appropriate spinal structure, they may improve understanding of the spinal motions during vibration. However, it is challenging to determine appropriate properties for the spine, inter-vertebral disks, ligaments, and muscles.

A human body model reflecting response to dual-axis excitation has not been reported to the authors' knowledge. Such a model is needed to represent the dynamic response of the seated human body (e.g., drivers and passengers of vehicles) exposed to simultaneous vertical and fore-and-aft vibration so as to predict ride discomfort. The objective of this study was to determine the required characteristics of a human body model for it to represent the vertical and fore-and-aft forces on the seat and the acceleration over the body surface of the human body with dual-axis vertical and fore-and-aft excitation, and identify how a human body model developed with single-axis excitation (Chapter 3) can be improved to work with dual-axis excitation. The study was also designed to investigate the contributions of the principal body segments to the dynamic responses with dual-axis vibration excitation, especially the primary resonance.

7.2 Method

7.2.1 Model description

The model developed in this study was represented by five rigid bodies: upper body, middle body, pelvis, thighs, and legs (Figure 7.1). Although simplified, the model represents the gross anatomy of the body.

The upper body was associated with the thoracic spine and combined thorax, head, neck, and upper limbs. The motions of the head and the seat-to-head transmissibility were not of interest in this study, so the head and neck were not modelled as separate entities in the model. The middle body was associated with the lumbar spine and can be considered to represent the abdomen including the viscera. The pelvis was associated with the segment from the fifth lumbar vertebra to the ischial tuberosities. These rigid bodies inter-connected by joints represent the thoracic spine (upper body), lumbar spine (middle body), and pelvis. Between the joints, the spine was assumed to be straight, assuming bending between individual vertebrae was small and could be represented by

rotation among the three rigid bodies. The vertebrae and disks were not modelled because the model was not designed to predict spinal forces.

The mass and inertia of the hands and forearms, that were assumed to rest on the thighs, were included in the mass and mass moments of inertia of the thighs. The feet were included in the segment representing the legs.

The five rigid bodies were inter-connected by pin joints, assuming no translational movements between the bodies. The axial and the shear deformations of the pelvis and thigh tissue at the seat-occupant interface were simulated using linear springs and dampers. The complete model is shown in Figure 7.1.

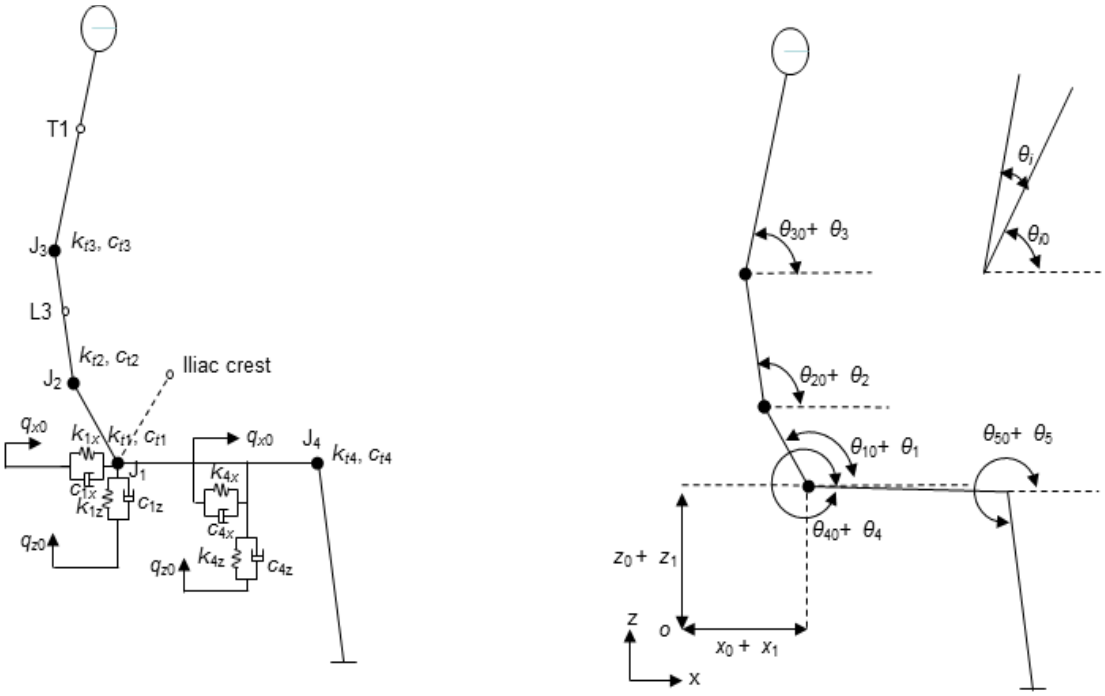

(a) (b)

Figure 7.1 A two-dimensional multi-body biodynamic model with dual-axis vibration: (a) mechanical properties; (b) motion description in arbitrary position. J_i, i = 1, 2, 3, and 4: revolute joint simulated with rotational spring k_{ti} and damper c_{ti}; k_{1x}, c_{1x}, shear stiffness and damping of pelvis tissue; k_{1z}, c_{1z}, axial stiffness and damping of pelvis tissue; k_{4x}, c_{4x}, shear stiffness and damping of thigh tissue; k_{4z}, c_{4z}, axial stiffness and damping of thigh tissue; q_{z0}, vertical vibration excitation; q_{x0}, fore-and-aft vibration excitation; $x_{10,}$ the horizontal coordinate of the pelvis joint in static equilibrium position; $z_{10,}$ the vertical coordinate of the pelvis joint in static equilibrium position; x_1, the horizontal oscillation of the pelvis joint; $z_{1,}$ the vertical oscillation of the pelvis joint; θ_{i0}, i = 1, 2, 3, 4, and 5, the initial inclination of each rigid body in static equilibrium position; θ_i, i = 1, 2, 3, 4, and 5, the rotational oscillation of each rigid body with respect to static equilibrium position.

The initial inclination of each body segment (i.e., θ_{i0}) was measured when the experiment was conducted (Chapter 4). The locations used for predicting transmissibility are the iliac crest, L3 and T1 (Figure 7.1). The distance between the iliac crest where the motion of the pelvis was measured and J1 was assumed to be the same as the distance between J1 and J2. The angle between the line connecting iliac crest and J1 and the horizontal line were also measured during the experiment. The location of L3 was assumed to be at the middle of the lumbar spine, (i.e., the middle body location). The distance between T1 and J3 along the thoracic spine (i.e., the upper body location) was assumed to be 80% of the total length of the thoracic spine.

7.2.2 Parameter identification

The equations of motion were derived with Lagrange formulation using the method adopted in Chapter 3 when developing a multi-body human body model with vertical excitation. The definitions of system mass matrix *M*, stiffness *K* and damping matrix *C* which were derived from the equations of motion were detailed in Appendix E.

The Simulink model was built in Matlab 7.9.0 (R2009b), details of which are shown in Appendix E.

The mechanical properties and the mass of each body segment were first identified by an optimisation procedure using the measured biodynamic responses of the seated human body (subject 8) exposed to single-axis vertical excitation as presented in Chapter 4. The optimization procedure identified the model parameters that minimized the mean square errors between the computed and measured vertical apparent masses and between the computed and measured fore-and-aft cross-axis apparent masses at the seat with single-axis vertical vibration at 1.0 ms^{-2} r.m.s. over the frequency range of 0.25 to 20 Hz. The optimized parameters reported in Chapter 3 were adopted as the initial values.

The objective function was defined as

$$E(\lambda) = \min(E_{M_z}(\lambda) + E_{M_x}(\lambda))^{1/2} \quad (7.1)$$

Where $E_{M_z}(\lambda)$, $E_{M_x}(\lambda)$ and are sums of squared-errors of the vertical apparent mass and the fore-and-aft cross-axis apparent mass. The errors between the measured phases and the calculated phases of the apparent mass and transmissibility were not included in the parameter identification.

$$E_{M_z}(\lambda)=\frac{1}{N}\sum_{i=1}^{N}(\left|M_{z_c}(f_i)\right|-\left|M_{z_t}(f_i)\right|)^2,$$

$$E_{M_x}(\lambda)=\frac{1}{N}\sum_{i=1}^{N}(\left|M_{x_c}(f_i)\right|-\left|M_{x_t}(f_i)\right|)^2. \quad (7.2)$$

where

N is the number of data samples containing the apparent mass or cross-axis apparent mass in the frequency range 0.25 to 20 Hz with a frequency resolution 0.25 Hz.

$M_{z_c}(f_i)$ and $M_{x_c}(f_i)$ are the model calculated vertical apparent mass and fore-and-aft cross-axis apparent mass at vibration frequency f_i (i=1, 2, ……, N), respectively;

$M_{z_t}(f_i)$ and $M_{x_t}(f_i)$ are the measured vertical apparent mass an fore-and-aft cross-axis apparent mass at vibration frequency f_i (i=1, 2, ……, N), respectively.

$\boldsymbol{\lambda}$ is the vector of the parameters of the model to be optimized. A total of 21 parameters were involved in the optimization procedure, with $\boldsymbol{\lambda}$ given by:

$\boldsymbol{\lambda}=[m_1, m_2, m_3, m_4, m_5, k_{1z}, c_{1z}, k_{1x}, c_{1x}, k_{4z}, c_{4z}, k_{4x}, c_{4x}, k_{t1}, c_{t1}, k_{t2}, c_{t2}, k_{t3}, c_{t3}, k_{t4}, c_{t4}]^{\mathrm{T}}$.

The set of identified parameters via the optimisation procedure was then assigned to the human body model in MATLAB/SIMULINK with the measured fore-and-aft and vertical accelerations on the seat surface (over a duration of 60 s with a sampling rate of 512 samples per second) used as the input motions. The same excitation was used for the simulation and the experiment so as to make the predicted response comparable to the experimental data. The Simulink model was run with ODE45 solver which solved the equations of motion numerically in the time domain. The time history of each degree-of-freedom (i.e., x_1, $z_1, \theta_1, \theta_2, \theta_3, \theta_4, \theta_5$) was output and saved. The time histories of the vertical and fore-and-aft forces, the vertical and fore-and-aft acceleration at the pelvis, L3 and T1 were obtained. The apparent mass and transmissibility were calculated using the CSD method which was used in Chapters 4 and 5. The length of FFT (Fast Fourier Transfer) was 2048. A Hanning window was used with an overlap of 50%. About 30 averagings were then conducted for the signal of 60-s duration.

The model parameters were finally slightly adjusted through comparing the model calculated biodynamic responses with the corresponding measured data. To provide a better match to the experimental data with dual-axis excitation, the vertical stiffness beneath the pelvis was reduced from 73605 N m^{-1} to 63605 N m^{-1} and the vertical damping of the tissue beneath thighs was increased from 1650 Ns m^{-1} to 8650 Ns m^{-1}, which was in line with the observation that human body tissue on the seat-occupant interface became softened and more damped with the addition of fore-and-aft vibration.

The final set of parameters is listed in Tables 7.1 to 7.4, where the stature of the human body, H, is 1.66 m, and the total mass of the body, M, is 63 kg.

Table 7.1 Length and centre of mass of each body segment [a].

	Length (m)	centre of mass
Upper body (l_3)	0.23H	0.50l_3
Middle body (l_2)	0.17H	0.55l_2
Pelvis (l_1)	0.08H	0.71l_1
Thighs (l_4)	0.20H	0.43l_4
Legs (l_5)	0.20H	0.43l_5

[a], data based on Dempster *et al.* (1967) and a NASA Reference Publication.

Table 7.2 Mass and second moments of inertia of each body segment.

	Mass (M=63 kg)		moment of inertia (kg m^2)[b]
Pelvis (m_1)	0.13M	8.19	0.025
Middle body (m_2)	0.16M	10.08	0.12
Upper body (m_3)	0.33M	20.79	1.20
Thighs (m_4)	0.26M	16.13	0.45
Legs (m_5)	0.12M	7.81	0.13

[b], the initial value of the moment of inertia were estimated on the basis of Dempster *et al.* (1967) and modified according to the optimized mass.

Table 7.3 Translational stiffness and damping.

Stiffness (N m^{-1})		Damping (Ns m^{-1})	
k_{1z}	64000[c]	c_{1z}	400
k_{1x}	75000	c_{1x}	15
k_{4z}	14600	c_{4z}	9000[c]
k_{4x}	10	c_{4x}	1500

[c], k_{1z} and c_{4z} was 73605 and 1650 respectively during the parameters identification based on the measured apparent mass and transmissibility with single-axis vertical vibration.

Table 7.4 Rotational stiffness and damping.

Stiffness (Nm rad^{-1})		Damping (Nms rad^{-1})	
k_{t1}	600	c_{t1}	50
k_{t2}	800	c_{t2}	450
k_{t3}	930	c_{t3}	500
k_{t4}	20	c_{t4}	2000

7.3 Prediction of apparent mass and transmissibility

The calibration of model is based on the vertical and fore-and-aft forces at the seat-occupant interface, vertical and fore-and-aft acceleration over the pelvis, L3, and T1 measured with a subject having a stature of 1.66 m and total body mass 63 kg (Chapters 4 and 5). The overall force on the seat surface and the accelerations on the pelvis and the spine were calculated with the dual-axis model and the parameters shown above. The power spectral density of the calculated vertical force at the seat, the vertical acceleration over the pelvis, L3 and T1 (Figure 7.2) had similar first resonance frequencies and modulus to the experimental data except the vertical acceleration over the pelvis being lower than the tested value between 6 Hz and 15 Hz. The calculated fore-and-aft force had the first mode at a similar frequency to that of the experimental value but the associated magnitude of the power spectral density was only half of the measured value (Figure 7.2(b)). The second mode around 6 Hz was observed in the

calculated fore-and-aft force, which was not evident in the measured value. The principle mode of the calculated fore-and-aft acceleration over the pelvis occurred at about 6 Hz, lower than the primary experimental resonance frequency (around 9 Hz) but had comparable peak magnitude (Figure 7.2(d)). The predicted fore-and-aft acceleration over L3 and T1 also had comparable resonance frequencies and modulus with the measured value except that the peak magnitude of the first mode of calculated fore-and-aft acceleration over L3 was lower than the experimental counterpart (Figure 7.2(f)).

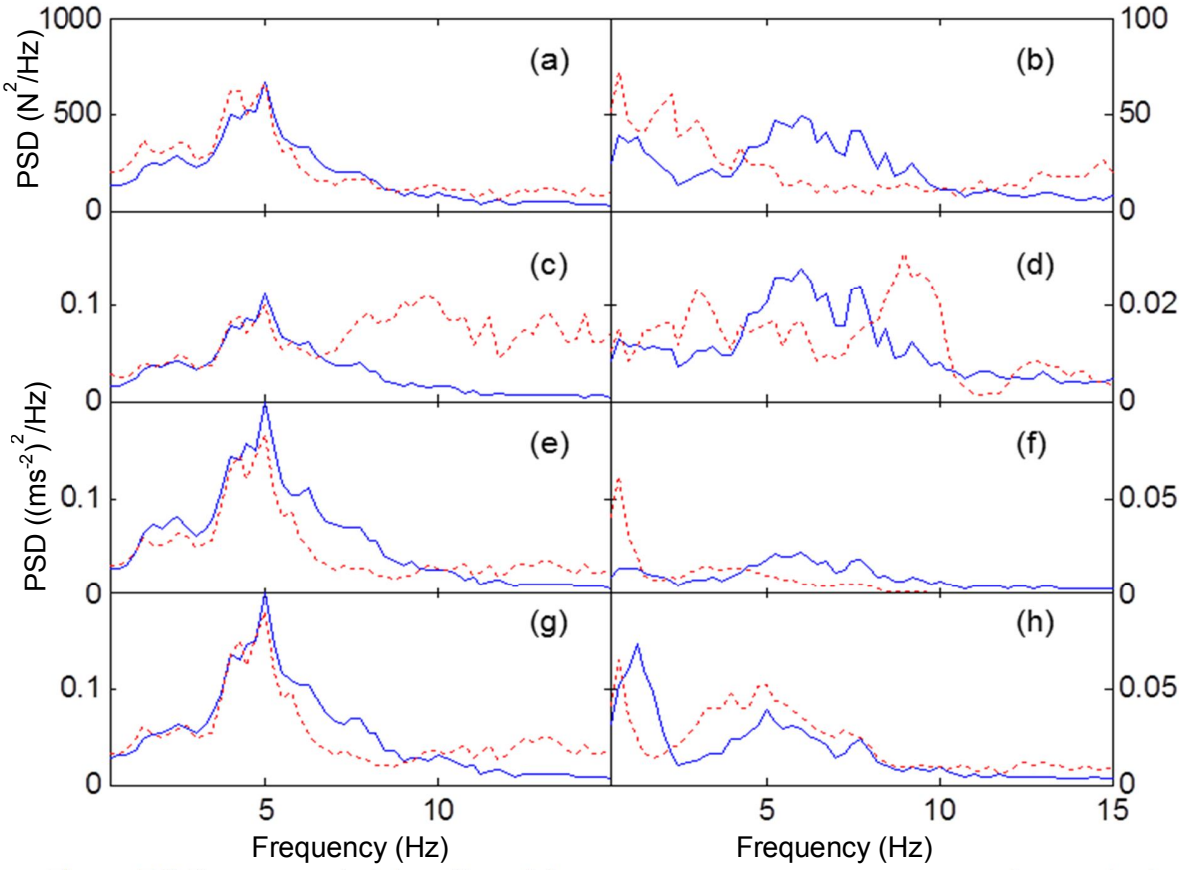

Figure 7.2 Power spectral densities of the overall dynamic response of the human body with dual-axis excitation: (a) vertical force at the seat; (b) fore-and-aft force at the seat; (c) vertical acceleration over the pelvis; (d) fore-and-aft acceleration over the pelvis; (e) vertical acceleration over L3; (f) fore-and-aft acceleration over L3; (g) vertical acceleration over T1; (h) fore-and-aft acceleration over T1. ——, calculated value; - - -, experimental value.

The model was further calibrated by comparing the calculated apparent mass and transmissibility to the measured values (Figure 7.3 and Figure 7.4). The calculated vertical apparent mass and fore-and-aft cross-axis apparent mass showed comparable resonance frequencies and modulus of the first peak with the corresponding experimental values (Figure 7.3). The calculated vertical transmissibility and fore-and-aft

cross-axis transmissibility also had similar first resonance frequencies and modulus to the experimental data. The main discrepancy was observed in the vertical transmissibility to the pelvis at frequencies greater than 5 Hz.

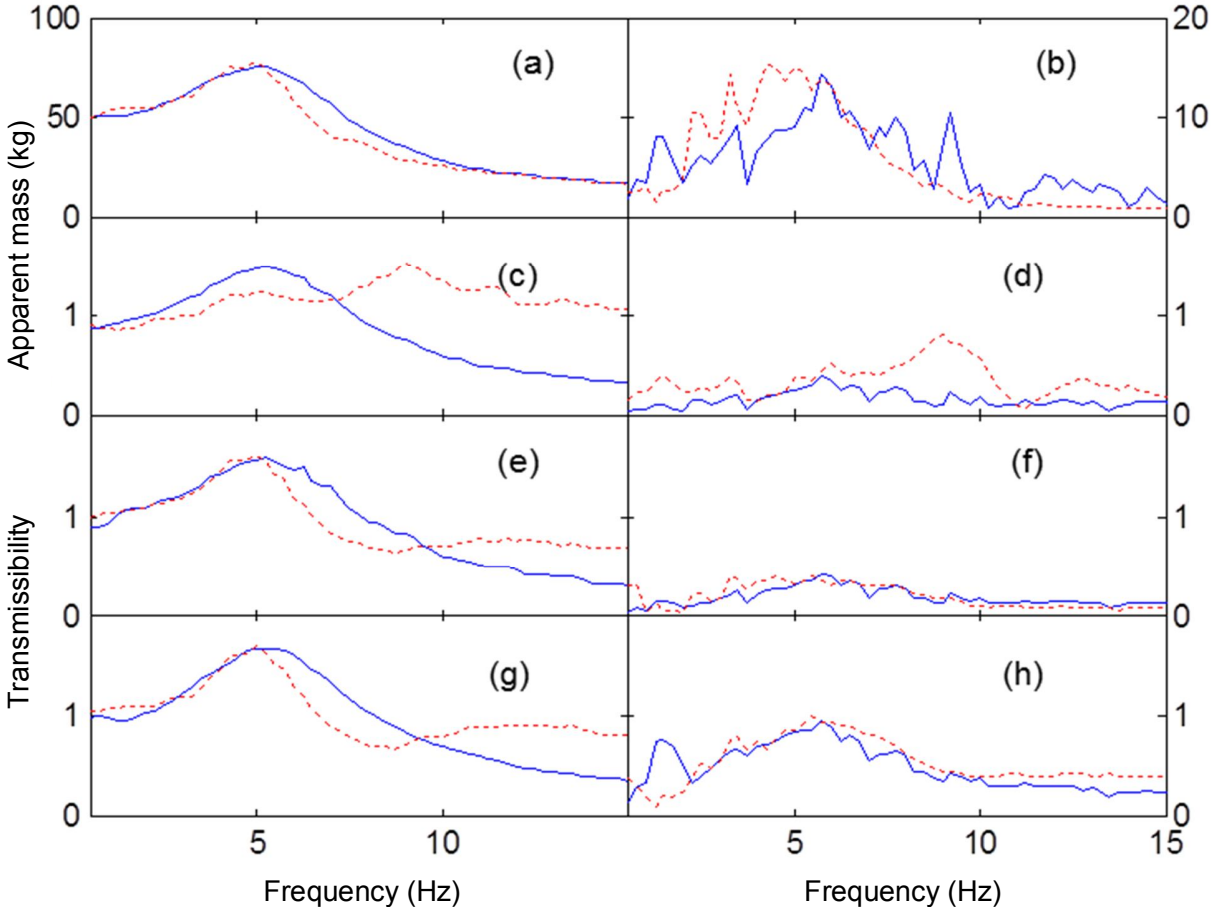

Figure 7.3 Apparent mass and transmissibility of the human body with dual-axis excitation: (a) vertical apparent mass; (b) fore-and-aft cross-axis apparent mass; (c) vertical transmissibility to the pelvis; (d) fore-and-aft cross-axis transmissibility to the pelvis; (e) vertical transmissibility to L3; (f) fore-and-aft cross-axis transmissibility to L3; (g) vertical transmissibility to T1; (h) fore-and-aft cross-axis transmissibility to T1. ——, calculated value; - - -, experimental value.

The calculated fore-and-aft apparent mass, the fore-and-aft transmissibility to the pelvis, L3 and T1 showed the same numbers of peaks and similar peak moduli to their experimental counterparts but resonated at higher frequencies (Figure 7.4). The calculated vertical cross-axis apparent mass and the transmissibility had similar number of peaks occurring at similar frequencies.

It is noted that there are only one or two modes in the vertical apparent mass and vertical transmissibility in Figure 7.3 while the vertical force and vertical acceleration in Figure 7.2.2 are more rugged. This is because the figures only show the output of the system rather than the transfer functions which are shown in Figure 7.3 In other words, peaks in Figure 7.2 are not necessarily attributed to any modes.

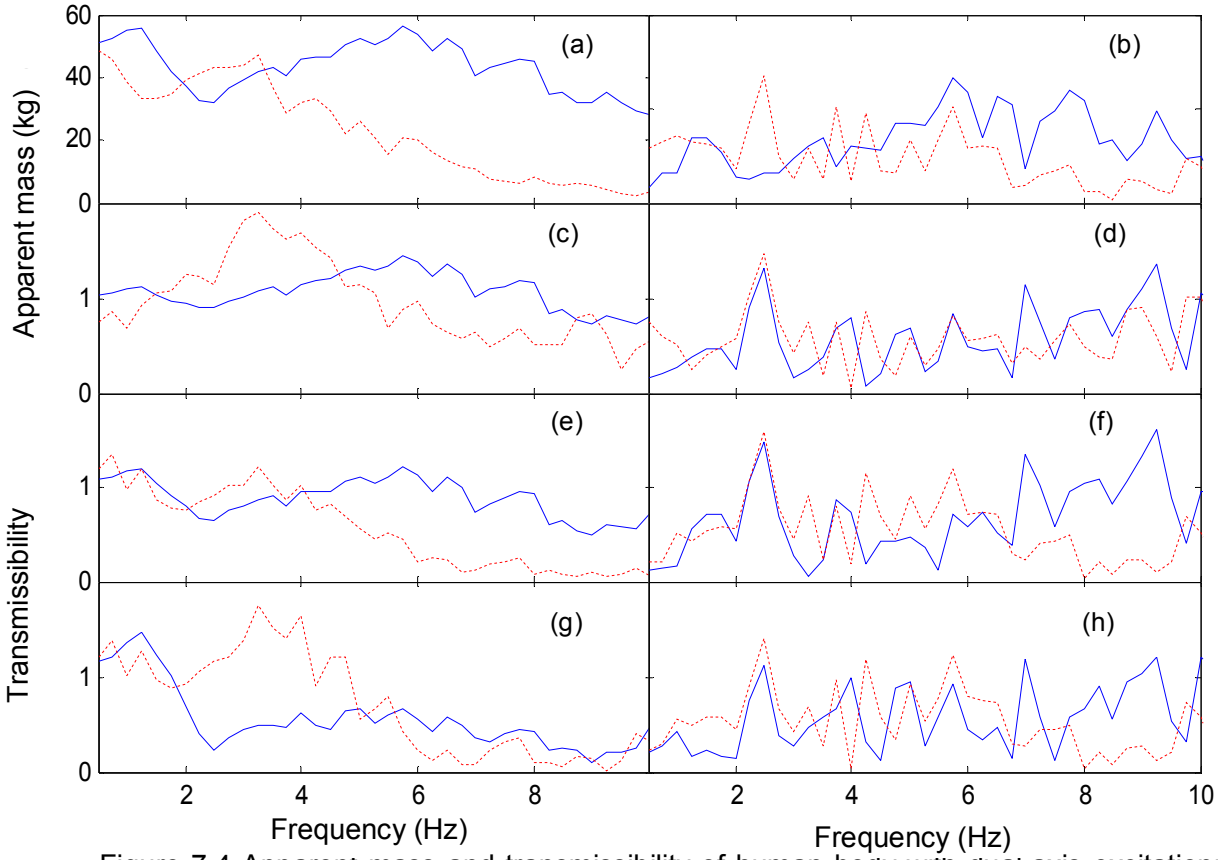

Figure 7.4 Apparent mass and transmissibility of human body with dual-axis excitation: (a) fore-and-aft apparent mass; (b) vertical cross-axis apparent mass; (c) fore-and-aft transmissibility to the pelvis; (d) vertical cross-axis transmissibility to the pelvis; (e) fore-and-aft transmissibility to L3; (f) vertical cross-axis transmissibility to L3; (g) fore-and-aft transmissibility to T1; (h) vertical cross-axis transmissibility to T1. ——, calculated value; - - -, experimental value.

7.4 Parameter sensitivity

The values of the six most influential mechanical parameters (i.e., k_{1z}, c_{4z}, k_{1x}, c_{4x}, k_{t1}, c_{t2}) were doubled so as to investigate how the biodynamic response with dual-axis excitation was influenced by changes of the mechanical properties of human body. The parameters to be changed were selected because they were observed to produce major variations in the resonance frequency and `peak modulus of the apparent mass with vertical excitation (Chapter 3).

The variations in the force and both the inline apparent mass and the cross-axis apparent mass in the frequency range of 0.5 to 15 Hz with increased vertical stiffness of tissue beneath the pelvis (i.e., k_{1z}) and increased vertical damping of tissue beneath the thighs (i.e., c_{4z}) are shown in Figure 7.5. Whether the primary resonance (either resonance frequency or peak modulus) is changed is checked firstly. If the primary resonance is changed little, the variation in the second resonance (or the response around the second resonance) is checked.

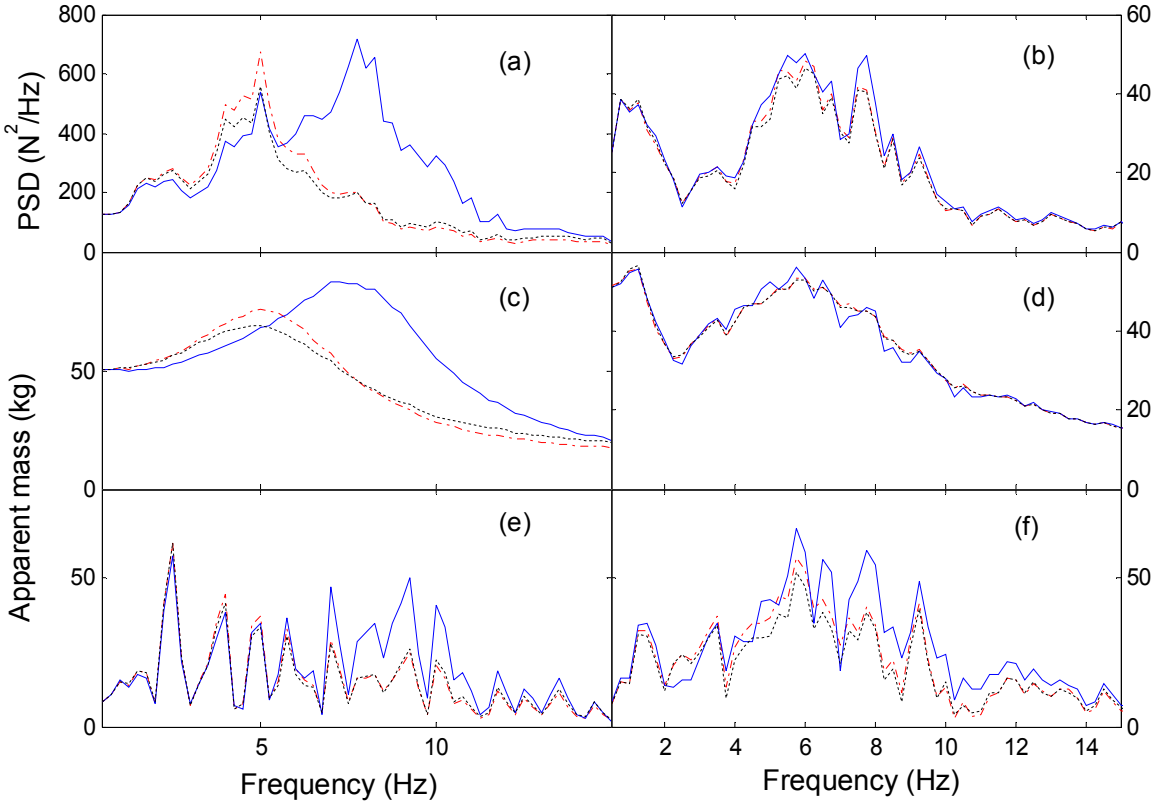

Figure 7.5 Effect of increasing the vertical stiffness of tissue beneath the pelvis (k_{1z}) and the vertical damping of tissue beneath the thighs (c_{4z}) on: (a) power spectral densities (PSDs) of the vertical force on the seat; (b) PSDs of the fore-and-aft force; (c) vertical apparent mass; (d) fore-and-aft apparent mass; (e) vertical cross-axis apparent mass; (f) fore-and-aft cross-axis apparent mass: —.—, nominal value (i.e., the value obtained with optimized parameters); ——, increased stiffness; - - -, increased damping.

The changes in the acceleration at the pelvis and T1 and both the inline and cross-axis transmissibility with the doubled k_{1z} and c_{4z} are shown in Figure 7.6. The peak magnitude of the PSD and the peak frequencies in the vertical acceleration at T1 and the pelvis were increased due to the increased stiffness (Figure 7.6(a) and Figure 7.6(c)), accompanied by the increase in the vertical transmissibility to T1 and to the pelvis, respectively (Figure 7.6(e) and Figure 7.6(g)). The vertical cross-axis

transmissibility to T1 and the pelvis increased only at frequencies greater than 6 Hz (Figure 7.6(i) and Figure 7.6(k)). Increasing the stiffness increased the PSD of the fore-and-aft acceleration at T1 and the pelvis marginally above 5 Hz (Figure 7.6(b) and Figure 7.6(d)), accompanied by an increase in the fore-and-aft cross-axis transmissibility to T1 and to the pelvis, respectively, in a similar frequency range (Figure 7.6(f) and Figure 7.6(h)). Increasing damping decreased the PSD of the vertical acceleration at T1 and the pelvis and the corresponding vertical transmissibility around resonance frequencies, but had little influence on the other responses.

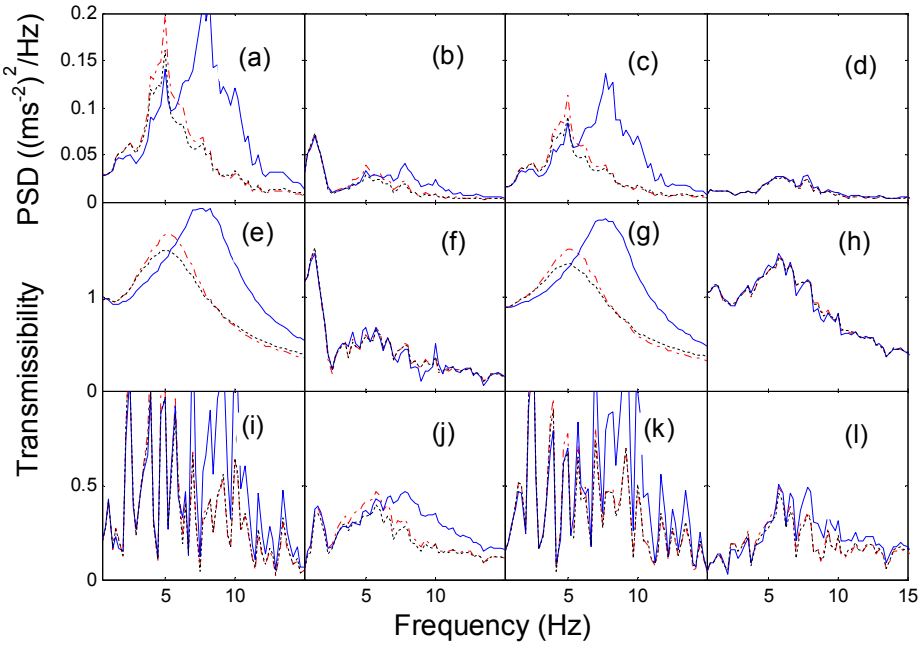

Figure 7.6 Effect of increasing the vertical stiffness of tissue beneath the pelvis (k_{1z}) and the vertical damping of tissue beneath the thighs (c_{4z}) on: (a) the power spectral density (PSD) of the vertical acceleration at T1; (b) the PSD of the fore-and-aft acceleration at T1 ; (c) the PSD of the vertical acceleration at the pelvis; (d) the PSD of the fore-and-aft acceleration at the pelvis; (e) the vertical transmissibility to T1; (f) the fore-and-aft transmissibility to T1; (g) the vertical transmissibility to the pelvis; (h) the fore-and-aft transmissibility to the pelvis; (i) the vertical cross-axis transmissibility to T1; (j) the fore-and-aft cross-axis transmissibility to T1; (k) the vertical cross-axis transmissibility to the pelvis; (l) the fore-and-aft cross-axis transmissibility to the pelvis. —.—, nominal value; ——, increased stiffness; - - -, increased damping.

The variations in the force and both the inline and cross-axis apparent mass in the frequency range of 0.5 to 15 Hz with increased fore-and-aft stiffness (k_{1x}) and fore-and-

aft damping (c_{4x}) of the tissues beneath thighs are shown in Figure 7.7. Neither increasing the fore-and-aft stiffness nor the fore-and-aft damping changed the spectra of the vertical force, the vertical apparent mass, or the vertical cross-axis apparent mass. Increasing stiffness did not change the spectra of the fore-and-aft force or the fore-and-aft apparent mass around the first peak but increased the force and apparent mass at frequencies greater than 5 Hz. Increased damping decreased the spectra of the fore-and-aft force and the fore-and-aft apparent mass at frequencies around the second peak between 3 to 8 Hz. Increased stiffness and increased damping had little effect on the fore-and-aft cross-axis apparent mass across the frequency range.

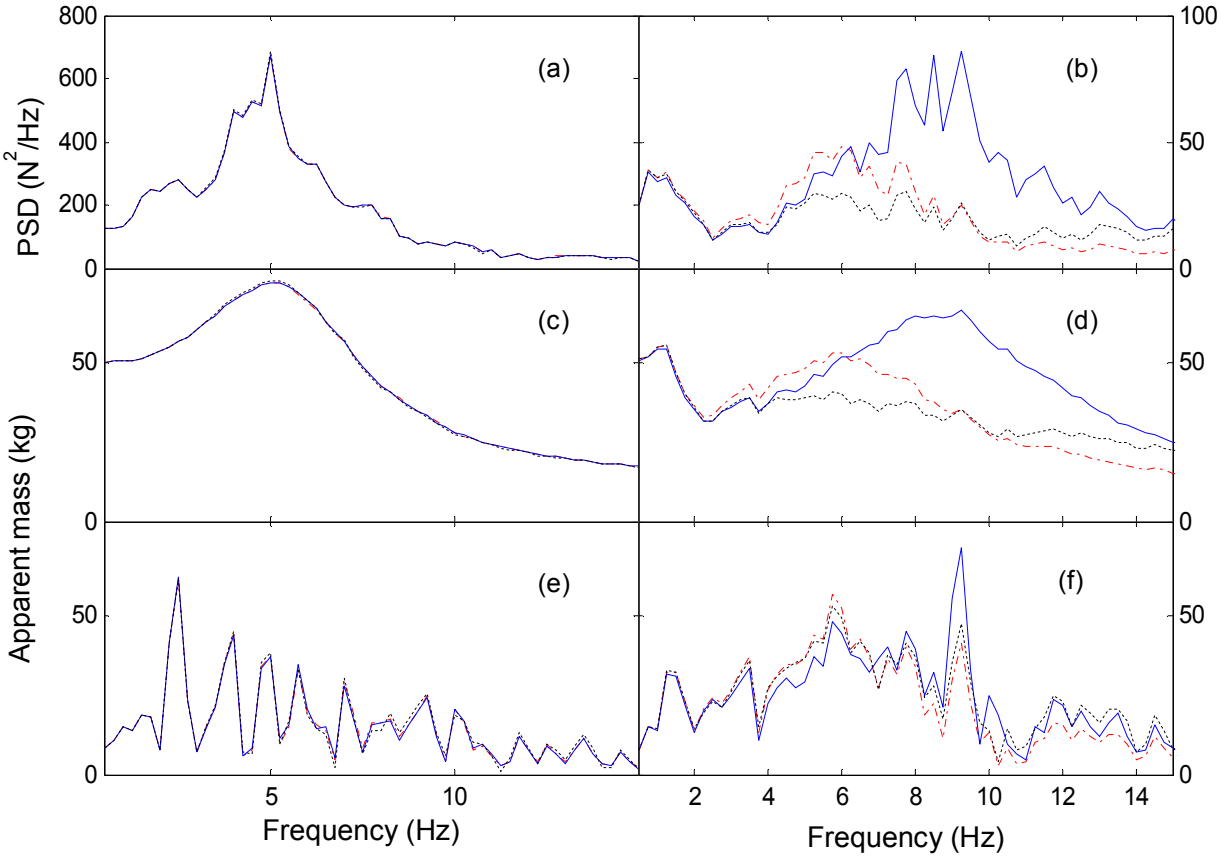

Figure 7.7 Effect of increasing fore-and-aft stiffness of tissue beneath the pelvis (i.e., k_{1x}) and the fore-and-aft damping of tissue beneath the thighs (i.e., c_{4x}) on the force response and the apparent mass. The keys are the same as Figure 7.5. —.—, nominal value; ——, increased stiffness; - - -, increased damping.

The change in the acceleration at the pelvis and T1 and the transmissibility with k_{1x} and c_{4x} doubled is shown in Figure 7.8. Neither increasing the fore-and-aft stiffness nor increasing the fore-and-aft damping affected the vertical acceleration responses or vertical transmissibility and fore-and-aft cross-axis transmissibility to T1 or the pelvis.

Increasing the stiffness (k_{1x}) increased the PSD of the fore-and-aft acceleration at T1 at frequencies greater than 7 Hz (Figure 7.8(b)) and was similar to the increase in the fore-and-aft transmissibility to T1 in the same frequency range (Figure 7.8(f)). Increasing the stiffness (k_{1x}) had little influence on the fore-and-aft cross-axis transmissibility to T1 (Figure 7.8(j)). There was no major effect of increasing damping (c_{4x}) on the PSD of the fore-and-aft acceleration on T1 (Figure 7.8(j)) and the transmissibility.

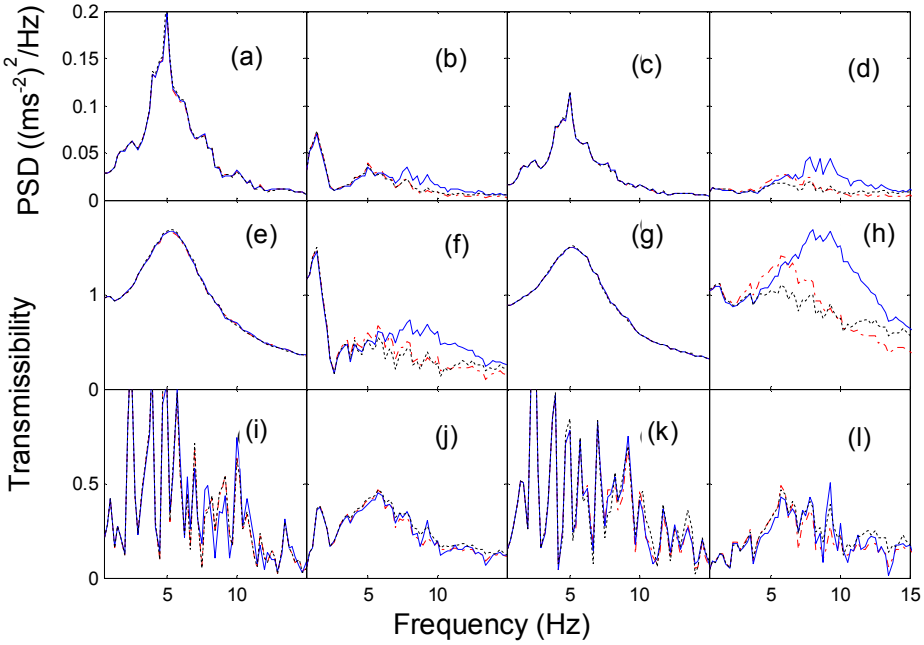

Figure 7.8 Effect of increasing the fore-and-aft stiffness of tissue beneath pelvis (i.e., k_{1x}) and the fore-and-aft damping of tissue beneath thighs (i.e., c_{4x}) on the resultant acceleration response and the associated components. The keys are the same as Figure 7.6. —.—, nominal value; ——, increasing stiffness; - - -, increasing damping.

With increasing stiffness (k_{1x}) there was an increase in the peak modulus and the peak frequency of the PSD of the fore-and-aft acceleration on the pelvis (Figure 7.8(d)) and the fore-and-aft transmissibility to the pelvis (Figure 7.8(h)) but not in the fore-and-aft cross-axis transmissibility to the pelvis. Increasing the damping (c_{4x}) decreased the PSD of the fore-and-aft acceleration and the fore-and-aft transmissibility at the frequencies between 5 to 8 Hz but did not change the fore-and-aft cross-axis transmissibility to the pelvis (Figure 7.8(l)).

With increased rotational stiffness k_{t1} and rotational damping c_{t2}, the variations in the force, and both the inline and cross-axis apparent mass, in the frequency range 0.5 to 15 Hz are shown in Figure 7.9. Increasing the rotational stiffness did not influence either the force or the apparent masses. A marginal reduction was observed with the PSD of the

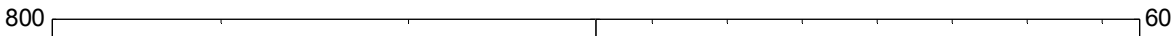

vertical force (Figure 7.9(a)) and the vertical apparent mass (Figure 7.9(c)) around the resonance frequency. A decrease in the fore-and-aft apparent mass (Figure 7.9(d)) and the power spectral densities of the fore-and-aft force (Figure 7.9 (b)) around their first peaks and the fore-and-aft cross-axis apparent mass (Figure 7.9(f)) between 4 to 8 Hz was observed.

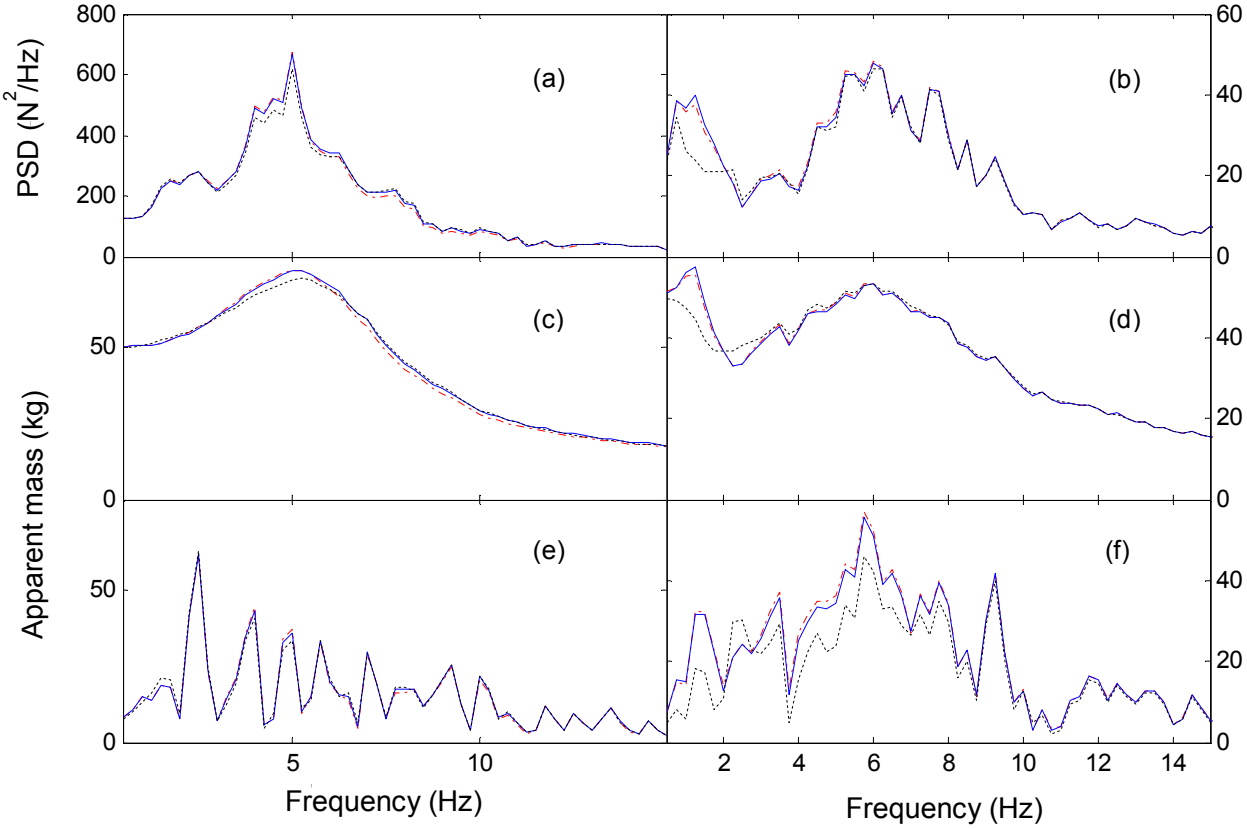

Figure 7.9 Effect of increasing the rotational damping, c_{t2}, and rotational stiffness, k_{t1}, on the force and the apparent mass. The keys are the same as in Figure 7.5. —.—, nominal value; ——, increasing rotational damping; - - -, increasing rotational stiffness.

The changes in the acceleration at the pelvis and at T1 and in both the inline and the cross-axis transmissibility with the same increase in rotational stiffness k_{t1} and rotational damping c_{t2} are shown in Figure 7.10. Increasing rotational stiffness did not influence any of the spectra of the monitored responses. Small reductions were observed in the PSD of the vertical acceleration at T1 (Figure 7.10(a)) and the vertical transmissibility to T1 (Figure 7.10(e)) around the resonance frequency but not in the acceleration and transmissibility to the pelvis. A decrease was observed in the fore-and-aft transmissibility to T1 (Figure 7.10(f)) and the magnitudes of the PSD of the fore-and-aft acceleration (Figure 7.10(b)) around their first peaks. A decrease was also observed in the fore-and-

aft cross-axis transmissibility between 4 to 8 Hz (Figure 7.10(j)). No effect of increasing the damping on the monitored variables associated the pelvis was observed.

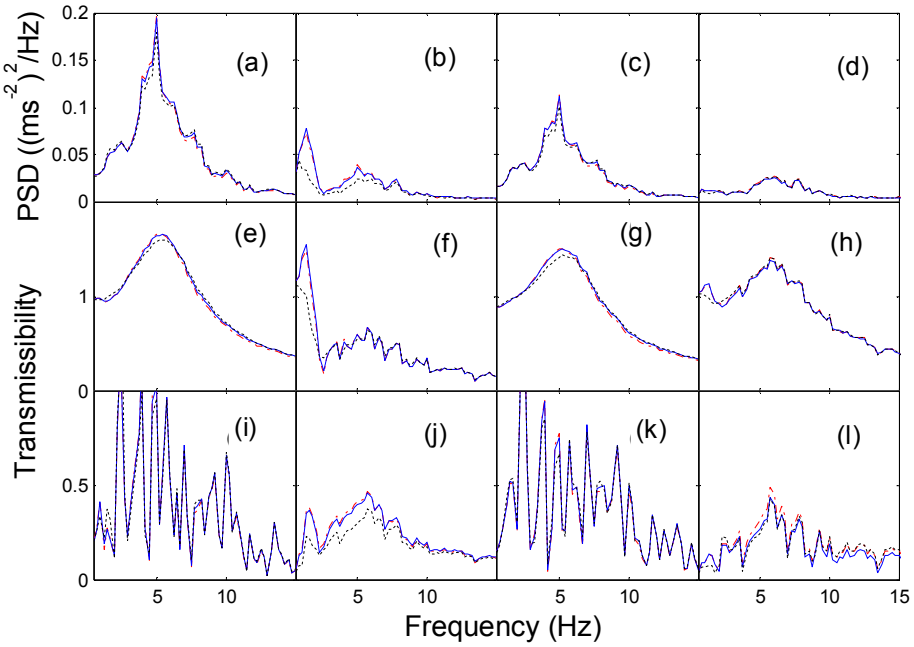

Figure 7.10 Effect of increasing rotational damping c_{t2} and rotational stiffness k_{t1} on the acceleration and the transmissibility. The keys are the same as in Figure 7.6. —.—, nominal value; ——, increasing rotational damping; - - -, increasing rotational stiffness.

7.5 Discussion

7.5.1 The necessary characteristics of a human body model for dual-axis excitation

To identify the necessary elements that should be included in a human body model with dual-axis excitation, the simplest model with a lumped mass connected to vertical and fore-and-aft springs and dampers was first formulated, as shown in Figure 7.11. The mass is able to move horizontally, with k_{1x} and c_{1x} simulating the shear properties of the body tissues at the seat-human body interface, and move vertically with k_{1z} and c_{1z} simulating the axial properties of the tissue. The model assumes that motion in the fore-and-aft direction results solely from fore-and-aft excitation while vertical motion is induced solely by vertical excitation, so the motions in the two directions are independent. This model can be regarded as the linear superposition of two models, each with a single degree-of-freedom, as shown in Figure 7.12.

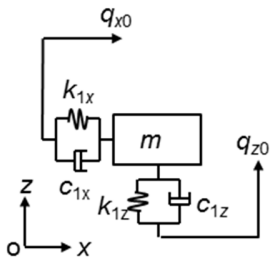

Figure 7.11 A human body model with two degrees-of-freedom for predicting the apparent mass in the vertical and fore-and-aft directions.

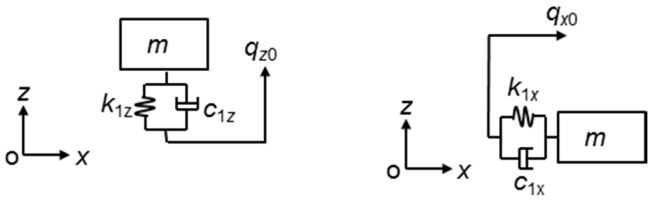

(a) (b)

Figure 7.12 Two single degree-of-freedom human body models for representing: (a) vertical apparent mass; (b) fore-and-aft apparent mass.

In practice, when there is dual-axis excitation, the response of the human body caused by the vertical excitation is coupled with the response caused by the fore-and-aft direction, which is not the same as that obtained using two single degree-of-freedom models as in Figure 7.12. So such a model is not suitable for representing the coupling effect of the dual-axis excitation on the biodynamic response.

A rotational element was introduced into the model in Figure 7.11 so as to produce a human body model with pitching motion as shown in Figure 7.13. The rotational element was introduced because a pitching motion of the upper body has been observed as a dominant vibration mode (Kitazaki and Griffin, 1997; Matsumoto and Griffin, 1998a). The two components of the body simulate the lower-body and the upper-body. The model has three degrees of freedom (i.e., vertical displacement of the lower-body, fore-and-aft displacement of the lower-body, and rotational displacement of the upper-body).

The vertical apparent mass and fore-and-aft apparent mass could be derived as

$$M_{zz} = \frac{\delta_1(M,C,K)}{s^2} - \frac{\delta_2(M,C,K)}{s^2}\left(\frac{Q_{x0}}{Q_{z0}}\right). \qquad (7.3)$$

$$M_{xx} = \frac{\varepsilon_1(M,C,K)}{s^2}\left(\frac{Q_{z0}}{Q_{x0}}\right) - \frac{\varepsilon_2(M,C,K)}{s^2}. \quad (7.4)$$

where Q_{x0} and Q_{z0} are the nominal Laplace expression of the fore-and-aft excitation (Figure 7.13, q_{x0}) and the vertical excitation (Figure 7.13, q_{z0}) in the frequency domain; M, C, and K are the mass matrix, damping matrix and stiffness matrix of the model. $\delta_1(M,C,K)$, $\delta_2(M,C,K)$ and $\varepsilon_1(M,C,K)$, $\varepsilon_2(M,C,K)$ are symbolic expressions consisting of system parameters.

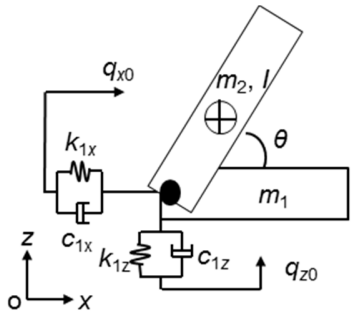

Figure 7.13 Three degree-of-freedom model for representing coupling effect of dual-axis excitation.

The vibrations in the two directions are coupled with each other in this model. It seems reasonable to suggest that a model of the human body with dual-axis excitation should have at least three degrees-of-freedom, one of which represents rotational motion.

7.5.2 The justification of time domain method

For the human body model with dual-axis excitation proposed in this study (Figure 7.1), the equations of motion were initially solved by performing the Laplace transform with respect to each independent coordinate and the inputs with the following assumption:

$$Q_{x0}=L(q_{x0}(t)); \; Q_{z0}=L(q_{z0}(t)), \quad (7.5)$$

where, $q_{x0}(t)$ is the fore-and-aft input displacement, q_{z0} (t) vertical input displacement, and L is Laplace calculator.

The symbolic expression of the shear deformation of the pelvis tissue (i.e., x_1) in the frequency domain, expressed as the formulation of the mass matrix, M, stiffness matrix, K, and damping matrix, C, of the system and the input frequency, f, was then defined as:

$$L(x_1) = q_1(f) = \Phi_0(M, C, K, f)Q_{x0} + \Phi_1(M, C, K, f)Q_{z0}. \quad (7.6)$$

Similarly, the symbolic expression of the axial deformation of the pelvis and rotational motion of the thighs with respect to joint 1 (Figure 7.1) were defined as Equations (7.7) and (7.8):

$$L(z_1) = q_2(f)$$

$$=(\Psi_0(M, C, K, f)+ \Psi_2(M, C, K, f)\,\Phi_0(M, C, K, f))\,Q_{z0}+(\Psi_1(M, C, K, f)+ \Psi_2(M, C, K, f)\Phi_1(M, C, K, f))Q_{z0}. \quad (7.7)$$

$$L(\theta_4) = q_6(f)$$

$$=(\zeta_0(M, C, K, f)+ \zeta_2\Phi_0(M, C, K, f))Q_{x0}+(\zeta_1(M, C, K, f)+ \zeta_2(M, C, K, f)\Phi_1(M, C, K, f))\,Q_{z0}. \quad (7.8)$$

The vertical apparent mass can thus be obtained as Equation (7.9):

$$M_{zz} = F_z/Q_{z0}\,(2\pi f)^2$$

$$= ((k_{1z}+c_{1z}\,(2\pi f))\,(q_2- Q_{z0}) + (k_{4z}+c_{4z}2\pi f)\,(q_2 +cos(\theta_{40})\,r_{c4}q_6- Q_{x0}))/(\,Q_{z0}(\pi f)^2). \quad (7.9)$$

The fore-and-aft apparent mass was obtained as Equation (7.10):

$$M_{xx}=F_x/Q_{x0}(2\pi f)^2$$

$$= ((k_{1x}+c_{1x}\,(2\pi f))\,(q_1- Q_{x0}) + (k_{4x}+c_{4x}\,(2\pi f))\,(q_1 +sin\,(\theta_{40})\,r_{c4}q_6- Q_{z0}))/\,(Q_{x0}\,(2\pi f)^2). \quad (7.10)$$

It is clear that the solution for the apparent mass with dual-axis excitation is dependent on both stimuli (Equations (7.9)-(7.10)). To predict the biodynamic response of the human body with dual-axis excitation using the above frequency domain method needs a close-form solution of the Laplace transform of the inputs. However, there are no mathematical functions for the Laplace transform of random signals. So the explicit expression of the ratio between the Laplace transform of the two inputs as a function of frequency was difficult to obtain. Although other frequency domain methods like the one based on modal superposition could be an alternative to solve the equations of motion, it was decided to calculate the response in the time domain with a Simulink model and calculate the transfer functions in the frequency domain using CSD method.

7.5.3 The application and limitations of the model

The model is expected to reflect the dynamic response of a real subject. The parameters have to be changed, e.g., length, mass, stiffness and damping, to match the data of other individuals.

The model in this study provided a reasonable prediction of the inline apparent masses and the cross-axis apparent masses, the inline transmissibilities and the cross-axis transmissibilities of the human body in the vertical and fore-and-aft directions when the body was exposed to simultaneous vertical and fore-and-aft excitation. However, the second peaks of the vertical acceleration at the pelvis and the vertical transmissibility to the pelvis were not well represented (Figure 7.3). The reason might be that the mechanical properties were predominately determined to provide a reasonable match to the vertical apparent mass. Consequently, the fitting of the first peak of the vertical acceleration at the pelvis which occurred at frequencies similar to the peak frequency of the vertical apparent mass was given the priority to. The second peak of the vertical acceleration at the pelvis which occurred at a high frequency was thus less fitted.

The mechanical properties of the model were based on parameter identification with the apparent mass with single-axis vertical vibration at 1.0 ms^{-2} r.m.s., as mentioned in Section 7.2.2. The identified parameters will vary when the vibration magnitude is changed, due to the nonlinearity reported in many of the previous studies. The parameters in the model will also vary between subjects. It was suggested that by varying anthropometric properties (e.g., body mass) and some of the key mechanical properties, such as the vertical stiffness of the spring representing the tissue beneath the pelvis, the model would be able to provide a reasonable representation of the biodynamic response of other individuals exposed to the same vibration. The suggestion was supported with the parameter sensitivity analysis presented in Section 7.4 (e.g., Figure 7.5). It is also noted that the model is expected to reflect the dynamic response of a real subject. The parameters have to be changed, e.g., length, mass, stiffness and damping, to match the data of other individuals.

The apparent mass and transmissibility of the body with single-axis excitation were similar to those with simultaneous vertical and fore-and-aft vibration, especially when the magnitude of the additional fore-and-aft vibration was less than that of the vertical vibration (e.g., Qiu and Griffin, 2010; Chapter 4). This implied that the combination of the mechanical properties of human body that reflect the biodynamic response with single-

axis excitation could largely determine the dynamic response with dual-axis vibration. Therefore, it seemed logical to use the parameters obtained by matching the response with single-axis vibration to predict the response with dual-axis vibration, and adjust only those parameters to which the response was sensitive.

With the introduction of the rotational element, the resultant biodynamic response with dual-axis vibration was assumed to be the superposition of the component due to the fore-and-aft excitation and that due to the vertical excitation. The assumption might be sensible when the magnitude of the simultaneous fore-and-aft vibration was lower than that of the vertical excitation, which was the case in the present study. However, when the magnitude of the fore-and-aft vibration is increased, more muscular activity may be involved to maintain the body balance and this may increase the nonlinearity. The dual-axis model proposed on the basis of the assumption of superposition might not work.

7.5.4 Understanding of the vibration modes

The vertical transmissibility to the pelvis and T1 was sensitive to an increase in the vertical stiffness of the pelvis tissue and an increase in the vertical damping of the thigh tissue in the similar way to the vertical apparent mass (Figure 7.5 and Figure 7.6). This implies that the force at the seat-occupant interface is associated with the motion of the pelvis and the spine when there is dual-axis excitation. The result was consistent with correlations in the experimental data showing that the resonance frequency of the vertical apparent mass with dual-axis excitation (a_z =1.0 ms^{-2} r.m.s., a_x =0.5 ms^{-2} r.m.s.) was related to the first resonance frequency of the vertical transmissibility to the pelvis and to T1 (p<0.05, Spearman; Chapter 4).

Increasing the fore-and-aft stiffness of the pelvis tissue increased the peak frequency and the associated modulus of the second resonances of the fore-and-aft apparent mass and the fore-and-aft transmissibility to the pelvis and T1. Increasing the rotational stiffness (i.e., k_{t1}) reduced the fore-and-aft apparent mass and the fore-and-aft transmissibility at low frequencies around the first mode but did not influence either the peak modulus or the peak frequency of the second mode. It was indicated that the second mode of the fore-and-aft apparent mass and fore-and-aft transmissibility was associated with fore-and-aft movement of upper-body caused by shear deformation of the pelvis tissue, while the first mode was attributed to fore-and-aft movement of the upper-body due to the pelvis pitch.

7.6 Conclusion

A multi-body dynamic human body model with five rigid bodies and seven degrees-of-freedom can provide a reasonable prediction of the frequency and modulus of the first resonance in the inline apparent masses and cross-axis apparent masses in the vertical and fore-and-aft directions, and the inline transmissibilities and cross-axis transmissibilities to the pelvis and the spine in the vertical and fore-and-aft directions when the human body is exposed to combined vertical and fore-and-aft excitation.

With dual-axis excitation, the resonance of the vertical apparent mass is sensitive to the vertical stiffness of tissues beneath the pelvis and closely related to the vertical motion of the pelvis and the spine. It has also been shown that the first mode of the fore-and-aft apparent mass and the fore-and-aft transmissibility can be attributed to the fore-and-aft movement of the upper-body due to the pelvis pitch, while the second mode can be attributed to the fore-and-aft movement of the upper-body caused by shear deformation of the pelvis tissue.

CHAPTER 8: A FINITE ELEMENT MODEL OF THE SEATED HUMAN BODY

8.1 Introduction

Various dynamic models of the human body have been proposed for predicting the biodynamic responses of the human body to whole-body vibration. Published models may be categorized as lumped-parameters models (e.g., Wei and Griffin, 1998; Qiu, 2007), multi-body models (e.g., Matsumoto and Griffin, 2001; Yoshimura *et al.*, 2005; Chapters 3 and 7), or finite element models (e.g., Pankoke *et al*., 2008). These models vary in terms of both the extent of the complexity of the model structure and their applications.

Finite element models of the human body have numerous elements connected by nodes (e.g., Pankoke *et al*., 2008) or a lumped spring-damper (e.g., Kitazaki and Griffin, 1997; Pankoke *et al*., 1998). Such models may depict the anatomy of the body with detailed skeletal structure and soft tissue in regions of interest such as the spine, back, pelvis and thighs. This type of model might be used to predict motion at the body surface and also internal forces associated with injury. However, the properties of the elements and materials are difficult to determine. Furthermore, such finite element models of the human body are complex and computational inefficient.

Some models have been developed to investigate relationships between mode shapes and human response. Modal analysis performed using 2D finite element methods has extracted seven mode shapes at frequencies less than 10 Hz (Kitazaki and Griffin, 1997). The fourth calculated mode shape, consisting of an entire body mode with vertical and fore-and-aft motion of the pelvis (due to deformation of tissue beneath the pelvis) moving in phase with vertical motion of the viscera corresponded to the primary resonance.

A planar finite element model of a sitting man consisting of rigid bodies representing the lower lumbar spine, upper torso, neck, head, arms, viscera, pelvis, and legs has been proposed (Pankoke *et al*., 1998). The model was designed to predict the dynamic response in different postures by adjusting the static force and moment on the pelvis relative to the predicted value in a standard posture, and by adjusting body weight parameters and body height parameters for individual subjects relative to the 50^{th} percentile male.

A combined car seat and occupant model for predicting seating comfort, the H-point, and backrest pressure was developed to assist seat design (Pankoke *et al.*, 2008). The

CASIMIR occupant model, with detailed geometry and dynamic characteristics of the lumbar spine, abdominal and dorsal musculature, abdominal cavity, upper-torso, arms, pelvis, legs, neck, and head was proposed but calibrated only with measures of vertical apparent mass and seat transmissibility.

Some other finite element models of the human body have been produced (e.g., ALASKA, PAM-CRASH, MADYMO, LSTC 50th percentile DUMMY). Most of these models are designed for crash analysis and are not suitable for predicting ride comfort. Some of the models may be computationally inefficient for optimising ride comfort because of unnecessary complexity in the model structure.

The multi-body models proposed in Chapter 3 and Chapter 7 are capable of representing the first resonance frequencies and the associated modulus of the dynamic response with vertical vibration and dual-axis vibration. However, simulation of the contact between the human body and the seat is oversimplified, and the models developed in the earlier chapters consisting of linear springs and dampers. The objective of this study was to develop a simple 3D finite element human body model with sufficient complexity and capacity to predict the vertical inline and fore-and-aft cross-axis apparent mass and the transmissibility to the lumbar spine. The model was developed to assist the prediction of vehicle ride dynamics and seating comfort. It is assumed that the nonlinear tissue is the main contributor to the nonlinearity observed in the apparent mass.

8.2 Proposed occupant-seat model

The 3-D occupant-seat finite element model was developed using the commercial software LS-DYNA. The human body model consisted of rigid bodies representing head-neck, arms, torso, pelvis, thighs, and legs-feet. Simple flat plates representing a horizontal rigid seat and a footrest that moved with the seat were included (Figure 8.1(a)).

The pelvis and the thighs were modelled as soft tissue and a simple bony structure (Figure 8.1 (b)). The proximal end of the thigh bone was at the ischial tuberosities. The soft tissue was initially assigned elastic material properties and the bone was rigid. All the other body parts were modelled as rigid bodies, each of which was assigned a uniform material property. The rigid bodies were meshed to represent only their inertial properties.

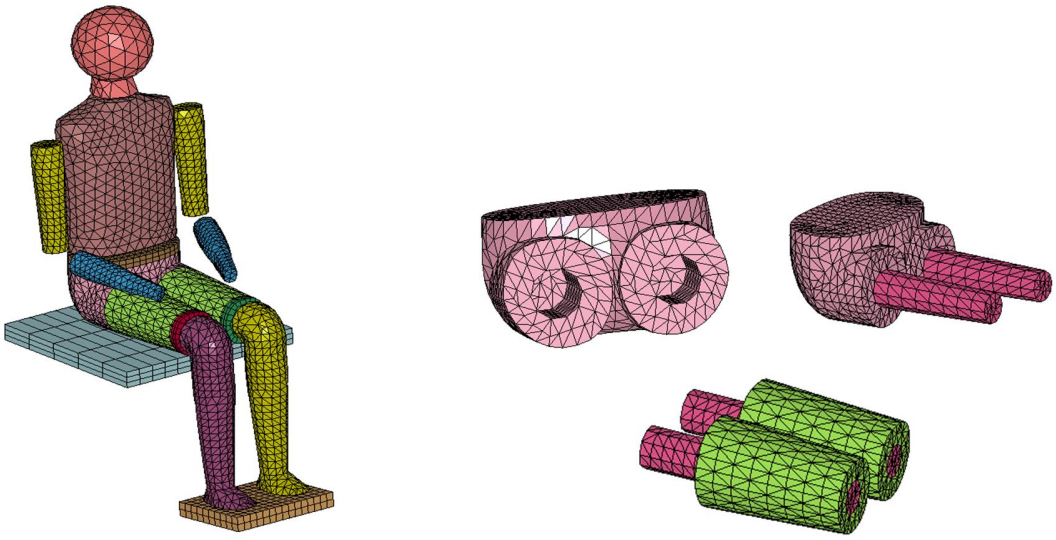

(a) (b)

Figure 8.1 Finite element model of the seated human body: (a) the complete human body; (b) the soft tissue and the bony structure of the pelvis and thigh.

The outer surface of the bone was connected with the inner surface of the pelvis and the thighs by shared common nodes. The same connection was applied between the pelvis tissue and the thigh tissue. The arms were rigidly connected to the torso. The head was connected to the torso via a spherical joint to identify the head motion around the resonance frequency in the vertical apparent mass on the seat. The torso was connected to the pelvis via a revolute joint so that it could only rotate in the sagittal plane. The revolute joint was used because the pitch motion of the upper body had been observed to contribute to the resonance in the apparent mass on the seat (e.g., Chapter 4). The connections between the thighs and the legs were also via revolute joints to identify effect of rotation of leg on the apparent mass on the seat (Nawayseh and Griffin, 2003).

The geometry of all body segments except the head was referred to the corresponding parts of the LSTC Front Impact Hybrid III -50th percentile Male (LSTC Dummy Models, 2010) for the width and length of the cross sections. The linkage lengths were based on values reported previously (Dempster *et al.*, 1967). The head was simplified as a solid sphere. The geometric dimensions were adjusted so that the ratios of the masses of these segments to the total mass were consistent with values defined in the literature

(Dempster *et al.*, 1967). The total mass of the human body model was 70 kg and the total height was 1.76 m (subject 2 in the experimental study in Chapter 4).

For all rigid and deformable parts of the model the density was 1.0 kg m^{-3}. The Young's modulus of the deformable bodies (i.e., the soft tissues of the pelvis and the thighs) was initially assigned a value of 5 x 10^6 N m^{-2}, which is in the range of the recommended values in LS-DYNA for low-density foam. It was later adjusted to 5.8 x 10^5 N m^{-2} to match the calculated apparent mass and transmissibility to the experimental values. The Poisson's ratio was 0.45 for the soft tissue. A Rayleigh damping of 0.1 was used for the whole model.

8.3 Calibration of the model

A random signal with a duration of 10-s, sampling rate 512 samples per second was used as the input. The magnitude of signal was at 0.5 ms^{-2} r.m.s. between 0.25 to 20 Hz. The signal was applied to the rigid seat as vertical acceleration. The reaction force on the seat surface and the acceleration on the seat surface and on the spine were saved with a sampling rate 512 samples per second. Apparent mass and transmissibility was calculated with the CSD method. The length of each FFT (Fast Fourier Transfer) was 2048. Hanning window was used with an overlap of 50%. Averaging was conducted among FFTs.

The model was first calibrated using the measured in-line and cross-axis apparent masses (subject 2). Figure 8.2 shows the moduli, phases and coherencies of the predicted apparent masses compared with their measured values.

The resonance frequency of the predicted vertical apparent mass was in good agreement with the resonance in the experimental apparent mass (Figure 8.2). The associated peak modulus of the apparent mass was close to the measured value, although the apparent mass at frequencies greater than 5 Hz was underestimated. The resonance frequency in the predicted fore-and-aft cross-axis apparent mass was similar to the measured value although the modulus of the predicted fore-and-aft cross-axis apparent mass at frequencies less than 5 Hz was less than the measured values.

8.4 Prediction of transmissibility and pressure distribution

The calibrated model was applied to predict both the body transmissibility and the pressure distribution at the interface between the rigid flat seat and the subject.

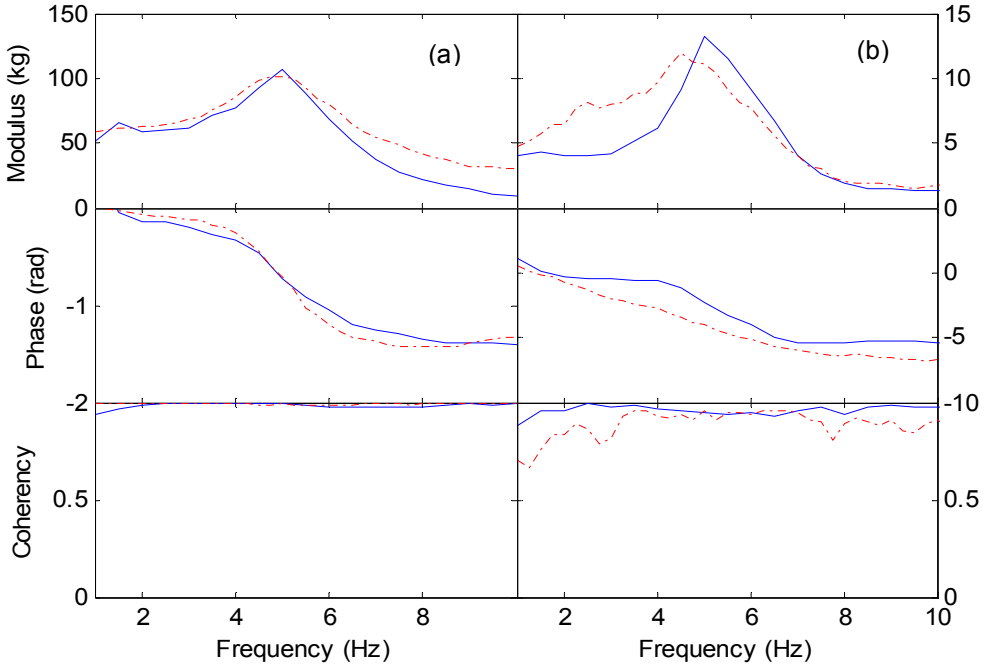

Figure 8.2 The calibration of the model with the measured apparent mass on the seat: ——, calculated values; —.—, experimental values. (a) vertical apparent mass; (b) fore-and-aft cross-axis apparent mass.

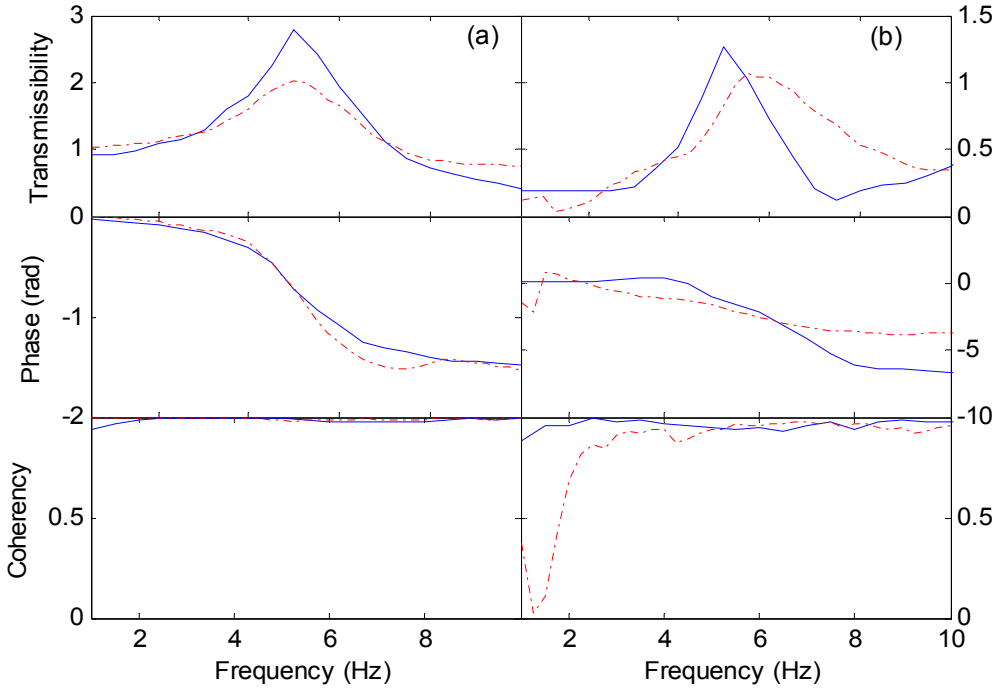

Figure 8.3 The transmissibility to the spine (L3) calculated with the model in comparison with experimental data: ——, calculated values; —.—, experimental value. (a) vertical transmissibility; (b) fore-and-aft cross-axis transmissibility.

The model provided a reasonable prediction of the modulus, the phase and coherencies of the transmissibility from the seat to the spine in both the vertical and the fore-and-aft directions (Figure 8.3). However, the peak vertical in-line transmissibility to the spine was slightly overestimated.

After a dynamic relaxation of the model so that it settled in its equilibrium position, the static pressure distribution was determined at the interface with the horizontal flat seat. The maximum pressure, which occurred around the ischial tuberosities (Figure 8.4(a)), was about 7.1 x 10^4 N m^{-2} compared with 4.2 x 10^4 N m^{-2} measured by Wu *et al.* (1998). With vertical random excitation at 0.5 ms^{-2} r.m.s., the maximum dynamic pressure still occurred at the ischial tuberosities (Figure 8.4(b)) and had a value of 10.1 x 10^4 N m^{-2} compared to maximum dynamic pressures of 5 x 10^4 N m^{-2} reported by Hinz *et al.* (2006b) and 6.0 x 10^4 N m^{-2} reported by Wu *et al.* (1998). In both of these other studies (Wu *et al.*, 1998; Hinz *et al.*, 2006b) the pressure distribution was measured for a person sitting on a flat rigid seat. The vibration used by Wu *et al.* (1998) was sinusoidal with a frequency of 5.0 Hz and magnitude of 2.0 ms^{-2} r.m.s. whereas the vibration used by Hinz *et al.* (2006b) was random with magnitude of 1.37 ms^{-2} r.m.s.

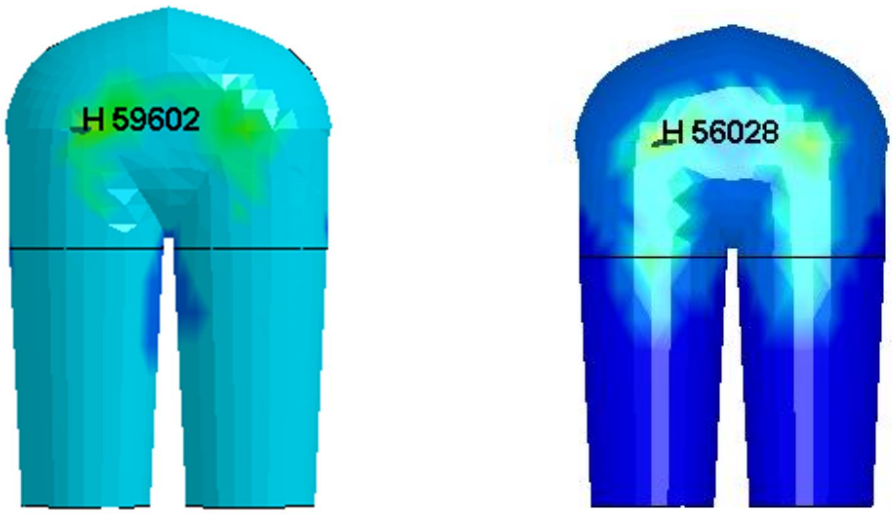

(a) (b)

Figure 8.4 Calculated pressure distributions: (a) static pressure distribution; (b) dynamic pressure distribution with vertical excitation at 0.5 ms^{-2} r.m.s. H 59602 and H 56028 are the elements where the maximum pressure occurred.

It is noted that although the geometry of the pelvis is symmetric, the elements on the pelvis and the pressure distribution are not symmetric. The asymmetric result is consistent with the previous experimental findings (e.g., Wu *et al.*, 1998).

8.5 Modal analysis of the model

The calibrated model was further applied to perform a modal analysis. Six modes were found at frequencies less than 10 Hz (Figure 8.5).

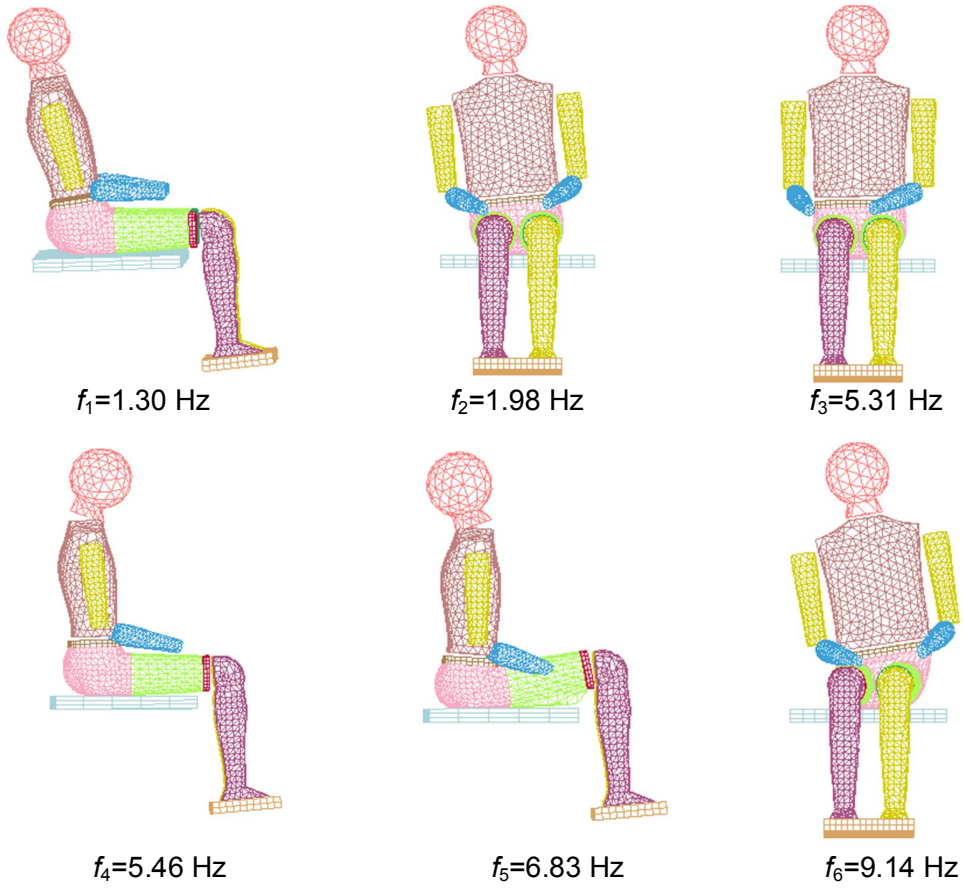

Figure 8.5 Modes shapes of the human body at frequencies less than 10 Hz.

The first mode at 1.30 Hz was dominated by pitch motion of the pelvis, accompanied by slight pitch of the thighs and vertical motion of the legs. The second mode at 1.98 Hz consisted of roll of the upper-body and the pelvis with lateral shear deformation of the soft tissues of the pelvis and the thighs. The third mode at 5.31 Hz involved yaw of the pelvis and the upper body with lateral shear deformation of buttocks tissue. The fourth mode at 5.46 Hz included pitch of the head out of phase with pitch of the pelvis and the torso. The legs moved up and down with the vertical motion and fore-and-aft shear

deformation of the buttocks tissue. The shape of the fifth mode at 6.83 Hz was similar to the fourth mode but with larger axial deformation of the pelvis tissue. Pitch of the thighs was also evident. The sixth mode at 9.15 Hz mainly consisted of lateral shear deformation of the soft tissue beneath the pelvis and roll of the upper-body, similar to the second mode.

8.6 Nonlinearity in dynamic response

Hyperelastic properties of soft tissues of the human body and animals have been reported (e.g., Zheng *et al*. 1999; Oomens *et al.*, 2003; Snedeker *et al*., 2005; Saraf *et al*., 2006; Loocke *et al*., 2008; Makhsous *et al*., 2008). The nonlinear force-deformation (or stress-strain) relationship observed in the soft tissue is similar to the behaviour of foam or rubber (e.g., Ippili, *et al.*, 2008). A few material models have been proposed to represent the constitutive relationships of soft tissue (e.g., Loocke *et al*., 2005; Loocke *et al*., 2008; MAT_MOONEY-RIVLIN_RUBBER, MAT_LOW_DENSITY_FOAM and MAT_VISCOELASTIC, as suggested in the LS-DYNA keyword user's manual, 2007).

When the vibration magnitude was increased from 0.5 to 1.0 ms^{-2} r.m.s., the resonance frequency of the measured vertical apparent mass was reduced from 5 Hz to 4.5 Hz (Chapter 4). To account for the shift of the resonance frequency, a piecewise material model was adopted for the tissue of the pelvis and the thighs. This type of material model simulates low density foam, which exhibits hyperelastic behaviour when compressed but recovers its original shape after unloading (LS-DYNA keyword user's manual, 2007). The non-linear stress-strain relation consisted of two straight lines (Figure 8.6).

The curve starts from the origin of the coordinate system. The coordinates of the end points of the first line and second line were determined by matching the predicted apparent mass to the experimental value measured with a vertical excitation at 0.5 ms^{-2} r.m.s. and 1.0 ms^{-2} r.m.s. The calibration was completed when: (a) resonance frequency of calculated apparent mass with vertical random excitation at 0.5 ms^{-2} r.m.s. was 5.0 Hz and (b) the predicted shift of the resonance frequency in the vertical apparent mass was 0.5 Hz (i.e., the shift in the resonance frequency of experimental apparent mass when the vibration magnitude was increased).

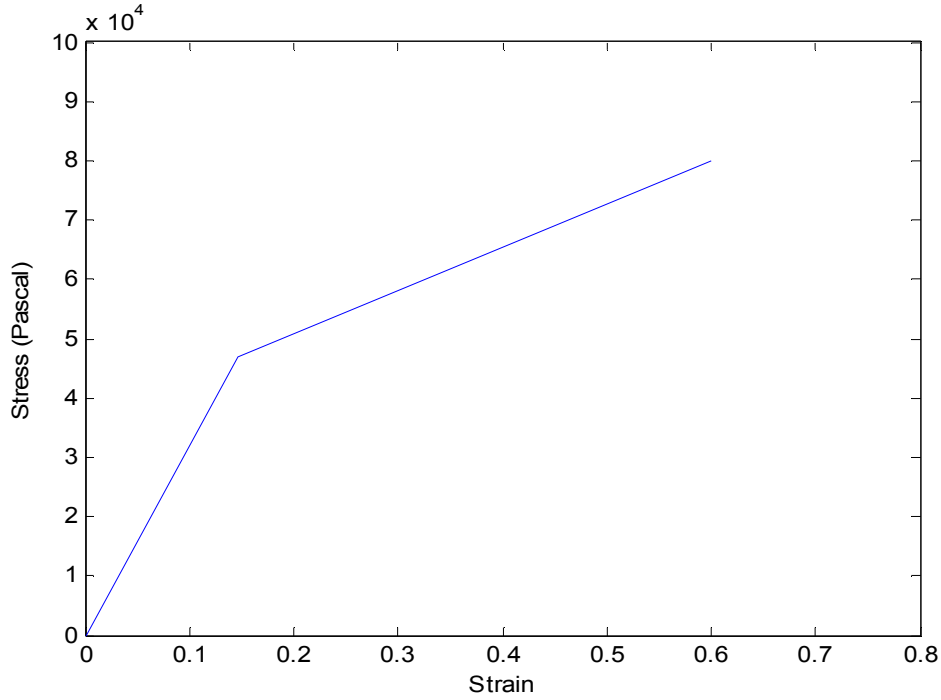

Figure 8.6 The nominal stress-strain curve for the compressive behaviour of the tissue beneath the pelvis and the thighs.

The calculated compressive deformation (i.e., the relative displacement between the node on the inner surface in contact with bone and the node on the outer surface of the buttocks in contact with the seat; see Figure 8.1(b)), vertical force and vertical apparent mass showed lower resonance frequencies with a high excitation magnitude than with a low excitation magnitude (Figure 8.7).

With the nonlinear tissue, the predicted resonance frequency of the deformation, the vertical force and the vertical apparent mass shifted from 5.5 to 3.0 Hz, 5.5 to 3.0 Hz, and 4.5 to 4.0 Hz, respectively.

With vertical excitations at both 0.5 and 1.0 ms^{-2} r.m.s., the maximum pressure occurred at the ischial tuberosities (see Figure 8.4 for pressure calculated with a linear tissue model at 0.5 ms^{-2} r.m.s.). The peak modulus of the PSD (power spectral density) of the maximum pressure at 1.0 ms^{-2} r.m.s. was four times that at 0.5 ms^{-2} r.m.s. (Figure 8.8). The r.m.s. (root mean square) value of the time history of the maximum pressure with vertical excitation at 0.5 ms^{-2} r.m.s. was 7.67 $x10^{8}$ Nm^{-2} while the value was 1.31 $x10^{9}$ Nm^{-2} with vertical excitation at 1.0 ms^{-2} r.m.s.

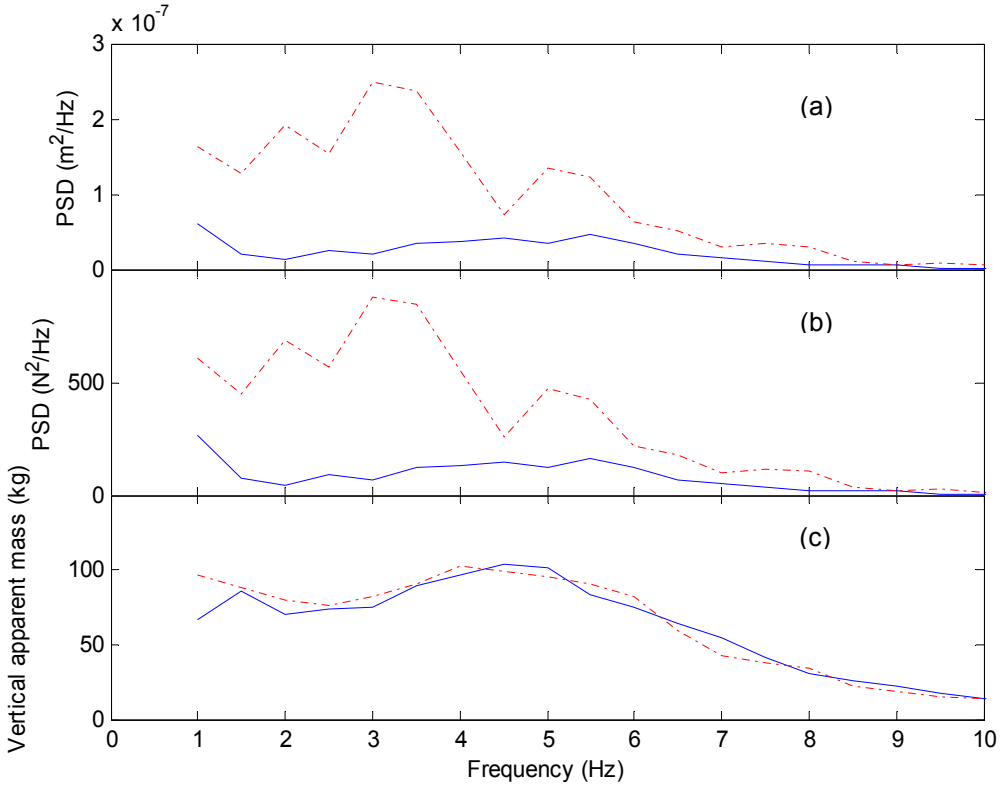

Figure 8.7 Calculated dynamic response with nonlinear tissue property: (a) compressive deformation of the tissue beneath the ischial tuberosities; (b) vertical force on the seat; (c) vertical apparent mass. ——, vertical excitation at 0.5 ms^{-2} r.m.s.; —.—, vertical excitation at 1.0 ms^{-2} r.m.s.

8.7 Discussion

8.7.1 Necessary complexity of a linear finite element model

The torso in the present model was simplified to be a single rigid body without spinal structure. This was because the deformation of the spine and the spinal forces were not of interest in this study. The bony structure in the pelvis and the thighs was less detailed than in some previous models (e.g., Pankoke *et al.*, 2008) but it was sufficient to predict the location where maximum pressure occurred and the approximate pressure at this location.

The force at the feet was less than at the seat (consistent with the findings of Nawayseh and Griffin, 2004) and by using the same excitation at both locations it was possible to take into account the effect of the footrest on the dynamic response at the seat (as suggested in Fairley and Griffin, 1989).

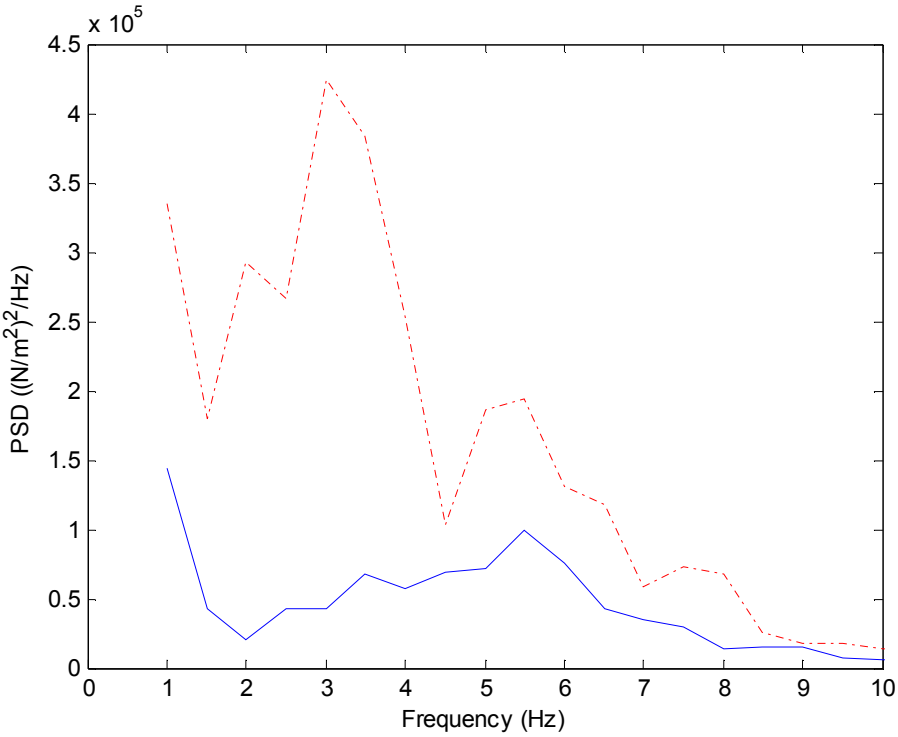

Figure 8.8 The power spectral density of the maximum pressure on the occupant-seat interface: ——, vertical excitation at 0.5 ms-2 r.m.s.; —.—, vertical excitation at 1.0 ms-2 r.m.s.

For this preliminary development of a simplified model, elastic material properties were used for the deformable tissues of the pelvis and the thighs and optimised to simulate the dynamic response at a typical vibration magnitude (i.e., 0.5 ms-2 r.m.s.). The linear material provided a sensible response as shown in Figures 8.2, 8.3 and 8.4. The model was further developed to include nonlinear characteristics of the soft tissue so as to improve predictions and take into account the nonlinear response observed in measurements of the apparent mass and pressure distribution of the body (Figures 8.7 and 8.8).

8.7.2 Vibration modes

The first mode of the model at 1.30 Hz involved pitch of the pelvis and might correspond to the first mode in the fore-and-aft apparent mass around 1 Hz as observed in experimental studies (e.g., Fairley and Griffin,1990; Nawayseh and Griffin, 2005). The second mode involved roll of the pelvis and lateral shear deformation of the pelvis tissue,

and had a natural frequency close to the second mode of the lateral apparent mass around 1.5 to 3 Hz (e.g., Fairley and Griffin, 1990).

The fourth mode at 5.46 Hz and the fifth mode at 6.83 Hz both involved pitch motion of the pelvis (and the upper-body), consistent with experimental data (Sandover and Dupuis, 1987). Up-and-down motions of the legs and feet were evident in both the fifth and the sixth modes, the natural frequencies of which were similar to the resonance frequency of the vertical apparent mass and the fore-and-aft cross-axis apparent mass at the feet (Nawayseh and Griffin, 2003).

8.7.3 Predicted nonlinearity in the vertical apparent mass

The use of the bi-linear material model for tissue appeared effective in reflecting the resonance shift in the vertical apparent mass associated with increasing vibration magnitude. These material properties are also suitable for low density foam, consistent with the assumption that the stiffness of the tissue beneath the pelvis and thighs was dependent on deformation when exposed to vibration (Figure 8.6). When the vibration magnitude was low (e.g., 0.5 ms^{-2} r.m.s.), the vertical force was relatively small. The compression of the tissue might be mainly within the scope of the first line in Figure 8.6. When the vibration magnitude was increased (e.g., to 1.0 ms^{-2} r.m.s.), the vertical force increased. It is possible that the vertical compression was mainly within the scope of the second line in Figure 8.6. However, the increases in the deformation (Figure 8.7(a)) and the force (Figure 8.7(b) were not proportional (Table 8.1). The r.m.s. value of the dynamic force at the seat increased by 70.6 % while the axial deformation increased by 85.6%. The disproportionate change in the force and deformation is reflected by a reduced stiffness shown by the second line of Figure 8.6.

Table 8.1 The r.m.s. value of the vertical force, the compressive deformation and the dynamic stiffness calculated with excitation at 0.5 $m.s^{-2}$ r.m.s. and 1.0 ms^{-2} r.m.s.

Excitation (ms^{-2} r.m.s.)	F_z (N r.m.s.)	Δl_z (m r.m.s.)	$DF_z=F_z.l^{-1}$ (Nm^{-1}r.m.s.)
0.5	30.64	5.02 x10^{-4}	6.10 x10^{4}
1.0	52.27	9.31 x10^{-4}	5.61 x10^{4}

8.8 Conclusions

A simplified finite element model of the seated human body has been developed and calibrated using the vertical apparent mass and the fore-and-aft cross-axis apparent mass measured on a seat. The calculated vertical inline apparent mass, the fore-and-aft cross-axis apparent mass, the vertical transmissibility to the lumbar spine, and the fore-and-aft cross-axis transmissibility to the lumbar spine had first resonance frequencies and peak modulus similar to the experimental data. The peak value of the predicted pressure distribution on a seat was observed at the similar region to the experiment results and the peak magnitudes had the same order.

The fourth mode of the model at 5.6 Hz, consisting of pitch motion of the upper-body and the pelvis, with axial and shear deformation of buttocks tissues, may be related to the principal resonance of the vertical apparent mass and transmissibility.

A decrease in the resonance frequency of the vertical apparent mass with increasing vibration magnitude was achieved by using a simplified bi-linear material model for the deformable tissue. It was shown that increasing magnitude of the vertical vibration introduced an increase in the axial deformation of the tissue by a larger percentage than the increase in the vertical force.

CHAPTER 9: GENERAL DISCUSSION

9.1 Introduction

The previous chapters have considered how resonances in the apparent mass and transmissibility, and their association, are affected by vibration magnitude (Chapters 4 and 5), coupling of dual-axis excitation (Chapters 4 and 5), and sitting posture (Chapter 6). The necessary characteristics of a model with a capacity to predict the inline and cross-axis apparent mass, transmissibility and the nonlinearity with single-axis and dual-axis excitation have been examined in Chapter 3 (a multi-body model with vertical excitation), Chapter 7 (a multi-body model with combined vertical and fore-and-aft excitation), and Chapter 8 (a finite element model simulating the nonlinearity). The main findings of these chapters are summarised and discussed in sections below.

9.2 Nonlinearity associated with vibration magnitude

The biodynamic responses associated with vertical excitation and fore-and-aft excitation both exhibited nonlinearity with changes in the magnitude of excitation (Chapters 4 and 5). The human tissue (or tissue from porcine, etc.) has also been reported to be load-dependent and exhibit nonlinear force-deflection behaviour (e.g., Zheng *et al*. 1999; Oomens *et al.*, 2003; Snedeker *et al*., 2005; Saraf *et al*., 2006; Loocke *et al*., 2008; Makhsous *et al*., 2008). It is therefore speculated that the nonlinear dynamic response occurs with a change in the mechanical properties of the human body.

With single-axis excitation, the experimental apparent mass and transmissibility calculated with the cross-spectral density, CSD method, are very close to the values calculated with the power spectra density, PSD method (Appendix F; also Nawayseh and Griffin, 2003; Nawayseh and Griffin, 2005). It is therefore assumed that the human body is linear within one vibration stimulus.

The mechanical properties are supposed to be changed only when the vibration characteristic is changed. If the human body which is exposed to single-axis excitation and represented by a single degree-of-freedom model (Figure 9.1), the natural frequency, the peak modulus and the phase lag of the transfer function (only the transmissibility is discussed in Section 9.2 as an example) are expressed by the Equations (9.1-9.3).

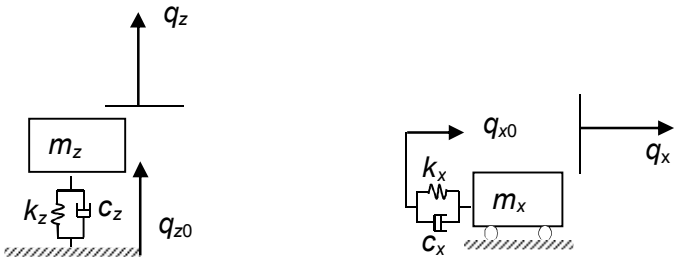

(a) (b)

Figure 9.1 Single degree-of-freedom model with: (a) vertical excitation; (b) fore-and-aft excitation.

$$\omega_{dz} = \omega_{nz}\sqrt{1-\frac{c_z^{\,2}}{m_z^{\,2}}} = \sqrt{\frac{k_z}{m_z}}\sqrt{1-\frac{c_z^{\,2}}{m_z^{\,2}}},$$

Or

$$\omega_{dx} = \omega_{nx}\sqrt{1-\frac{c_x^{\,2}}{m_x^{\,2}}} = \sqrt{\frac{k_x}{m_x}}\sqrt{1-\frac{c_x^{\,2}}{m_x^{\,2}}}. \tag{9.1}$$

$$\left|\frac{q_z}{q_{z0}}\right| = \frac{1}{\sqrt{\left(k_z-\omega^2 m_z\right)^2+\left(\omega^2 c_z\right)^2}},$$

Or

$$\left|\frac{q_x}{q_{x0}}\right| = \frac{1}{\sqrt{\left(k_x-\omega^2 m_x\right)^2+\left(\omega^2 c_x\right)^2}}. \tag{9.2}$$

$$\phi_z = -\tan^{-1}\frac{\omega c_z}{k_z-\omega^2 m_z},$$

Or

$$\phi_x = -\tan^{-1}\frac{\omega c_x}{k_x-\omega^2 m_x}. \tag{9.3}$$

Assuming that mass is constant when changing the magnitude of excitation (i.e., q_{z0} or q_{x0}), an increase in the phase lag could be attributed to either a decrease in the stiffness or an increase in the damping factor (Equation (9.3)).

With increasing magnitude of vertical excitation (i.e., q_{z0}), the increase in the phase lag (Chapter 4; ϕ_z in Equation (9.3)) and the decrease in the natural frequency (i.e., ω_{dz} in Equation (9.1)) were possibly caused by a decrease in the stiffness (i.e., k_z). An increase in the damping could also contribute to an increased phase and a decreased natural frequency, as suggested by Equations (9.1) and (9.3). However, an increase in the damping (i.e., c_z) would introduce a smaller peak modulus (the maximum value of $\left|\frac{q_z}{q_{z0}}\right|$, as suggested by Equation (9.2)). This is not consistent with the experimental finding that there is no significant reduction in peak modulus in the vertical transmissibility (see Chapter 4). It is therefore difficult to tell whether the damping factor was increased or not with the frequency resolution of 0.25 Hz employed in the study.

With increasing magnitude of fore-and-aft excitation, the decrease in the modulus of the first peak in the fore-and-aft transmissibility (Chapter 5; the maximum value of $\left|\frac{q_x}{q_{x0}}\right|$ in Equation (9.2)) and the increase in the phase lag (Chapter 5; ϕ_x in Equation (9.3)) were possibly caused by an increase in the damping (i.e., c_x). A decrease in the stiffness (i.e., k_x) could also increase the phase lag (Equation (9.3)), it will reduce the natural frequency (i.e., ω_{dx} in Equation (9.1)). However, the first resonance frequency in the fore-and-aft transmissibility was not observed to be changed significantly (see Chapter 5). It is possible that the stiffness was not decreased, or the decrease was not large enough to introduce a detectable deviation in the first resonance frequency in the fore-and-aft transmissibility with the frequency resolution of 0.25 Hz employed.

9.3 Nonlinearity associated with coupling effect

The uncorrelated signals in the experiments in this thesis means the coherency of two inputs is very close to 0 (about 10% in the experiment) so the transfer functions could be calculated with the CSD method which is normally used for single-axis case (Bendat and Piersol, 1986). However, with dual-axis excitation, the vertical excitation still produces response in the fore-and-aft direction, e.g., fore-aft force, similar to single-axis vertical excitation producing fore-aft force. Similarly, with dual-axis excitation, the fore-aft excitation still produces response in the vertical direction, e.g., vertical force, similar to single-axis fore-aft excitation producing vertical force. This is the coupling effect. Although the vertical force generated by the fore-aft excitation is small compared to the

vertical force generated with vertical excitation, it does contribute to the change in the vertical apparent mass with dual-axis excitation, compared to that with single-axis vertical excitation.

9.3.1 Effect of *x*-axis excitation on the *z*-axis response

With increasing magnitude of the additional fore-and-aft excitation from 0 to 1.0 ms^{-2} r.m.s. while the magnitude of vertical excitation was held constant at 1.0 ms^{-2} r.m.s., the resonance frequency in both the vertical apparent mass and the vertical body transmissibility decreased (Chapter 4).

A Poisson ratio of around 0.45 has been reported for human body tissue (e.g., Li *et al*., 2001). The observed coupling influence of *x*-axis excitation on the z-axis response is suggested to be associated with the Poisson's effect of human body tissue. When the human body is exposed to vertical excitation, the buttock tissue is compressed (Figure 9.2(b)) relative to the initial shape (Figure 9.2(a)). With dual-axis excitation, the compression of the tissue is not only caused by the vertical excitation but also caused by the fore-and-aft excitation (Figure 9.2(c)). It is possible that the total deflection of tissue with dual-axis excitation is greater than that with single-axis excitation. It seems that the dynamic stiffness was reduced due to the increased compression when there was combined vertical and fore-and-aft excitation during the experiment, analogous to the softening effect associated with increasing the magnitude of the single-axis vertical excitation.

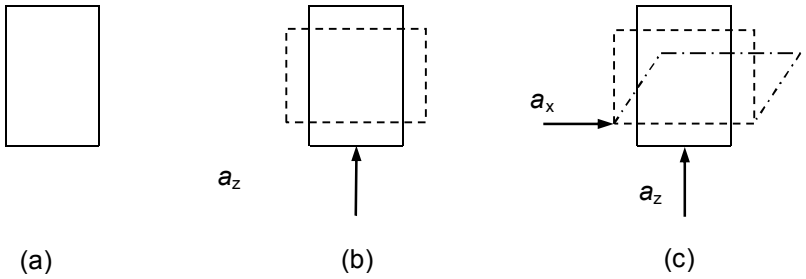

Figure 9.2 Deformation of buttocks tissue with single-axis vertical vibration and combined vertical and fore-and-aft vibration: (a) ——, initial position of buttocks tissue; (b) - - -, buttocks tissue position undergoing vertical vibration; (c) —.—, buttocks tissue position exposed to vertical vibration and fore-and-aft vibration.

9.3.2 Effect of *z*-axis excitation on the *x*-axis response

With increasing magnitude of the additional vertical excitation from 0 to 1.0 ms^{-2} r.m.s. while the magnitude of fore-and-aft excitation was held constant at 1.0 ms^{-2} r.m.s., the

modulus of the first peak in the fore-and-aft apparent mass and fore-and-aft body transmissibility decreased (Chapter 5).

The observed coupling influence of z-axis excitation on the *x*-axis response is also suggested to be associated with the Poisson's effect of human body tissue. When the human body is exposed to single-axis fore-and-aft excitation, the buttock tissue is compressed in the fore-and-aft direction (Figure 9.3(b)) relative to the initial shape (Figure 9.3(a)). With dual-axis excitation, the fore-and-aft deformation of the tissue is not only caused by the fore-and-aft vertical excitation but also caused by the vertical excitation (Figure 9.3(c)).

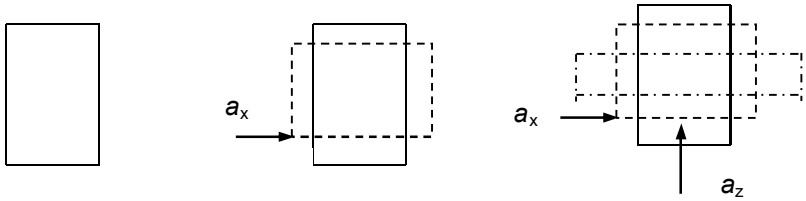

Figure 9.3 Deformation of buttocks tissue with single-axis fore-and-aft excitation and combined fore-and-aft and vertical excitation: (a) ——, initial position of buttocks tissue; (b) - - -, buttocks tissue position undergoing fore-and-aft excitation; (c) —.—, buttocks tissue position exposed to fore-and-aft excitation and vertical excitation.

The total fore-and-aft deflection of tissue with dual-axis excitation may be expected to be greater than that with single-axis excitation alone. It seems that the fore-and-aft damping is increased due to the increased compression when there was combined fore-and-aft and vertical excitation. This was similar to increased damping with increased magnitude of single-axis fore-and-aft excitation, which was discussed in Section 9.2. It is still difficult to determine whether the stiffness of the tissue is changed or not. This is because the first resonance frequency in the fore-and-aft apparent mass was not significantly change with the addition of the vertical excitation when using a frequency resolution of 0.25 Hz.

It is noted that the discussion in Sections 9.2 and 9.3 was conducted that assuming that the tissue was the main source of the nonlinearity that was observed in both the apparent mass and the transmissibility (as suggested by Huang, 2008).

9.4 The necessary complexity of human body models

The complexity of a mathematical model is determined by the application of the model. The human body models proposed in this research are designed to represent both the inline and the cross-axis dynamic response at the seat surface and over the body

surface with single-axis and dual-axis excitation. The models were also required to have the capability to reflect an effect of posture change on the biodynamic response.

The intent of predicting cross-axis response at the seat surface requires including rotational connections between the segments that represent thighs and pelvis. Therefore, the pelvis and thighs are simulated with rigid bodies, each of which is able to move vertically, horizontally, and rotate in the sagittal plane. Similarly, predictions of the biodynamic responses in the vertical and fore-and-aft directions over the spine require rotational joints between the elements which represent the thoracic spine and the lumbar spine. Simulating body segments with rigid bodies not only enables the model to represent a coupling effect between *z*-axis excitation and *x*-axis excitation but also makes it possible to model different sitting postures. For example, by varying the initial inclination of the spine and pelvis, the model is able to take into account the effect of a change in the geometry on the apparent mass when changing from a normal posture to an erect posture or to a slouched posture. By adding sets of springs and dampers to the thoracic spine or lumbar spine, the model could be used to investigate the effect of backrest contact on the apparent mass at the seat. By varying the inclination of the thighs and legs, the model is able to simulate the effect of the height of a footrest (e.g., Nawayseh and Griffin, 2004) and the distance between the footrest and the seat (e.g., Toward and Griffin, 2010).

Rotational connections are essential for a human body model with dual-axis excitation to be able to model the coupling effect caused by the two perpendicular excitations. With the additional fore-and-aft input applied to the horizontal sets of springs and dampers at the seat-occupant interface, the multi-body model that worked for vertical excitation also worked for dual-axis excitation. However, some of the key parameters (e.g., the vertical stiffness of the pelvis tissue, the vertical damping of the tissue beneath the thighs) for the single-axis model were changed to match the transfer functions obtained with dual-axis model. This is because the resonance shift with dual-axis excitation is assumed to be due to the nonlinearity of the tissue beneath the pelvis and thigh, i.e., the coupling effect as discussed in Section 9.3.2.

Although the upper torso, arms and legs are rigid bodies and contain no bony structure, a finite element human model with the buttocks represented by flexible bodies containing a simple pelvis bony structure has the ability to provide sensible predictions of the apparent mass at the seat, transmissibility to the spine, and pressure distribution at the

seat. It seems unwise to develop a complicated human body model with detailed muscle and skeleton structure for the cervical spine, thoracic spine, lumbar spine, and pelvis for the applications in this study.

It is noted that the modelling places an emphasis on reflecting the primary resonance, especially the resonance frequencies of the transfer functions (i.e., apparent mass and transmissibility to the spine). The second mode is much less profound and little is unknown about how it is generated. Features that are needed to reflect the second modes are worth identifying in the future studies.

CHAPTER 10: GENERAL CONCLUSIONS

10.1 General conclusions

With vertical excitation, the resonance frequency in the vertical inline and fore-and-aft cross-axis apparent mass and transmissibility to the spine and pelvis (and the pitch motion of pelvis) reduce with the addition of the fore-and-aft excitation, similar to the softening effect caused by increasing magnitude of single-axis vertical excitation. The primary resonance frequency in the dynamic response associated with vertical excitation in the normal upright posture is less than that in an erect posture but greater than that in a slouched posture. The association between the apparent mass and the transmissibility varies with the magnitude of vertical vibration and the addition of fore-and-aft excitation.

With fore-and-aft excitation, the peak modulus in the fore-and-aft inline and vertical cross-axis apparent mass and transmissibility to the spine and pelvis (and the pitch motion of pelvis) reduce with increasing magnitude of fore-and-aft excitation and the addition of vertical excitation. The first resonance frequency in the apparent mass and the transmissibility to the pelvis and the spine with fore-and-aft excitation is greater in an erect posture than in a normal upright posture and in a slouched posture. The association between the apparent mass and the transmissibility also vary with the magnitude of fore-and-aft excitation and the addition of vertical excitation.

A seven degree-of-freedom multi-body model can provide sensible predictions of the first resonance frequencies and the associated peak modulus in the vertical apparent mass and transmissibility and fore-and-aft cross-axis apparent mass and transmissibility with dual-axis excitation (Chapter 7). The predictions were achieved by reducing the axial stiffness of the pelvis tissue and the axial damping of the thigh tissue in the model with single-axis vertical excitation (as developed in Chapter 3). The multi-body model (Chapter 7) suggests that the first mode in the fore-and-aft apparent mass and the fore-and-aft transmissibility to the upper body (see Chapter 5) is caused by fore-and-aft movement of the upper body which arises from pitch motion of the pelvis. The model also indicates that the second mode is associated with fore-and-aft movement of the upper body caused by shear deformation of pelvis tissue.

With the deformable bodies (i.e., pelvis tissue and thigh tissue) simulated with nonlinear low density foam material model (Chapter 8), a finite element model is able to reflect the resonance shift seen in the vertical apparent mass with increasing vibration magnitude.

The model suggests that increasing magnitudes of vertical vibration increase the axial deformation of the tissue by a greater percentage than the increase in vertical force. With this characteristic, a finite element model predicts a reduction in the resonance frequencies of the vertical apparent mass, the axial deformation of the pelvis tissue, and the maximum pressure at the seat-occupant interface when increasing magnitude of vertical excitation.

10.2 Recommendations

The finite element model in this research used low density foam material to represent the nonlinear force-deflection properties of the pelvis tissue. As the tensile and shear behaviour of this type of material is governed by Young's modulus, it has no capability to model the nonlinear cross-axis response (i.e., the nonlinearity seen in the fore-and-aft cross-axis apparent mass). Other nonlinear material types may be investigated for modelling both the nonlinear inline and the nonlinear cross-axis dynamic response (e.g., Mooney-Rivlin-Rubber in the LS-DYNA platform). Whatever nonlinear material is used, it will be difficult to determine the parameters needed to quantify the nonlinear performance of the material. The samples used in the measurements of tissue properties reported so far are either from cadavers or animals. Tests with living humans are not conducted with dynamic excitation and how well they reflect human tissue properties in dynamic vibration conditions has yet to be identified.

Previous studies, and the research in this thesis, show that sitting posture can change the resonance frequency and the peak modulus in the apparent mass and transmissibility (Chapter 6). The multi-body models (in Chapter 3 and Chapter 7), and the finite element model (in Chapter 8), were calibrated only with experimental data in the normal upright posture. It is desirable to fit the models to the dynamic responses in other postures (e.g., an erect posture and a slouched posture) by adjusting the inclination, stiffness, and damping of the body segments. Identifying how the model parameters vary with sitting posture will advance understanding of the effect of posture on the dynamic response of the body.

Nonlinear changes in pressure distribution with changes in vertical excitation have been measured experimentally (e.g., Wu *et al.*, 1998; Hinz *et al.*, 2006b) and calculated using the finite element model in Chapter 8. It is desirable to measure the pressure distribution over the seat-occupant interface with dual-axis excitation with various combinations of vibration magnitudes. It may be hypothesised that the pressure distribution with

orthogonal excitation will exhibit similar nonlinearity to that with increasing magnitude of single-axis excitation.

APPENDICES

The appendices below show the information of:

Appendix A shows the solutions of equations of motion of the human body model developed in Chapter 3.

Appendix B shows the apparent mass and transmissibility associated with vertical excitation at vibration magnitudes which have not been shown in Chapter 4.

Appendix C shows the apparent mass and transmissibility associated with fore-and-aft excitation at vibration magnitudes which have not been shown in Chapter 5.

Appendix D shows the apparent mass and transmissibility in a normal upright posture, an erect posture and a slouched posture at different vibration magnitudes (Chapter 6).

Appendix E shows the Simulink model of the equations of motion of seated human body exposed to dual-axis excitation (Chapter 7). The corresponding coefficients are also appended.

Appendix F compares the apparent mass and transmissibility calculated with CSD method and PSD method.

APPENDIX A: SOLUTIONS OF THE EQUATIONS OF MOTION OF SINGLE-AXIS HUMAN BODY MODEL (Chapter 3)

Assuming that $q_1 = x_1, q_2 = z_1, q_3 = \theta_1, q_4 = \theta_2, q_5 = \theta_3, q_6 = \theta_4, q_7 = \theta_5$, Q_1, Q_2, Q_3, Q_4, Q_5, Q_6, Q_7 are Laplace transform of q_1, q_2, q_3, q_4, q_5, q_6 and q_7 respectively.

θ_{10}=150º; θ_{20}=100º; θ_{30}=50º; θ_{40}=350º; θ_{50}=280º;

sin10=sin(θ_{10}); sin20=sin(θ_{20}); sin30=sin(θ_{30}); sin40=sin(θ_{40}); sin50=sin(θ_{50});

cos10=cos(θ_{10}); cos20=cos(θ_{20}); cos30=cos(θ_{30}); cos40=cos(θ_{40}); cos50=cos(θ_{50});

cos1020=cos(θ_{10}-θ_{20}); cos1030=cos(θ_{10}-θ_{30}); cos2030=cos(θ_{20}-θ_{30}); cos4050=cos(θ_{40}-θ_{50});

s=2pi$f$;

Q_1=Q;

Q_2=-(H_1+H_2Q);

Q_3=(D_2H_1+D_2H_2Q-D_1Q);

Q_4=(F_1Q-F_2H_1-F_2H_2Q);

Q_5=(G_2H_1-G_1Q+G_2H_2Q);

Q_6=(B_3H_1+B_3H_2Q-B_1-B_2Q);

Q_7=(E_2H_1+E_2H_2Q+E_3-E_1Q);

Where,

Q=(-$A_{13}D_2H_1$+$A_{14}F_2H_1$-$A_{15}G_2H_1$+$A_{16}B_1$-$A_{16}B_3H_1$-$A_{17}E_2H_1$-$A_{17}E_3$)/(A_{11}-$A_{13}D_1$-$A_{13}D_2H_2$+$A_{14}F_1$-$A_{14}H_2$-$A_{15}G_1$+$A_{15}G_2H_2$-$A_{16}B_2$+$A_{16}B_3H_2$-$A_{17}E_1$+$A_{17}E_2H_2$);

B_1=A_{68}/($A_{66}A_{77}$-$A_{76}A_{67}$);

B_2=($A_{61}A_{77}$-$A_{71}A_{67}$)/($A_{66}A_{77}$-$A_{76}A_{67}$);

B_3=($A_{62}A_{77}$-$A_{72}A_{67}$)/($A_{66}A_{77}$-$A_{76}A_{67}$);

C_1=($A_{41}A_{55}$-$A_{45}A_{51}$)/($A_{44}A_{55}$-$A_{45}A_{54}$);

C_2=($A_{42}A_{55}$-$A_{45}A_{52}$)/($A_{44}A_{55}$-$A_{45}A_{54}$);

C_3=($A_{43}A_{55}$-$A_{45}A_{53}$)/($A_{44}A_{55}$-$A_{45}A_{54}$);

D_1=($A_{31}A_{55}$-$A_{35}A_{51}$-$A_{34}C_1$+$A_{35}A_{54}C_1$)/($A_{33}A_{55}$-$A_{34}C_3$-$A_{35}A_{53}$+$A_{35}A_{54}C_3$);

$D_2=(A_{32}A_{55}-A_{35}A_{52}-A_{34}C_2+A_{35}A_{54}C_2)/(A_{33}A_{55}-A_{34}C_3-A_{35}A_{53}+A_{35}A_{54}C_3)$;

$E_1=(A_{71}-A_{76}B_2)/A_{77}$;

$E_2=(A_{72}-A_{76}B_3)$;

$E_3=A_{76}B_1/A_{77}$;

$F_1=C_3D_1-C_1$;

$F_2=C_3D_2-C_2$;

$G_1=(A_{51}-A_{53}D_1+A_{54}F_1)/A_{55}$;

$G_2=(A_{52}-A_{53}D_2+A_{54}F_2)/A_{55}$;

$H_1=A_{28}/(A_{22}-A_{23}D_2+A_{24}F_2-A_{25}G_2-A_{26}B_3-A_{27}E_2)$;

$H_2=(A_{24}F_1-A_{23}D_1-A_{25}G_1-A_{26}B_2-A_{27}E_1)/(A_{22}-A_{23}D_2+A_{24}F_2-A_{25}G_2-A_{26}B_3-A_{27}E_2)$;

$A_{11}= k_{1x}+m_1s^2+m_2s^2+k_{4x}+c_{1x}s+m_3s^2+m_4s^2+m_5s^2+c_{4x}s$;

$A_{13}= m_2s^2l_1\sin10+m_3s^2l_1\sin10+m_1s^2r_1\sin10$;

$A_{14}= m_3s^2l_2\sin20+m_2s^2r_2\sin20$;

$A_{15}=m_3s^2r_3\sin30$;

$A_{16}= m_5s^2l_4\sin40-m_4s^2r_4\sin40-k_{4x}r_{c4}\sin40-c_{4x}sr_{c4}\sin40$;

$A_{17}= m_5s^2r_5\sin50$;

$A_{22}= m_1s^2+m_2s^2+k_{4z}+m_3s^2+c_{1z}s+m_4s^2+m_5s^2+k_{1z}+c_{4z}s$;

$A_{23}=-m_3s^2l_1\cos10-m_1s^2r_1\cos10-m_2s^2l_1\cos10$;

$A_{24}= -m_3s^2l_2\cos20-m_2s^2r_2\cos20$;

$A_{25}= -m_3s^2r_3\cos30$;

$A_{26}= c_{4z}sr_{c4}\cos40+k_{4z}r_{c4}\cos40+m_4s^2r_4\cos40+m_5s^2l_4\cos40$;

$A_{27}= m_5s^2r_5\cos50$;

$A_{28}= -c_{4z}s-k_{1z}-k_{4z}-c_{1z}s$;

$A_{31}= m_2s^2l_1\sin10+m_3s^2l_1\sin10+m_1s^2r_1\sin10$;

$A_{32}= -m_3s^2l_1\cos10-m_2s^2l_1\cos10-m_1s^2r_1\cos10$;

$A_{33}= I_1s^2+m_2s^2l_1^2+m_3s^2l_1^2+k_{t1}+c_{t1}s+k_{t2}+c_{t2}s$;

$A_{34}= m_2 s^2 r_2 l_1 \cos 1020 + m_3 s^2 l_2 l_1 \cos 1020 - k_{t2} - c_{t2} s;$

$A_{35}= m_3 s^2 r_3 l_1 \cos 1030;$

$A_{41}= m_2 s^2 l_1 \sin 10 + m_3 s^2 l_1 \sin 10 + m_1 s^2 r_1 \sin 10;$

$A_{42}= -m_2 s^2 r_2 \cos 20 - m_3 s^2 l_2 \cos 20;$

$A_{43}= m_3 s^2 l_2 l_1 \cos 1020 + m_2 s^2 r_2 l_1 \cos 1020 - k_{t2} - c_{t2} s;$

$A_{44}= c_{t2} s + l_2 s^2 + m_3 s^2 l_2^2 + m_2 s^2 r_1^2 + k_{t2} + k_{t3} + c_{t3} s;$

$A_{45}= m_3 s^2 r_3 l_2 \cos 2030 - k_{t3} - c_{t3} s;$

$A_{51}= m_3 s^2 r_3 \sin 30;$

$A_{52}= -m_3 s^2 r_3 \cos 20;$

$A_{53}= l_3 s^2 + m_3 s^2 r_3 l_1 \cos 1030;$

$A_{54}= m_3 s^2 r_3 l_2 \cos 2030 - k_{t3} - c_{t3} s;$

$A_{55}= m_3 s^2 r_3^2 + k_{t3} + c_{t3} s;$

$A_{61}= m_5 s^2 l_4 \sin 40 - c_{4x} s r_{c4} \sin 40 - k_{4x} r_{c4} \sin 40 + k_{t1} + m_4 s^2 r_4 \sin 40 + c_{t2} s;$

$A_{62}= k_{4z} r_{c4} s \cos 40 + k_{4z} r_{c4} \cos 40 - m_5 s^2 l_4 \cos 40 - m_4 s^2 r_4 \cos 40;$

$A_{66}= l_4 s^2 + c_{t1} s + m_5 s^2 l_4^2 + k_{4x} r_{c4}^2 (\sin 40)^2 + m_4 s^2 r_{c4}^2 + k_{4z} r_{c4}^2 (\cos 40)^2 + c_{4z} r_{c4}^2 s (\cos 40)^2 + c_{4x} s r_{c4}^2 (\sin 40)^2 + k_{t1} + k_{t4} + c_{t4} s;$

$A_{67}= m_5 s^2 r_5 l_4 \cos 4050 + k_{t4} + c_{t4} s$

$A_{68}= -k_{4z} r_{c4} s \cos 40 - k_{4z} r_{c4} \cos 40;$

$A_{71}= m_5 s^2 r_5 \sin 50;$

$A_{72}= m_5 s^2 r_5 \cos 50;$

$A_{76}= m_5 s^2 r_5 l_4 \cos 4050;$

$A_{77}= l_5 s^2 + m_5 s^2 r_5^2 + k_{t4} + c_{t4} s.$

APPENDIX B: TRANSMISSIBILITY ASSOCIATED WITH VERTICAL VIBRATION (Chapter 4)

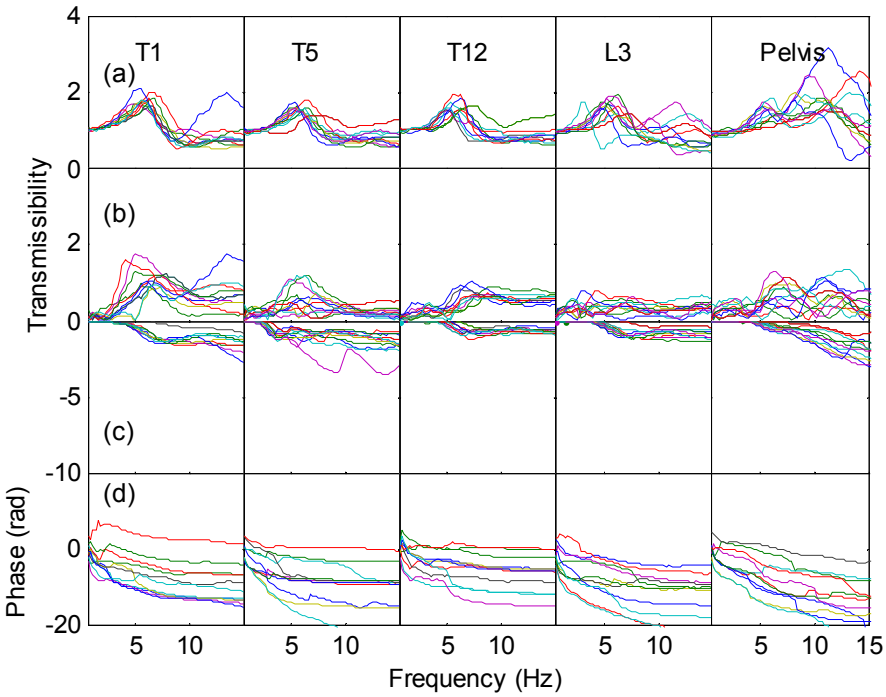

Figure B.1 Modulus and phase of individual transmissibility from vertical seat motion to upper body motion of 12 subjects with vertical vibration at 0.25 ms^{-2} r.m.s.: (a) the vertical transmissibility and phase; (b) the fore-and-aft cross-axis transmissibility and phase.

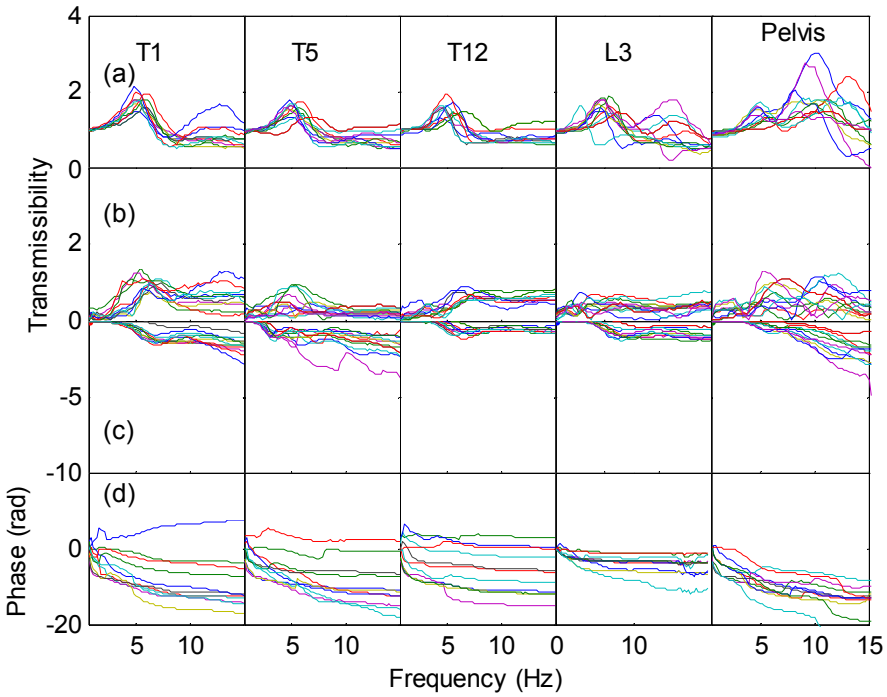

Figure B.2 Modulus and phase of individual transmissibility from vertical seat motion to upper body motion of 12 subjects with vertical vibration at 0.5 ms^{-2} r.m.s.: (a) the vertical transmissibility and phase; (b) the fore-and-aft cross-axis transmissibility and phase.

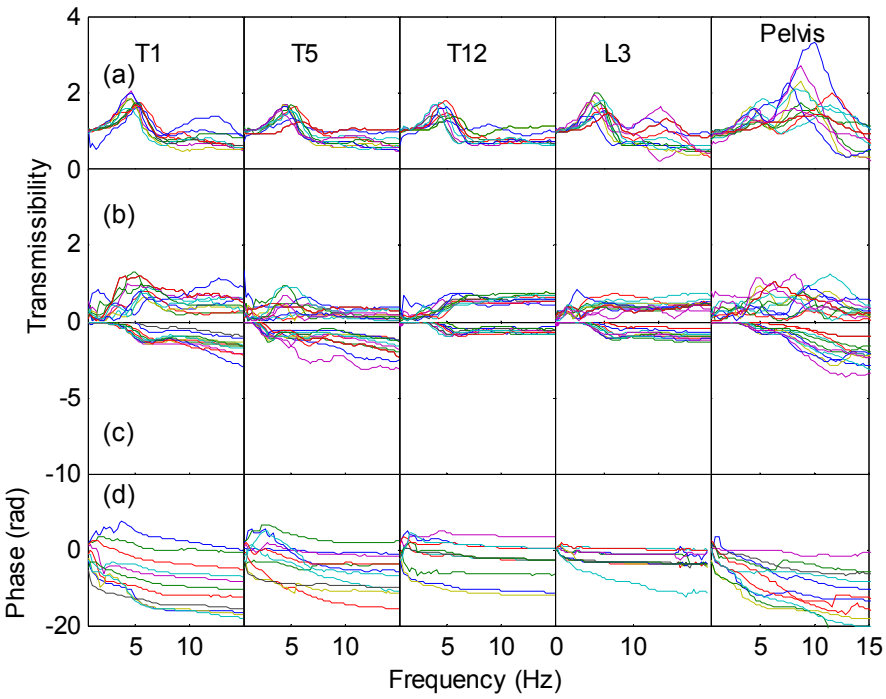

Figure B.3 Modulus and phase of individual transmissibility from vertical seat motion to upper body motion of 12 subjects with 1.0 ms^{-2} r.m.s. vertical vibration and 0.25 ms^{-2} r.m.s. fore-and-aft vibration: (a) the vertical transmissibility and phase; (b) the fore-and-aft cross-axis transmissibility and phase.

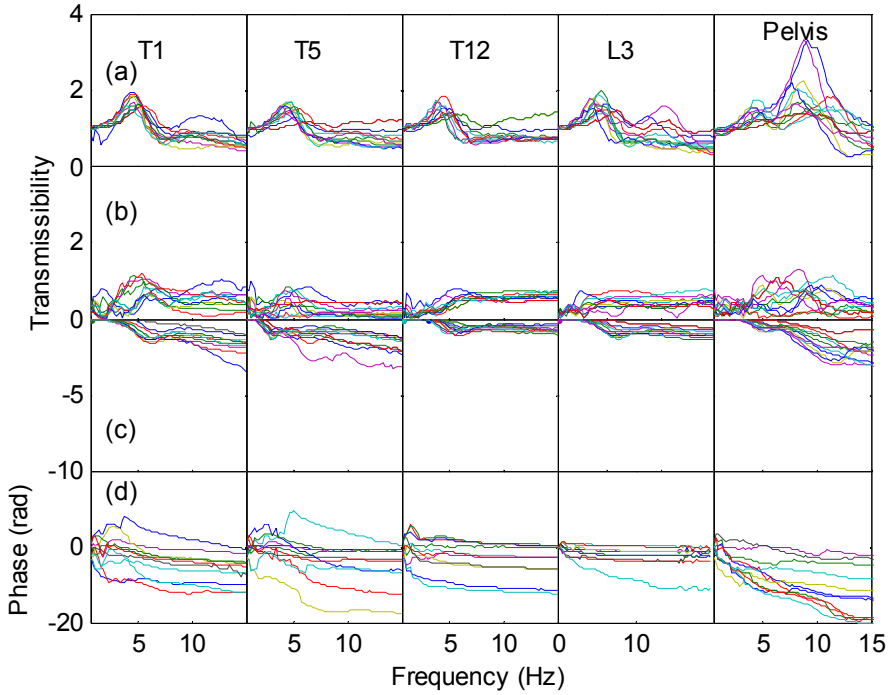

Figure B.4 Modulus and phase of individual transmissibility from vertical seat motion to upper body motion of 12 subjects with 1.0 ms^{-2} r.m.s. vertical vibration and 0.5 ms^{-2} r.m.s. fore-and-aft vibration: (a) the vertical transmissibility and phase; (b) the fore-and-aft cross-axis transmissibility and phase.

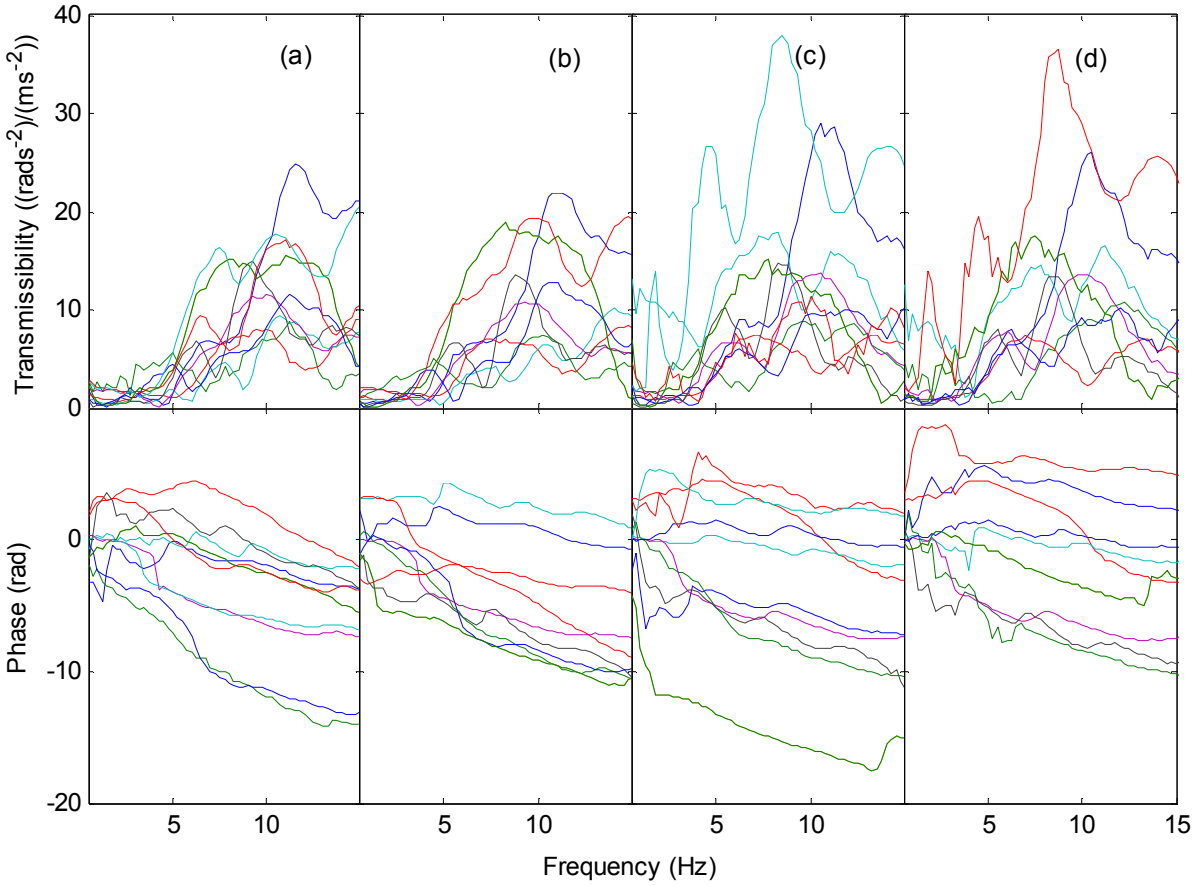

Figure B.5 Individual transmissibility from vertical seat motion to pitch of the pelvis of 12 subjects: (a) pitch transmissibility with single-axis vertical vibration at 0.25 ms^{-2} r.m.s.; (b) pitch transmissibility with single-axis vertical vibration at 0.5 ms^{-2} r.m.s.; (c) pitch transmissibility with 1.0 ms^{-2} r.m.s. vertical vibration and 0.25 ms^{-2} r.m.s. fore-and-aft vibration; (d) pitch transmissibility with 1.0 ms^{-2} r.m.s. vertical vibration and 0.5 ms^{-2} r.m.s. fore-and-aft vibration.

APPENDIX C: TRANSMISSIBILITY ASSOCIATED WITH FORE-AND-AFT VIBRATION (Chapter 5)

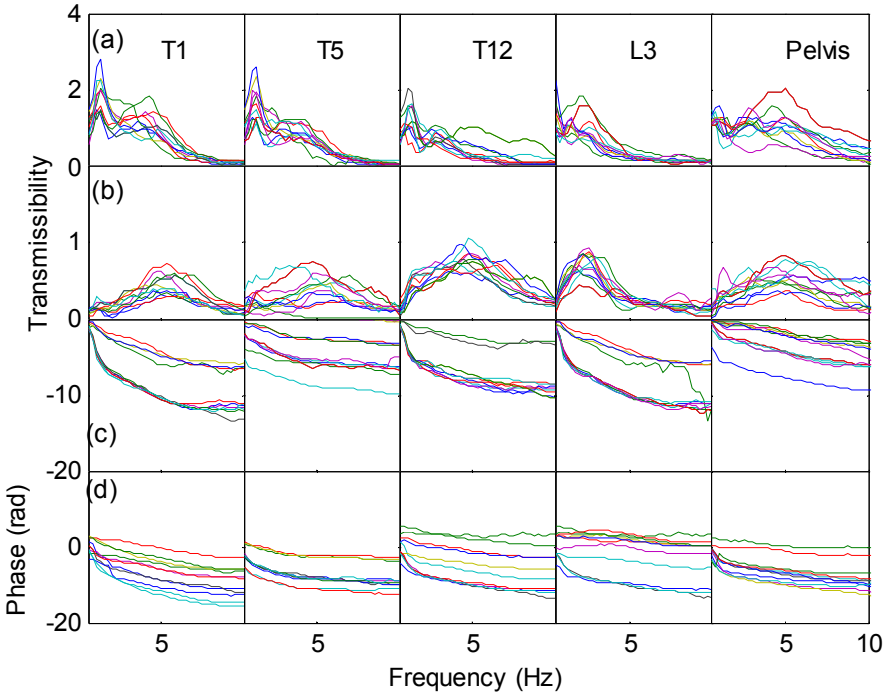

Figure C.1 Modulus and phase of individual transmissibility from fore-and-aft seat motion to upper body motion of 12 subjects with fore-and-aft vibration at 0.25 ms^{-2} r.m.s.: (a) the fore-and-aft transmissibility and phase; (b) the vertical cross-axis transmissibility and phase.

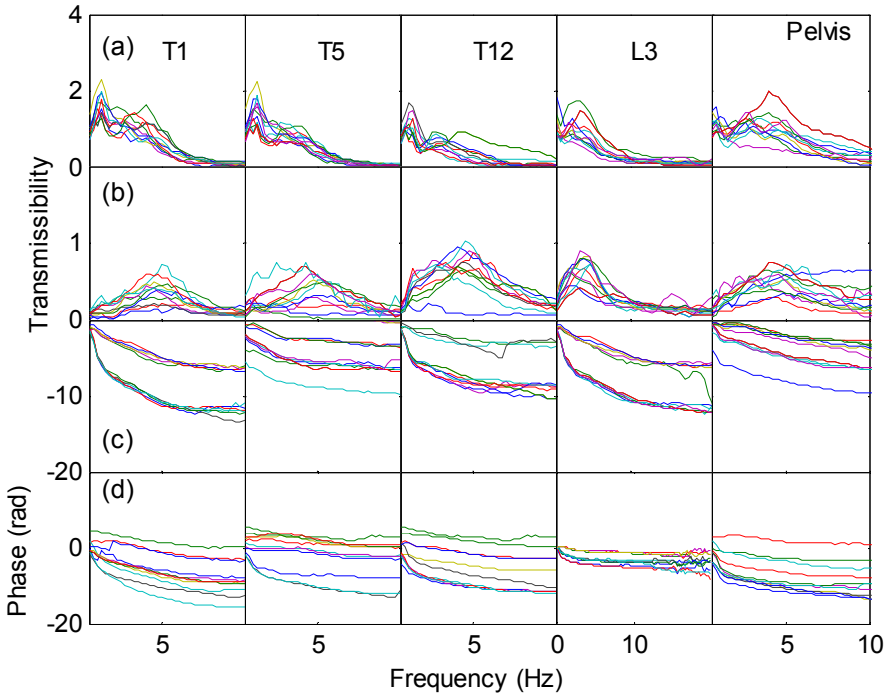

Figure C.2 Modulus and phase of individual transmissibility from fore-and-aft seat motion to upper body motion of 12 subjects with fore-and-aft vibration at 0.5 ms^{-2} r.m.s.: (a) the fore-and-aft transmissibility and phase; (b) the vertical cross-axis transmissibility and phase.

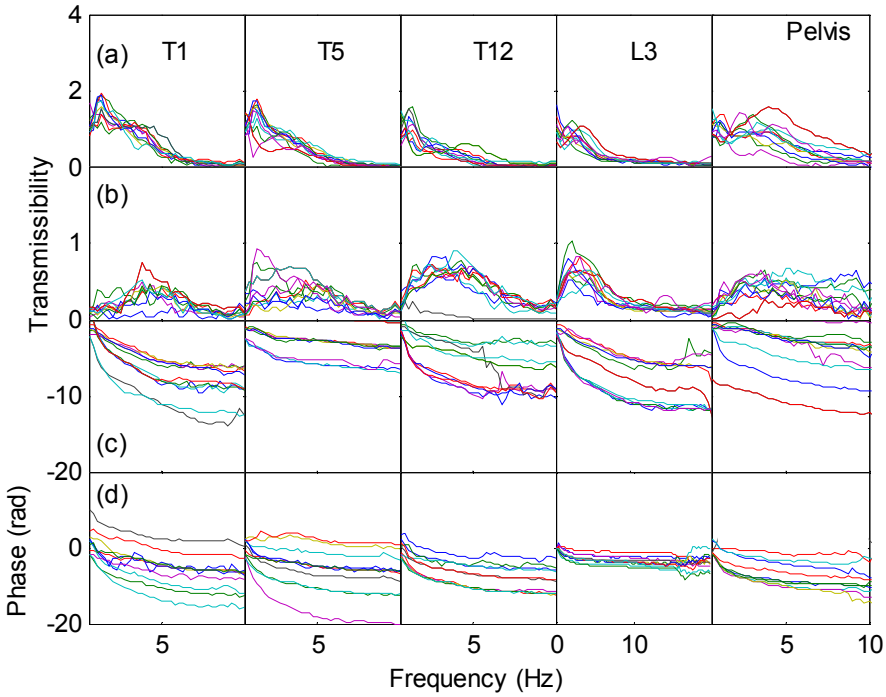

Figure C.3 Modulus and phase of individual transmissibility from fore-and-aft seat motion to upper body motion of 12 subjects with 1.0 ms^{-2} r.m.s. fore-and-aft vibration and 0.25 ms^{-2} r.m.s. vertical vibration: (a) the fore-and-aft transmissibility and phase; (b) the vertical cross-axis transmissibility and phase.

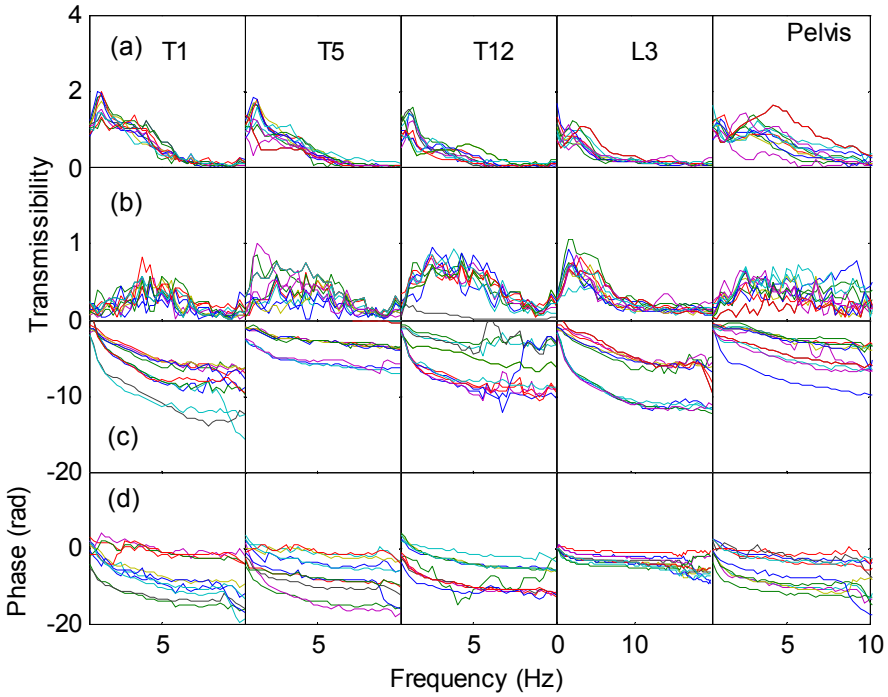

Figure C.4 Modulus and phase of individual transmissibility from fore-and-aft seat motion to upper body motion of 12 subjects with 1.0 ms^{-2} r.m.s. fore-and-aft vibration and 0.5 ms^{-2} r.m.s. vertical vibration: (a) the fore-and-aft transmissibility and phase; (b) the vertical cross-axis transmissibility and phase.

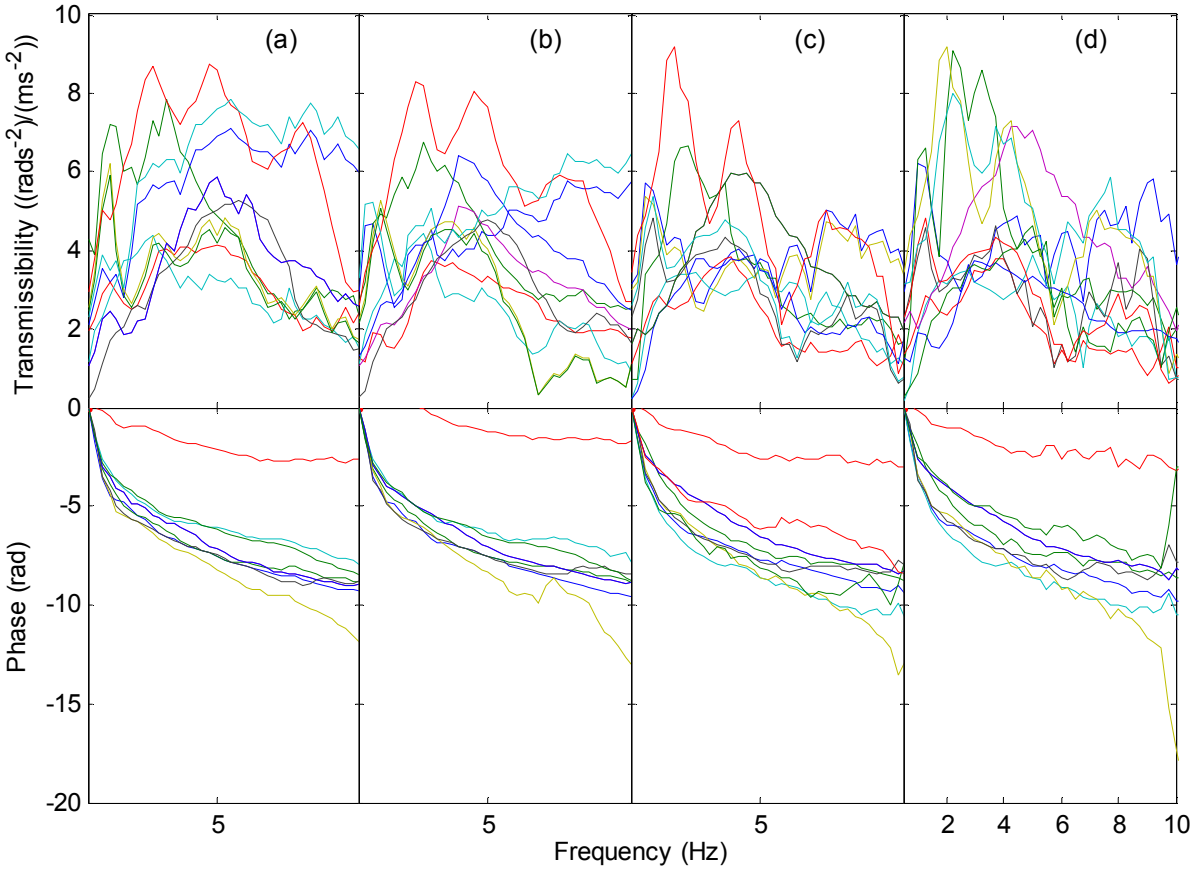

Figure C.5 Individual transmissibility from fore-and-aft seat motion to pitch of the pelvis of 12 subjects: (a) pitch transmissibility with single-axis fore-and-aft vibration at 0.25 ms^{-2} r.m.s.; (b) pitch transmissibility with single-axis fore-and-aft vibration at 0.5 ms^{-2} r.m.s.; (c) pitch transmissibility with 1.0 ms^{-2} r.m.s. fore-and-aft vibration and 0.25 ms^{-2} r.m.s. vertical vibration; (d) pitch transmissibility with 1.0 ms^{-2} r.m.s. fore-and-aft vibration and 0.5 ms^{-2} r.m.s. vertical vibration.

APPENDIX D: APPARENT MASS AND TRANSMISSIBILITY IN DIFFERENT POSTURES (Chapter 6)

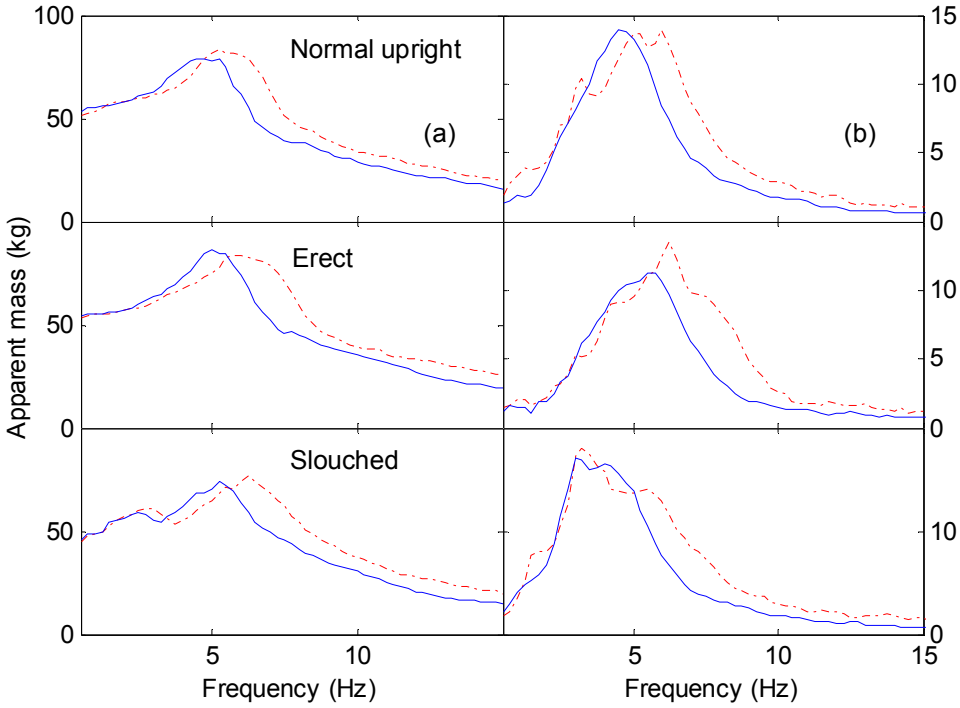

Figure D.1 Effect of vibration magnitude on vertical apparent mass, (a) and fore-and-aft cross-axis apparent mass, (b) in three sitting postures: —.—, a_z =0.25 ms^{-2} r.m.s.; - - -, a_z =1.0 ms^{-2} r.m.s. (medians of 12 subjects).

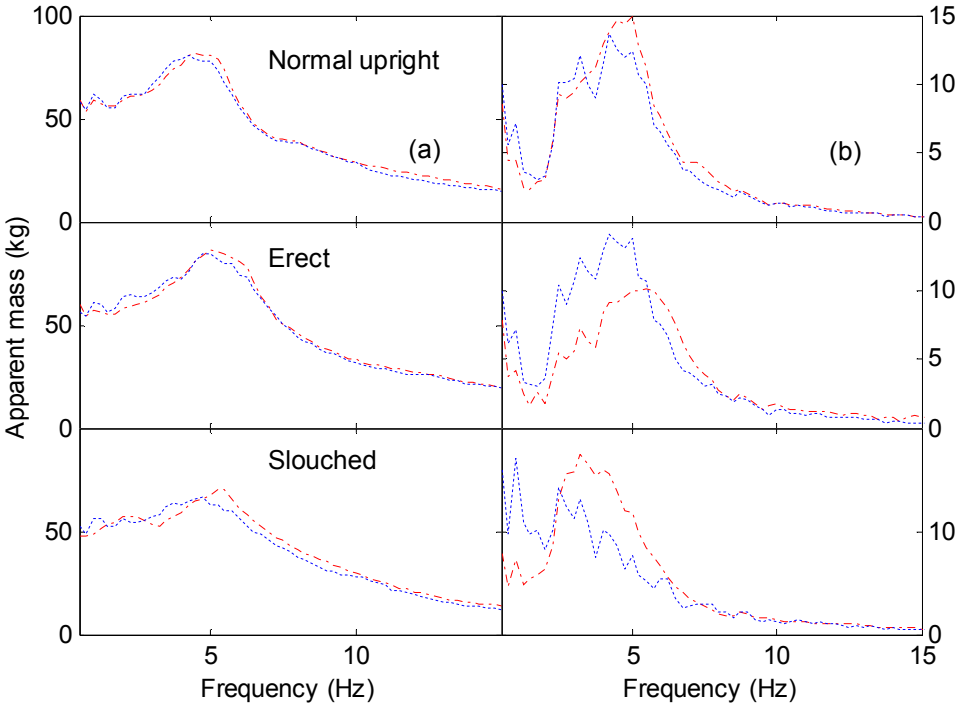

Figure D.2 Effect of vibration magnitude on vertical apparent mass, (a) and fore-and-aft cross-axis apparent mass, (b) in three sitting postures: —.—, a_z =1.0 ms^{-2} r.m.s., a_x =0.25 ms^{-2} r.m.s.; - - -, a_z =1.0 ms^{-2} r.m.s., a_x =1.0 ms^{-2} r.m.s. (medians of 12 subjects).

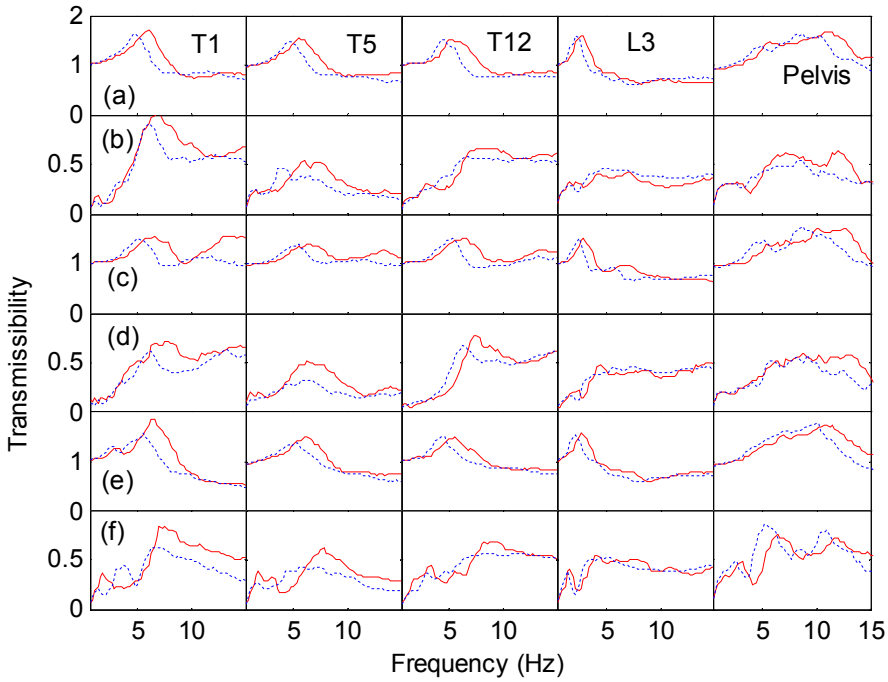

Figure D.3 Effect of vibration magnitude on the transmissibility from vertical seat motion to each measurement location in three sitting postures: effect of vibration magnitudes. ——, a_z=0.25 ms^{-2} r.m.s.; - - -, a_z=1.0 ms^{-2} r.m.s. (a) vertical transmissibility in the normal upright posture; (b) fore-and-aft cross-axis transmissibility in the normal upright posture; (c) vertical transmissibility in the erect posture; (d) fore-and-aft cross-axis transmissibility in the erect posture; (e) vertical transmissibility in the slouched posture; (f) fore-and-aft cross-axis transmissibility in the slouched posture.(medians of 12 subjects).

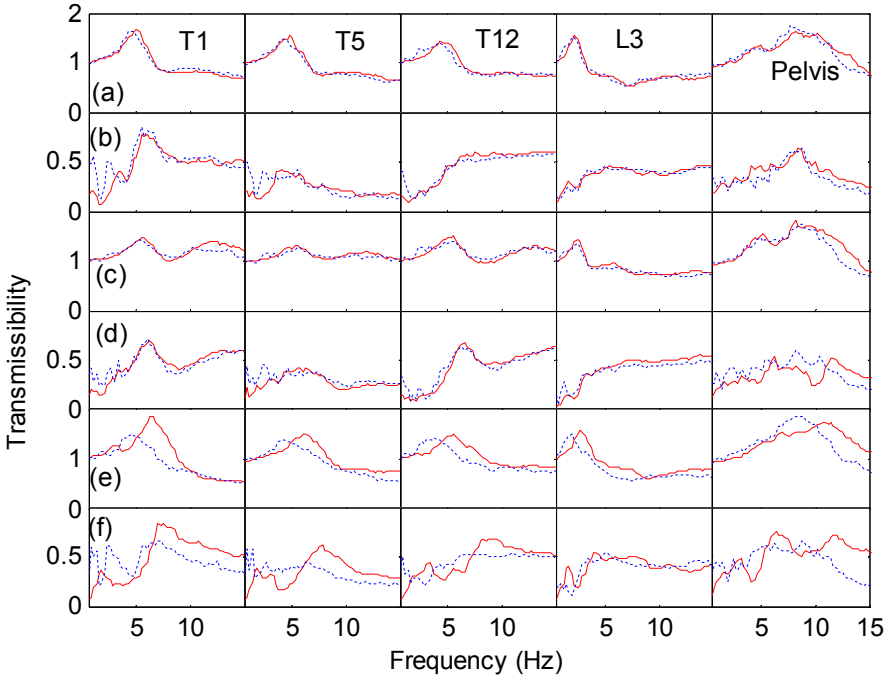

Figure D.4 Effect of vibration magnitude on the transmissibility from vertical seat motion to each measurement location in three sitting postures: effect of vibration magnitudes. ——, a_z =1.0, a_x=0.25 ms^{-2} r.m.s.; - - -, a_z =1.0, a_x =1.0 ms^{-2} r.m.s. (a) vertical transmissibility in the normal upright posture; (b) fore-and-aft cross-axis transmissibility in the normal upright posture; (c) vertical transmissibility in the erect posture; (d) fore-and-aft cross-axis transmissibility in the erect posture; (e) vertical transmissibility in the slouched posture; (f) fore-and-aft cross-axis transmissibility in the slouched posture (medians of 12 subjects).

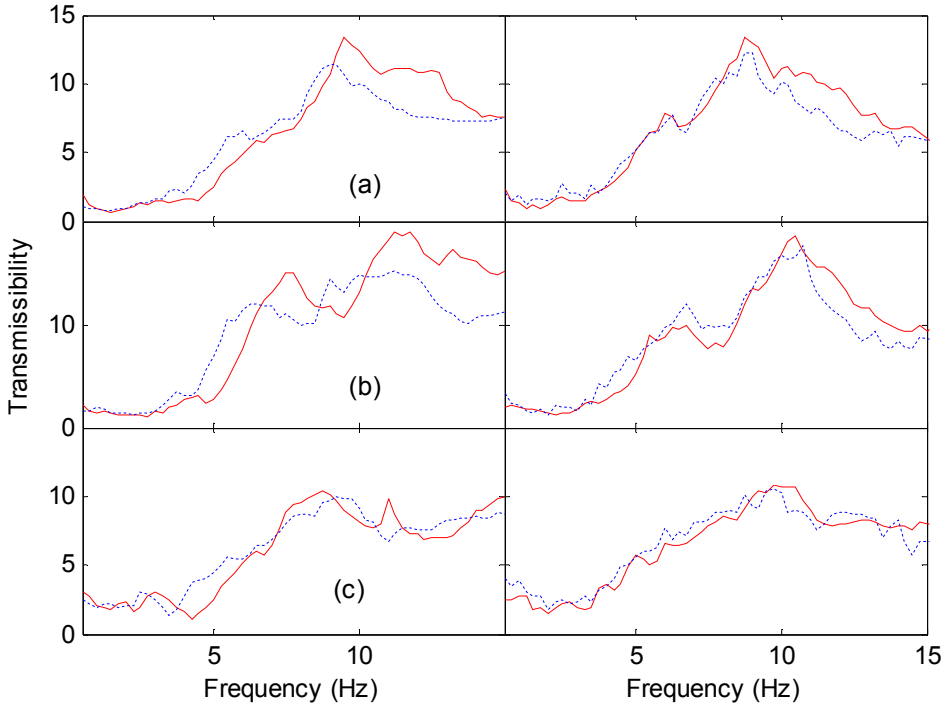

Figure D.5 transmissibility from vertical seat motion to pelvis pitch motion of 12 subjects in three sitting postures: effect of vibration magnitudes. Left column, single-axis vertical vibration, ——, a_z=0.25 ms^{-2} r.m.s.; - - -, a_z=1.0 ms^{-2} r.m.s.; right column, dual-axis vibration, ——, a_z =1.0, a_x=0.25 ms^{-2} r.m.s.; - - -, a_z =1.0, a_x =1.0 ms^{-2} r.m.s. (a) pitch transmissibility in the normal upright posture; (b) pitch transmissibility in the erect posture; (c) pitch transmissibility in the slouched posture.

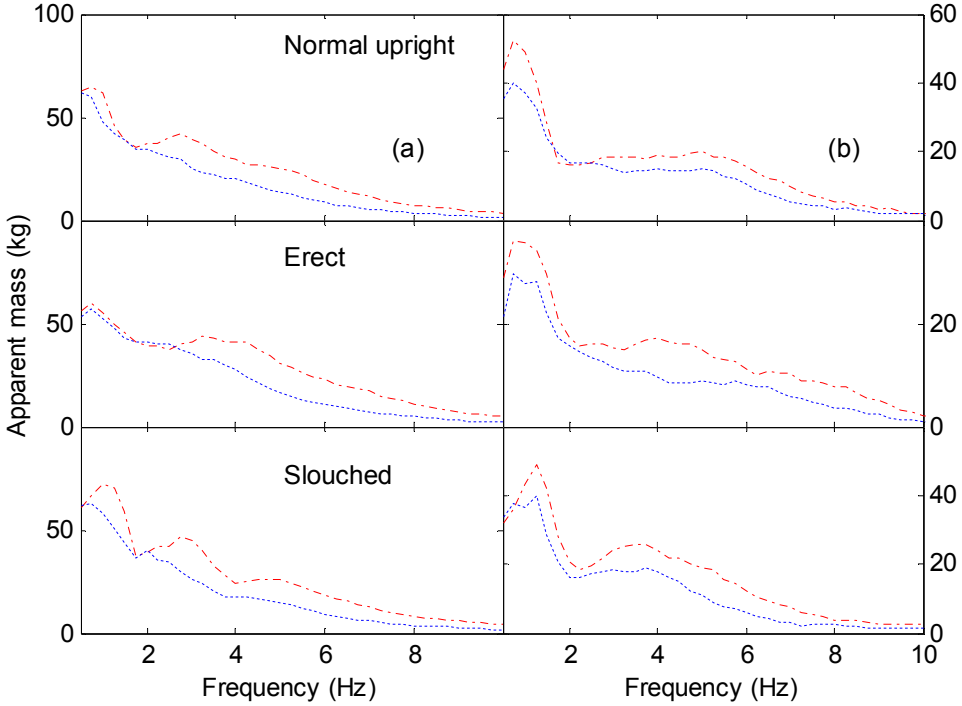

Figure D.6 Effect of vibration magnitude on fore-and-aft apparent mass, (a) and vertical cross-axis apparent mass, (b) in three sitting posture: —.—, a_x =0.25 ms^{-2} r.m.s.; - - -, a_x =1.0 ms^{-2} r.m.s. (medians of 12 subjects).

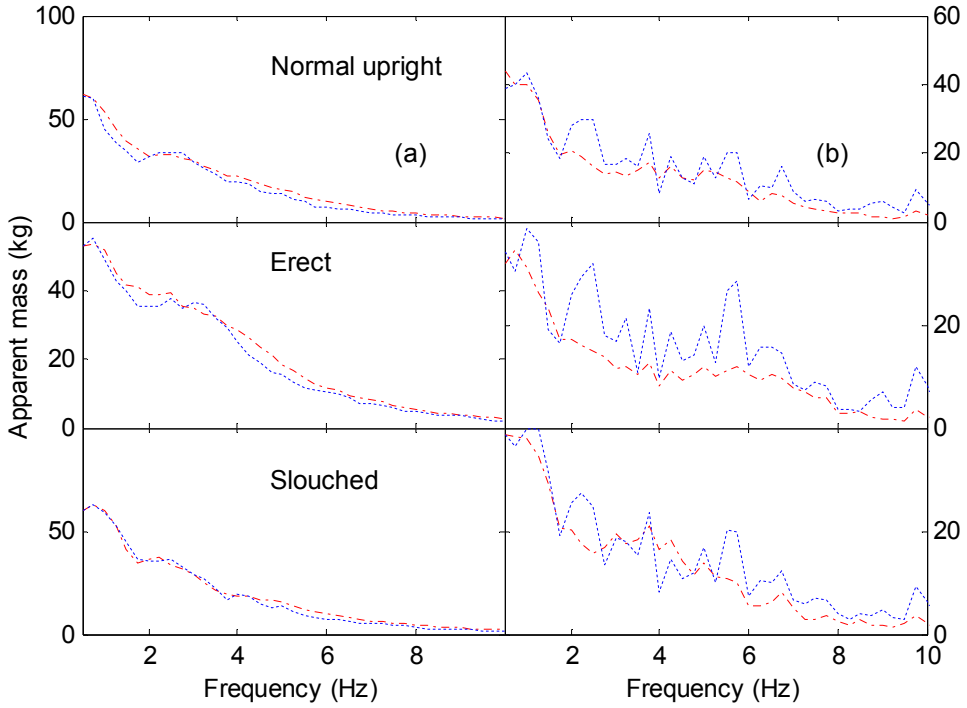

Figure D.7 Effect of vibration magnitude on fore-and-aft apparent mass, (a) and vertical cross-axis apparent mass, (b) in three sitting posture: —.—, a_x =1.0, a_z =0.25 ms^{-2} r.m.s.; - - -, a_x =1.0, a_z =1.0 ms^{-2} r.m.s. (medians of 12 subjects).

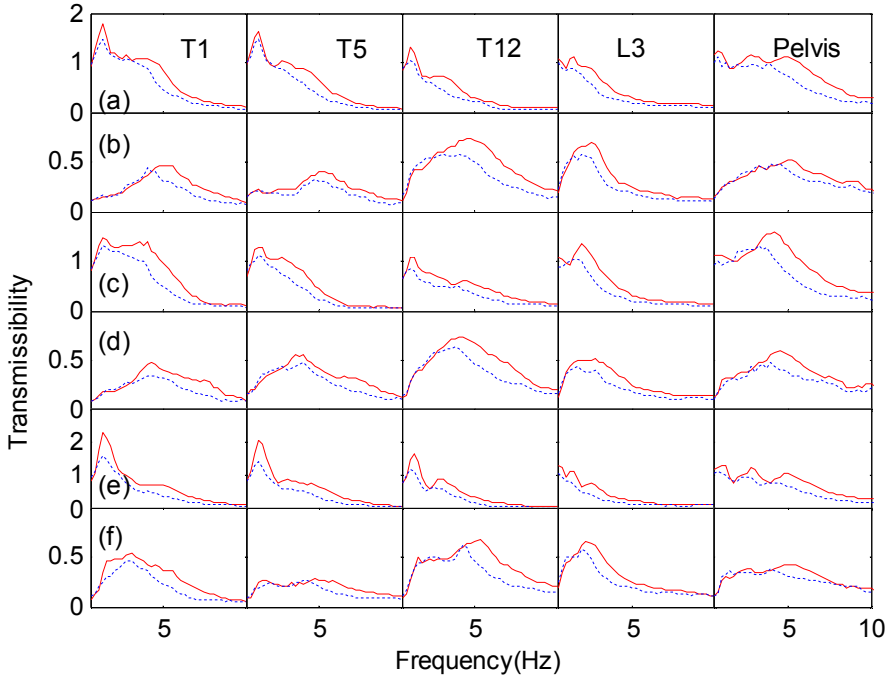

Figure D.8 Effect of vibration magnitude on the transmissibility from fore-and-aft seat motion to each measurement location in three sitting postures: effect of vibration magnitudes. ——, a_x=0.25 ms^{-2} r.m.s.; - - -, a_x=1.0 ms^{-2} r.m.s. (a) fore-and-aft transmissibility in the normal upright posture; (b) vertical cross-axis transmissibility in the normal upright posture; (c) fore-and-aft transmissibility in the erect posture; (d) vertical cross-axis transmissibility in the erect posture; (e) fore-and-aft transmissibility in the slouched posture; (f) vertical cross-axis transmissibility in the slouched posture (medians of 12 subjects).

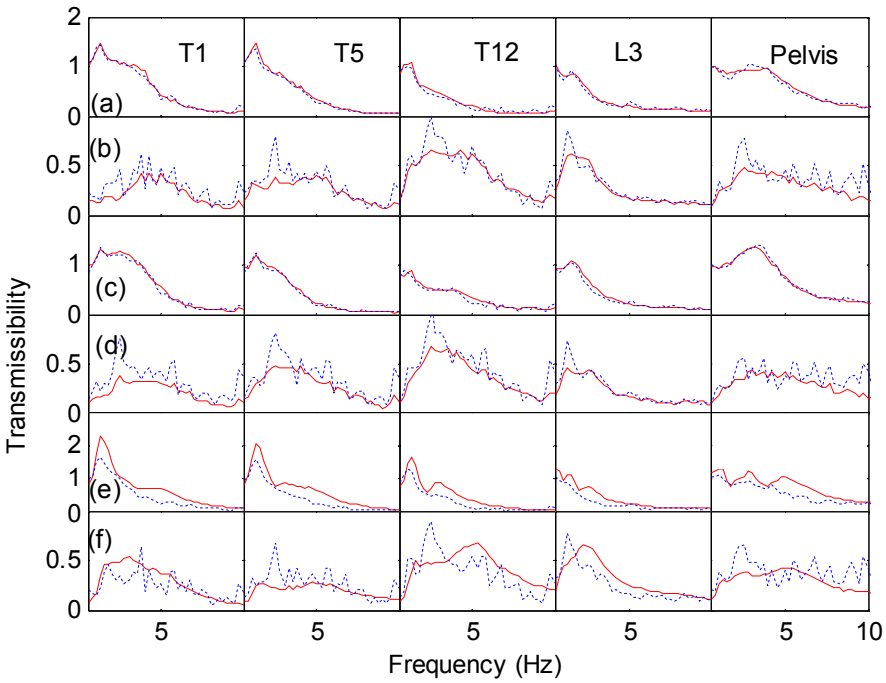

Figure D.9 Effect of vibration magnitude on the transmissibility from fore-and-aft seat motion to each measurement location in three sitting postures: effect of vibration magnitudes. ——, a_x =1.0, a_z=0.25 ms^{-2} r.m.s.; - - -, a_x =1.0, a_z =1.0 ms^{-2} r.m.s. (a) fore-and-aft transmissibility in the normal upright posture; (b) vertical cross-axis transmissibility in the normal upright posture; (c) fore-and-aft transmissibility in the erect posture; (d) vertical cross-axis transmissibility in the erect posture; (e) fore-and-aft transmissibility in the slouched posture; (f) vertical cross-axis transmissibility in the slouched posture (medians of 12 subjects).

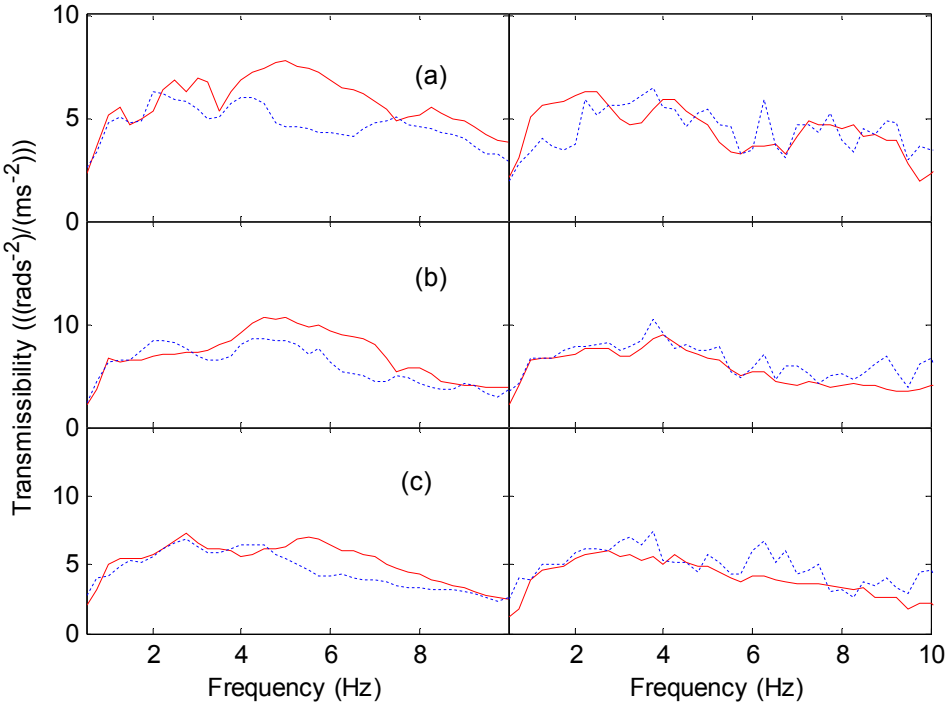

Figure D.10 transmissibility from fore-and-aft seat motion to pelvis pitch motion of 12 subjects in three sitting postures: effect of vibration magnitudes. Left column, single-axis fore-and-aft vibration, ——, a_x=0.25 ms^{-2} r.m.s.; - - -, a_x=1.0 ms^{-2} r.m.s.; right column, dual-axis vibration, ——, a_x =1.0, a_z=0.25 ms^{-2} r.m.s.; - - -, a_x =1.0, a_z =1.0 ms^{-2} r.m.s. (a) pitch transmissibility in the normal upright posture; (b) pitch transmissibility in the erect posture; (c) pitch transmissibility in the slouched posture.

APPENDIX E: THE SIMULINK MODEL OF THE HUMAN BODY AND THE COEFFICIENTS FOR EQUATIONS OF MOTION (Chapter 7)

Assuming that θ_{10}=150º; θ_{20}=100º; θ_{30}=50º; θ_{40}=350º; θ_{50}=280º;

sin10=sin(θ_{10}); sin20=sin(θ_{20}); sin30=sin(θ_{30}); sin40=sin(θ_{40}); sin50=sin(θ_{50});

cos10=cos(θ_{10}); cos20=cos(θ_{20}); cos30=cos(θ_{30}); cos40=cos(θ_{40}); cos50=cos(θ_{50});

cos1020=cos(θ_{10}-θ_{20}); cos1030=cos(θ_{10}-θ_{30}); cos2030=cos(θ_{20}-θ_{30}); cos4050=cos(θ_{40}-θ_{50});

$M_{11}=m_1+m_2+m_3+m_4+m_5$;

$M_{12}=0$;

$M_{13}=-(m_1r_1\sin10+m_2l_1\sin10+m_3l_1\sin10)$;

$M_{14}=-(m_2r_2\sin20+m_3l_2\sin20)$;

$M_{15}=-m_3r_3\sin30$;

$M_{16}=-(m_4r_4\sin40+m_5l_4\sin40)$;

$M_{17}=-m_5r_5\sin50$;

$K_{11}=k_{1x}+k_{4x}$;

$K_{12}=0$;

$K_{13}=0$;

$K_{14}=0$;

$K_{15}=0$;

$K_{16}=-k_{4x}r_{c4}\sin40$;

$K_{17}=0$;

$C_{11}=c_{1x}+c_{4x}$;

$C_{12}=0$;

$C_{13}=0$;

$C_{14}=0$;

$C_{15}=0$;

C_{16}=-$c_{4x}r_{c4}$sin40;

C_{17}=0;

M_{21}=0;

M_{22}= m_1+m_2+m_3+m_4+m_5;

M_{23}= $m_1r_1$cos10+ $m_2l_1$cos10+ $m_3l_1$cos10;

M_{24}= m_2 $r_2$cos20+ $m_3l_2$cos20;

M_{25}= m_3 $r_3$cos30;

M_{26}= m_4 $r_4$cos40+ m_5 $l_4$cos40;

M_{27}= m_5 $r_5$cos50;

K_{21}=0;

K_{22}=k_{1z}+k_{4z};

K_{23}=0;

K_{24}=0;

K_{25}=0;

K_{26}= k_{4z} r_{c4}cos40;

K_{27}=0;

C_{21}=0;

C_{22}= c_{1z}+c_{4z};

C_{23}=0;

C_{24}=0;

C_{25}=0;

C_{26}= c_{4z} r_{c4}cos40;

C_{27}=0;

M_{31}=-(m_1 $r_1$sin10+ m_2 $l_1$sin10+ m_3 $l_1$sin10);

M_{32}= $m_1r_1$cos10+ $m_2l_1$cos10+ $m_3l_1$cos10;

$M_{33}= m_1 r_1^2+ m_2 l_1^2+ m_3 l_1^2+ I_1;$

$M_{34}= m_2 l_1 r_2 \cos 1020+ m_3 l_1 l_2 \cos 1020;$

$M_{35}= m_3 l_1 r_3 \cos 1030;$

$M_{36}=0;$

$M_{37}=0;$

$K_{31}=0;$

$K_{32}=0;$

$K_{33}=k_{t1}+k_{t2};$

$K_{34}=-k_{t2};$

$K_{35}=0;$

$K_{36}=-k_{t1};$

$K_{37}=0;$

$C_{31}=0;$

$C_{32}=0;$

$C_{33}= c_{t1}+c_{t2};$

$C_{34}=-c_{t2};$

$C_{35}=0;$

$C_{36}=-c_{t1};$

$C_{37}=0;$

$M_{41}=-(m_2 r_2 \sin 20+m_3 l_2 \sin 20);$

$M_{42}= m_2 r_2 \cos 20+ m_3 l_2 \cos 20;$

$M_{43}= m_2 l_1 r_2 \cos 1020+ m_3 l_1 l_2 \cos 1020;$

$M_{44}= m_2 r_2^2+ m_3 l_1^2+ I_2;$

$M_{45}= m_3 l_2 r_3 \cos 2030;$

$M_{46}=0;$

$M_{47}=0;$

K_{41}=0;

K_{42}=0;

K_{43}=-k_{t2};

K_{44}= k_{t2}+ k_{t3};

K_{45}=-k_{t3};

K_{46}=0;

K_{47}=0;

C_{41}=0;

C_{42}=0;

C_{43}=-c_{t2};

C_{44}= c_{t2}+ c_{t3};

C_{45}=- c_{t3};

C_{46}=0;

C_{47}=0;

M_{51}=-$m_3 r_3$sin30;

M_{52}= m_3 $r_3$cos30;

M_{53}= m_3 $l_1 r_3$cos1030;

M_{54}= m_3 $l_2 r_3$cos2030;

M_{55}= $m_3 r_3^2$+I_3;

M_{56}=0;

M_{57}=0;

K_{51}=0;

K_{52}=0;

K_{53}=0;

K_{54}=-k_{t3};

K_{55}=k_{t3};

K_{56}=0;

K_{57}=0;

C_{51}=0;

C_{52}=0;

C53=0;

C_{54}=-c_{t3};

C_{55}=c_{t3};

C_{56}=0;

C_{57}=0;

M_{61}=-($m_4r_4$sin40+$m_5l_4$sin40);

M_{62}= $m_4r_4$cos40+ m_5 $l_4$cos40;

M_{63}=0;

M_{64}=0;

M_{65}=0;

M_{66}= $m_4r_4^2$+ $m_5l_4^2$+I_4;

M_{67}= m_5 l_4 $r_5$cos4050;

K_{61}=-$k_{4x}r_{c4}$sin40;

K_{62}= k_{4z} r_{c4}cos40;

K_{63}=-k_{t1};

K_{64}=0;

K_{65}=0;

K_{66}=k_{t4}+k_{t1}+$k_{4z}r_{c4}^2$;

K_{67}=- k_{t4};

C_{61}=- $c_{4x}r_{c4}$sin40;

C_{62}= $c_{4z}r_{c4}$cos40;

C_{63}=-c_{t1};

C_{64}=0;

C_{65}=0;

C_{66}= c_{t4}+c_{t1}+$c_{4z}{r_{c4}}^2$;

C_{67}=-c_{t4};

M_{71}=-$m_5 r_5$sin50;

M_{72}= m_5 $r_5$cos50;

M_{73}=0;

M_{74}=0;

M_{75}=0;

M_{76}= m_5 $l_4 r_5$cos4050;

M_{77}= $m_5{r_5}^2$+I_5;

K_{71}=0;

K_{72}=0;

K_{73}=0;

K_{74}=0;

K_{75}=0;

K_{76}=-k_{t4};

K_{77}=k_{t4};

C_{71}=0;

C_{72}=0;

C_{73}=0;

C_{74}=0;

C_{75}=0;

C_{76}=-c_{t4};

C_{77}=c_{t4}.

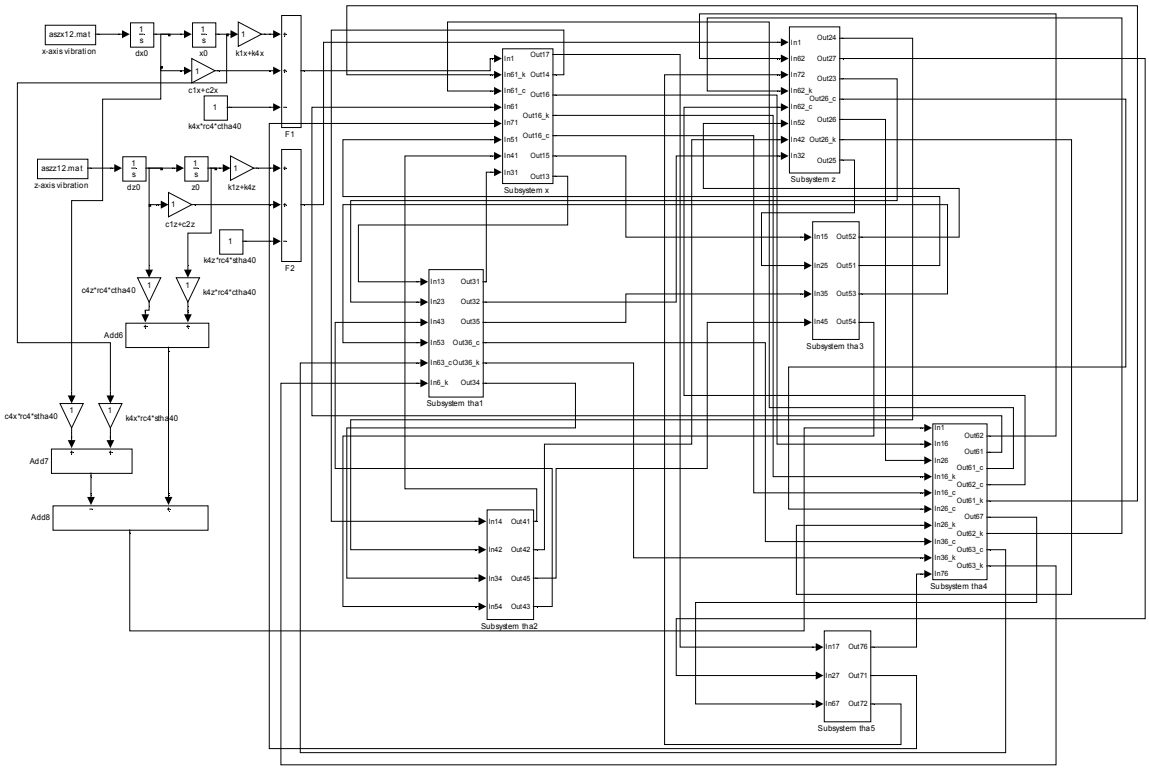

Figure E.1 The Simulink model of the of human body exposed to dual-axis excitation.

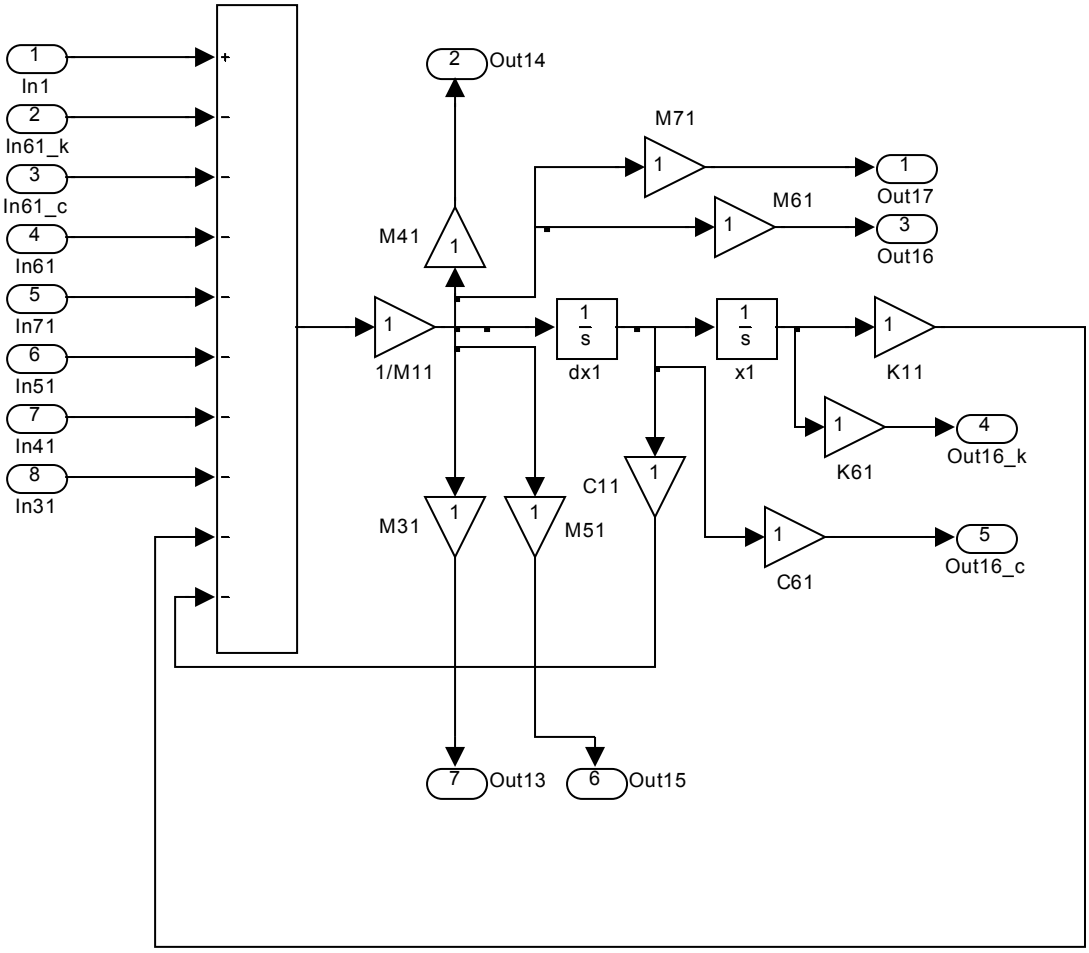

Figure E.2 The subsystem *x*.

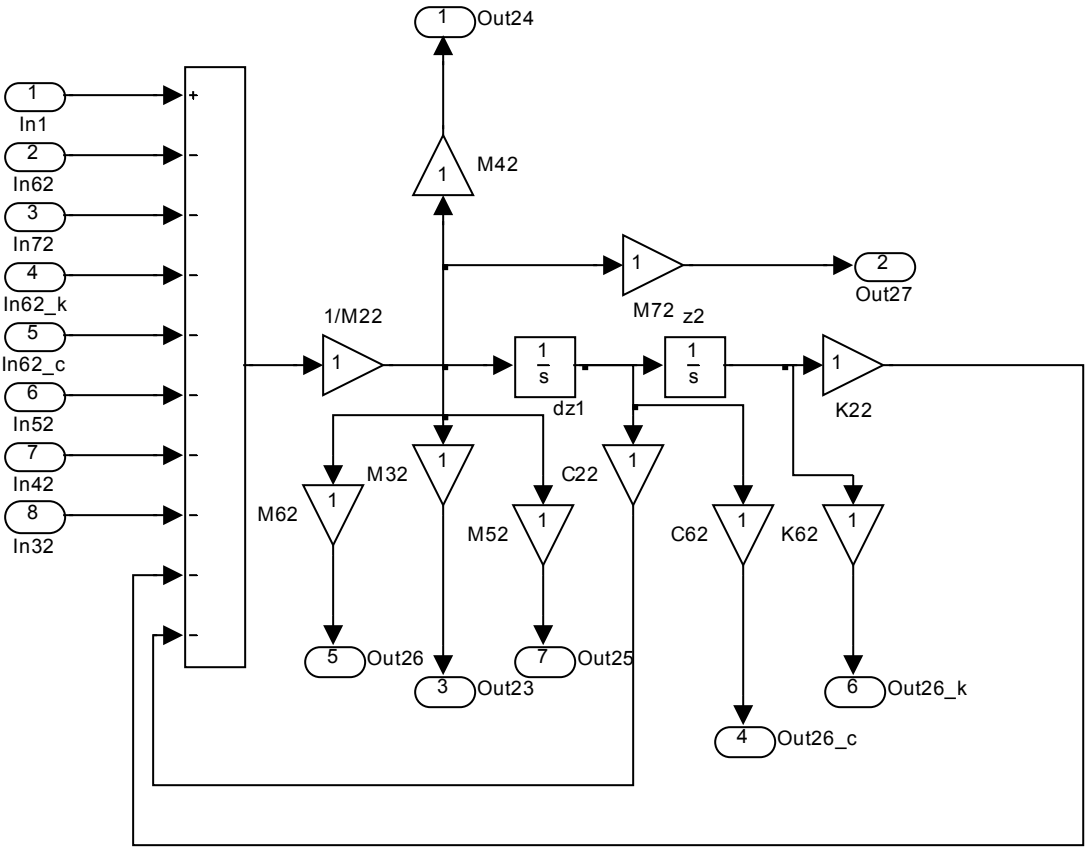

Figure E.3 The subsystem *z*.

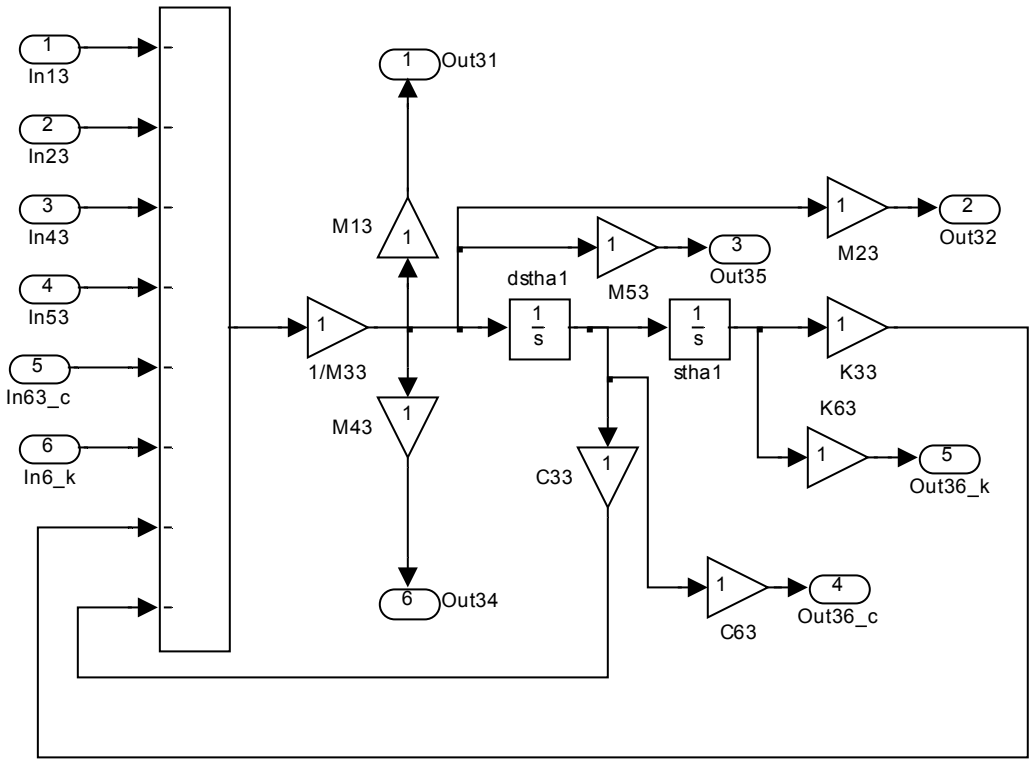

Figure E.4 The subsystem θ_1.

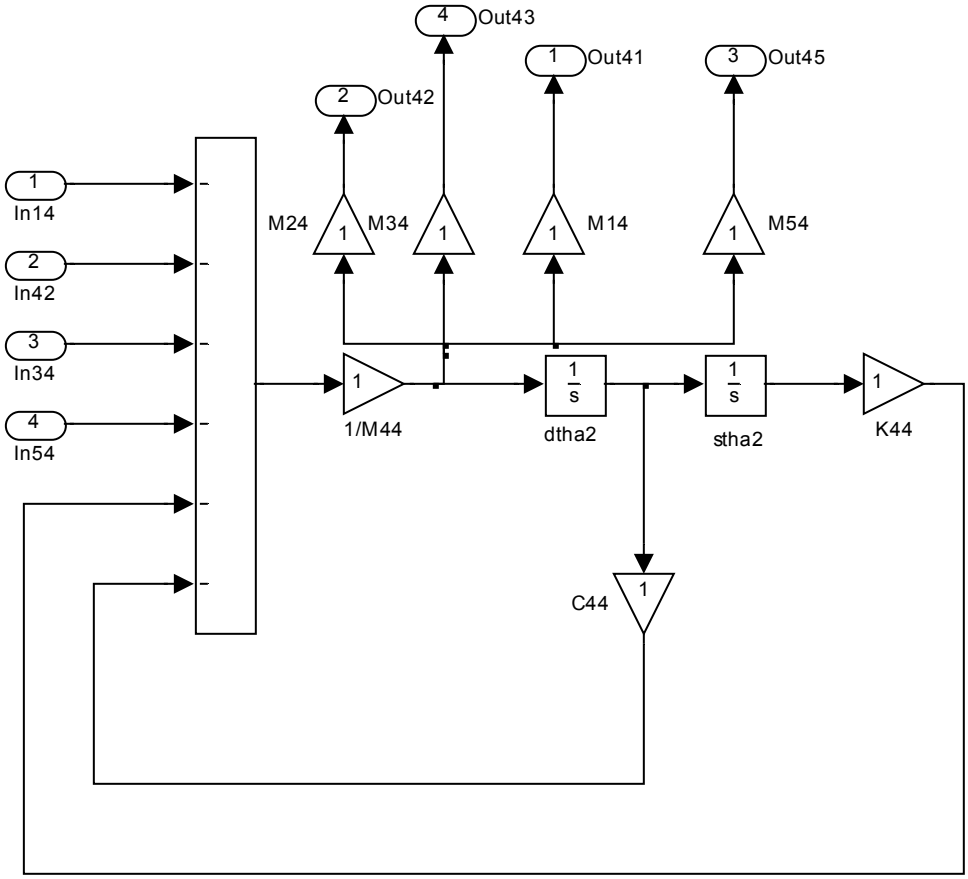

Figure E.5 The subsystem θ_2.

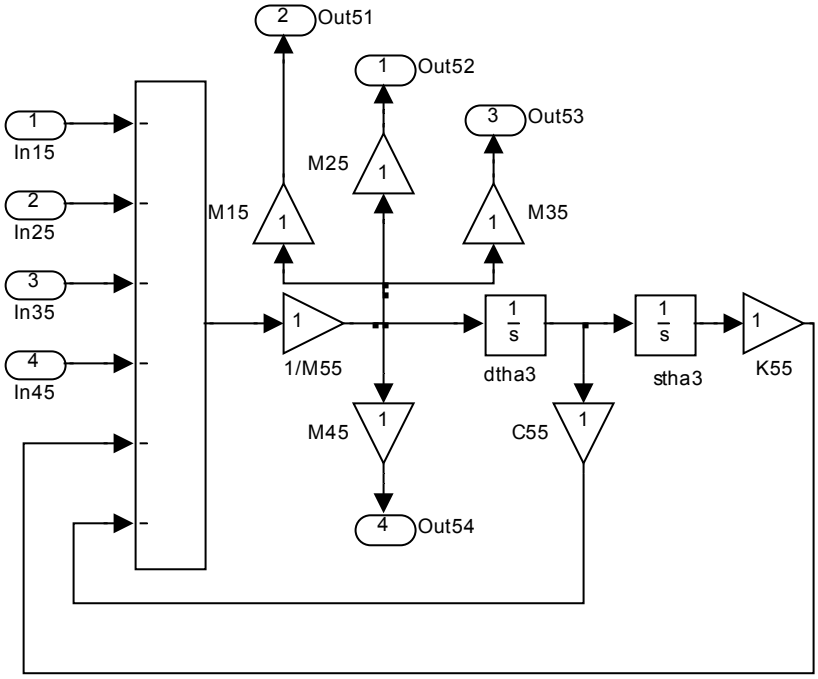

Figure E.6 The subsystem θ_3.

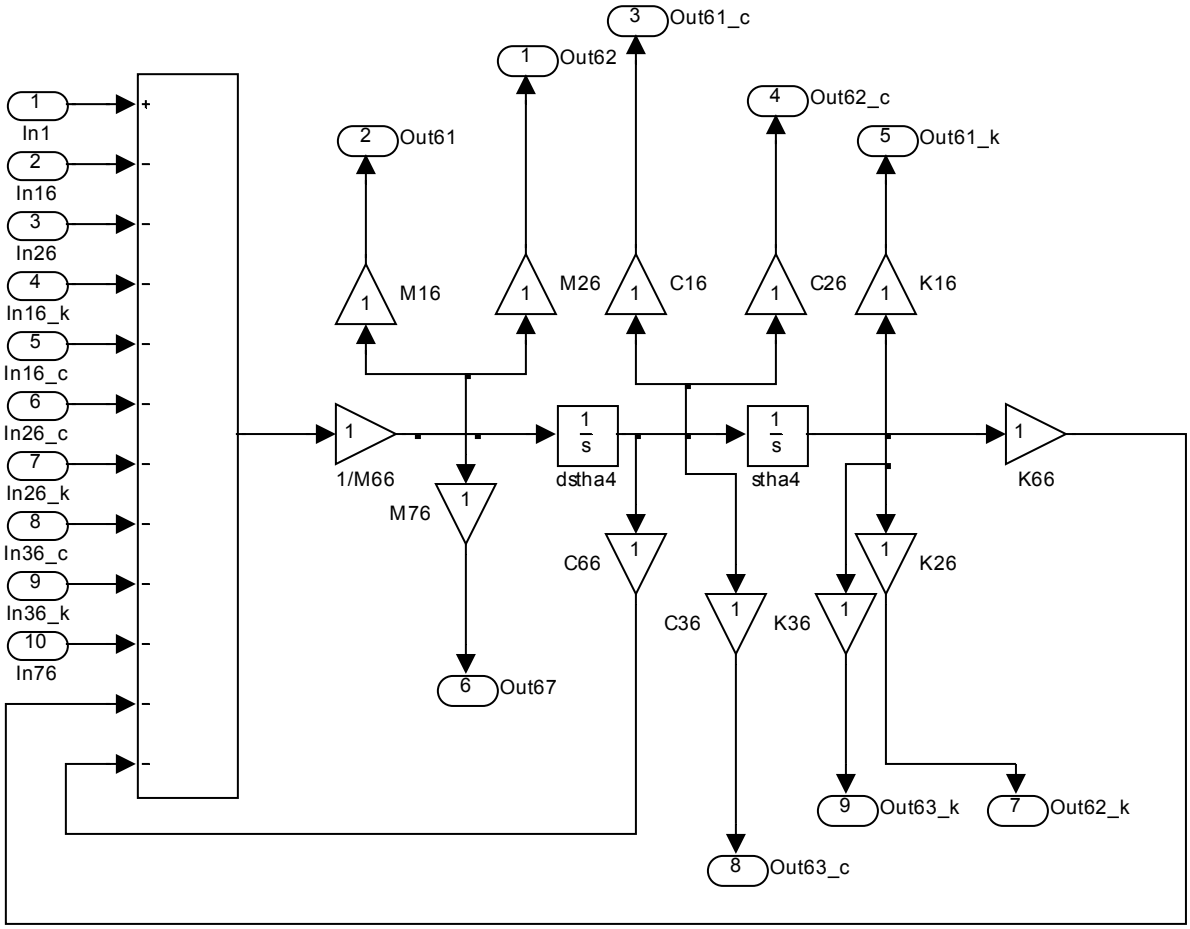

Figure E.7 The subsystem θ_4.

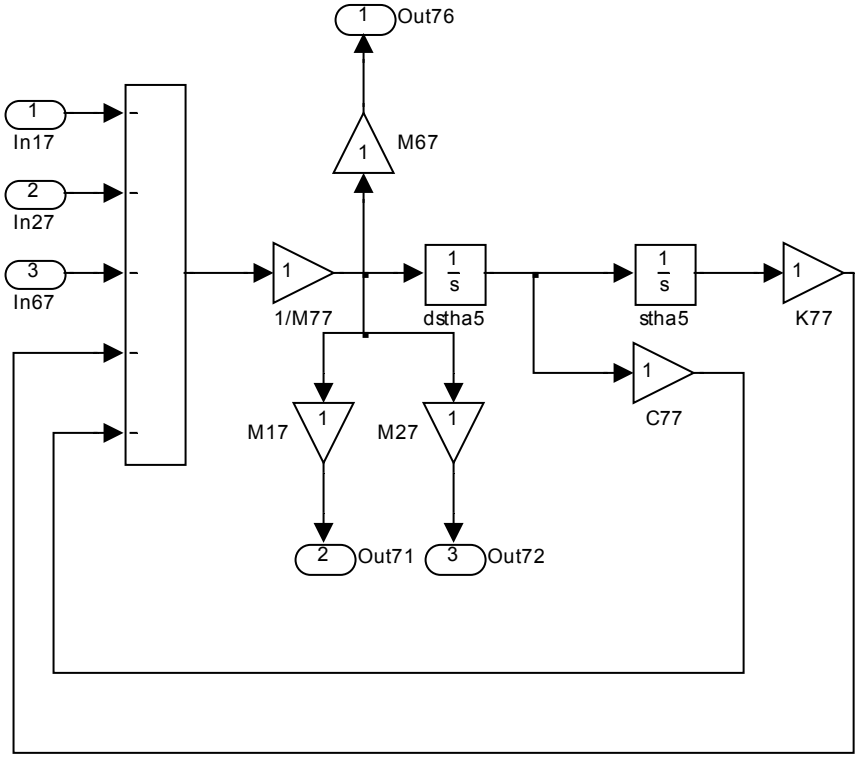

Figure E.8 The subsystem θ_5.

APPENDIX F: comparisons between the results obtained with CSD method and PSD method (Chapter 9)

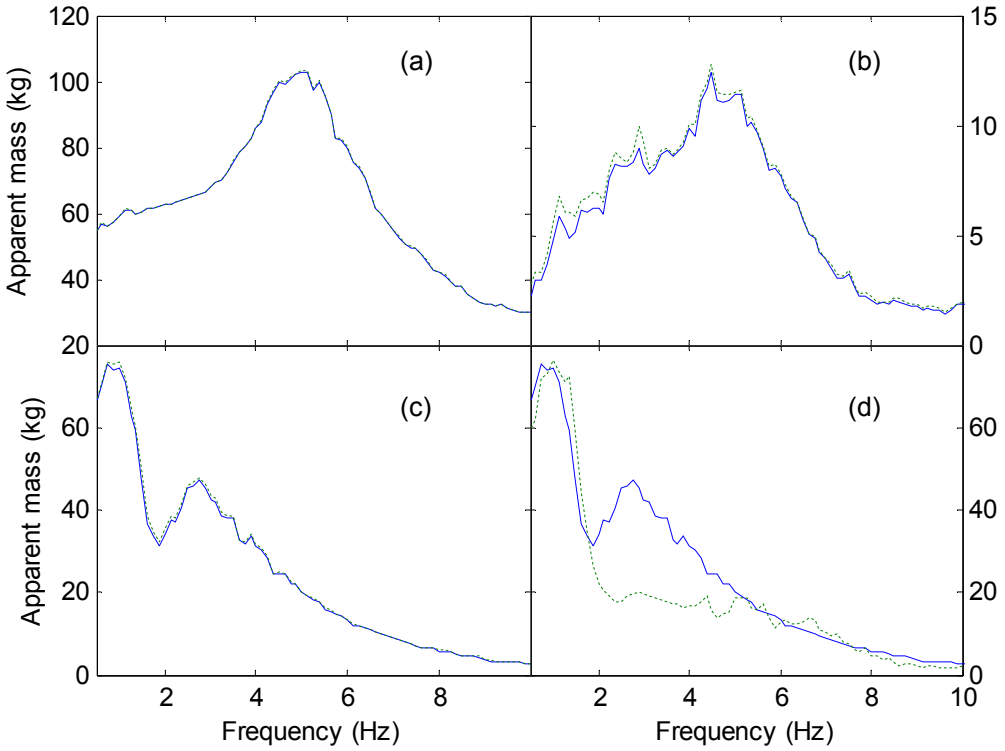

Figure F.1 Comparison of the apparent mass calculated with CSD method and PSD method: ——, CSD method; - - -, PSD method. (a) vertical apparent mass with vertical vibration at 0.5 ms^{-2} r.m.s.; (b) fore-and-aft cross-axis apparent mass with vertical vibration at 0.5 ms^{-2} r.m.s.; (c) fore-and-aft apparent mass with fore-and-aft vibration at 0.5 ms^{-2} r.m.s.; (d) vertical cross-axis apparent mass with fore-and-aft vibration at 0.5 ms^{-2} r.m.s. (individual data of subject 2).

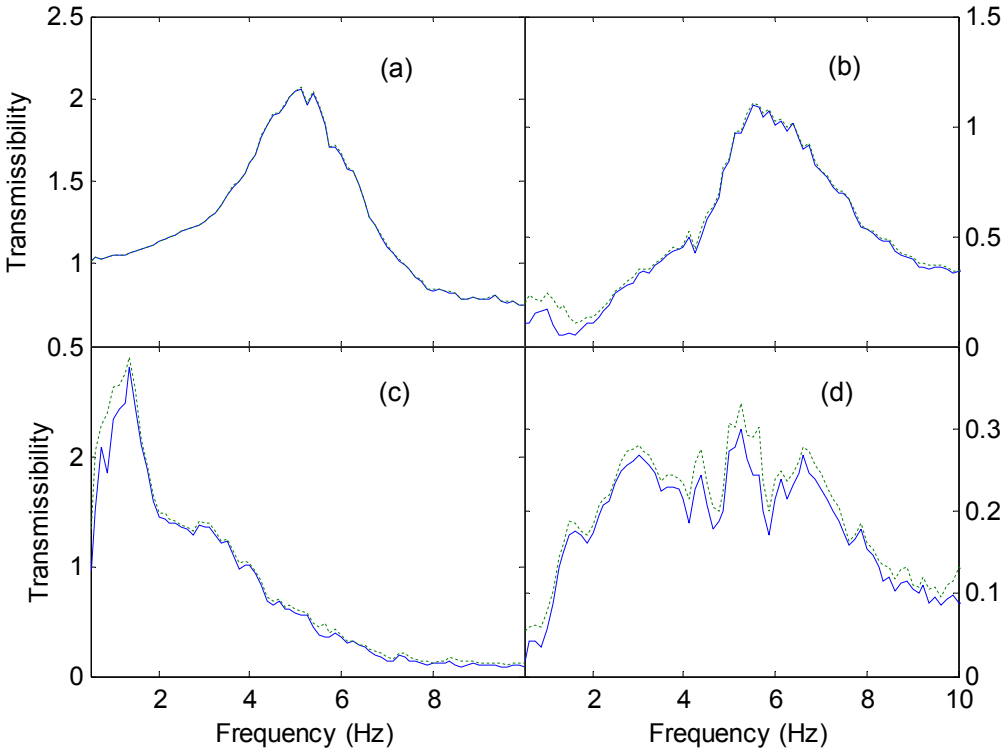

Figure F.2 Comparison of the transmissibility calculated with CSD method and PSD method: ——, CSD method; - - -, PSD method. (a) vertical transmissibility with vertical vibration at 0.5 ms^{-2} r.m.s.; (b) fore-and-aft cross-axis transmissibility with vertical vibration at 0.5 ms^{-2} r.m.s.; (c) fore-and-aft transmissibility with fore-and-aft vibration at 0.5 ms^{-2} r.m.s.; (d) vertical cross-axis transmissibility with fore-and-aft vibration at 0.5 ms^{-2} r.m.s. (individual data of subject 2).

REFERENCES

Bendat, JS, Piersol, AG (1986) Random Data Analysis and Measurement Procedures, 2nd Edition, Wiley, New York.

Boileau PE, Wu X and Rakheja S (1998) Definition of a range of idealized values to characterize seated body biodynamic response under vertical vibration. Journal of Sound and Vibration 215 (1), 841–862.

Cho Y and Yoon YS (2001) Biomechanical model of human on seat with backrest for evaluating ride quality. International Journal of Industrial Ergonomics 27 (5), 331-345.

Coermann RR (1962) The mechanical impedance of the human body in sitting and standing positions at low frequencies. Human Factors 4, 227–253.

Dempster WT and Gaughran RL (1967) Properties of body segments based on size and weight. American Journal of Anatomy 120 (1), 33-54.

Fairley TE and Griffin MJ (1989) The apparent mass of the seated human body: vertical vibration. Journal of Biomechanics 22 (2), 81–94.

Fairley TE and Griffin MJ (1990) The apparent mass of the seated human body in the fore-and-aft and lateral direction. Journal of Sound and Vibration 139 (2), 299–306.

Fleury G and Mistrot P (2006) Numerical assessment of fore-and-aft suspension performance to reduce whole-body vibration of wheel loader drivers. Journal of Sound and Vibration 298 (3), 672–687.

Griffin MJ (1989) Vertical vibration of seated subjects: effect of posture, vibration level, and frequency. Aviation, Space and Environmental Medicine 46 (3), 269-276.

Griffin MJ (1990) Handbook of Human Vibration. London: Academic Press Limited.

Hagbarth KE, Hagglund JV, Nordin M and Wallin EU (1985) Thixotropic behaviour of human finger flexor muscles with accompanying changes in spindle and reflex responses to stretch. Journal of Physiology 368, 323 – 342.

Hinz B, Blüthner R, Menzel G, Rützel S, Seidel H, and Wölfel HP (2006a) Apparent mass of seated men -Determination with single- and multi-axis excitations at different magnitudes. Journal of Sound and Vibration 298(3), 788-809.

Hinz B, Rutzel S, Bluthner R, Menzel G, Wö fel HP and Seidel H (2006b) Apparent mass of seated man - First determination with a soft seat and dynamic seat pressure distributions. Journal of Sound and Vibration 298 (3), 704-724.

Hinz B, Seidel H, Bräuer D, Menzel G, Blüthner R and Erdmann U (1988) Dimensional accelerations of lumbar vertebrae and estimation of internal spinal load during sinusoidal vertical whole-body vibration: a pilot study. Clinical Biomechanics 3 (4), 241-248.

Holmlund P, Lundstrom R and Lindberg L (2000) Mechanical impedance of the human body in vertical direction. Applied Ergonomics 31 (4), 415–422.

Homma I and Hagbarth KE (2000) Thixotropic of rib cage respiratory muscles in normal subjects. Journal of Applied Physiology 89 (5), 1753-1758.

Huang Y and Griffin MJ (2006) Effect of voluntary periodic muscular activity on nonlinearity in the apparent mass of the seated human body during vertical random whole-body vibration. Journal of Sound and Vibration 298 (3), 824-840.

Huang Y (2008) Mechanism of nonlinear biodynamic response of the human body exposed to whole-body vibration. PhD thesis, University of Southampton, England.

Huang Y and Griffin MJ (2008) Non-linear dual-axis biodynamic response of the semi-supine human body during vertical whole-body vibration. Journal of Sound and Vibration 312 (1-2), 296 – 315.

International Organization for Standardization (2001) Vibration and shock – Range of idealized values to characterize seated-body biodynamic response under vertical vibration. ISO 5982.

Ippili RK, Davies P, Bajaj AK and Hagenmeyer L (2008) Nonlinear multi-body dynamic model of seat–occupant system with polyurethane seat and H-point prediction. International Journal of Industrial Ergonomics 38 (5-6), 368-383.

Kim SK, White SW, Bajaj AK and Davies P (2003) Simplified models of the vibration of mannequins in car seats. Journal of Sound and Vibration 264 (1), 49-90.

Kim TH, Kim YT and Yoon YS (2005) Development of a biomechanical model of the human body in a sitting posture with vibration transmissibility in the vertical direction. Industrial Ergonomics 35 (9), 817-829.

Kitazaki S and Griffin MJ (1997) A modal analysis of whole-body vertical vibration using a finite element model of the human body. Journal of Sound and Vibration 200 (1), 83-103.

Kitazaki S and Griffin MJ (1998) Resonance behaviour of the seated human body and effects of posture. Journal of Biomechanics 31 (2), 143 – 149.

Lakie M, Walsh EG and Wright GW (1979) Passive wrist movements-a large thixotropic effect. Journal of Physiology 300, 36–37.

Lakie M (1986) Vibration causes stiffness changes (thixotropic behaviour) in relaxed human muscle. United Kingdom Group Informal Meeting on Human Response to Vibration, Loughborough, England, 22-23 September.

Lee RA and Pradko F (1968) Analytical analysis of human vibration. Society of Automotive Engineers, Paper No. 680091.

Lewis CH (2001) An adaptive electro-mechanical model for simulating the driving point force response of the human body with different input motions. United Kingdom Group Meeting on Human Responses to Vibration, Farnborough, England, 12–14 September.

Li J, Luo XY, Kuang ZB (2001) A nonlinear anisotropic model for porcine aortic heart valves. Journal of Biomechanics 34 (10), 1279–1289.

Liang CC and Chiang FC (2006) A study on biodynamic models of seated human subjects exposed to vertical vibration. International Journal of Industrial Ergonomics 36 (10), 869-890.

Liang CC and Chiang FC (2008) Modelling of a seated human body exposed to vertical vibrations in various automotive postures. Industrial Health 46 (2), 125-167.

Livermore Software Technology Corporation (2007) LS-DYNA keyword user's manual, Volume I.

Loocke MV, Lyons CG, Simms CK (2005) A validated model of passive muscle in compression. Journal of Biomechanics 39 (16), 2999–3009.

Loocke MV, Lyons CG, Simms CK (2008) Viscoelastic properties of passive skeletal muscle in compression: Stress-relaxation behaviour and constitutive modelling. Journal of Biomechanics 41 (7), 1555–1566.

LSTC Dummy Models (2010) LSTC Front Impact Hybrid III -50th percentile Male http://www.oasys-software.com/dyna/en/fe-models/lstc_dummies.shtml.

Lundström R and Holmlund P (1998) Absorption of energy during whole-body vibration exposure. Journal of Sound and Vibration 215 (4), 789 – 799.

Makhsous M, Venkatasubramanian G, Chawla A, Pathak Y, Priebe M, Rymer WZ and Lin F (2008) Investigation of soft-tissue stiffness alteration in denervated human tissue using an ultrasound indentation system. The Journal of Spinal Cord Medicine 31 (1), 88-96.

Mansfield NJ (1995) Distortion of the dynamic response of the pelvis when exposed to whole-body sinusoidal vibration. United Kingdom Group Meeting on Human Responses to Vibration, Silsoe, England, 18–20 September.

Mansfield NJ (1997) A consideration of alternative non-linear lumped parameter models of the apparent mass of a seated person. United Kingdom Group Meeting on Human Responses to Vibration, Southampton, England. 17–19 September.

Mansfield NJ (1998) Non-linear biodynamic response of the seated person to whole-body vibration. PhD thesis, University of Southampton, England.

Mansfield NJ and Griffin MJ (2000) Non-linearity in apparent mass and transmissibility during exposure to whole-body vertical vibration. Journal of Biomechanics 33 (8), 933–941.

Mansfield NJ and Griffin MJ (2002) Effects of posture and vibration magnitude on apparent mass and pelvis rotation during exposure to whole-body vertical vibration. Journal of Sound and Vibration 253 (1), 93 – 107.

Mansfield NJ, Lundström R, Lenzuni P, and Nataletti P (2006) Effect of vibration magnitude, vibration spectrum and muscle tension on apparent mass and cross axis transfer functions during whole-body vibration exposure. Journal of Biomechanics 39 (16), 3062-3070.

Mansfield NJ and Maeda S (2005a) Effect of backrest and torso twist on the apparent mass of the seated body exposed to vertical vibration. Industrial Health 43 (3), 413–420.

Mansfield NJ and Maeda S (2005b) Comparison of the apparent mass of the seated human measured using random and sinusoidal vibration. Industrial Health 43 (1), 233–240.

Mansfield NJ and Maeda S (2006) Comparison of the apparent masses and cross-axis apparent masses of seated humans exposed to single and dual-axis whole-body vibration. Journal of Sound and Vibration 298 (3), 841-853.

Matsumoto Y and Griffin MJ (2001) Modelling the dynamic mechanisms associated with the principal resonance of the seated human body. Clinical Biomechanics 16 (suppl1), 31-44.

Matsumoto Y and Griffin MJ (1998a) Movement of the upper-body of seated subjects exposed to vertical whole-body vibration at the principal resonance frequency. Journal of Sound and Vibration 215 (4), 743 –762.

Matsumoto Y and Griffin MJ (1998b) Dynamic response of the standing human body exposed to vertical vibration: influence of posture and vibration magnitude, Journal of Sound and Vibration 212 (1), 85–107.

Matsumoto Y and Griffin MJ (2002a) Non-linear characteristics in the dynamic responses of seated subjects exposed to vertical whole-body vibration. Journal of Biomechanical Engineering 124 (5), 527 – 532.

Matsumoto Y and Griffin MJ (2002b) Effect of muscle tension on non-linearities in the apparent mass of seated subjects exposed to vertical whole-body vibration. Journal of Sound and Vibration 253 (1), 77–92.

Messenger AJ and Griffin MJ (1989) Effects of anthropometric and postural variables on the transmission of whole-body vertical vibration from seat-to-head. Institute of Sound and Vibration Research, University of Southampton, England. Technical Report 172.

Muksian R and Nash CD (1974) A model for the response of seated humans to sinusoidal displacements of the seat. Journal of Biomechanics 7 (3), 209–215.

National Aeronautics and Space Administration (1978) Anthropometric source book, volume1: anthropometry for designers. NASA Reference Publication 1024.

Nawayseh N and Griffin MJ (2009) A model of the vertical apparent mass and the fore-and-aft cross-axis apparent mass of the human body during vertical whole-body vibration. Journal of Sound and Vibration 319 (1-2), 719-730.

Nawayseh N and Griffin MJ (2003) Non-linear dual-axis biodynamic response to vertical whole-body vibration. Journal of Sound and Vibration 268 (3), 503 – 523.

Nawayseh N and Griffin MJ (2004) Tri-axial forces at the seat and backrest during whole-body vertical vibration. Journal of Sound and Vibration 277 (1-2), 309 – 326.

Nawayseh N and Griffin MJ (2005) Non-linear dual-axis biodynamic response to fore-and-aft whole-body vibration. Journal of Sound and Vibration 282 (3-5), 831-862.

Oomens, CWJ, Bosboom, EMH, Bressers, OFJT, Bouten, CVC, Bader, DL (2003) Can loaded interface characteristics influence strain distribution in muscle adjacent to bony prominences? Computer Methods in Biomechanics and Biomedical Engineering 6 (3), 171-180.

Paddan GS and Griffin MJ (1988a) The transmission of translational seat vibration to the head - I. Vertical seat vibration. Journal of Biomechanics 21 (3), 191-197.

Paddan GS and Griffin MJ (1988b) The transmission of translational seat vibration to the head - II. Horizontal seat vibration. Journal of Biomechanics 21 (3), 199-206.

Paddan GS and Griffin MJ (1998) A review of the transmission of translational seat vibration to the head. Journal of Sound and Vibration 215 (4), 863–882.

Pankoke S, Buck B, and Woelfel HP (1998) Dynamic FE model of sitting man adjustable to body height, body mass, body posture used for calculating internal forces in the lumbar vertebral disks. Journal of Sound and Vibration 215 (4), 827-839.

Pankoke S and Siefert A (2008) Latest development in occupant simulation techniques related to seating comfort and human response and human response to vibration: finite element occupant model CASIMIR, United Kingdom Conference on Human Responses to Vibration: Leicester, England, 15-17 September.

Park SJ, Park SC, Kim JH and Kim CB (1999) Biomechanical parameters on body segments of Korean adults. International Journal of Industrial Ergonomics 23 (1-2), 23-31.

Qiu Y (2007) A seat-occupant model for the prediction of backrest transmissibility in the fore-and-aft direction. United Kingdom Conference on Human Responses to Vibration, Leicester, England, 10-12 September.

Qiu Y and Griffin MJ (2003) Transmission of fore-aft vibration to a car seat using field tests and laboratory simulation. Journal of Sound and Vibration 264 (1), 135-155.

Qiu Y and Griffin MJ (2009) Biodynamic responses of the seated human body to single-axis and dual-axis vibration. Proceedings of 4th International Conference on Whole Body Vibration Injuries, Montreal, Canada, 2-4 June.

Qiu Y and Griffin MJ (2010) Biodynamic responses of the seated human body to single-axis and dual-axis vibration. Industrial Health 48 (5), 615-627.

Qiu Y and Griffin MJ (2011) Modeling the fore-and-aft apparent mass of the human body and the transmissibility of seat backrests. Vehicle System Dynamics 49 (5), 703-722.

Rakheja S, Stiharu I, and Boileau P-É (2002) Seated occupant apparent mass characteristics under automotive postures and vertical vibration. Journal of Sound and Vibration 253 (1), 57–75.

Sandover J (1978) Modelling human responses to vibration. Aviation, Space and Environmental Medicine 49 (1), 335–339.

Sandover J and Dupuis H (1987) A reanalysis of spinal motion during vibration. Ergonomics 30 (6), 975 - 985.

Saraf H, Ramesh KT, Lennon AM, Merkle KC and Roberts JC (2007) Mechanical properties of soft human tissues under dynamic loading. Journal of Biomechanics 40 (9), 1960–1967.

Smith SD (1994) Non-linear resonance behaviour in the human exposed to whole body vibration. Shock and Vibration 1 (5), 439 – 450.

Smith SD (2000) Modelling differences in the vibration response characteristics of the human body. Journal of Biomechanics 33, 1513 – 1516. Supplementary material: Human vibration data collection, analysis, and modelling http://www.elsevier.nl:80/inca/publications/store/3/2/1).

Snedeker JG., Barbezat M, Niederer P, Schmidlin FR, Farshad M (2005) Strain energy density as a rupture criterion for the kidney: impact tests on porcine organs, finite element simulation, and a baseline comparison between human and porcine tissues. Journal of Biomechanics 38 (5), 993–1001.

Stein GJ, Zahoranský R, Gunston TP, Burström L, Meyer L (2008) Modelling and simulation of a fore-and-aft driver's seat suspension system with road excitation. International Journal of Industrial Ergonomics 38 (5-6), 396–409.

Stein GJ, Múčka P, Chmúrny R (2006) Preliminary results on an x-direction apparent mass model of human body sitting in a cushioned, suspended seat. Journal of Sound and Vibration 298 (3), 688–703.

Siefert A, Pankoke P, Hofmann J and Contratto MS (2008) Analysis of static and dynamic properties of foam and trim materials for seat cushions: experimental investigations, numerical implementation and simulation of human exposure to vibrations. United Kingdom Conference on Human Responses to Vibration. Leicester, England, 15-17 September.

Siefert A, Pankoke S and Wolfel HP (2008) Virtual optimization of car passenger seats: Simulation of static and dynamic effects on drivers' seating comfort. International Journal of Industrial Ergonomics 38 (5-6), 410-424.

Subashi GHMJ, Nawayseh N, Matsumoto Y and Griffin MJ (2009) Nonlinear subjective and dynamic responses of seated subjects exposed to horizontal whole-body vibration. Journal of Sound and Vibration 321 (1-2), 416–434.

Tanner RI (1985) Engineering Rheology. Oxford engineering science series 14, Oxford: Clarendon press.

Toward MGR (2002) Apparent mass of the human body in the vertical direction: effect of input spectra. United Kingdom Group Meeting on Human Responses to Vibration, Loughborough, England, 18–20 September.

Toward MGR (2003) Apparent mass of the human body in the vertical direction: effect of seat backrest. United Kingdom Group Meeting on Human Responses to Vibration, Gosport, England, 17–19 September.

Toward MGR and Griffin MJ (2010) Apparent mass of the human body in the vertical direction: Effect of a footrest and a steering wheel. Journal of Sound and Vibration 329 (9), 1586-1596.

Toward MGR and Griffin (2011) Apparent mass of the human body in the vertical direction: inter-subject variability. Journal of Sound and Vibration 330 (4), 827–841.

Toward MGR and Griffin MJ (2009) Apparent mass of the human body in the vertical direction: Effect of seat backrest. Journal of Sound and Vibration 327 (3-5), 657–669.

Valencia FP and Munro RR (1985) An electromyographic study of the lumbar multifidus in man. Electromyography and Clinical Neurophysiology 2 (4), 205 – 221.

Van Loocke M, Lyons CG and Simms CK (2006) A validated model of passive muscle in compression. Journal of Biomechanics 39 (16), 2999–3009.

Van Loocke. M, Lyons CG and Simms CK (2008) Viscoelastic properties of passive skeletal muscle in compression: Stress-relaxation behaviour and constitutive modelling. Journal of Biomechanics 41 (7), 1555–1566.

Verver, MM (2004) Numerical tools for comfort analyses of automotive seating. Dissertation, Technische Universiteit Eindhoven, Eindhoven.

Wang W, Rakheja S and Boileau P-É (2004) Effects of sitting postures on biodynamic response of seated occupants under vertical vibration. International Journal of Industrial Ergonomics 34 (4), 289–306.

Wei L and Griffin MJ (1998) Mathematical models for the apparent mass of the seated human body exposed to vertical vibration. Journal of Sound and Vibration 212 (5), 855 – 874.

Wittmann TJ and Phillips NS (1969) Human body nonlinearity and mechanical impedance analysis. Journal of Biomechanics 2 (3), 281 – 288.

Yoshimura T, Nakai K and Tamaoki G (2005) Multi-body dynamics modelling of seated human body under exposure to whole-body vibration. Industrial Health 43 (3), 441–447.

Wu X, Rakheja S and Boileau P- É (1999) Distribution of human-seat interface pressure on a soft automotive seat under vertical vibration. International Journal of Industrial Ergonomics 24 (5), 545-557.

Zheng G, Qiu Y and Griffin MJ (2009) Planar multi-body modelling of the in-axis and cross-axis apparent mass of the seated human body with vertical whole body vibration. United Kingdom Conference on Human Responses to Vibration, Loughborough, England, 7-9 September.

Zheng YP, Mak Arthur FT, Lue B (1999) Objective assessment of limb tissue elasticity: Development of a manual indentation procedure. Journal of Rehabilitation Research and Development 36 (2), 71-85.